


Spring 1993

Recognition of Quadric Surfaces From Range Data: An Analytical Approach

Ivan X. D. D'Cunha
Old Dominion University

Follow this and additional works at: https://digitalcommons.odu.edu/ece_etds

 Part of the [Artificial Intelligence and Robotics Commons](#), and the [Electrical and Computer Engineering Commons](#)

Recommended Citation

D'Cunha, Ivan X.. "Recognition of Quadric Surfaces From Range Data: An Analytical Approach" (1993). Doctor of Philosophy (PhD), dissertation, Electrical/Computer Engineering, Old Dominion University, DOI: 10.25777/aktp-h874
https://digitalcommons.odu.edu/ece_etds/174

This Dissertation is brought to you for free and open access by the Electrical & Computer Engineering at ODU Digital Commons. It has been accepted for inclusion in Electrical & Computer Engineering Theses & Dissertations by an authorized administrator of ODU Digital Commons. For more information, please contact digitalcommons@odu.edu.

**RECOGNITION OF QUADRIC SURFACES FROM RANGE DATA:
AN ANALYTICAL APPROACH**

by

Ivan X. D. D'Cunha
B.E. June 1987, Osmania University, India
M.S. December 1989, Old Dominion University

A Dissertation Submitted to the Faculty of
Old Dominion University in Partial Fulfillment
of the Requirements of

DOCTOR OF PHILOSOPHY
ELECTRICAL ENGINEERING

OLD DOMINION UNIVERSITY
May, 1993

Approved by:

Nicolas Alvarez, Director

ABSTRACT

RECOGNITION OF QUADRIC SURFACES FROM RANGE DATA: AN ANALYTICAL APPROACH

Ivan X. D. D'Cunha
Old Dominion University, 1992
Director: Dr. Nicolas Alvertos

The problem of recognizing and positioning of objects in three-dimensional space is important for robotics and navigation applications. In recent years, digital range data, also referred to as range images or depth maps, have been available for the analysis of three-dimensional objects owing to the development of several active range finding techniques. The distinct advantage of range images is the explicitness of the surface information available. Many industrial and navigational robotics tasks will be more easily accomplished if such explicit information can be efficiently interpreted.

In this dissertation, a new technique based on analytic geometry for the recognition and description of three-dimensional quadric surfaces from range images is presented. Beginning with the explicit representation of quadrics, a set of ten coefficients are determined for various three-dimensional surfaces. For each quadric surface, a unique set of two-dimensional curves which serve as a feature set is obtained from the various angles at which the object is intersected with a plane. Based on a discriminant method, each of the curves is classified as a parabola, circle,

ellipse, hyperbola, or a line. Each quadric surface is shown to be uniquely characterized by a set of these two-dimensional curves, thus allowing discrimination from the others.

Before the recognition process can be implemented, the range data have to undergo a set of pre-processing operations, thereby making it more presentable to classification algorithms. One such pre-processing step is to study the effect of median filtering on raw range images. Utilizing a variety of surface curvature techniques, reliable sets of image data that approximate the shape of a quadric surface are determined. Since the initial orientation of the surfaces is unknown, a new technique is developed wherein all the rotation parameters are determined and subsequently eliminated. This approach enables us to position the quadric surfaces in a desired coordinate system.

Experiments were conducted on raw range images of spheres, cylinders, and cones. Experiments were also performed on simulated data for surfaces such as hyperboloids of one and two sheets, elliptical and hyperbolic paraboloids, elliptical and hyperbolic cylinders, ellipsoids and the quadric cones. Both the real and simulated data yielded excellent results. Our approach is found to be more accurate and computationally inexpensive as compared to traditional approaches, such as the three-dimensional discriminant approach which involves evaluation of the rank of a matrix.

Finally, we have proposed one other new approach, which involves the formulation of a mapping between the explicit and implicit forms of representing quadric surfaces. This approach, when fully realized, will yield a three-dimensional discriminant, which will recognize quadric surfaces based upon their component surface patches. This approach is faster than prior approaches and at the same time is invariant to pose and orientation of the surfaces in three-dimensional space.

DEDICATION

*To my parents Marcel and Helen for their
love and support.*

ACKNOWLEDGEMENTS

I am grateful to Dr. Nicolas Alvertos for his guidance and support with this research. Without his encouragement and motivation, this work would have been an unfulfilled dream. My sincere thanks to Dr. David Livingston for spending endless hours helping bring this manuscript to its present form. I would also like to thank Dr. John W. Stoughton for lending me the moral support when needed. I wish to thank Dr. Philip Wohl and Dr. Vishnu Lakdawala for their enthusiasm and reviewing this dissertation.

I also wish to thank Mr. Mike Goode of the Automation Technology Branch of NASA Langley Research Center for trusting us with this project. His help whenever needed is sincerely appreciated. I would also like to thank the secretaries at our department, Bev, Valerie, Alicia, Jenny, and all my friends and colleagues at school for having put up with me for all these years.

Above all, my sincere thankfulness to God for blessing me with good health and for being on my side all times.

Table of Contents

LIST OF TABLES	vii
LIST OF FIGURES	x
CHAPTER 1: INTRODUCTION.	3
1.1 Introduction	1
1.2 Range Image and Data Acquisition	1
1.3 Definition of Object Recognition Problem	2
1.4 Objectives and Organization of the Dissertation	3
CHAPTER 2: BACKGROUND	5
2.1 Introduction	5
2.2 Literature Review	5
2.3 Differential Geometry of Surfaces: Mean and Gaussian Curvatures	8
2.4 Three-Dimensional Discriminant	12
2.4.1 Translation	13
2.4.2 Rotation	13
CHAPTER 3: QUADRIC SURFACE REPRESENTATION	19
3.1 Introduction	19
3.2 Quadric Surface Description	19

3.3 Recognition Scheme	23
3.3.1 Median Filtering	24
3.3.2 Segmentation	28
3.3.3 Three-Dimensional Coefficients Evaluation	28
3.3.4 Evaluation of the Rotation Matrix	33
3.3.5 Product Terms Elimination Method	38
3.3.6 Translation of the Rotated Object	44

CHAPTER 4: QUADRIC SURFACE CHARACTERIZATION AND

RECOGNITION	47
4.1 Introduction	47
4.2 Two-Dimensional Discriminant	48
4.3 Quadric Surface Description and Representation	49
4.3.1 Ellipsoid	49
4.3.2 Circular (Elliptic) cylinder	55
4.3.3 Sphere	62
4.3.4 Quadric circular (elliptic) cone	66
4.3.5 Hyperboloid of one sheet	70
4.3.6 Hyperboloid of two sheets	82
4.3.7 Elliptic paraboloid	90
4.3.8 Hyperbolic paraboloid	95
4.3.9 Hyperbolic cylinder	99
4.3.10 Parabolic cylinder	100
4.3.11 Parallelepiped	106

4.4 Mapping of Explicit to Implicit Representation for Quadric Surfaces	107
CHAPTER 5: EXPERIMENTAL RESULTS	112
5.1 Introduction	112
5.2 Median Filtering on Range Images	113
5.3 Application of the Recognition Process to the Processed Image Data	156
5.4 Application of the Rotation Alignment Algorithm	162
5.5 Application of Three-Dimensional Discriminant Technique	166
CHAPTER 6: CONCLUSIONS	171
6.1 Overview	171
6.2 Advantages of the Recognition Scheme	174
6.3 Future Goals and Research Directions	175
REFERENCES	176
APPENDIX A	180
APPENDIX B	187
APPENDIX C	190
APPENDIX D	193
APPENDIX E	198

LIST OF TABLES

Table 2-1	Surface classification using the three-dimensional discriminant approach	18
Table 4-1	Intersection of ellipsoid with planes	55
Table 4-2	Intersection of quadric cylinder with planes	62
Table 4-3	Intersection of sphere with planes	64
Table 4-4	Intersection of quadric cone with planes	73
Table 4-5	Intersection of hyperboloid of one sheet with planes	82
Table 4-6	Intersection of hyperboloid of two sheets with planes	88
Table 4-7	Intersection of elliptic paraboloid with planes	95
Table 4-8	Intersection of hyperbolic paraboloid with planes	96
Table 4-9	Intersection of the hyperbolic cylinder with planes	100
Table 4-10	Intersection of the parabolic cylinder with planes	103
Table 4-11	Intersection of the parallelepiped with planes	106
Table 4-12	Various curves intercepted by quadric surfaces when intersected with the planes $z = k$ and $y = k$	108
Table 4-13	Feature vector (representing the presence or absence of curves) for each of the quadric surfaces	109
Table 5-1	Comparison of coefficients evaluated for the original and the processed images of a sphere	159

Table 5-2	Comparison of coefficients evaluated for the original and the processed images of a cylinder	160
Table 5-3	Curves intercepted by the two planes, $z = k$ and $y = k$, with real raw and processed range data of the sphere	161
Table 5-4	Curves intercepted by the two planes, $z = k$ and $y = k$, with real raw and processed range data of the cylinder	161
Table 5-5	Curves intercepted by the two planes, $z = k$ and $y = k$, with real raw and processed range data of the quadric cone	162
Table 5-6	New coefficients of the raw image data of sphere after alignment	163
Table 5-7	New coefficients of the 3 x 3 median filtered image data of sphere after alignment	163
Table 5-8	New coefficients of the 5 x 5 median filtered image data of sphere after alignment	164
Table 5-9	New coefficients of the raw image data of cylinder after alignment	164
Table 5-10	New coefficients of the 3 x 3 median filtered image data of cylinder after alignment	165
Table 5-11	New coefficients of the 5 x 5 median filtered image data of cylinder after alignment	165
Table 5-12	New coefficients of an unknown simulated data obtained after alignment	167
Table 5-13	New coefficients of an unknown simulated data obtained after alignment	

Table 5-14	New coefficients of an unknown simulated data obtained after alignment	168
Table 5-15	Surface characterization using 3-D discriminant approach for simulated data	169

LIST OF FIGURES

Figure 2-1	Shape of a surface in the vicinity of an elliptic, hyperbolic, and parabolic point	10
Figure 2-2	A set of eight view-independent surface types for a visible surface	11
Figure 2-3	Two right-handed rectangular coordinate systems	14
Figure 2-4	Relation between the coordinates of P upon translation	14
Figure 2-5	Two rectangular coordinate systems having the same origin	15
Figure 3-1	Quadric representations of Real ellipsoid, Hyperboloid of one sheet, Hyperboloid of two sheets, and Real quadric cone	20
Figure 3-2	Quadric representations of Elliptic paraboloid, Hyperbolic paraboloid, Elliptic cylinder, and Parabolic cylinder	21
Figure 3-3	Quadric representations of Hyperbolic cylinder and Parallelepiped	22
Figure 3-4	Raw range image of the sphere	25
Figure 3-5	3 x 3 median filtered image of the raw sphere	25
Figure 3-6	5 x 5 median filtered image of the raw sphere	27
Figure 3-7	7 x 7 median filtered image of the raw sphere	27
Figure 3-8	Rotation transformation of the coordinate system	36
Figure 4-1	List of all quadric surfaces	50
Figure 4-2	Ellipsoid detailed view: horizontal intersections	53

Figure 4-3	Ellipsoid detailed view: vertical intersections	54
Figure 4-4	Cylinder detailed view: horizontal intersections	58
Figure 4-5	Cylinder detailed view: vertical intersections	60
Figure 4-6	Cylinder: lateral view	61
Figure 4-7	Intersection of a plane and a sphere	65
Figure 4-8	Quadric cone detailed view: horizontal intersections	69
Figure 4-9	Quadric cone detailed view: vertical intersections	71
Figure 4-10	Quadric cone: Lateral view	72
Figure 4-11	Hyperboloid of one sheet detailed view: horizontal intersections and $z = 0$	76
Figure 4-12	Hyperboloid of one sheet detailed view: horizontal intersections and $z = -c$	78
Figure 4-13	Hyperboloid of one sheet detailed view: vertical intersections	80
Figure 4-14	Hyperboloid of one sheet: lateral view	81
Figure 4-15	Hyperboloid of two sheets detailed view: horizontal intersections	85
Figure 4-16	Hyperboloid of two sheets detailed view: vertical intersections	87
Figure 4-17	Hyperboloid of two sheets: lateral view	89
Figure 4-18	Elliptic paraboloid detailed view: horizontal intersections	92
Figure 4-19	Elliptic paraboloid detailed view: vertical intersections	94
Figure 4-20	Hyperbolic paraboloid detailed view: horizontal intersections	97

Figure 4-21	Hyperbolic paraboloid detailed view: vertical intersections	98
Figure 4-22	Hyperbolic cylinder detailed view: horizontal intersections	101
Figure 4-23	Hyperbolic cylinder detailed view: vertical intersections	102
Figure 4-24	Parabolic cylinder detailed view: horizontal intersections	104
Figure 4-25	Parabolic cylinder detailed view: vertical intersections	105
Figure 5-1	Raw range image of the sphere with its background	114
Figure 5-2	Raw range image of the sphere after segmentation	114
Figure 5-3	3 x 3 median filtered image of the raw sphere	115
Figure 5-4	5 x 5 median filtered image of the raw sphere	116
Figure 5-5	7 x 7 median filtered image of the raw sphere	116
Figure 5-6a	First derivative with respect to x-axis of the sphere raw image	117
Figure 5-6b	First derivative with respect to y-axis of the sphere raw image	118
Figure 5-6c	Second derivative with respect to x-axis of the sphere raw image	119
Figure 5-6d	Second derivative with respect to y-axis of the sphere raw image	120
Figure 5-7a	First derivative with respect to x-axis of the sphere filtered with a mask size of 3 x 3	121
Figure 5-7b	First derivative with respect to y-axis of the sphere filtered sphere filtered with a mask size of 3 x 3	122
Figure 5-7c	Second derivative with respect to x-axis of the sphere filtered with a mask size of 3 x 3	123

Figure 5-7d	Second derivative with respect to y-axis of the sphere filtered with a mask size of 3 x 3	124
Figure 5-8a	First derivative with respect to x-axis of the sphere filtered with a mask size of 5 x 5	125
Figure 5-8b	First derivative with respect to y-axis of the sphere filtered with a mask size of 5 x 5	126
Figure 5-8c	Second derivative with respect to x-axis of the sphere filtered with a mask size of 5 x 5	127
Figure 5-8d	Second derivative with respect to y-axis of the sphere filtered with a mask size of 5 x 5	128
Figure 5-9a	First derivative with respect to x-axis of the sphere filtered with a mask size of 7 x 7	129
Figure 5-9b	First derivative with respect to y-axis of the sphere filtered with a mask size of 7 x 7	130
Figure 5-9c	Second derivative with respect to x-axis of the sphere filtered filtered with a mask size of 7 x 7	131
Figure 5-9d	Second derivative with respect to y-axis of the sphere filtered filtered with a mask size of 7 x 7	132
Figure 5-10	Sign plot for the original range image of the sphere	134
Figure 5-11	Sign plot for the 3 x 3 filtered image of the sphere	135
Figure 5-12	Sign plot for the 5 x 5 filtered image of the sphere	136
Figure 5-13	Sign plot for the 7 x 7 filtered image of the sphere	137
Figure 5-14	Raw range image of the cylinder with its background	139
Figure 5-15	Raw range image of the cylinder after segmentation	139
Figure 5-16	3 x 3 median filtered image of the raw cylinder	140

Figure 5-17	5 x 5 median filtered image of the raw cylinder	140
Figure 5-18a	First derivative with respect to x-axis of the cylinder raw image	141
Figure 5-18b	First derivative with respect to y-axis of the cylinder raw image	142
Figure 5-18c	Second derivative with respect to x-axis of the cylinder raw image	143
Figure 5-18d	Second derivative with respect to y-axis of the cylinder raw image	144
Figure 5-19a	First derivative with respect to x-axis of the cylinder filtered with a mask size of 3 x 3	145
Figure 5-19b	First derivative with respect to y-axis of the cylinder filtered with a mask size of 3 x 3	146
Figure 5-19c	Second derivative with respect to x-axis of the cylinder filtered with a mask size of 3 x 3	147
Figure 5-19d	Second derivative with respect to y-axis of the cylinder filtered with a mask size of 3 x 3	148
Figure 5-20a	First derivative with respect to x-axis of the cylinder filtered with a mask size of 5 x 5	149
Figure 5-20b	First derivative with respect to y-axis of the cylinder filtered with a mask size of 5 x 5	150
Figure 5-20	Second derivative with respect to x-axis of the cylinder filtered with a mask size of 5 x 5	151
Figure 5-20d	Second derivative with respect to y-axis of the cylinder filtered with a mask size of 5 x 5	152

Figure 5-21	Sign plot for the original cylinder	153
Figure 5-22	Sign plot for the 3 x 3 filtered cylinder image	154
Figure 5-23	Sign plot for the 5 x 5 filtered cylinder image	155
Figure 5-24	Best-fit plot for the sphere raw image	157
Figure 5-25	Best-fit plot for the cylinder	158
Figure 6-1	Delta rocket composed of cylindrical and conical shapes	172
Figure 6-2	Conical domes and cylinderlike body make up the space probe	173
Figure 6-3	Cylindrical space station with a half sphere dome top	173

CHAPTER ONE

INTRODUCTION

1.1 Introduction

One of the most important tasks in computer vision is that of three-dimensional object recognition. Success has been limited to the recognition of symmetric objects. Recently, research has concentrated on the recognition of small numbers of asymmetric objects as well as objects placed in complex scenes. Unlike the recognition procedure developed for intensity-based images, the recent development of active and passive sensors extracting quality range information has led to the involvement of explicit geometric representations of the objects for the recognition schemes [1, 2]. Location and description of three-dimensional objects from natural light images are often difficult to determine. However, range images give a more detailed and direct geometric description of the shape of the three-dimensional object. A brief introduction to range images and the laser range-finder is presented in Section 1.2. In Section 1.3, a precise global definition of the object recognition problem is discussed. The objective of this dissertation and its relevance to the global three-dimensional problem is presented in Section 1.4.

1.2 Range Image and Data Acquisition

Range images share the same format as intensity images, i.e., both of these images are two-dimensional arrays of numbers, the only difference being that the numbers in the range images represent the distances between a sensor focal plane to points in space. The laser range-finder or tracker [3] is currently the most widely used sensor. The laser range-finder makes use of a laser beam which scans the surfaces in

the scene of observation from left to right and top to bottom. Thus the distances obtained measure both depth and scanning angle. The principle of triangulation is utilized to obtain the three-dimensional coordinate of each pixel. Unless a specific algorithm demands a special form of the range images, it is usually this depth information which is utilized for the recognition process. Active triangulation techniques use an extra source of light to project some pattern onto the objects to be measured, thereby reducing complexity of the stereo matching problem [4, 5]. Many industrial and navigational robotic tasks such as target identification and tracking, automated assembly, bin picking, mobile robots, etc., will be better accomplished if such explicit depth information can be efficiently obtained and accurately interpreted.

Modeling human vision is a complex process. To date, machine vision systems can hardly perform a fraction of the capabilities of the human visual system. An efficient mechanism which can acquire relevant information from the three-dimensional world and subsequently form models of the real world will, to some extent, bridge the gap between machine and human capabilities.

1.3 Definition of the Object Recognition Problem

Three-dimensional object recognition is vast problem. In the course of the succeeding text, we will give a somewhat precise definition of this problem.

In the real world, the things human see and feel are primarily solid objects. When people view objects for the first time, they attempt to collect information from various aspects of the object. This process of collecting and forming information about unknown objects is known as model formation [8]. After gaining familiarity with many objects, we are able to identify objects from any arbitrary viewpoint without further investigation.

The human vision system has the capability of analyzing and determining not only the color but also the spatial orientation of objects relative to a fixed coordinate

system. Since we are interested in an automatic, computerized process to recognize objects, the input data we use must be compatible with available digital computers. Hence, two-dimensional matrices of numerical values usually known as digitized sensor data, constitute the information that is processed to describe or recognize three-dimensional objects. The sensor used for this process can be a passive sensor, like a camera, or an active sensor, such as a laser range mapper. Summarizing, the three-dimensional recognition problem constitutes a detailed completion of model formation of the object leading to an in-depth knowledge of its shape and orientation with respect to a fixed view of the real world.

1.4 Objectives and Organization of the Dissertation

An approach based on two-dimensional analytic geometry to recognize a series of three-dimensional objects is presented in this dissertation. Among the various three-dimensional objects considered are the hyperboloids of one and two sheets, ellipsoids, spheres, circular and elliptical quadric cones, circular and elliptical cylinders, parabolic and hyperbolic cylinders, elliptic and hyperbolic paraboloids, and parallelepipeds.

The difficulties in recognizing three-dimensional objects stems from the complexity of the scene, the number of objects in the database and the lack of *a priori* information about the scene. Techniques vary based upon the difficulty of the recognition problem. In our case we attempt to recognize segmented objects in range images.

Location and orientation of three-dimensional objects has always been the most complex issue in many computer vision applications. Algorithms for a robust three-dimensional recognition system must be view-independent. Herein, we have developed a technique to determine the three-dimensional object location and orientation in range images. Once the object lies in a desired stable rest position, our proposed recognition scheme quickly and accurately classifies it as one of the objects mentioned above. In comparison to most of the present day methods utilized for range image object

recognition, our proposed approach attacks the problem in a different manner and is computationally inexpensive.

Chapter Two reviews some of the earlier and current work in this area. It includes a review of some of the mathematical concepts associated with three-dimensional object recognition. A mathematical quadric classification method based on a three-dimensional discriminant is discussed while in this chapter. In chapters Three and Four we discuss, in detail, our proposed three-dimensional approach. Chapter Three addresses the various pre-processings steps involved prior to the application of the recognition algorithm. Median filtering, segmentation, three-dimensional coefficient evaluation, and rotation alignment being some of them. The demerits of existing schemes in the area of three-dimensional object recognition and the uniqueness and improvizations brought about through our recognition procedures are also discussed in Chapter Three. In Chapter Four, after a brief discussion of the practical merits of using planar intersections, characteristic feature vectors are obtained for each of the quadric surfaces under investigation. Results are summarized in Chapter Five. A large set of real range images of spheres, cylinders, and cones were utilized to test the proposed recognition scheme. Results obtained for simulated data of other quadric surfaces, namely, hyperboloids and paraboloids are also tabulated in Chapter Five. Chapter Six concludes with a discussion of possible areas for future investigation.

CHAPTER TWO

BACKGROUND

2.1 Introduction

Past and present research in the field of three-dimensional object recognition is reviewed in Section 2.2. Surface curvatures which are widely utilized in this research area are briefly reviewed in Section 2.3. Section 2.4 investigates a three-dimensional approach to classification and reduction of quadrics as presented by Olmstead [24], wherein various invariant features of the quadratic form under translation and rotation are discussed.

2.2 Literature Review

Many of the currently available techniques for describing and recognizing three-dimensional objects are based on the principle of segmentation. Segmentation is the process in which range data is divided into smaller regions (mostly squares) [4]. These small regions are approximated as planar surfaces or curved surfaces based upon the surface mean and Gaussian curvatures. Regions sharing similar curvatures are subsequently merged. This process is known as region growing. Other approaches [6-10] characterize the surface shapes while dealing with the three-dimensional recognition problem. Levine et al. [11] briefly review various works in the field of segmentation, where segmentation has been classified into region-based and edge-based approaches. Again surface curvatures play an important role for characterization in each of these approaches.

Grimson et al. [12] discuss a scheme utilizing local measurements of three-dimensional positions and surface normals to identify and locate objects from a known

set. Objects are modeled as polyhedra with a set number of degrees of freedom with respect to the sensors. The authors claim a low computational cost for their algorithm. Although they have limited the experiments to one model, i.e., data obtained from one object, they claim that the algorithm can be used for multiple object models. Also, only polyhedral objects with a sufficient number of planar surfaces can be used in their scheme.

Another paper by Faugeras et al. [13] describes surfaces by curves and patches which are further represented using linear parameters such as points, lines and planes. Their algorithm initially reconstructs objects from range data and consequently utilizes certain constraints of rigidity to recognize objects while positioning. They arrive at the conclusion that for an object to be recognized, at least a certain area of the object should be visible (approx. 50%). They claim their approach could be used for images obtained using ultrasound, stereo, and tactile sensors.

Hu and Stockman [14] have employed structured light as a technique for three-dimensional surface recognition. The objects are illuminated using a controlled light source of a regular pattern, thereby creating artificial features on the surfaces which are consequently extracted. They claim to have solved the problem known as "grid line identification." From the general constraints, a set of geometric and topological rules are obtained which are effectively utilized in the computation of grid labels which are further used for finding three-dimensional surface solutions. Their results infer that consistent surface solutions are obtained very fast with good accuracy using a single image.

Recognition of polyhedral objects involves the projection of several invariant features of three-dimensional bodies onto two-dimensional planes [15]. Recently, recognition of three-dimensional objects based upon their representation as a linear combination of two-dimensional images has been investigated [16]. Transformations such as rotation and translation have been considered for three-dimensional objects in

terms of the linear combination of a series of two-dimensional views of the objects. Instead of using transformations in three-dimensions, it has been shown that the process is the equivalent of obtaining two-dimensional transformations of several two-dimensional images of the objects and combining them together to obtain the three-dimensional transformation. This procedure appears computationally intensive.

Most of the techniques and algorithms mentioned above have a common criterion for classifying the three-dimensional objects in the final phase. They have a database of all the objects they are trying to recognize and hence try to match features from the test samples to the features of the objects in the database.

Fan et al. [17] use graph theory for decomposing segmentations into subgroups corresponding to different objects. Matching of the test objects with the objects in the database is performed in three steps: the screener, which makes an initial guess for each object; the graph matcher, which conducts an exhaustive comparison between potential matching graphs and computes three-dimensional transformation between them; and finally, the analyzer, which based upon the results from the earlier two modules conducts a split and merge of the object graphs. The distinguishing aspect of this scheme is that the authors used occluded objects for describing their proposed method.

As has been mentioned, most of the present research on three-dimensional objects utilize range imagery rather than stereo images. But at the same time, it should be noted that it was stereo imagery which, to a large extent, was initially used to investigate the problem of three-dimensional object recognition.

Forsyth et al. [18] use stereo images to obtain a range of invariant descriptors in three-dimensional model-based vision. Initially, they demonstrate a model-based vision system that recognizes curved plane objects irrespective of the pose. Based upon image data, models are constructed for each object and the pose is computed. However, they mainly describe three-dimensional objects with planar faces.

Lee and Hahn [19] have actually dealt with an optimal sensing strategy. Their main objective is to obtain valuable and effective data or information from three-dimensional objects, which subsequently could be used to describe and recognize natural quadric surfaces. Other works on stereo vision can be found in references 20, 21, 22 and 23.

The visible-invariant surface characteristics mentioned before are the Gaussian curvature (K) and the mean curvature (H), which are referred to collectively as surface curvatures. Mean curvature is an extrinsic surface property, whereas Gaussian curvature is intrinsic. In the following section we briefly describe these two widely used invariant surface characteristics for three-dimensional objects.

2.3 Differential Geometry of Surfaces: Mean and Gaussian Curvatures

Mean and Gaussian curvatures [8] are identified as the local second-order surface characteristics that possess several desirable invariance properties and represent extrinsic and intrinsic surface geometry, respectively. The explicit parametric form of a general surface S in E^3 (three-dimensional Euclidean space) with respect to a known coordinate system is given as

$$S = \left\{ (x(u,v), y(u,v), z(u,v)) : (u,v) \in D \right\}, \quad (2.1)$$

where D is any surface patch and is a subset of E^2 .

However if the depth maps are assumed to be in the form of a graph surface (Monge patch surface) [8], then S can be written as

$$S = \left\{ (x,y,z(x,y)), (x,y) \in D \right\},$$

where $z(x,y)$ is the depth at a point (x,y) in a given range image.

The representations for the Gaussian and the mean curvatures are as follows:

Gaussian curvature, K , is defined by, (2.2)

$$\frac{\partial^2 z}{\partial x^2} \cdot \frac{\partial^2 z}{\partial y^2} - \frac{\left[\frac{\partial^2 z}{\partial x \partial y} \right]^2}{\left\{ 1 + \left(\frac{dz}{dx} \right)^2 + \left(\frac{dz}{dy} \right)^2 \right\}^2}.$$

Mean curvature, H , is defined by, (2.3)

$$\frac{\partial^2 z}{\partial x^2} + \frac{\partial^2 z}{\partial y^2} + \frac{\partial^2 z}{\partial x^2} \cdot \left[\frac{\partial z}{\partial y} \right]^2 + \frac{\frac{\partial^2 z}{\partial y^2} \cdot \left[\frac{\partial z}{\partial x} \right]^2 - 2 \cdot \frac{\partial z}{\partial x} \cdot \frac{\partial z}{\partial y} \cdot \frac{\partial^2 z}{\partial x \partial y}}{2 \left\{ 1 + \left[\frac{\partial z}{\partial x} \right]^2 + \left[\frac{\partial z}{\partial y} \right]^2 \right\}^{3/2}}.$$

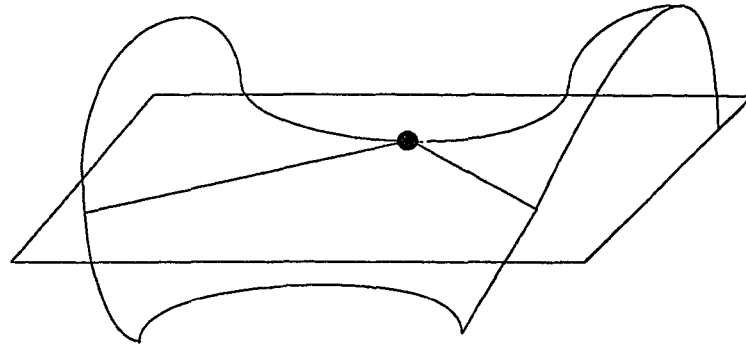
Both of these curvatures are invariant to translation and rotation of the object as long as the object surface is visible.

Based upon the sign of the Gaussian curvature, individual points in the surface are locally classified into three surface types as shown in Figure 2-1:

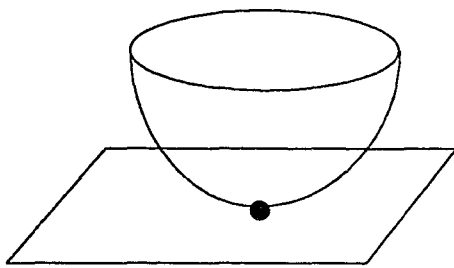
- (a) $K > 0$ implies an elliptic surface point,
- (b) $K < 0$ implies a hyperbolic surface point, and
- (c) $K = 0$ implies a parabolic surface point.

Besl and Jain in their paper [8] have shown that the Gaussian and mean curvatures together can be utilized to give a set of eight different surfaces as shown in Figure 2-2:

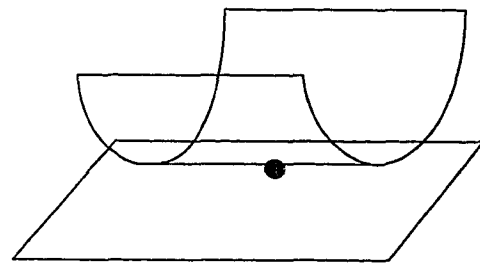
- 1) $H < 0$ and $K > 0$ implies a peak surface.
- 2) $H > 0$ and $K > 0$ implies a pit surface.
- 3) $H < 0$ and $K = 0$ implies a ridge surface.
- 4) $H > 0$ and $K = 0$ implies a valley surface.



(b) Hyperbolic point ($K < 0$)



(a) Elliptic point ($K > 0$)



(c) Parabolic point ($k = 0$)

Figure 2-1. Shape of a surface in the vicinity of an elliptic, hyperbolic, and parabolic point.

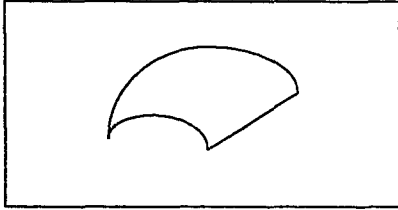
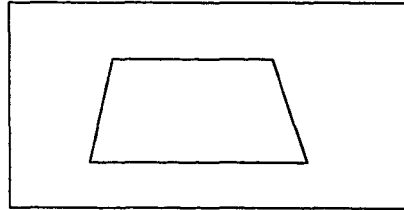
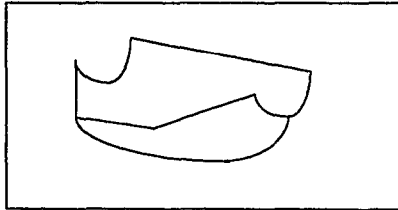
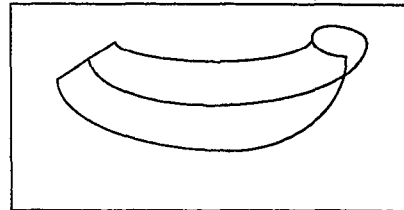
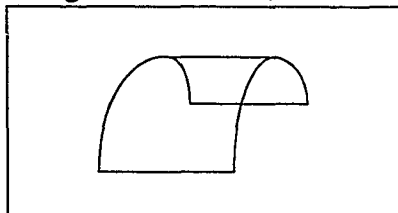
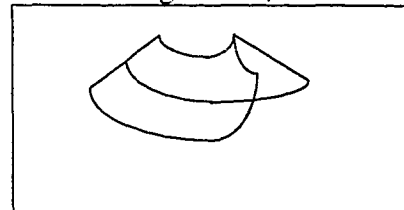
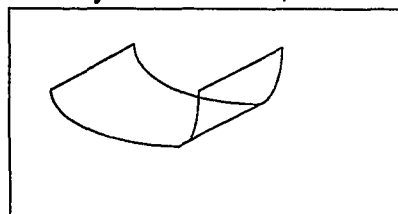
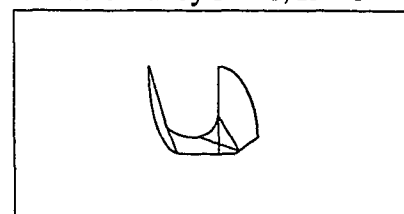
Peak Surface $H < 0, K > 0$ Flat Surface $H = 0, K = 0$ Pit Surface $H > 0, K > 0$ Minimal Surface $H = 0, K < 0$ Ridge Surface $H < 0, K = 0$ Saddle Ridge $H < 0, K < 0$ Valley Surface $H > 0, K = 0$ Saddle Valley $H > 0, K < 0$ 

Figure 2-2. A set of eight view-independent surface types for a visible surface.

- 5) $H = 0$ and $K = 0$ implies a flat surface.
- 6) $H = 0$ and $K < 0$ implies a minimal surface.
- 7) $H < 0$ and $K < 0$ implies a saddle ridge surface.
- 8) $H > 0$ and $K < 0$ implies a saddle valley surface.

2.4 Three-Dimensional Discriminant

In this section we investigate a three-dimensional approach to classification and reduction of quadrics as presented by Olmstead [24], which looks into the invariants of the quadratic form under translation and rotation of three-dimensional objects.

The general quadric surface of second degree in the three variables x , y , and z can be written in the form

$$F(x,y,z) = ax^2 + by^2 + cz^2 + 2fyz + 2gzx + 2hxy + 2px + 2qy + 2rz + d = 0$$

Associated with $F(x,y,z)$ are two matrices: e and \mathbf{E} , where

$$e = \begin{bmatrix} a & h & g \\ h & b & f \\ g & f & c \end{bmatrix}$$

and

$$\mathbf{E} = \begin{bmatrix} a & h & g & p \\ h & b & f & q \\ g & f & c & r \\ p & q & r & d \end{bmatrix}.$$

Let the determinant of \mathbf{E} be denoted by Δ , and the determinant of e be denoted by D . Also let the cofactors of each element of Δ be denoted by the corresponding capital letters. Three-dimensional surfaces are classified as singular or non-singular, based upon \mathbf{E} being singular or non-singular. Examples of non-singular surfaces are ellipsoids, hyperboloids, and paraboloids. The other quadrics are singular.

Let us now consider the two basic transformations, namely translation and rotation, and try to arrive at some invariant features. Consider the two rectangular right-handed coordinate systems as shown in Figure 2-3. Any point in space has two sets of coordinates, one for each set of axes. The problem is to find a relationship between these two sets of coordinates so that one can convert from one coordinate system to the other.

2.4.1 Translation

Inspecting Figure 2-4, we see that the coordinates of O' and P in the xyz system are (x_0, y_0, z_0) and (x, y, z) , respectively, and the coordinates of P in the $x'y'z'$ system are (x', y', z') . The two sets of coordinates of P are related by the following translation equations:

$$x = x' + x_0. \quad (2.4)$$

$$y = y' + y_0. \quad (2.5)$$

$$z = z' + z_0. \quad (2.6)$$

The set of equations, (2.4), (2.5), and (2.6) relate the coordinates of a point in the $x'y'z'$ system to its coordinates in the xyz system. Direct substitution of equations (2.4) - (2.6) into $F(x, y, z)$ results in the following theorem:

Theorem 2.1. For any quadric surface, the coefficients of the second degree terms, and therefore the matrix e , are invariant under translation.

2.4.2 Rotation

Consider the two rectangular coordinate systems as shown in Figure 2-5. With respect to the $x'y'z'$ system, let the direction cosines of the x , y , and z axes be $(\lambda_1, \nu_1, \nu_1)$, $(\lambda_2, \nu_2, \nu_2)$, and $(\lambda_3, \nu_3, \nu_3)$, respectively. Then with respect to the xyz system, the direction cosines of the x' , y' , and z' axes are $(\lambda_1, \lambda_2, \lambda_3)$, (ν_1, ν_2, ν_3) , and (ν_1, ν_2, ν_3) , respectively.

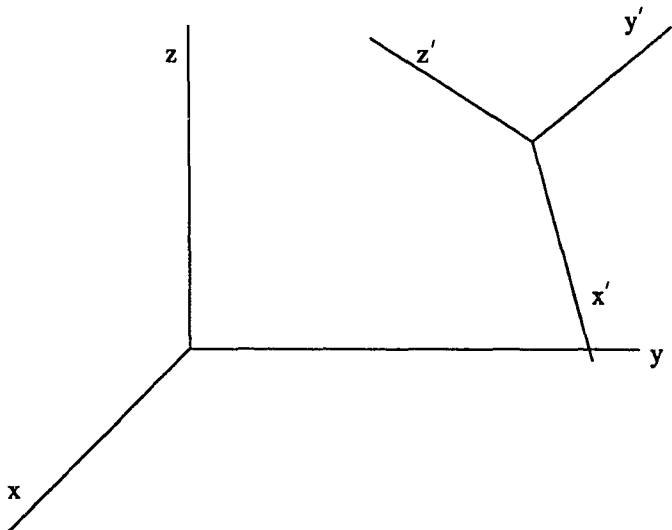


Figure 2-3. Two right-handed rectangular coordinate systems.

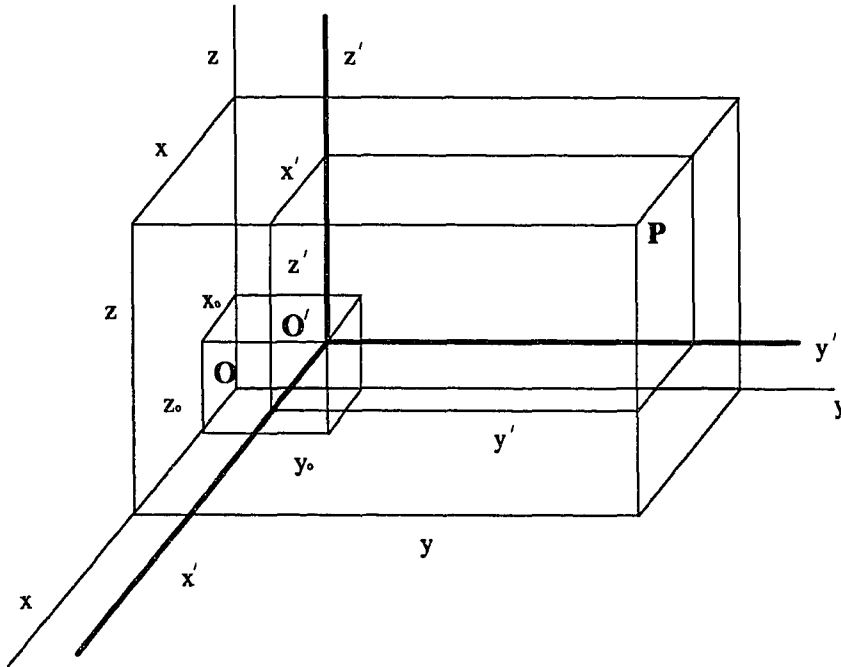


Figure 2-4. Relation between the coordinates of P upon translation.

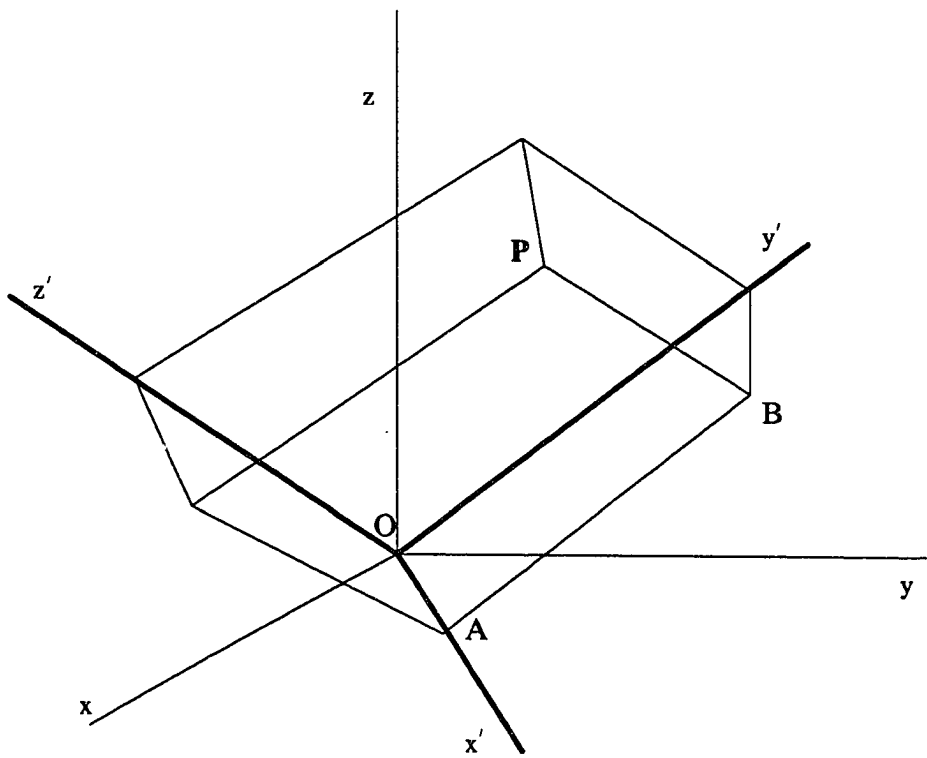


Figure 2-5. Two rectangular coordinate systems having the same origin.

For any point, P, whose coordinates in the two systems are (x,y,z) and (x',y',z') , the following two sets of rotation equations are obtained:

$$\begin{aligned}x &= \lambda_1 x' + \nu_1 y' + \nu_1 z', \\y &= \lambda_2 x' + \nu_2 y' + \nu_2 z', \\z &= \lambda_3 x' + \nu_3 y' + \nu_3 z',\end{aligned}$$

and

$$\begin{aligned}x' &= \lambda_1 x + \lambda_2 y + \lambda_3 z, \\y' &= \nu_1 x + \nu_2 y + \nu_3 z, \\z' &= \nu_1 x + \nu_2 y + \nu_3 z,\end{aligned}$$

which gives rise to the rotation matrix

$$A = \begin{bmatrix} \lambda_1 & \nu_1 & \nu_1 \\ \lambda_2 & \nu_2 & \nu_2 \\ \lambda_3 & \nu_3 & \nu_3 \end{bmatrix}, \quad (2.7)$$

where the elements of the rows (or columns) are direction cosines of perpendicular directions. Direct calculation results in the following theorem:

Theorem 2.2. The determinant D of the rotation matrix A is equal to 1.

Before arriving at a particular set of invariant features of a quadric, we first describe a plane of symmetry of a certain type, called a principal plane.

Definition 2.1 A principal plane is a diametrical plane that is perpendicular to the chord it bisects [24].

Consider the matrix e again:

$$e = \begin{bmatrix} a & h & g \\ h & b & f \\ g & f & c \end{bmatrix}.$$

The eigen-values of the matrix e can be calculated from

$$\begin{vmatrix} a - k & h & g \\ h & b - k & f \\ g & f & c - k \end{vmatrix} = 0.$$

This cubic equation in k is called the characteristic equation of the matrix e . Its roots are called the characteristic roots of e . The quantities given below are found to be invariant as a consequence of the following theorem [25].

Theorem 2.3 If the second degree equation $F(x,y,z)=0$ is transformed by means of a translation or a rotation with fixed origin, the following quantities are invariant:

$D, \Delta, \rho_3, \rho_4, I, J, k_1, k_2,$ and k_3 , where D, Δ are the determinants of the matrices e and E , respectively; and ρ_3 and ρ_4 are the ranks of the matrices e and E , respectively. Also

$$I = a + b + c,$$

$$J = ab + ac + bc - f^2 - g^2 - h^2,$$

and finally $k_1, k_2,$ and k_3 are the characteristic roots of e .

Based upon the above set of invariants, surface classifications are listed in Table 2-1.

In Chapters Three and Four, we discuss our proposed recognition scheme in detail.

Number	Surface	ρ_3	ρ_4	Sign of Δ	k's same sign
1	Real ellipsoid	3	4	-	yes
2	Hyperboloid of one sheet	3	4	+	no
3	Hyperboloid of two sheets	3	4	-	no
4	Real quadric cone	3	3		no
5	Elliptic paraboloid	2	4	-	yes
6	Hyperbolic paraboloid	2	4	+	no
7	Real elliptic cylinder	2	3		yes
8	Hyperbolic cylinder	2	3		no
9	Parabolic cylinder	1	3		

Table 2-1. Surface classification using the three-dimensional discriminant approach. ρ_3 is the rank of matrix e and ρ_4 is the rank of matrix E . The characteristic roots of the matrix e are referred by k's.

CHAPTER THREE

QUADRIC SURFACE REPRESENTATION

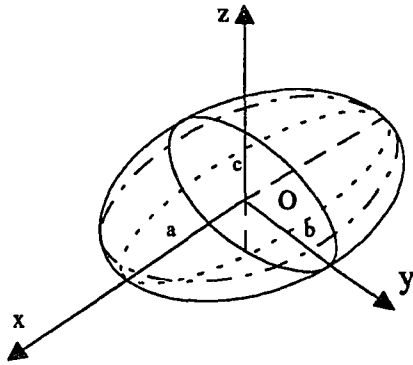
3.1 Introduction

Section 3.2 considers the various three-dimensional quadric surfaces used in the recognition process. While describing each of these objects, we will be considering the surfaces with their centers aligned to the origin of our coordinate system. Section 3.3 explains our quadric recognition algorithm in detail. This section also addresses the acquisition of range data and the necessary pre-processing steps, the representation of quadric surfaces by a second degree polynomial, and the rotation alignment algorithm whereby each of the quadric surfaces are placed in a coordinate system of our choice. The merits of the proposed technique are addressed while considering the improvizations brought about in the recognition of three-dimensional objects (especially quadrics) in Section 3.4.

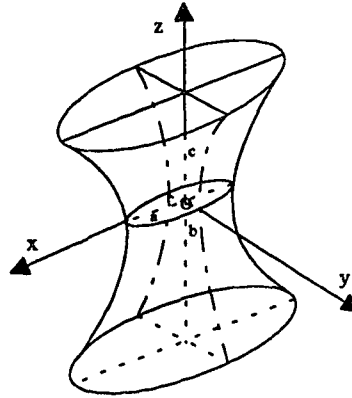
3.2 Quadric Surface Description

In this section by means of Figures 3-1, 3-2, and 3-3, we illustrate and represent the following three-dimensional quadric surfaces which are considered for the recognition process: ellipsoids, the hyperboloids of one and two sheets, quadric cones, elliptic paraboloids, hyperbolic paraboloids, elliptic cylinders, hyperbolic cylinders, parabolic cylinders, and parallelepipeds.

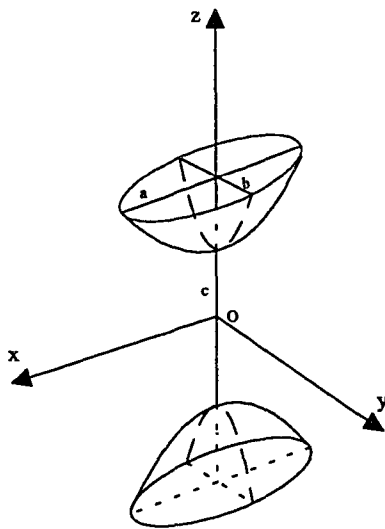
Most three-dimensional objects of practical use consist of at least one of the surfaces described above. All the representations of surfaces which were described above hold true under ideal conditions, i.e., when the source data is perfect, exact pose and orientation of the objects are known, the system is noiseless, etc. However in the real



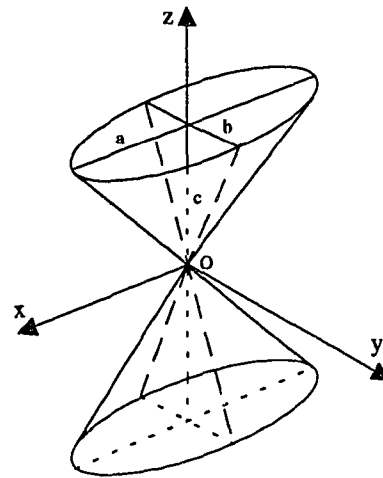
Real Ellipsoid: $\frac{x^2}{a^2} + \frac{y^2}{b^2} + \frac{z^2}{c^2} = 1$



Hyperboloid of one sheet: $\frac{x^2}{a^2} + \frac{y^2}{b^2} - \frac{z^2}{c^2} = -1$

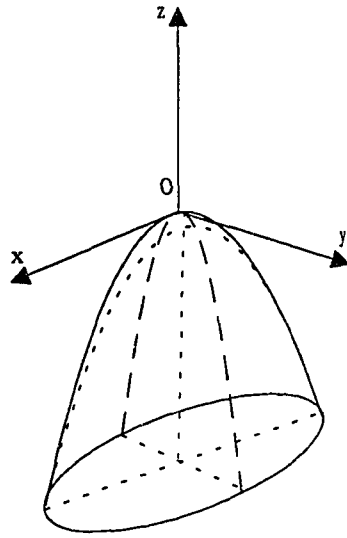


Hyperboloid of two sheets: $\frac{x^2}{a^2} + \frac{y^2}{b^2} - \frac{z^2}{c^2} = -1$

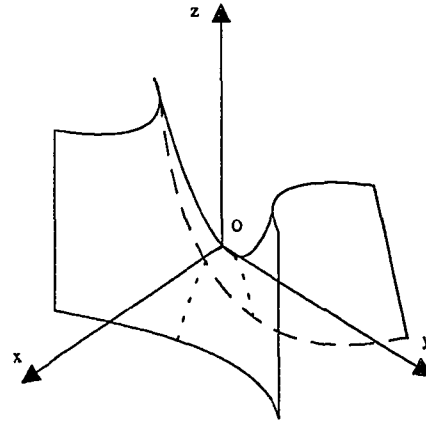


Real quadric cone: $\frac{x^2}{a^2} + \frac{y^2}{b^2} - \frac{z^2}{c^2} = 0$

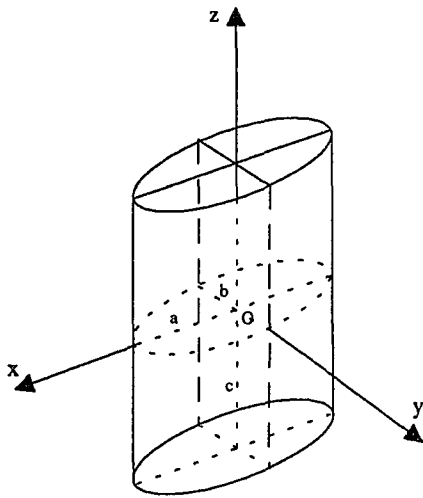
Figure 3-1. Quadric representations of Real ellipsoid, Hyperboloid of one sheet, Hyperboloid of two sheets, and real quadric cone.



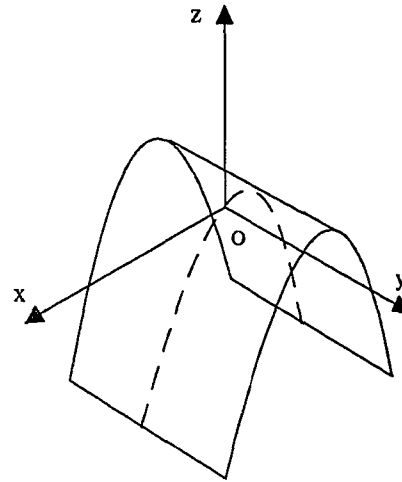
Elliptic paraboloid: $\frac{x^2}{a^2} + \frac{y^2}{b^2} + 2z = 0$



Hyperbolic paraboloid: $\frac{x^2}{a^2} - \frac{y^2}{b^2} + 2z = 0$

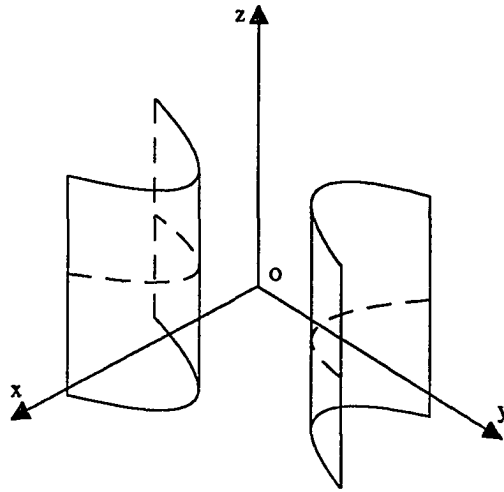


Elliptic cylinder: $\frac{x^2}{a^2} + \frac{y^2}{b^2} = 1$

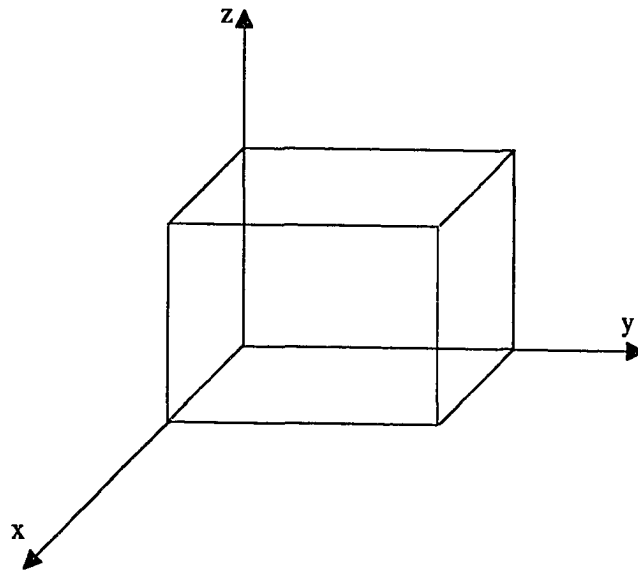


Parabolic cylinder: $x^2 + 2rz = 0$

Figure 3-2. Quadric representations of Elliptic paraboloid, Hyperbolic paraboloid, Elliptic cylinder, and Parabolic cylinder.



Hyperbolic cylinder: $\frac{x}{a^2} - \frac{y^2}{b^2} = -1$



Parallelepiped

Figure 3-3. Quadric representations of Hyperbolic cylinder and Parallelepiped.

world, practically none of these conditions hold true. Any set of data, whether it is derived or generated from a passive (camera) or an active sensor (laser range mapper), can at best be approximated to a second-degree polynomial. Whether this polynomial accurately represents a surface or not, and if so, how these coefficients (representation) can be chosen to come close to recognizing a three-dimensional object, is the whole issue of the recognition problem.

In the next few sections, while formulating our recognition scheme, we describe one such technique which generates ten coefficients (which are sufficient under ideal conditions) to describe all the objects of interest [26].

However, before elaborating on the recognition scheme, an overview of the technique is presented. The recognition scheme utilizes a two-dimensional discriminant (which is a measure for distinguishing two-dimensional curves) to recognize three-dimensional surfaces. Instead of utilizing the ten generated coefficients and attempting to recognize the surface from its quadric representation, the quadrics are identified using the information resulting from the intersection of the surface with different planes. If the surface is one of those listed above, there are five possible two-dimensional curves that may result from such intersections, (i) a circle, (ii) an ellipse, (iii) a parabola, (iv) a hyperbola, and (v) a line. Thus, a feature or pattern vector with five independent components can be formed for characterizing each of the surfaces.

3.3 Recognition Scheme

Our recognition scheme consists of the following steps:

- (1) acquisition of the range data and conducting the pre-processing steps,
- (2) description and representation of objects as general second degree surfaces,
- (3) determination of the location and orientation of the objects with respect to a desired coordinate system,

- (4) performance of the rotation and translation transformations of the object so as to place it in a stable desired coordinate system,
- (5) use of the principle of two-dimensional discriminants to classify the various curves obtained by intersecting the surfaces with planes, and
- (6) acquisition of an optimal set of planes sufficient enough to distinguish and recognize each of the quadric surfaces. Angular bounds within which every surface yields a distinct set of curves are determined in step 6.

The range data, as mentioned in Chapter One, is a pixel-by-pixel depth value from the point of origin of the laser to the point where the beam impinges on a surface. The objects are scanned from left-to-right and top-to-bottom. A grid frame may consist of 256 x 256 pixels. Before this range data is applied to the object classifier, it has to undergo the following pre-processing steps:

- a) median filtering, and
- b) segmentation.

3.3.1 Median Filtering

Conventionally, a rectangular window of size $M \times N$ is used in two dimensional median filtering. As in our case [27], experiments were performed with square windows of mask sizes 3×3 and 5×5 . Salt and pepper noise in the range images used in this research was uniformly distributed throughout. Irrespective of the mask size, the range information at every pixel in the image is replaced by the median of the pixels contained in the $M \times M$ window centered at that point. Referring to Figure 3-4 and keeping in mind that the black pixels correspond to the background and the white pixels to the object, black pixels inside the object are referred to as pepper noise and white pixels in the black background are referred to as salt noise. Figure 3-5 is obtained as a result of a 3×3 mask being moved over the entire image. The image looks as sharp as the original image though some of the noise still exists. A 5×5 and

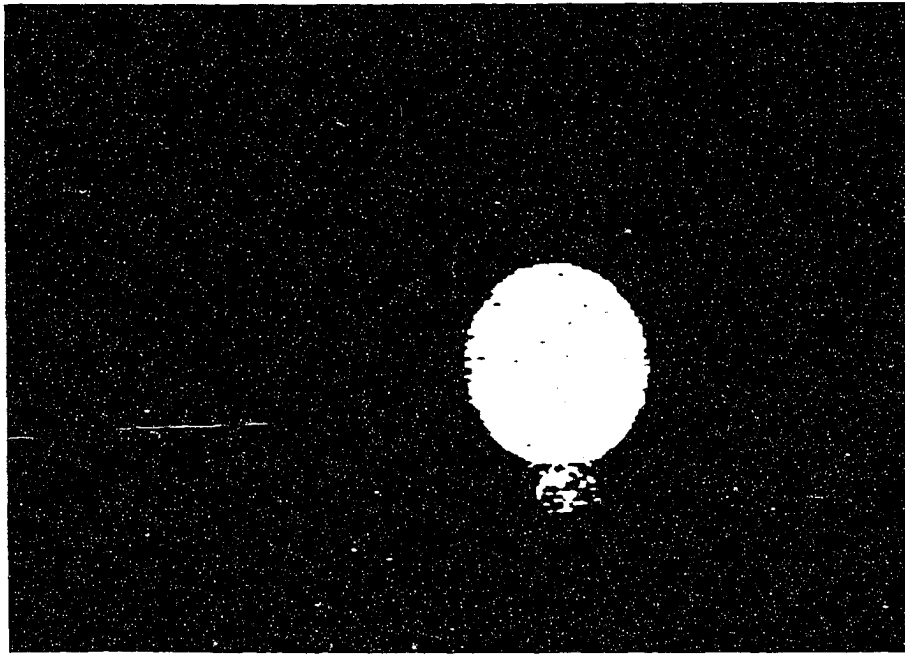


Figure 3-4. Raw range image of the sphere.

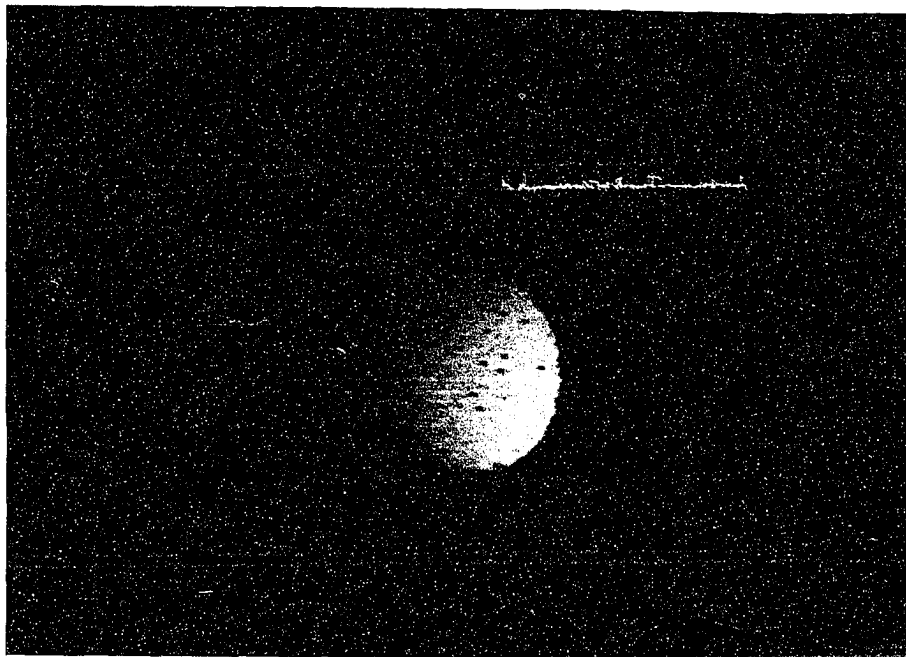


Figure 3-5. 3 x 3 median filtered image of the raw sphere.

a 7 x 7 mask removes all of the visual salt and pepper noise, but the images as seen in Figures 3-6 and 3-7 respectively, to some extent, have lower contrast than the original image.

Once a range image is filtered using a median filter of different masks, the next concern is to study the changes to the original data which have been brought about by filtering. Evaluating curvatures is one good way of distinguishing similarities and dissimilarities among the filtered images and the original range data.

First and second order derivatives are evaluated along the x and y axes to check the uniformity of the original and the filtered images. Approximating, the first-order derivative for a pixel $(A_{i,j})$ centered at i,j is given as:

$$\frac{\partial A}{\partial x} \approx \frac{1}{2\varepsilon} [(A_{i+1,j+1} - A_{i,j+1}) + (A_{i+1,j} - A_{i,j})]$$

and

$$\frac{\partial A}{\partial y} \approx \frac{1}{2\varepsilon} [(A_{i+1,j+1} - A_{i+1,j}) + (A_{i,j+1} - A_{i,j})].$$

Similarly approximating, the second order derivatives for a pixel centered at $A_{i,j}$ is given as:

$$\frac{\partial^2 A}{\partial x^2} \approx \frac{1}{\varepsilon^2} [A_{i-1,j} - 2A_{i,j} + A_{i+1,j}]$$

and

$$\frac{\partial^2 A}{\partial y^2} \approx \frac{1}{\varepsilon^2} [A_{i,j-1} - 2A_{i,j} + A_{i,j+1}],$$

where ε represents the spacing between picture cell centers.

A sign map, which shows the relationships among two neighboring pixels with respect to the depth value, was also generated to check the effect of median filtering on the original data. Sign maps of some of the experimented quadric surfaces are illustrated in Chapter Five.

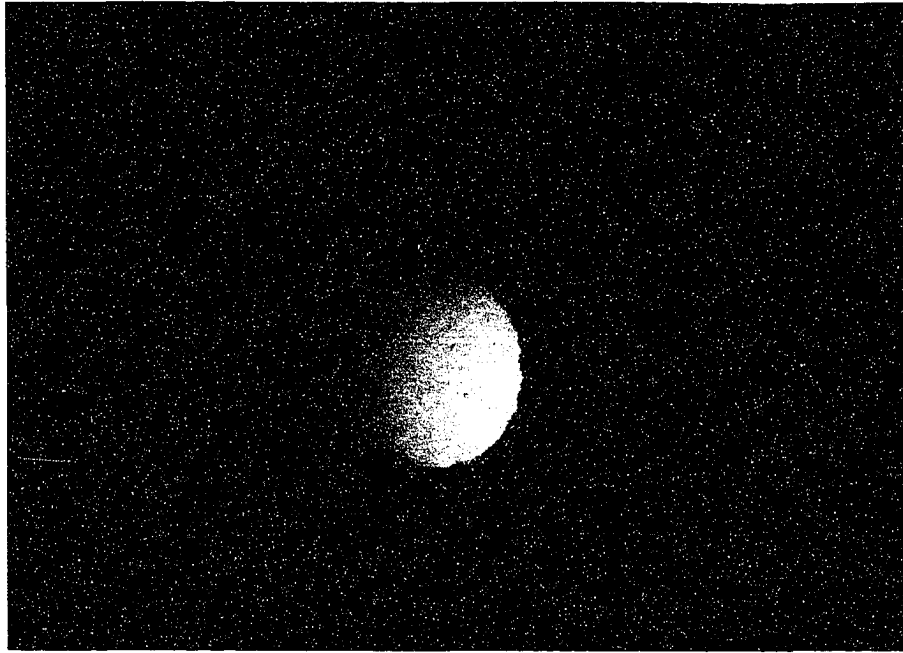


Figure 3-6. 5 x 5 median filtered image of the raw sphere.

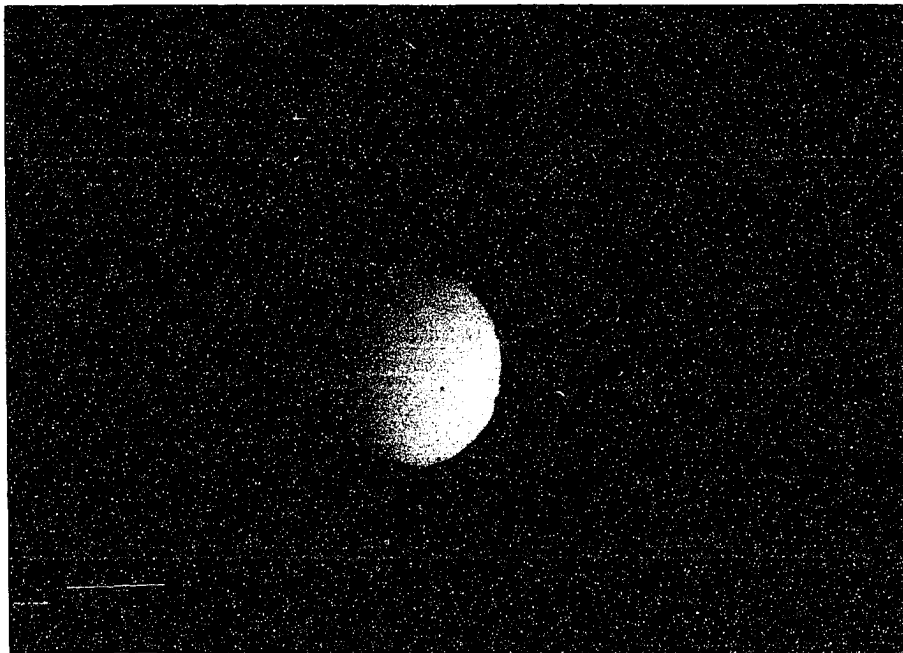


Figure 3-7. 7 x 7 median filtered image of the raw sphere.

3.3.2 Segmentation

Since isolated objects instead of complex scenes are considered, a simple thresholding whereby the object is separated from the background is utilized for the segmentation process. In the case where objects are irregular or a scene consists of a cluster of objects, Gaussian and mean curvatures have to be utilized to sub-divide the scene into planar or curved surfaces. Each surface is then recognized separately. Range image segmentation has been extensively studied by Levine et al. [9].

Now that the available range data has been processed to eliminate salt and pepper noise, we can now utilize the image data to obtain the quadric surface which best fits the data. To achieve this goal, we need to determine the coefficients of a second degree polynomial representation for the three-dimensional surface.

3.3.3 Three-Dimensional Coefficients Evaluation

Our objective is to obtain a surface described by Equation (3.1) from a given set of data (range) points. We assume that the data is a set of range-image samples obtained from a single surface which can be described by a quadric equation.

$$F(x,y,z) = ax^2 + by^2 + cz^2 + 2fyz + 2gzx + 2hxy + 2px + 2qy + 2rz + d = 0. \quad (3.1)$$

We shall therefore define the best description to be the one which minimizes the mean-squared error (MSE) between the range data and the quadric [26].

Equation (3.1) in vector notation becomes

$$F(x,y,z) = \mathbf{a}^T \mathbf{p} = 0, \quad (3.2)$$

where $\mathbf{a}^T = [a \ b \ c \ 2f \ 2g \ 2h \ 2p \ 2q \ 2r \ d]$ and $\mathbf{p}^T = [x^2 \ y^2 \ z^2 \ yz \ zx \ xy \ x \ y \ z \ 1]$.

The error measure for any data point (x,y,z) can be measured by evaluating $F(x,y,z)$. If this point lies exactly on the surface then, $F(x,y,z) = 0$, meaning that the error is zero.

The mean-squared error, E , is defined as

$$E = \min_{\mathbf{a}} \sum_S \|F\|_2. \quad (3.3)$$

In vector notation, Equation (3.3) becomes

$$E = \min_{\mathbf{a}} \sum_S \mathbf{a}^T \mathbf{p} \mathbf{p}^T \mathbf{a} = \min_{\mathbf{a}} \mathbf{a}^T \mathbf{R} \mathbf{a}, \quad (3.4)$$

where \mathbf{R} is the scatter matrix for the data set equal to

$$\mathbf{R} = \sum_S \mathbf{p} \mathbf{p}^T. \quad (3.5)$$

Minimizing E leads to a trivial solution of $\mathbf{a} = 0$, implying all the coefficients are zero.

We therefore attempt to find the minimum of $\mathbf{a}^T \mathbf{R} \mathbf{a}$ with respect to \mathbf{a} , subject to some constraint $K(\mathbf{a}) = k$.

Let

$$G(\mathbf{a}) = \mathbf{a}^T \mathbf{R} \mathbf{a} \quad (3.6)$$

and

$$K(\mathbf{a}) = \mathbf{a}^T \mathbf{K} \mathbf{a}, \quad (3.7)$$

where \mathbf{K} is another undetermined constant matrix. Using Lagrange's method [28], we write the function

$$U = G(\mathbf{a}) - \lambda K(\mathbf{a}), \quad (3.8)$$

where λ again is an undetermined constant. To find a minimum solution for U , we form

$$\frac{\partial U}{\partial \mathbf{a}} = 2(\mathbf{R} - \lambda \mathbf{K}) \mathbf{a} = 0. \quad (3.9)$$

Solving $\frac{\partial U}{\partial \mathbf{a}} = 0$ and $K(\mathbf{a}) = k$ simultaneously, we find \mathbf{a} and λ to give a minimum solution. We wish to evaluate the constraint $K(\mathbf{a})$ such that it gives a non-zero solution for \mathbf{a} for all the quadric surfaces of interest.

In order to determine the function of the coefficient vector \mathbf{a} which is invariant to translation and rotation, we write the quadric equation as

$$F(x,y,z) = F(\mathbf{v}) = \mathbf{v}^t \mathbf{D} \mathbf{v} + 2\mathbf{v}^t \mathbf{q} + d = 0, \quad (3.10)$$

where

$$\mathbf{v} = \begin{bmatrix} x \\ y \\ z \end{bmatrix}, \quad (3.11)$$

$$\mathbf{D} = \begin{bmatrix} a & h & g \\ h & b & f \\ g & f & c \end{bmatrix} \quad (3.12)$$

and

$$\mathbf{q} = \begin{bmatrix} p \\ q \\ r \end{bmatrix}. \quad (3.13)$$

After carrying out the transformations, translation and rotation, it is observed that the second-order terms and the eigen-values are the only invariants of \mathbf{D} under translation and rotation, respectively.

We now derive a function of the eigen-values of \mathbf{D} , i.e., $f(\lambda)$, which will allow us to obtain all of the quadrics of interest. The constraint should be in a quadratic form, such that when we substitute it in

$$\frac{\partial u}{\partial \mathbf{a}} = 2(\mathbf{R} - \lambda \mathbf{K})\mathbf{a} = 0, \quad (3.14)$$

we get a linear equation from which we can solve for \mathbf{a} .

From reference 29, a good choice for the constraint $f(\lambda)$ is

$$f(\lambda) = \sum_i \lambda_i^2 = 1, \quad (3.15)$$

i.e.,

$$\sum \lambda_i^2 = \text{tr}(D^2) = a^2 + b^2 + c^2 + 2f^2 + 2g^2 + 2h^2. \quad (3.16)$$

Writing it in the form of equation $K(a) = \mathbf{a}^T K \mathbf{a}$:

$$\text{tr}(D^2) = \mathbf{a}^T \begin{bmatrix} K_2 & 0 \\ 0 & 0 \end{bmatrix} \mathbf{a}, \quad (3.17)$$

where the constraint matrix K_2 is

$$K_2 = \begin{bmatrix} 1 & 0 & 0 & 0 & 0 & 0 \\ 0 & 1 & 0 & 0 & 0 & 0 \\ 0 & 0 & 1 & 0 & 0 & 0 \\ 0 & 0 & 0 & 1/2 & 0 & 0 \\ 0 & 0 & 0 & 0 & 1/2 & 0 \\ 0 & 0 & 0 & 0 & 0 & 1/2 \end{bmatrix}. \quad (3.18)$$

Equation $R\mathbf{a} = \lambda K\mathbf{a}$, can now be written as

$$\begin{bmatrix} C & B \\ B^T & A \end{bmatrix} \begin{bmatrix} \beta \\ \alpha \end{bmatrix} = \lambda \begin{bmatrix} K_2 & 0 \\ 0 & 0 \end{bmatrix} \begin{bmatrix} \beta \\ \alpha \end{bmatrix}, \quad (3.19)$$

where C is the 6×6 scatter matrix for the quadratic terms a , b , and c ; B is the 6×4 scatter matrix for the mixed terms $2f$, $2g$, and $2h$ and A is the 4×4 scatter matrix for the linear and constant term, i.e., $2p$, $2q$, $2r$, and d . β is the 6×1 vector of the quadratic coefficients and α is the 4×1 vector of the linear and the constant coefficients.

Solving Equation (3.19), we get

$$C\beta + B\alpha = \lambda K_2\beta \quad (3.20)$$

and

$$B^T\beta + A\alpha = 0. \quad (3.21)$$

From Equation (3.21) we get

$$\alpha = -A^{-1}B^T\beta. \quad (3.22)$$

Substituting α in Equation (3.20), we have

$$(C - BA^{-1}B^T)\beta = \lambda K_2\beta. \quad (3.23)$$

Labeling $(C - BA^{-1}B^T)$ as M , we have

$$M\beta = \lambda K_2\beta, \quad (3.24)$$

which appears similar to an eigen-value problem. Writing K_2 as H^2 , where,

$$H = \begin{bmatrix} 1 & 0 & 0 & 0 & 0 & 0 \\ 0 & 1 & 0 & 0 & 0 & 0 \\ 0 & 0 & 1 & 0 & 0 & 0 \\ 0 & 0 & 0 & 1/\sqrt{2} & 0 & 0 \\ 0 & 0 & 0 & 0 & 1/\sqrt{2} & 0 \\ 0 & 0 & 0 & 0 & 0 & 1/\sqrt{2} \end{bmatrix}, \quad (3.25)$$

$$H^{-1} = \begin{bmatrix} 1 & 0 & 0 & 0 & 0 & 0 \\ 0 & 1 & 0 & 0 & 0 & 0 \\ 0 & 0 & 1 & 0 & 0 & 0 \\ 0 & 0 & 0 & \sqrt{2} & 0 & 0 \\ 0 & 0 & 0 & 0 & \sqrt{2} & 0 \\ 0 & 0 & 0 & 0 & 0 & \sqrt{2} \end{bmatrix}. \quad (3.26)$$

We can write $M\beta = \lambda K_2\beta$ as $M\beta = \lambda H H\beta$, or $H^{-1}M H^{-1}H\beta = \lambda H\beta$.

Let $\beta' = H\beta$ and $M' = H^{-1}M H^{-1}$, where M' is a real symmetric matrix, then

$$M'\beta' = \lambda\beta'. \quad (3.27)$$

M' has six λ_i 's and six corresponding B_i 's.

For the minimum error solution, we choose the eigen-vector corresponding to the smallest eigen-value, i.e.,

$$\beta_i = H^{-1}B'_i. \quad (3.28)$$

Solving for $\alpha_i = -A^{-1}B^TB_i$, we have our solution.

Once the procedure described in Section 3.3.3 has been performed, the median filtered range data can be described as

$$F(x,y,z) = ax^2 + by^2 + cz^2 + 2fyz + 2gzx + 2hxy + 2px + 2qy + 2rz + d = 0, \quad (3.29)$$

where the values of the coefficients $a, b, c, f, g, h, p, q, r$, and d are known. Generally speaking, all of the objects in the experiments generate all ten coefficients as is shown in Chapter Five. The question now is: How can we distinguish one object from the another and how accurately can we describe the recognized object? In the following sections of this chapter and Chapter Four, we describe the necessary scheme to solve the recognition problem of quadric surfaces.

3.3.4 Evaluation of the Rotation Matrix

The determination of the location and orientation of a three-dimensional object is one of the central problems in computer vision applications. It is observed that most of the methods and techniques which try to solve this problem require considerable pre-processing such as detecting edges or junctions, fitting curves or surfaces to segmented images and computing high order features from the input images. Since three-dimensional object recognition depends not only on the shape of the object but also the pose and orientation of the object as well, any definite information about the object's orientation will aid in selecting the right features for the recognition process.

In this research we suggest a method based on analytic geometry, whereby all the rotation parameters of any object placed in any orientation in space are determined and

eliminated systematically. With this approach we are in a position to place the three-dimensional object in a desired stable position, thereby eliminating the orientation problem. We can then utilize the shape information to explicitly represent the three-dimensional surface.

Any quadric surface can be represented by Equation (3.29) in terms of a second degree polynomial of variables x , y , and z .

Let (x,y,z) describe the coordinates of any point in our coordinate system. As shown in Figure 3-8(b), consider a rotation of angle α about the z axis, i.e. in the xy -plane. Then the new coordinates in terms of the old are represented as

$$x = x'\cos\alpha + y'\sin\alpha$$

and

$$y = -x'\sin\alpha + y'\cos\alpha;$$

i.e., the rotation matrix is

$$R_{\alpha} = \begin{bmatrix} \cos\alpha & \sin\alpha & 0 \\ -\sin\alpha & \cos\alpha & 0 \\ 0 & 0 & 1 \end{bmatrix}.$$

Next, as shown in Figure 3-8(c), consider a rotation about the x' axis by an angle β , i.e., in the $y'z$ plane, of the same point. The resultant coordinates and the old coordinates are now related by the following equations:

$$y' = y''\cos\beta + z'\sin\beta$$

and

$$z = -y''\sin\beta + z'\cos\beta,$$

where the rotation matrix is

$$R_{\beta} = \begin{bmatrix} 1 & 0 & 0 \\ 0 & \cos\beta & \sin\beta \\ 0 & -\sin\beta & \cos\beta \end{bmatrix}.$$

Finally as shown in Figure 3-8(d), consider a rotation about the y'' axis by an angle γ , i.e., in the $x'z'$ plane, then

$$z' = z''\cos\gamma + x''\sin\gamma$$

and

$$x' = -z''\sin\gamma + x''\cos\gamma.$$

The rotation matrix for the above transformation is

$$R_{\gamma} = \begin{bmatrix} \cos\gamma & 0 & -\sin\gamma \\ 0 & 1 & 0 \\ \sin\gamma & 0 & \cos\gamma \end{bmatrix}.$$

Observing that

$$\begin{bmatrix} x \\ y \\ z \end{bmatrix} = R_{\alpha}R_{\beta}R_{\gamma}\begin{bmatrix} x'' \\ y'' \\ z'' \end{bmatrix},$$

we obtain the following:

$$x = x''(\cos\alpha\cos\gamma + \sin\alpha\sin\beta\sin\gamma) + y''\sin\alpha\cos\beta + z''(-\sin\gamma\cos\alpha + \cos\gamma\sin\alpha\sin\beta),$$

$$y = x''(-\cos\gamma\sin\alpha + \sin\gamma\sin\beta\cos\alpha) + y''\cos\beta\cos\alpha + z''(\sin\gamma\sin\alpha + \cos\gamma\sin\beta\cos\alpha)$$

and

$$z = x''\sin\gamma\cos\beta - y''\sin\beta + z''\cos\gamma\cos\beta.$$

After substituting the new x , y , and z coordinates into Equation (3.29), we get an entire set of new coefficients for x''^2 , y''^2 , z''^2 , $y''z''$, $x''z''$, $x''y''$, x'' , y'' , and z'' .

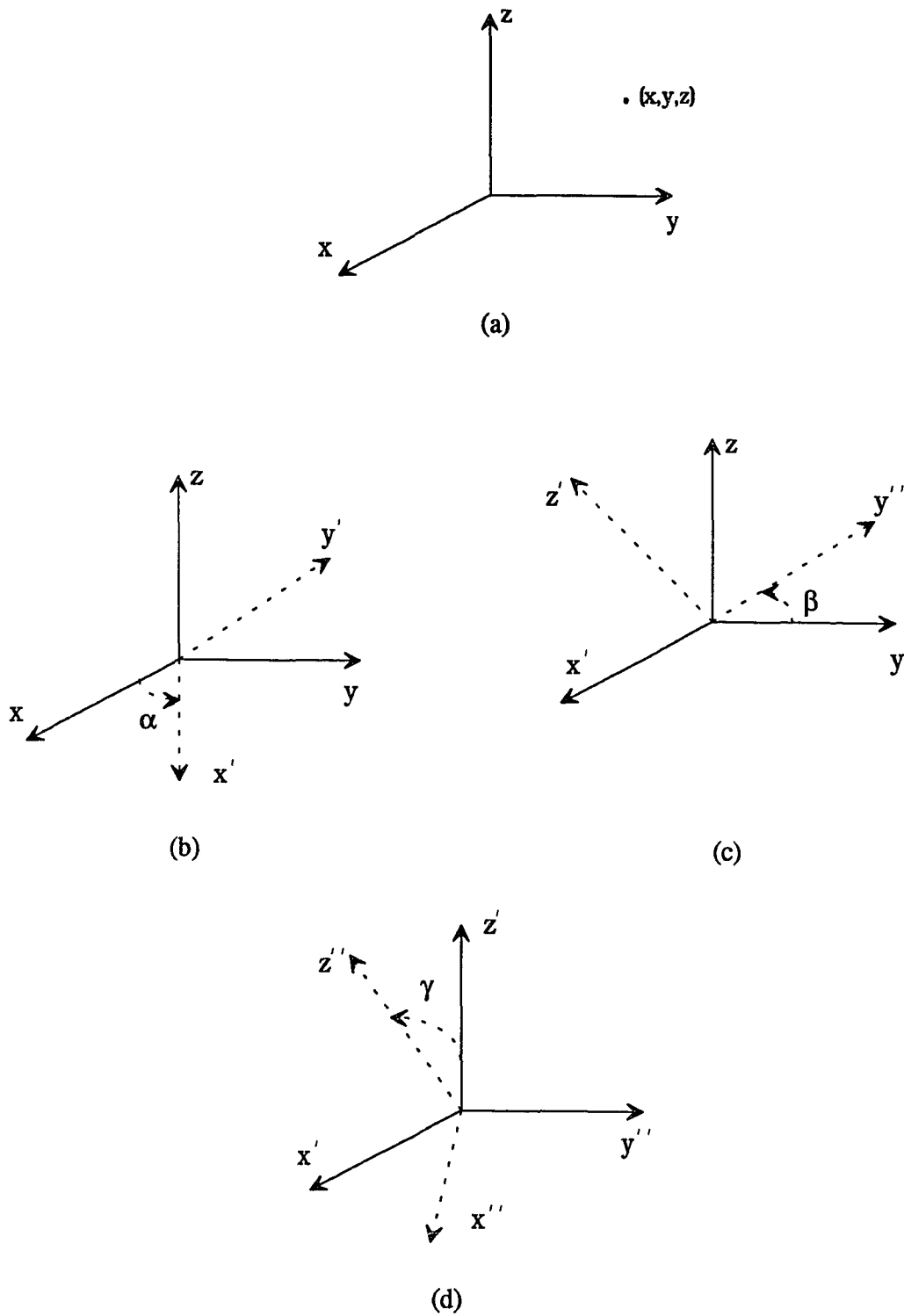


Figure 3-8. Rotation transformation of the coordinate system.

These new coefficients are listed below.

$$\begin{aligned}
 a'' &= \cos^2\gamma [a \cdot \cos^2\alpha + b \cdot \sin^2\alpha] + \sin^2\beta \sin^2\gamma [a \cdot \sin^2\alpha + b \cdot \cos^2\alpha] \\
 &+ 2\sin\alpha \sin\beta \sin\gamma \cos\alpha \cos\gamma (a - b) + c \cdot \sin^2\gamma \cos^2\beta \\
 &+ \sin 2\alpha [h \cdot \sin^2\beta \sin^2\gamma] + \sin 2\gamma [-f \cdot \sin\alpha \cos\beta + g \cdot \cos\alpha \cos\beta \\
 &+ h \cdot \cos^2\alpha \sin\beta - h \cdot \sin\beta \sin^2\alpha] + \sin 2\beta \sin^2\gamma (f \cdot \cos\alpha + g \cdot \sin\alpha) - h \cdot \sin 2\alpha \cos^2\gamma.
 \end{aligned} \tag{3.30}$$

$$\begin{aligned}
 b'' &= (a \cdot \sin^2\alpha + b \cdot \cos^2\alpha) \cos^2\beta + c \cdot \sin^2\beta + \sin 2\beta [-f \cdot \cos\alpha - g \cdot \sin\alpha] \\
 &+ h \cdot \sin 2\alpha \cos^2\beta.
 \end{aligned} \tag{3.31}$$

$$\begin{aligned}
 c'' &= \sin^2\gamma (a \cdot \cos^2\alpha + b \cdot \sin^2\alpha) + (a \cdot \sin^2\alpha + b \cdot \cos^2\alpha) \cos^2\gamma \sin^2\beta \\
 &+ 2\sin\alpha \sin\beta \sin\gamma \cos\alpha \cos\gamma (b - a) + c \cdot \cos^2\gamma \cos^2\beta + \sin 2\alpha [h \cdot \cos^2\gamma \sin^2\beta - h \cdot \sin^2\gamma] \\
 &+ \cos^2\gamma \sin 2\beta [f \cdot \cos\alpha + g \cdot \sin\alpha] + \sin 2\gamma [f \cdot \sin\alpha \cos\beta - g \cdot \cos\alpha \cos\beta - h \cdot \cos 2\alpha \sin\beta].
 \end{aligned} \tag{3.32}$$

$$\begin{aligned}
 2f'' &= \left[(b \cdot \cos^2\alpha + a \cdot \sin^2\alpha + h \cdot \sin 2\alpha - c) \sin 2\beta + (2g \cdot \sin\alpha + 2f \cdot \cos\alpha) \cos 2\beta \right] \cos\gamma \\
 &+ \left[((b - a) \sin 2\alpha - 2h \cdot \cos 2\alpha) \cos\beta + (2g \cdot \cos\alpha - 2f \cdot \sin\alpha) \sin\beta \right] \sin\gamma.
 \end{aligned} \tag{3.33}$$

$$\begin{aligned}
 2g'' &= \sin 2\gamma \left[-\cos^2\alpha (a - b \cdot \sin^2\beta) - \sin^2\alpha (-a \cdot \sin^2\beta + b) + c \cdot \cos^2\beta \right] \\
 &+ \sin 2\gamma \left[\sin 2\beta (f \cdot \cos\alpha + g \cdot \sin\alpha) + h \cdot \sin 2\alpha (1 + \sin^2\beta) \right] \\
 &+ \cos 2\gamma \left[\sin 2\alpha \sin\beta (a - b) + 2h \cdot \sin\beta \cos 2\alpha + \cos\beta (2g \cdot \cos\alpha - 2f \cdot \sin\alpha) \right].
 \end{aligned} \tag{3.34}$$

$$\begin{aligned}
 2h'' &= \sin 2\beta \sin\gamma [a \cdot \sin^2\alpha + b \cdot \cos^2\alpha - c + h \cdot \sin 2\alpha] + \cos 2\beta \sin\gamma [2g \cdot \sin\alpha + 2f \cdot \cos\alpha] \\
 &+ \cos\beta \cos\gamma [\sin 2\alpha (a - b) + 2h \cdot \cos 2\alpha] + \sin\beta \cos\gamma [2f \cdot \sin\alpha - 2g \cdot \cos\alpha].
 \end{aligned} \tag{3.35}$$

$$2p'' = 2\cos\gamma [p \cdot \cos\alpha - q \cdot \sin\alpha] + 2\sin\beta \sin\gamma [p \cdot \sin\alpha + q \cdot \cos\alpha] + 2r \cdot \sin\gamma \cos\beta. \tag{3.36}$$

$$2q'' = 2\cos\beta [p \cdot \sin\alpha + q \cdot \cos\alpha] - 2r \cdot \sin\beta. \tag{3.37}$$

$$2r'' = 2\cos\gamma \sin\beta [p \cdot \sin\alpha + q \cdot \cos\alpha] + 2\sin\gamma [-p \cdot \cos\alpha + q \cdot \sin\alpha] + 2r \cdot \cos\gamma \cos\beta. \tag{3.38}$$

$$d'' = d. \tag{3.39}$$

As seen from the above expressions, all of the coefficients are affected by the rotations α , β , and γ except for the constant d'' .

In order to eliminate the product terms $2f''$, $2g''$, and $2h''$, expressions (3-33) - (3.35) must be set equal to zero and solved simultaneously. As seen from these three expressions, each of them is a function of the rotation angles α , β , and γ . It is not possible to analytically find the rotation angles which eliminate the product terms. Instead, in the next section we present an iterative technique which performs the elimination of the product terms.

3.3.5 Product Terms Elimination Method

The product terms yz , xz , and xy in $F(x,y,z)$, denote the rotation terms which are to be eliminated. Elimination of all these rotation terms will place the three-dimensional surface on a coordinate system plane parallel to our coordinate system.

Observe that in the presence of a single rotation term, say yz , Equation (3.29) takes the form

$$F(x,y,z) = ax^2 + by^2 + cz^2 + 2fyz + 2px + 2qy + 2rz + d = 0.$$

The equation of the trace of the surface in the yz plane is obtained by setting $x = 0$. An appropriate rotation about the origin in the yz plane by an angle β will eliminate the yz term.

However, in the presence of two or more rotation terms, trying to eliminate a second rotation term will force the previously eliminated rotation term to reappear. Therefore, there will be at least two rotation terms present. The approach we propose is an iterative process, whereby at each stage the object is rotated in each of the coordinate planes, sequentially. The procedure is repeated until all the product terms are eliminated, i.e., the coefficients f , g , and h converge to zero in the limit.

Since our aim is to eliminate the rotation terms xy , yz , and xz , let's exclusively consider the coefficients of these rotation terms, namely f , g , and h evaluated in Section 3.3.4. In our iterative procedure we are able to eliminate all of the product terms. For example, suppose we wish to eliminate the term xy . By a specific rotation of α about the z axis, we will be able to accomplish our goal. However, while executing this process, the orientation of the object about the two planes yz and xz , i.e., the angles the object make with these two planes have been changed. If we wish to eliminate the yz term, the object has to be rotated about the x axis by an angle β . However, in this instance, while performing the process, the previously eliminated xy term reappears though the magnitude of its present orientation has been reduced. Hence by iterating the above process, an instance occurs when all the coefficients of the product terms converge to zero in the limit.

Consider the Equations (3.33), (3.34), and (3.35). First eliminate the coefficient h , i.e, the xy term. This can be accomplished by rotating the object about the z axis by an angle α , whereas $\beta=\gamma=0$. Under these circumstances the new coefficients are as shown below.

$$2f_{11} = 2g \cdot \sin\alpha_1 + 2f \cdot \cos\alpha_1,$$

$$2g_{11} = 2g \cdot \cos\alpha_1 - 2f \cdot \sin\alpha_1,$$

and

$$2h_{11} = (a - b)\sin 2\alpha_1 + 2h \cdot \cos 2\alpha_1 = 0,$$

$$\text{where } \cot 2\alpha_1 = \frac{b - a}{2h}.$$

As seen above, the coefficient h has been forced to 0. The first digit of the subscript refers to the iteration number, whereas the second digit of the subscript denotes the number of times the object has been rotated by a specific angle. The remaining coefficients a , b , c , p , q , and r also reflect changes brought about by the above rotation.

The new coefficients are

$$a_{11} = a \cdot \cos^2 \alpha_1 + b \cdot \sin^2 \alpha_1 - 2h \cdot \sin \alpha_1 \cos \alpha_1,$$

$$b_{11} = b \cdot \cos^2 \alpha_1 + a \cdot \sin^2 \alpha_1 + 2h \cdot \sin \alpha_1 \cos \alpha_1,$$

$$c_{11} = c,$$

$$2p_{11} = 2p \cdot \cos \alpha_1 - 2q \cdot \sin \alpha_1,$$

$$2q_{11} = 2p \cdot \sin \alpha_1 + 2q \cdot \cos \alpha_1,$$

and

$$2r_{11} = 2r.$$

The new quadric equation is

$$F(x,y,z) = a_{11}x^2 + b_{11}y^2 + c_{11}z^2 + 2f_{11}yz + 2g_{11}xz + 2p_{11}x + 2q_{11}y + 2r_{11}z + d = 0.$$

Consider the second step wherein the coefficient corresponding to the yz term is forced to zero. In this particular case, the object has to be rotated by an angle β about the x axis, where $\alpha=\gamma=0$. Under these circumstances, the new rotation coefficients (signifying the product terms) become

$$2f_{12} = (b_{12} - c_{12})\sin 2\beta_1 + 2f_{11} \cdot \cos 2\beta_1 = 0,$$

$$\text{where } \cot 2\beta_1 = \frac{c_{11} - b_{11}}{2f_{11}},$$

$$2g_{12} = 2g_{11} \cdot \cos \beta_1,$$

and

$$2h_{12} = -2g_{11} \cdot \sin \beta_1.$$

At the same time the other coefficients become

$$a_{12} = a_{11},$$

$$b_{12} = c_{11} \cdot \sin^2 \beta_1 + b_{11} \cdot \cos^2 \beta_1 - 2f_{11} \cdot \sin \beta_1 \cos \beta_1,$$

$$c_{12} = b_{11} \cdot \sin^2 \beta_1 + c_{11} \cdot \cos^2 \beta_1 + 2f_{11} \cdot \sin \beta_1 \cos \beta_1,$$

$$2p_{12} = 2p_{11},$$

$$2q_{12} = 2q_{11} \cdot \cos \beta_1 - 2r_{11} \cdot \sin \beta_1,$$

and

$$2r_{12} = 2q_{11} \cdot \sin \beta_1 + 2r_{11} \cdot \cos \beta_1.$$

The new quadric equation is:

$$F(x,y,z) = a_{12}x^2 + b_{12}y^2 + c_{12}z^2 + 2g_{12}xz + 2h_{12}xy + 2p_{12}x + 2q_{12}y + 2r_{12}z + d = 0.$$

In the final step of the initial iteration, the coefficient corresponding to the xz term is forced to zero. In this case, the object is to be rotated by an angle γ about the y axis, whereas $\alpha = \beta = 0$. Under these circumstances, the new rotation coefficients become

$$2f_{13} = 2h_{12} \cdot \sin \gamma_1 = -2g_{11} \cdot \sin \beta_1 \sin \gamma_1,$$

$$2g_{13} = (a_{13} - c_{13}) \sin 2\gamma_1 + (2g_{11} \cdot \cos \alpha_1 - f_{11} \cdot \sin \alpha_1) \cos \beta_1 \cos 2\gamma_1 = 0,$$

$$\text{where } \cot 2\gamma_1 = \frac{c_{12} - a_{12}}{2g_{12}},$$

and

$$2h_{13} = 2h_{12} \cdot \cos \gamma_1 = -2g_{11} \cdot \sin \beta_1 \cos \gamma_1.$$

Let's now carefully analyze the coefficients of xy , yz , and zx obtained in the final step of the first iteration. Consider, for instance, the coefficient corresponding to the yz term. It is observed that while proceeding from one step to the other, the new coefficients are getting multiplied by the sine or cosine of the concerned angle. This implies that in every succeeding step these coefficients are decreasing in their magnitude. To justify the above statement, let us now consider all the coefficients obtained in the second iteration.

At the end of stage 1 of the second iteration, the rotation coefficients become

$$2f_{21} = 2f_{13} \cdot \cos\alpha_2 = -2g_{11} \cdot \sin\beta_1 \sin\gamma_1 \cos\alpha_2,$$

$$2g_{21} = -2f_{13} \cdot \sin\alpha_2 = 2g_{11} \cdot \sin\beta_1 \sin\gamma_1 \sin\alpha_2,$$

and

$$2h_{21} = 0, \text{ where } \cot 2\alpha_2 = \frac{b_{13} - a_{13}}{2h_{13}}.$$

At the end of the second stage of the second iteration, the rotation coefficients become

$$2f_{22} = 0 \text{ where } \cot 2\beta_2 = \frac{c_{21} - b_{21}}{2f_{21}},$$

$$2g_{22} = 2g_{11} \cdot \sin\beta_1 \sin\gamma_1 \sin\alpha_2 \cos\beta_2,$$

and

$$2h_{22} = -2g_{11} \cdot \sin\beta_1 \sin\gamma_1 \sin\alpha_2 \sin\beta_2.$$

Similarly at the end of the final stage of the second iteration, the rotation coefficients reduce to

$$2f_{23} = -2g_{11} \cdot \sin\beta_1 \sin\gamma_1 \sin\alpha_2 \sin\beta_2 \sin\gamma_2,$$

$$2g_{23} = 0 \text{ where } \cot 2\alpha_2 = \frac{b_{13} - a_{13}}{2h_{13}},$$

and

$$2h_{23} = -2g_{11} \cdot \sin\beta_1 \sin\gamma_1 \sin\alpha_2 \sin\beta_2 \cos\gamma_2.$$

The terms α_2 , β_2 , and γ_2 are the respective rotation angles along the z, x, and y axes in the second iteration. Hence it is observed with each iteration that the rotation coefficients get smaller and smaller in magnitude and eventually disappear in the limit.

We are now in a position to formulate a rotation matrix whose elements correspond to the directional cosines of the x, y, and z axes of the rotated object.

The rotation matrix = $R_\gamma R_\beta R_\alpha$,

where

$$R_\alpha = \begin{bmatrix} \cos\alpha & \sin\alpha & 0 \\ -\sin\alpha & \cos\alpha & 0 \\ 0 & 0 & 1 \end{bmatrix},$$

$$R_\beta = \begin{bmatrix} 1 & 0 & 0 \\ 0 & \cos\beta & \sin\beta \\ 0 & -\sin\beta & \cos\beta \end{bmatrix},$$

and

$$R_\gamma = \begin{bmatrix} \cos\gamma & 0 & -\sin\gamma \\ 0 & 1 & 0 \\ \sin\gamma & 0 & \cos\gamma \end{bmatrix}.$$

Subsequently,

$$R_\gamma R_\beta R_\alpha = \begin{bmatrix} \cos\alpha\cos\gamma - \sin\alpha\sin\beta\sin\gamma & \cos\gamma\sin\alpha + \sin\gamma\sin\beta\cos\alpha & -\sin\gamma\cos\beta \\ -\cos\beta\sin\alpha & \cos\beta\cos\alpha & \sin\beta \\ \sin\gamma\cos\alpha + \cos\gamma\sin\alpha\sin\beta & \sin\alpha\sin\gamma - \cos\gamma\sin\beta\cos\alpha & \cos\beta\cos\gamma \end{bmatrix}, \quad (3.40)$$

where

$$\alpha = \sum_{i=1}^n \alpha_i, \quad \beta = \sum_{i=1}^n \beta_i, \quad \text{and} \quad \gamma = \sum_{i=1}^n \gamma_i. \quad n \text{ corresponds to the iteration where all the rota-}$$

tion terms go to zero in the limit.

Once the rotation terms, i.e., xy , yz , and xz are eliminated, the three-dimensional surface has the representation of

$$F(x,y,z) = Ax^2 + By^2 + Cz^2 + 2Px + 2Qy + 2Rz + D = 0, \quad (3.41)$$

where A , B , C , P , Q , and R are the coefficients resulting after the elimination of the rotation terms. A natural question to ask is: Can the terms of the first degree be eliminated by means of a translation? The answer is sometimes they can and sometimes they cannot. The case, where the term can be eliminated, is supported by the following theorem.

3.3.6 Translation of the Rotated Object

Theorem 3.2. The terms of the first degree of an equation of a quadric surface can be eliminated by means of a translation if and only if the surface has a center, in which case the first degree terms are eliminated if and only if the new origin is a center [24].

The method of completing squares is the easiest to determine the coordinates of the new origin. Consider Equation (3.41). Grouping the like terms:

$$Ax^2 + 2Px + By^2 + 2Qy + Cz^2 + 2Rz + D = 0 \quad \Rightarrow$$

$$A \left[x^2 + 2P \frac{x}{A} \right] + B \left[y^2 + 2Q \frac{y}{B} \right] + C \left[z^2 + 2R \frac{z}{C} \right] + D = 0.$$

Upon completing squares, we get

$$A \left[x + \frac{P}{A} \right]^2 + B \left[y + \frac{Q}{B} \right]^2 + C \left[z + \frac{R}{C} \right]^2 + D - \left[\frac{P^2}{A} + \frac{Q^2}{B} + \frac{R^2}{C} \right] = 0, \quad (3.42)$$

where $-P/A$, $-Q/B$, and $-R/C$ are the coordinates of the new origin.

3.4 Summary and Problem Identification

All of the above procedures performed until now result in a second degree polynomial describing an unknown object, the center of the object lying at the origin of our coordinate system. Had the test data been simulated, the three-dimensional discriminant approach which was mentioned in Chapter One could be used to describe and recognize the object. Since the test data is not simulated, we should utilize a recognition algorithm which will distinguish and recognize each of the test surfaces from one another.

The intersection of a surface with a plane generates a curve. The nature of this curve depends solely on what type of object is intersected and with which particular plane and in which orientation. Since we have no knowledge of the surface type, a priori, one approach is to intersect the surface with a series of planes. We need to determine the optimum number of planes which will uniquely characterize each of the quadric surfaces.

Our goal is to derive a consistent method for determining the minimum number of planes necessary to intersect a given quadric surface so that the generated conics uniquely characterize the surface. This goal includes the derivation and formulation of the angular bounds for which a particular plane intersecting a surface generates the same two-dimensional curve. In summary, each of the quadric surfaces is represented

by a unique five-tuple, whose elements signify the presence or absence of the following curves: circle, ellipse, hyperbola, parabola, and a line.

Chapter Four covers the description and recognition of each of the three-dimensional surfaces we have above mentioned in Section 3.2. A distinct pattern vector is obtained for each of the surfaces.

CHAPTER FOUR

QUADRIC SURFACE CHARACTERIZATION AND RECOGNITION

4.1 Introduction

Our proposed method utilizes a two-dimensional discriminant which is a measure for distinguishing curves. Since the ten generated coefficients described in Section 3.3.3 of Chapter Three give a three-dimensional representation of the surfaces, we propose to identify the quadrics using the information resulting from the intersection of the surface with different planes. If the surface is one of those considered for the recognition process (see figures 3-1, 3-2, and 3-3), there are five possible two-dimensional curves that may result from such intersections: (i) a circle, (ii) an ellipse, (iii) a parabola, (iv) a hyperbola, and (v) a line. Thus, a feature or pattern vector with five independent components can be formed for characterizing each of the surfaces.

The two-dimensional discriminant criteria we use to recognize each of the two-dimensional curves created by planes intersecting the various quadric surfaces is discussed in Section 4.2. In Section 4.3 the results of Chapter Three are used to completely implement our recognition algorithm. Concomitantly, we derive a consistent method for determining the minimum number of planes that are necessary to intersect a given three-dimensional surface so that the generated conics uniquely characterize the surface. The formulation of a three-dimensional discriminant similar to the two-dimensional discriminant is presented in Section 4.4. The mapping between the explicit and implicit representations of quadric surfaces is also examined in this section.

4.2 Two-Dimensional Discriminant

Given a conic of the form

$$F(x,y) = Ax^2 + Bxy + Cy^2 + Dx + Ey + F = 0,$$

the discriminant $\delta = B^2 - 4AC$ characterizes it as one of the following [30]:

If $\delta = B^2 - 4AC < 0$, then the conic is an ellipse or a circle.

If $\delta = B^2 - 4AC = 0$, then the conic is a parabola.

If $\delta = B^2 - 4AC > 0$, then the conic is a hyperbola.

Our objective is to derive a consistent method for determining the minimum number of planes required to intersect a given three-dimensional surface so that the generated conics uniquely characterize the surface. This includes the derivation and formulation of the angular bounds for which a particular intersecting plane yields the same two-dimensional curve.

The three-dimensional surfaces (objects) to be recognized are listed below:

- (a) an ellipsoid,
- (b) a circular cylinder,
- (c) a sphere,
- (d) a quadric cone,
- (e) a hyperboloid of one sheet,
- (f) a hyperboloid of two sheets,
- (g) an elliptic paraboloid,
- (h) a hyperbolic cylinder,
- (i) a parabolic cylinder,
- (j) a hyperbolic paraboloid, and
- (k) a parallelepiped.

4.3 Quadric Surface Description and Representation

As discussed in Section 3.2 of Chapter Three, we now assume that the three-dimensional objects have undergone two basic transformations, rotation and translation. Consequently the product terms in the representation $F(x,y,z)$ for a particular surface have been eliminated and the center of the surface lies at the origin of our specified coordinate system. As illustrated in Figure 4-1, all of the surfaces are contained in the xy plane with their centers at O (the origin). For each surface, the characterization is performed in two steps. Initially we consider the intersection of each object with two planes (horizontal and vertical). This step does not require that the surface undergoes a translation transformation. We refer to plane 1 as the one that intersects the object parallel to the xy plane, i.e., z constant. Also refer to plane 2 as the one that intersects the object parallel to the xz plane, i.e., y constant. In the second step, the minimum set of intersecting planes needed to yield a unique feature vector (the various curves serve as features) is determined. In this step we assume that the object has undergone the translation transformation. The following sections describe the representation procedure for each of the quadric surfaces listed in Section 4.2.

4.3.1 Ellipsoid

Step 1:

Consider the equation of an ellipsoid resting on a plane parallel to the xy plane and its axis of revolution parallel to the z axis. Equation (3.1) reduces to the form

$$F(x,y,z) = ax^2 + by^2 + cz^2 + 2px + 2qy + 2rz + d = 0, \quad (4.1)$$

which further reduces to

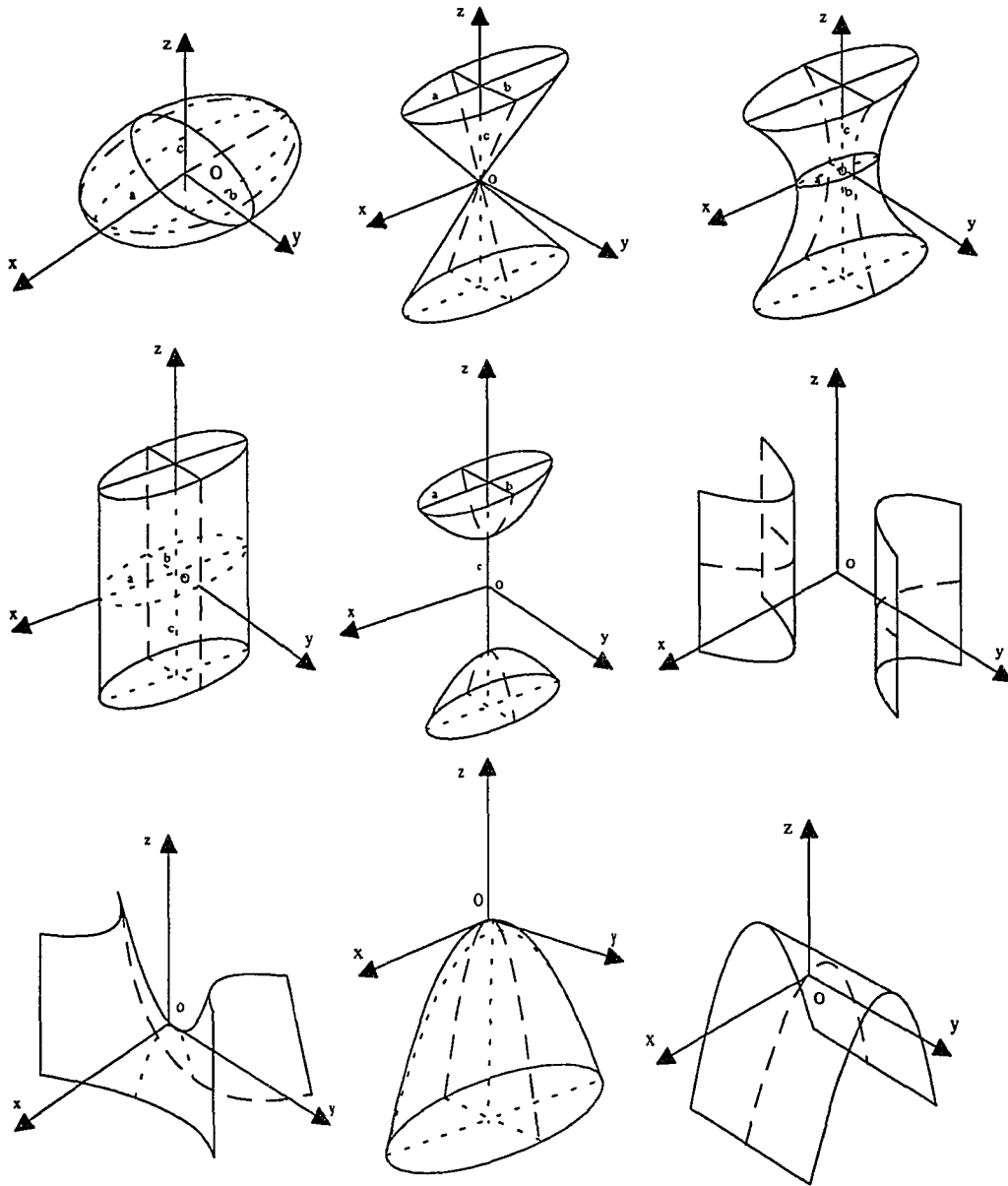


Figure 4-1. Quadric surfaces from left to right and top to bottom: ellipsoid, quadric cone, hyperboloid of one sheet, elliptic cylinder, hyperboloid of two sheets, hyperbolic cylinder, hyperbolic paraboloid, elliptic paraboloid, and parabolic cylinder.

$$\frac{\left[x + \frac{p}{a}\right]^2}{\frac{1}{a}} + \frac{\left[y + \frac{q}{b}\right]^2}{\frac{1}{b}} + \frac{\left[z + \frac{r}{c}\right]^2}{\frac{1}{c}} - 1 = 0, \quad (4.2)$$

where $a > 0$, $b > 0$, $c > 0$ and we have assumed the scaling $d = \frac{p^2}{a} + \frac{q^2}{b} + \frac{r^2}{c} - 1$.

It should be noted that the coefficients a , b , c , p , q , r , and d are all known; $\sqrt{\frac{1}{a}}$, $\sqrt{\frac{1}{b}}$, and $\sqrt{\frac{1}{c}}$ are the semi-major and minor axes of the ellipsoid, respectively; and $[-p/a, -q/b, -r/c]$ are the coordinates of the center of the ellipsoid.

Consider the intersection of the ellipsoid with plane **1**, i.e., $z = k$, where $\frac{-r}{c} - \sqrt{\frac{1}{c}} < k < \frac{-r}{c} + \sqrt{\frac{1}{c}}$, then,

$$\frac{\frac{(y + \frac{q}{b})^2}{\frac{1}{b} - \frac{(ck + r)^2}{bc}}}{\frac{1}{a} - \frac{(ck + r)^2}{ac}} - 1 = 0, \quad (4.3)$$

which is the equation of an ellipse.

Let's now consider the intersection of the ellipsoid with plane **2**, i.e., $y = k$, where $\frac{-q}{b} - \sqrt{\frac{1}{b}} < k < \frac{-q}{b} + \sqrt{\frac{1}{b}}$, then,

$$\frac{\frac{(x + \frac{p}{a})^2}{\frac{1}{a} - \frac{(bk + q)^2}{ab}}}{\frac{1}{c} - \frac{(bk + q)^2}{bc}} - 1 = 0, \quad (4.4)$$

which is again the equation of an ellipse. For the case when the two minor axes are equal, the surface is called a spheroid. Also, when all the axes are equal, i.e., $a = b = c$, the surface is a sphere. Intersection of the sphere with planes is discussed in Section 4.3.3.

Step 2:

As mentioned before, we assume that the ellipsoid has undergone a translation, such that its center aligns with the origin of our desired coordinate system as shown in Figure 4-2. Hence its representation can be assumed as

$$\frac{X^2}{A^2} + \frac{Y^2}{B^2} + \frac{Z^2}{C^2} = 1, \quad (4.5)$$

where A, B, and C are the major and minor semi-axes, respectively, of the ellipsoid. As seen in step 1, intersection of the ellipsoid with any $Z = |k|$, $-C \leq k \leq C$, will be an ellipse. Let us now determine the bounds within which inclined sub-planes of $Z = |k|$ still result in an elliptic intersection with the ellipsoid.

Consider the points E(A,0,0), F(0,B,0), and G(0,0,K), where $K > 0$. The equation of the plane containing these points is:

$$BKX + AKY + ABZ - ABK = 0.$$

Solving for Z and substituting in Equation (4.5) yields the curve of intersection:

$$X^2(B^2C^2 + B^2K^2) + Y^2(A^2C^2 + A^2K^2) + 2AK^2BXY + \dots = 0. \quad (4.6)$$

In the above equation only terms which are necessary to determine the intercepted curve are retained. Proceeding with the discriminant test,

$$\delta = 4A^2B^2[-C^4 - 2C^2K^2].$$

Since the discriminant is always negative, the intercepts are ellipses. Angular bounds in terms of an angle are not needed in this case, since the only occasion the intercepts are different than ellipses is when two of the semi-axes are equal. Under that circumstance, we arrive at a circular intercept. Figure 4-3 illustrates vertical planes intersecting the ellipsoid. Table 4-1 summarizes the result obtained above.

DETAILED VIEW: HORIZONTAL INTERSECTIONS

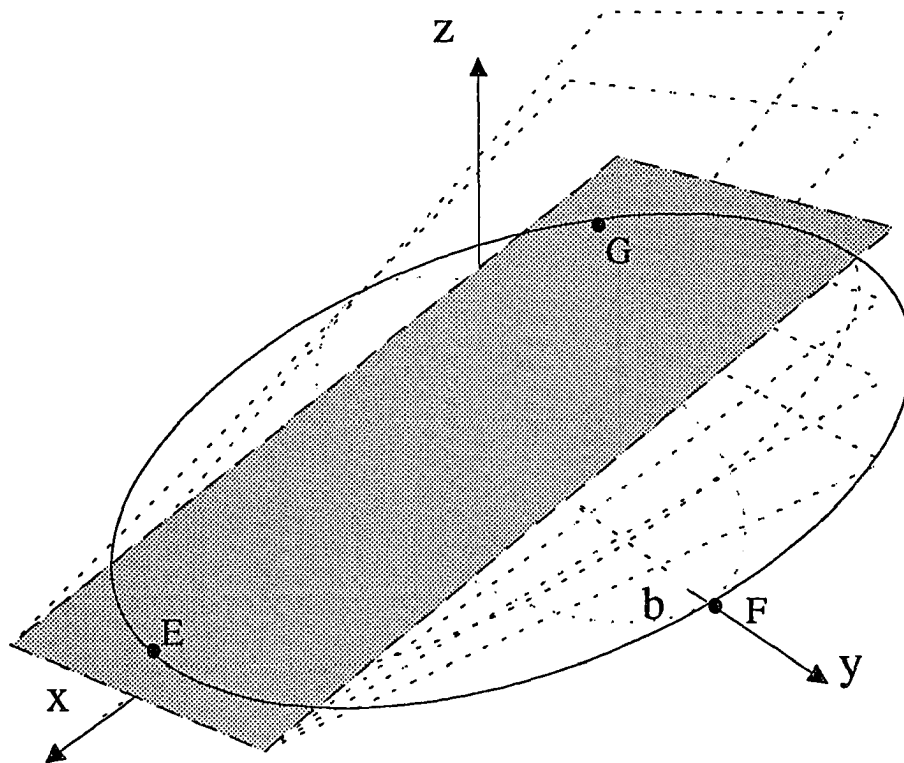


Figure 4-2. The plane parallel to the x-axis and all its inclined sub-planes generate ellipses. In the case of a spheroid all intersections are ellipses except when the plane is parallel to one of the axes under which case the intersection is a circle.

DETAILED VIEW: VERTICAL INTERSECTIONS

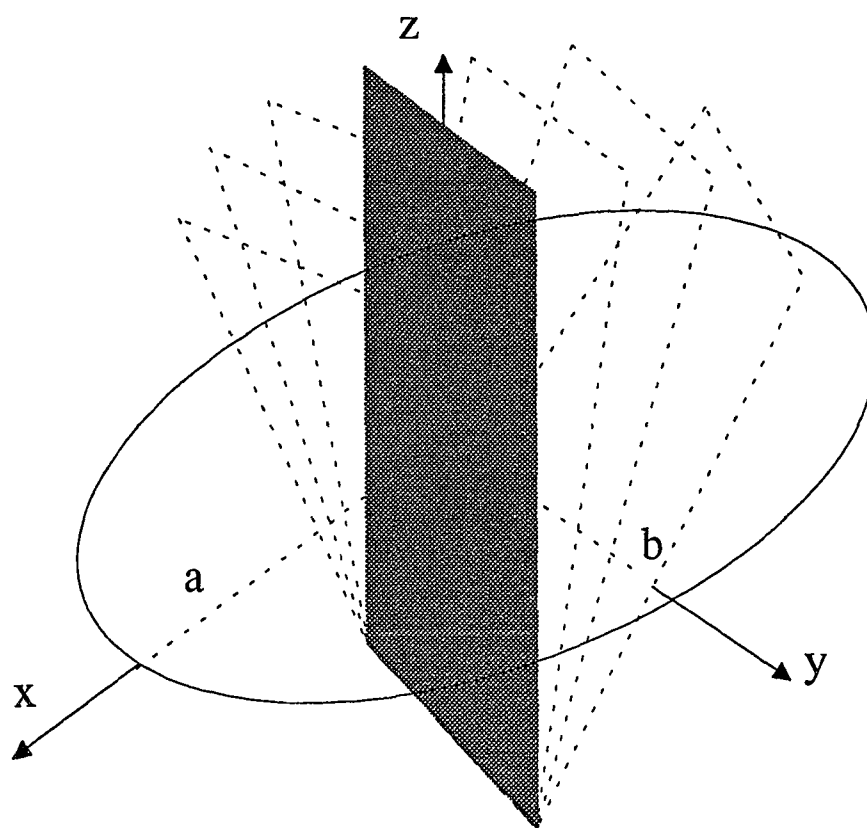


Figure 4-3. The plane parallel to the z-axis and all its inclined sub-planes generate ellipses. In the case of a spheroid all intersections are ellipses except when the plane is parallel to one of the axes under which case the intersection is a circle.

PLANE	INTERSECTION
$Z = K$	Ellipse
$Y = K$	Ellipse
Any inclined sub-planes to $Z=K, Y=K$	Ellipse

Table 4-1. Intersection of ellipsoid with planes.

4.3.2 Circular (elliptic) cylinder

Step 1:

Consider the general representation of a circular cylinder resting on a plane parallel to the xy plane and its axis of revolution parallel to the z axis. Its representation then reduces to

$$F(x,y,z) = bx^2 + by^2 + 2px + 2qy + d = 0, \quad (4.7)$$

which is the same as

$$F(x,y,z) = \frac{\left[y + \frac{q}{b}\right]^2}{\frac{1}{b}} + \frac{\left[x + \frac{p}{b}\right]^2}{\frac{1}{b}} - 1 = 0, \quad (4.8)$$

only if $d = \frac{q^2}{b} + \frac{p^2}{b} - 1$ and also $b > 0$.

In the case of the elliptic cylinder, Equation (4.7) becomes

$$F(x,y,z) = ax^2 + by^2 + 2px + 2qy + d = 0,$$

which further reduces to

$$F(x,y,z) = \frac{\left[y + \frac{q}{b}\right]^2}{\frac{1}{b}} + \frac{\left[x + \frac{p}{a}\right]^2}{\frac{1}{a}} - 1 = 0, \quad (4.9)$$

only if $d = \frac{q^2}{b} + \frac{p^2}{a} - 1$ and $a > 0, b > 0$.

Intersection of the circular or elliptic cylinder with plane **1** would not affect its representation, since it is independent of the variable z . Hence the resultant curve intercepted is the same as represented by Equations (4.7) or (4.9), which is an equation of a circle or an ellipse, respectively.

Consider the case where the circular cylinder is intersected with plane **2**, i.e., $y = k$, where $\frac{-q}{b} - \sqrt{\frac{1}{b}} < k < \frac{-q}{b} + \sqrt{\frac{1}{b}}$. Then,

$$\left[x + \frac{p}{a}\right]^2 = \frac{1}{b} - \left[\frac{bk + q}{b}\right]^2. \quad (4.10a)$$

Solving for x generates the equation of a pair of parallel lines. A similar result is obtained when the elliptic cylinder is intersected with plane **2**, namely

$$\left[x + \frac{p}{a}\right]^2 = \frac{1}{a} - \frac{b}{a} \left[\frac{bk + q}{b}\right]^2. \quad (4.10b)$$

Step 2:

As with the ellipsoid, consider the elliptic cylinder to have undergone the translation transformation. Its center is aligned with the origin of the coordinate system as shown in Figure 4-4. Let the height of the cylinder be $2L$. The representation of the elliptic cylinder can be assumed as

$$\frac{X^2}{A^2} + \frac{Y^2}{B^2} = 1, \quad (4.11)$$

where A and B are the major and minor semi-axes of the cylinder. Intersection of the cylinder with any plane $Z = |k|$, $-L \leq k \leq L$, is an ellipse. The angular bounds within which an inclined plane will still result in an elliptic intersection is determined next.

Consider the intersection of the plane passing through the points $E(A,0,0)$, $F(-A,0,K)$, and $G(0,-B,0)$ with the cylinder as shown in Figure 4-4. The equation of the plane containing these points is:

$$BKX - AKY + 2ABZ - ABK = 0.$$

Solving for X ,

$$X = \frac{AKY - 2ABZ + ABK}{BK}.$$

Substituting X in Equation (4.11) results in

$$2K^2Y^2 + 4B^2Z^2 - 4BKYZ + \dots = 0.$$

The discriminant results in a quantity less than zero. Hence the intersection is an ellipse.

Given any two planes, $a_1x + b_1y + c_1z + d_1 = 0$, and $a_2x + b_2y + c_2z + d_2 = 0$, the angle of intersection is given as

$$\cos\theta = \frac{|a_1a_2 + b_1b_2 + c_1c_2|}{\sqrt{a_1^2 + b_1^2 + c_1^2}\sqrt{a_2^2 + b_2^2 + c_2^2}}.$$

Hence, in the above case the intersections with respect to the plane $z = 0$ and all the planes inclined to it (which we will refer to as inclined-sub planes), yield ellipses for

$$\cos\theta \leq \frac{2AB}{\sqrt{(A^2K^2 + 4A^2B^2 + B^2K^2)}}.$$

DETAILED VIEW: HORIZONTAL INTERSECTIONS

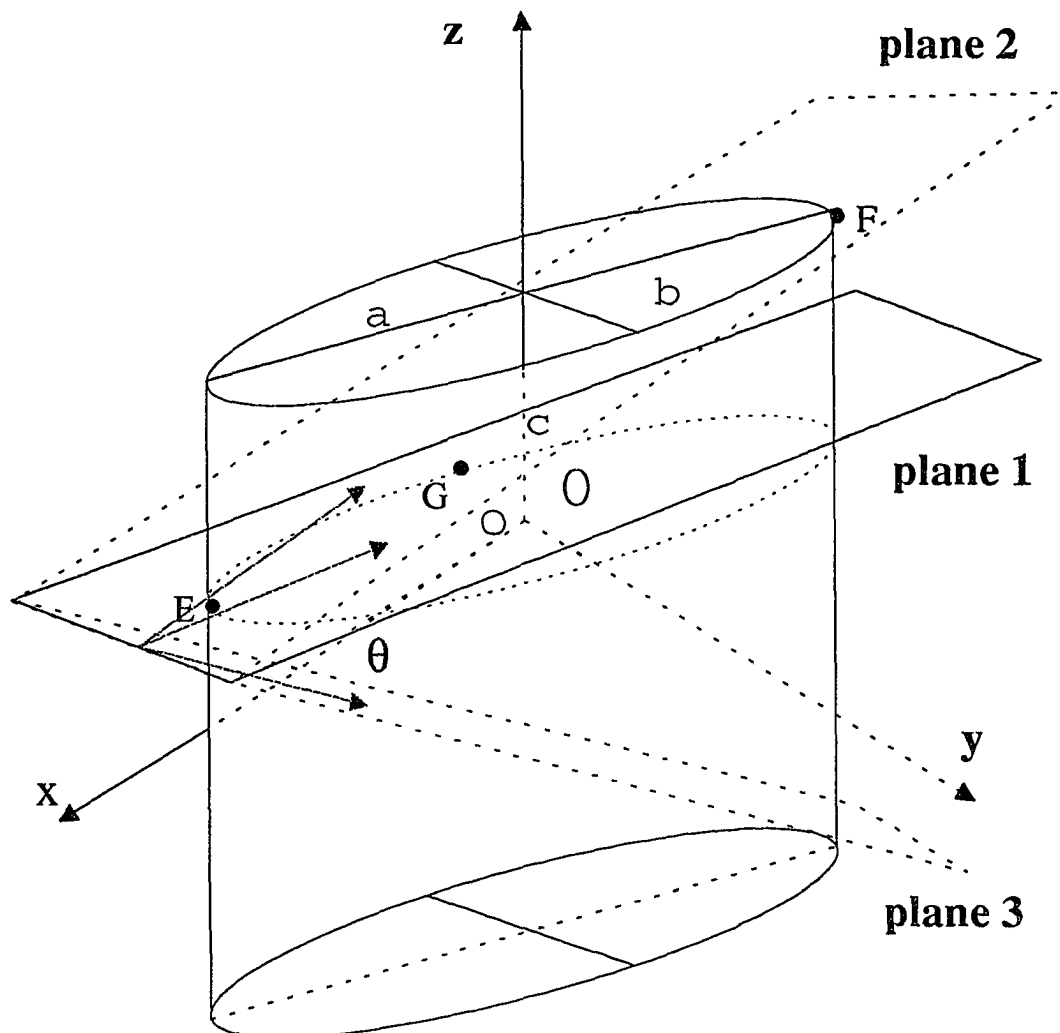


Figure 4-4. Plane 1 and the planes parallel to it within the range $-L$ to L (length of the cylinder) intersect the cylinder in parallel lines. Plane 2 and plane 3 are the inclined sub-planes of plane 1 which determine the maximum range or inclination (with plane 1) wherein similar curves (ellipses) are generated. θ is the angular bound for the inclination in terms of an angle.

The angular bounds with respect to the plane $X = K, -A \leq K \leq A$, and its inclined sub-planes is determined next.

Intersection of the plane $X = K$ or $Y = K$ and the cylinder results in an intersection of a pair of straight lines. The equation of the plane passing through the points $H(0,B,-L)$, $I(0,-B,-L)$, and $J(K,0,L)$, $|K| > 0$, as shown in Figure 4-5, is

$$KZ - 2LX + LK = 0.$$

Solving for X ,

$$X = \frac{K(Z + L)}{2L}.$$

Substituting in Equation (4.11), yields the interception

$$\frac{K^2(Z + L)^2}{4L^2A^2} + \frac{Y^2}{B^2} = 1,$$

which is an ellipse.

All intersections of the inclined plane $X = K, |K| > 0$, yield degenerate ellipses. In terms of the angle of intersection,

$$\cos\theta < \frac{2L}{\sqrt{A^2 + 4K^2}}.$$

Figure 4-6 illustrates a lateral view of all the possible curves intercepted by the intersection of the cylinder and the planes. Table 4-2 summarizes the results obtained above.

DETAILED VIEW : VERTICAL INTERSECTIONS

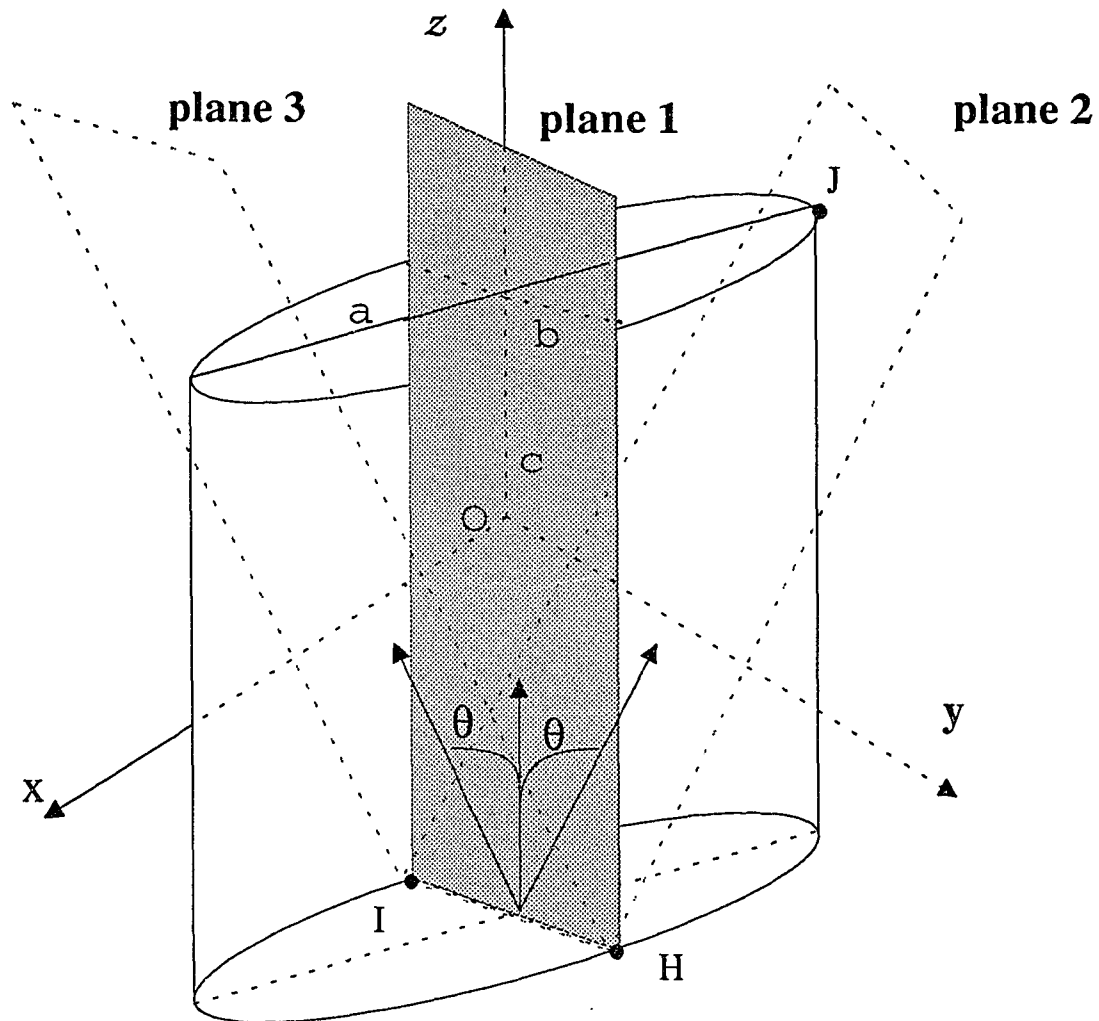


Figure 4-5. Plane 1 and the planes parallel to it within the range $-a$ to a intersect the cylinder in parallel lines. Plane 2 and plane 3 are the inclined sub-planes of plane 1 which determine the maximum range or inclination (with plane 1) wherein similar curves (degenerate ellipses) are generated. θ is the angular bound for this inclination in terms of an angle.

LATERAL VIEW

INTERSECTION OF A PLANE AND A QUADRIC CYLINDER

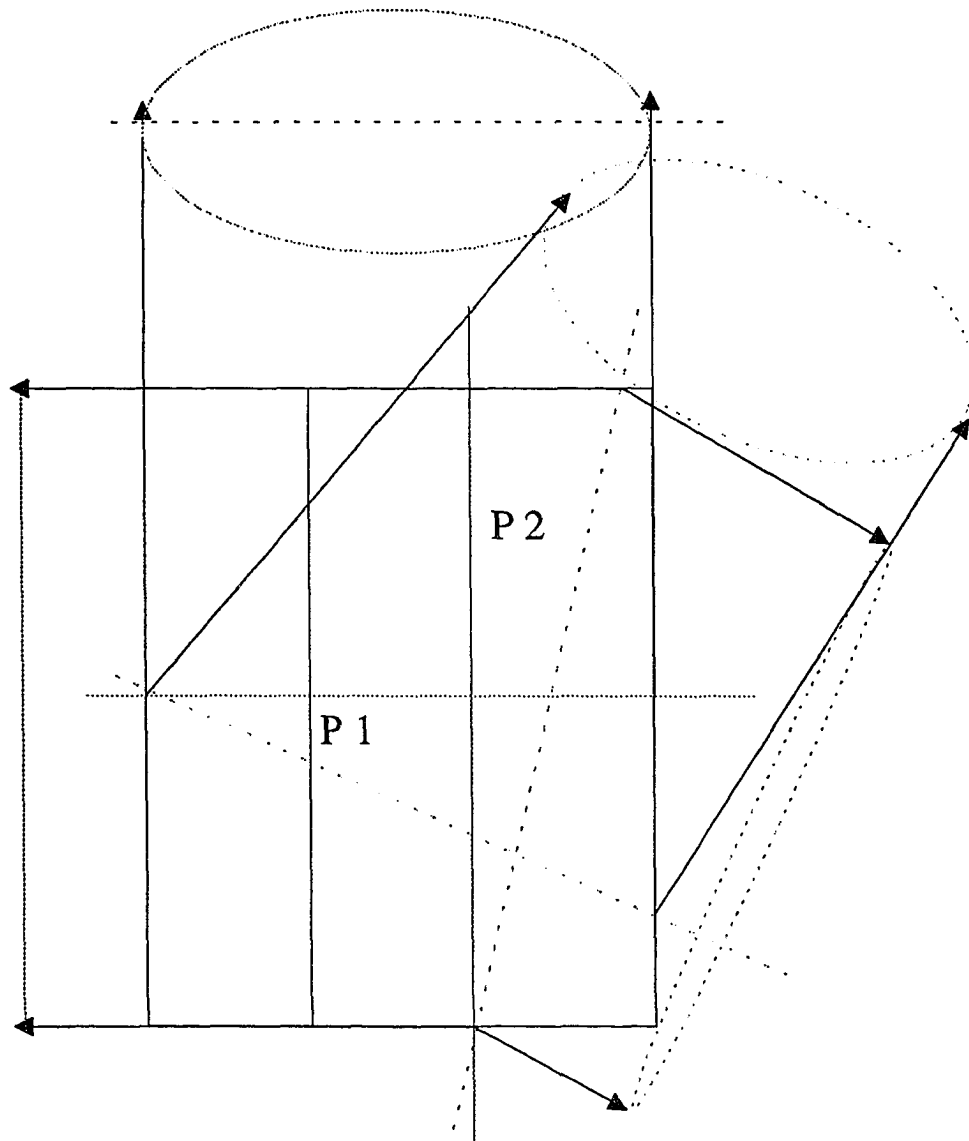


Figure 4-6. Plane P1 and its inclined sub-plane generate ellipses. Though plane P2 generates a pair of lines, its inclined sub-planes start generating degenerate ellipses as the inclination start to increase.

PLANE	INTERSECTION
$Z = K$	Circle, Ellipse
$X = K$	Lines
Inclined sub-planes of $Z=K$	Ellipse
Inclined sub-planes of $X=K$	Lines

Table 4-2. Intersection of quadric cylinder with planes.

4.3.3 Sphere

Step 1:

As mentioned in Section 4.1., the sphere is a special case of an ellipsoid, where the three semi axes are all equal. Equation (4.1) thus reduces to

$$F(x,y,z) = ax^2 + ay^2 + az^2 + 2px + 2qy + 2rz + d = 0, \quad (4.12)$$

which further reduces to

$$\frac{\left[x + \frac{p}{a}\right]^2}{\frac{1}{a}} + \frac{\left[y + \frac{q}{a}\right]^2}{\frac{1}{a}} + \frac{\left[z + \frac{r}{a}\right]^2}{\frac{1}{a}} - 1 = 0, \quad (4.13)$$

only if $d = \frac{p^2}{a} + \frac{q^2}{b} + \frac{r^2}{a} - 1$.

Consider the case when the sphere is intersected with plane **1**, i.e., $z = k$, where

$$\frac{-r}{a} - \sqrt{\frac{1}{a}} < k < \frac{-r}{a} + \sqrt{\frac{1}{a}}. \text{ Then,}$$

$$\frac{\left[x + \frac{p}{a}\right]^2}{\frac{1}{a} - \left[\frac{ak + r}{a}\right]^2} + \frac{\left[y + \frac{q}{a}\right]^2}{\frac{1}{a} - \left[\frac{ak + r}{a}\right]^2} - 1 = 0, \quad (4.14)$$

which is the equation of a circle.

A similar equation results when the sphere is intersected with plane 2, in which case $y = k$, where $\frac{-q}{a} - \sqrt{\frac{1}{a}} < k < \frac{-q}{a} + \sqrt{\frac{1}{a}}$, and subsequently Equation (4.13) becomes

$$\frac{\left[x + \frac{p}{a}\right]^2}{\frac{1}{a} - \left[\frac{ak + q}{a}\right]^2} + \frac{\left[z + \frac{r}{a}\right]^2}{\frac{1}{a} - \left[\frac{ak + q}{a}\right]^2} - 1 = 0. \quad (4.15)$$

Step 2:

Figure 4-7 illustrates the sphere which has undergone translation and has its center aligned with the origin of our desired coordinate system. The representation of the sphere thus becomes:

$$\frac{X^2}{A^2} + \frac{Y^2}{A^2} + \frac{Z^2}{A^2} = 1, \quad (4.16)$$

where A is the radius of the sphere. As seen in step 1, intersection of the sphere with any $Z = |K|$, $-A \leq K \leq A$, will be a circle. Next, we determine the bounds within which inclined sub-planes of the $Z = |K|$ plane still result in circular intersections with the sphere.

Consider the points $E(0,0,K)$, $F(A,0,0)$, and $G(0,-A,0)$, where $K > 0$. The equation of the plane passing through these points is

$$-YK + AZ + KX - AK = 0.$$

Solving for Z and substituting in Equation (4.16), yields the equation of the intercept as

$$(A^2 + K^2)X^2 + Y^2(A^2 + K^2) - 2K^2XY + \dots = 0,$$

where only the necessary terms to determine the nature of the intercepted curve are retained. Proceeding with the discriminant test,

$$\delta = -4A^2[1 + 2K^2].$$

Since the discriminant is negative, the intercepts are ellipses or circles. Angular bounds are not needed since none of the other curves are ever intercepted. Similar results are obtained while considering inclined sub-planes of $X = |K|$ or $Y = |K|$. Figure 4-7 shows a lateral view of all the curves intersected in a sphere by various planes. Table 4-3 summarizes the various results obtained above.

PLANE	INTERSECTION
$Z = K$	Circle
$Y = K$	Circle
$X = K$	Circle
Any inclined sub-planes to $X=K$, $Y=K$, and $Z=K$	Ellipse

Table 4-3. Intersection of sphere with planes.

INTERSECTION OF A PLANE AND A SPHERE

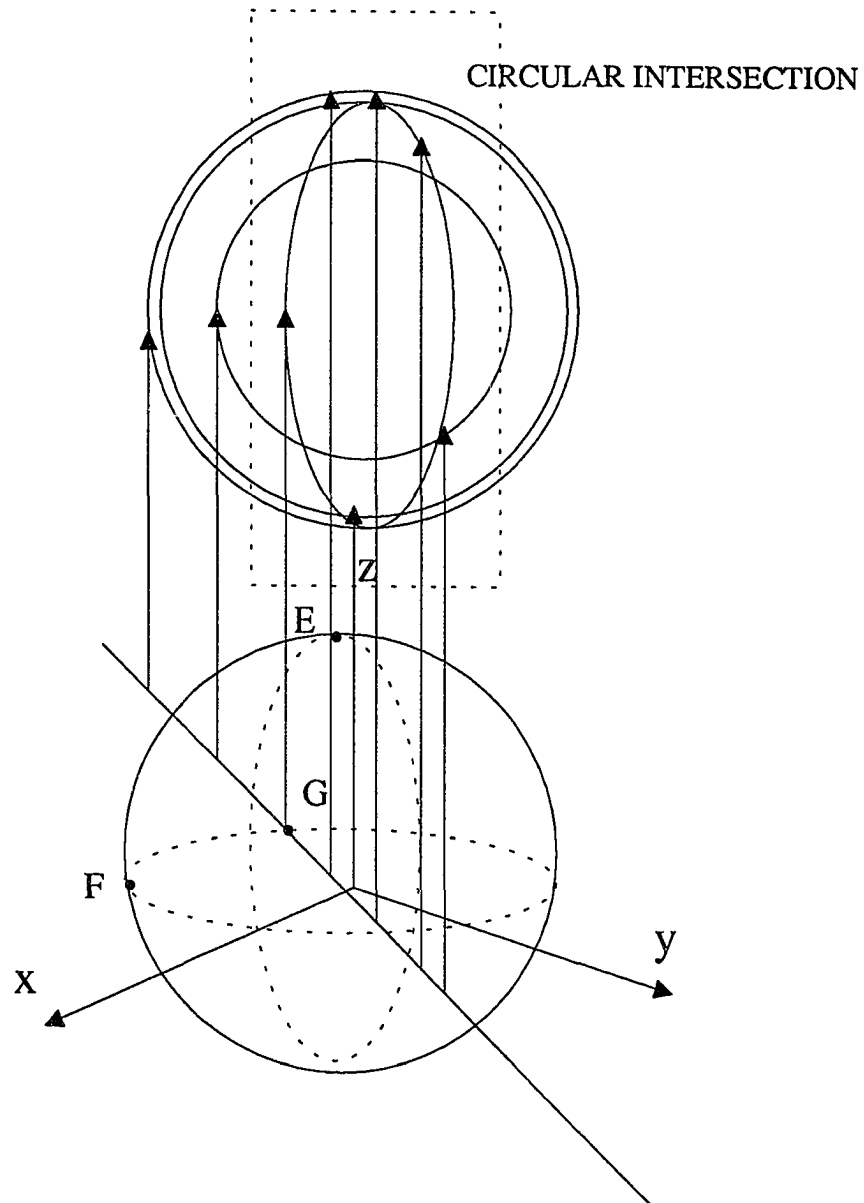


Figure 4-7. The intersection of plane and a sphere results in a circular line of intersection.

4.3.4 Quadric circular (elliptic) cone

Step 1:

The general representation of a circular cone on a plane parallel to the xy plane and its axis of revolution parallel to the z axis is

$$F(x,y,z) = bx^2 + by^2 + cz^2 + 2px + 2qy + 2rz + d = 0, \quad (4.17)$$

where $bc < 0$ and $d = \frac{p^2}{b} + \frac{q^2}{b} + \frac{r^2}{c}$.

From Equation (4.17), upon completing squares, we have

$$F(x,y,z) = b\left[x + \frac{p}{b}\right]^2 + b\left[y + \frac{q}{b}\right]^2 + c\left[z + \frac{r}{c}\right]^2 + d - \frac{p^2}{b} - \frac{q^2}{b} - \frac{r^2}{c} = 0. \quad (4.18)$$

Since $d = \frac{p^2}{b} + \frac{q^2}{b} + \frac{r^2}{c}$, Equation (4.18) becomes

$$F(x,y,z) = \frac{\left[x + \frac{p}{b}\right]^2}{\frac{1}{b}} + \frac{\left[y + \frac{q}{b}\right]^2}{\frac{1}{b}} - \frac{\left[z + \frac{r}{c}\right]^2}{\frac{-1}{c}} = 0. \quad (4.19)$$

In the case of the elliptic cone, Equation (4.17) reduces to

$$F(x,y,z) = \frac{\left[x + \frac{p}{a}\right]^2}{\frac{1}{a}} + \frac{\left[y + \frac{q}{b}\right]^2}{\frac{1}{b}} - \frac{\left[z + \frac{r}{c}\right]^2}{\frac{-1}{c}} = 0, \quad (4.20)$$

where $ab > 0$, $ac < 0$, and $bc < 0$. If $c < 0$, i.e., $b > 0$, the intersection of the cone represented by Equation (4.19) with plane 1 , i.e., $z = k$, where $\frac{-r}{c} - \sqrt{\frac{-1}{c}} < k < \frac{-r}{c} + \sqrt{\frac{-1}{c}}$, would generate

$$\frac{\left[x + \frac{p}{b}\right]^2}{\frac{1}{b}} + \frac{\left[y + \frac{q}{b}\right]^2}{\frac{1}{b}} = \frac{\left[k + \frac{r}{c}\right]^2}{-\frac{1}{c}}, \quad (4.21)$$

where $-\frac{1}{c}$ is a positive quantity. The above equation is that of a circle. The elliptic cone on the other hand which is represented by Equation (4.20), upon intersection with plane 1, i.e., $z = k$, where $\frac{-r}{c} - \sqrt{\frac{-1}{c}} < k < \frac{-r}{c} + \sqrt{\frac{-1}{c}}$, would generate

$$\frac{\left[x + \frac{p}{a}\right]^2}{\frac{1}{a}} + \frac{\left[y + \frac{q}{b}\right]^2}{\frac{1}{b}} = \frac{\left[k + \frac{r}{c}\right]^2}{-\frac{1}{c}}, \quad (4.22)$$

which is an ellipse. The intersection of the circular cone with plane 2, i.e., $y=k$, where $\frac{-q}{b} - \sqrt{\frac{1}{b}} < k < \frac{-q}{b} + \sqrt{\frac{1}{b}}$, would generate

$$\frac{\left[x + \frac{p}{b}\right]^2}{\frac{1}{b}} - \frac{\left[z + \frac{r}{c}\right]^2}{-\frac{1}{c}} = \frac{\left[k + \frac{q}{b}\right]^2}{\frac{1}{b}}, \quad (4.23)$$

where $-\frac{1}{c}$ is a positive quantity. Equation (4.23) represents a hyperbola. A similar result is obtained when the elliptic cylinder is intersected with plane 2.

Step 2:

The quadric representation of the elliptic cone illustrated in Figure 4-8 is

$$\frac{X^2}{A^2} + \frac{Y^2}{B^2} - \frac{Z^2}{C^2} = 0. \quad (4.24)$$

Intersection of the cone with horizontal planes $z = k$, where $-c < k < c$, generates ellipses as intercepts. Let us consider the horizontal plane $Z = -C$ and determine the various intercepts formed by its inclined sub-planes. The equation of the plane passing through the points $E(A,0,-C)$, $F(0,-B,-C)$, and $G(0,0,L)$ where $-C < L < C$, is

$$-A(C+L)Y + ABZ + B(C+L)X - ABL = 0.$$

Substituting Z in Equation (4.24) results in

$$B^2[C^2 - (C+L)^2]X^2 + A^2[C^2 - (C+L)^2]Y^2 - 2AB(C+L)^2XY + \dots = 0,$$

thereafter,

$$\delta = 4A^2B^2[(C+L)^4 - (L^2+2LC)^2].$$

Analyzing δ leads to the following bounds:

For $L \geq 0$ the intersections are hyperbolas.

For all values of L , $-C < L < 0$, except for $L = -C + \frac{C}{\sqrt{2}}$, the intersections are ellipses.

For the one particular case where $L = -C + \frac{C}{\sqrt{2}}$, the intersection is a parabola. In terms of θ , the angle between the $Z = -C$ plane and its inclined sub-plane is

$$\cos\theta = \frac{AB}{\sqrt{A^2(C+L)^2 + A^2B^2 + B^2(C+L)^2}}.$$

Next, consider the intersections formed by the plane $X = 0$ and its sub-planes.

Substituting $X = 0$ in Equation (4.24) leads to the intersection

$$\frac{Y^2}{B^2} - \frac{Z^2}{C^2} = 0,$$

which is a degenerate hyperbola. For all $-A < X < A$, the intercepts are hyperbolas.

DETAILED VIEW : HORIZONTAL INTERSECTIONS

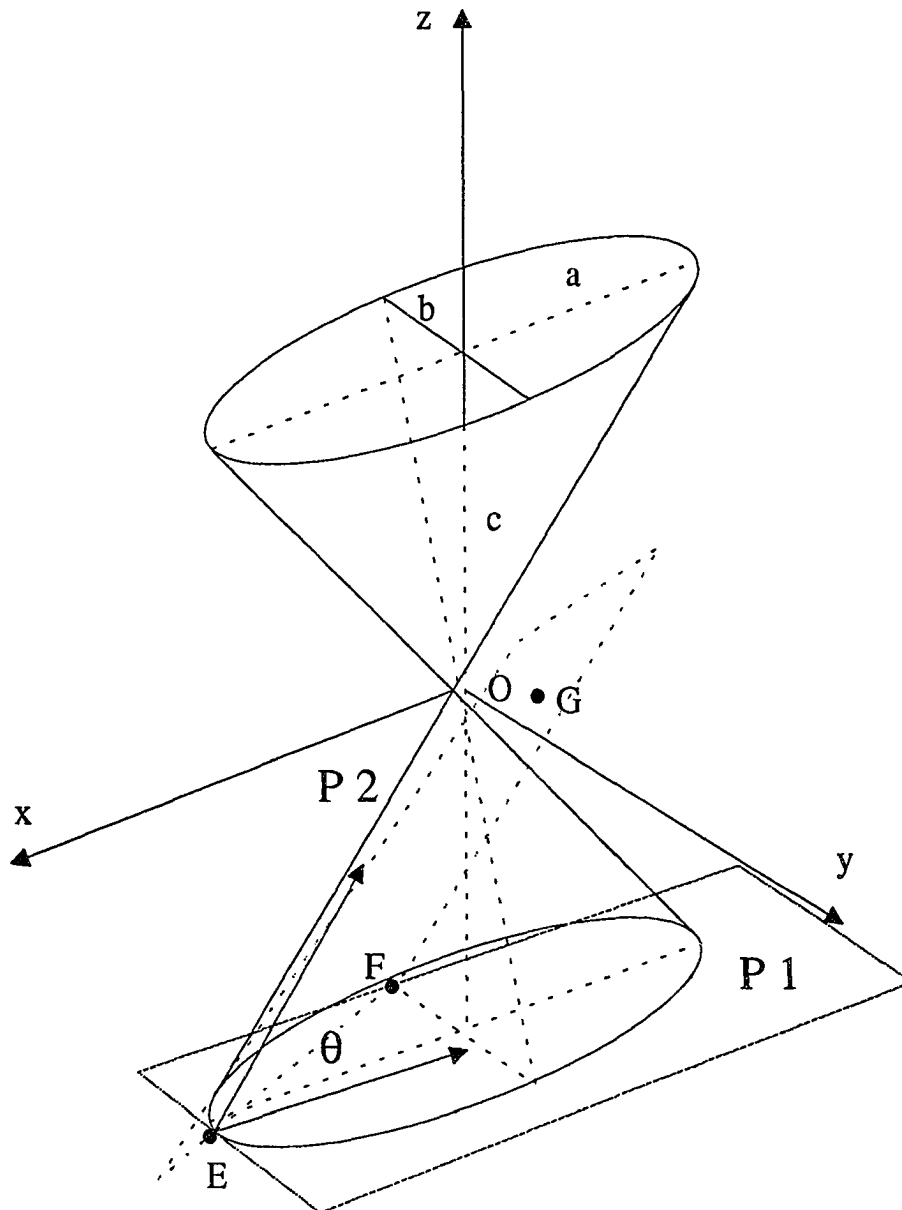


Figure 4-8. Plane P1 and planes parallel to it within the range $-c$ to c (except the one passing through the origin) generate ellipses. Plane P2 is the inclined sub-plane which denotes the maximum inclination or range (of plane P1) within which ellipses are generated. θ is the angular bound in terms of the angle.

The equation of the plane passing through the points $H(0,-B,-C)$, $I(0,B,-C)$, and $J(L,0,C)$, where $L > 0$ is

$$LZ - 2CX + LC = 0.$$

Solving for Z and substituting in Equation (4.24) leads to the representation of the intercept as

$$X^2[L^2 - 4A^2]B^2 + L^2A^2Y^2 + 4A^2B^2XL + \dots = 0. \quad (4.25)$$

Solving $L^2 - 4A^2$, indicates the following conditions for the various intercepts:

For $L = 2A$, the intercept is a parabola.

For all values of L , $-2A < L < 2A$, the intercepts are hyperbolas.

For all $L > 2A$, the intercepts are ellipses.

Figure 4-9 illustrates all of the above results. The angle between the $X = 0$ plane and its inclined sub-planes for the above obtained interceptions is

$$\cos\theta < \frac{+2C}{\sqrt{(L^2 + 4C^2)}}.$$

Figure 4-10 shows a lateral view of all possible curves intercepted in a quadric cone by the various planes. Table 4-4 summarizes all of the results obtained in this section.

4.3.5 Hyperboloid of one sheet

Step 1:

The general representation of a hyperboloid of one sheet resting on a plane parallel to the xy plane and its axis of revolution parallel to the z axis is

$$bx^2 + by^2 + cz^2 + 2px + 2qy + 2rz + d = 0, \quad (4.26)$$

where base of the cylinder is circular and $bc < 0$.

DETAILED VIEW : VERTICAL INTERSECTIONS

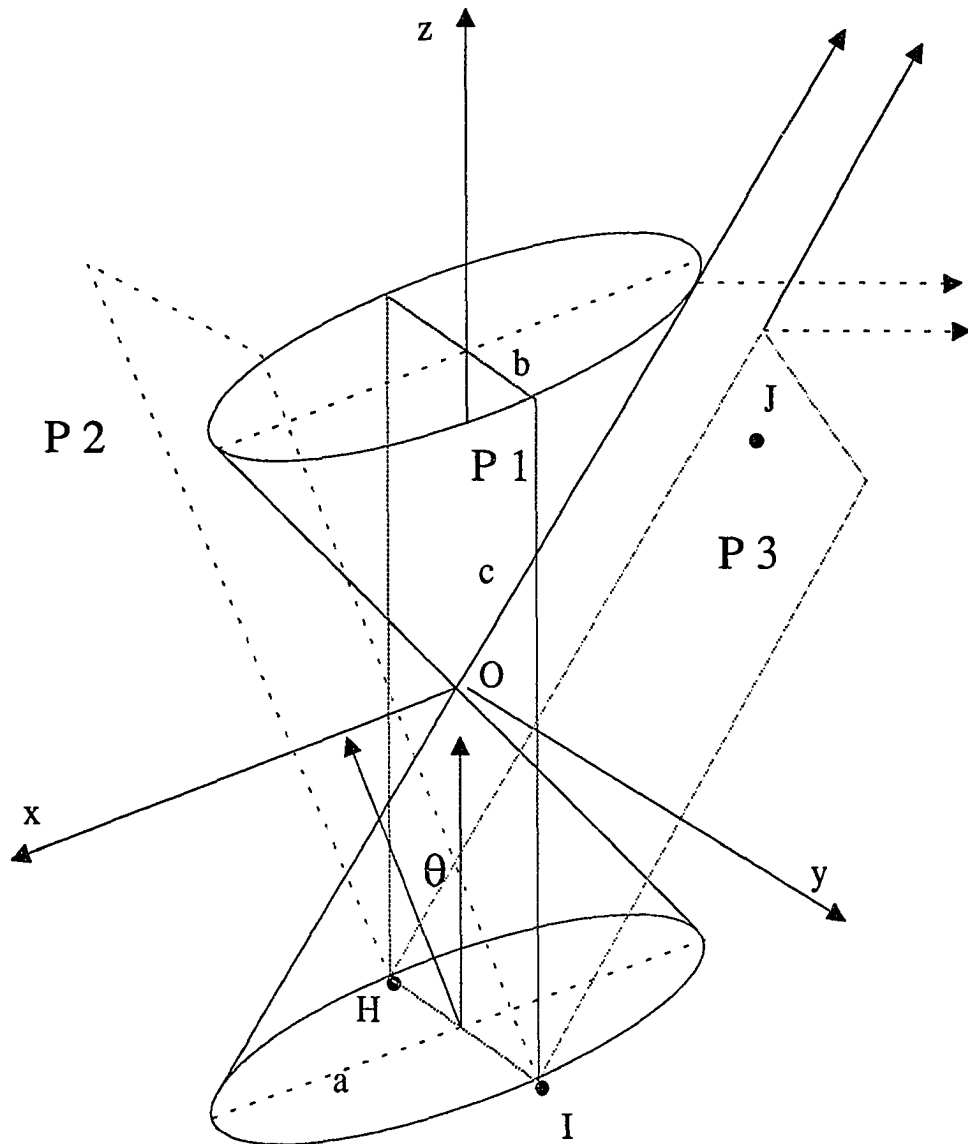


Figure 4-9. Plane P1 and planes parallel to it within the range $-b$ to b generates degenerate hyperbolas. Plane P2 is the inclined sub-plane which shows the outer region or the maximum inclination (of plane P1) within which hyperbolas are intercepted. θ is the angular bound in terms of the angle. Plane P3 is the only exception where the intersection is a parabola. In this case the inclination of the plane P3 is equal to the base angle of the cone.

LATERAL VIEW

INTERSECTION OF A PLANE AND A CONE

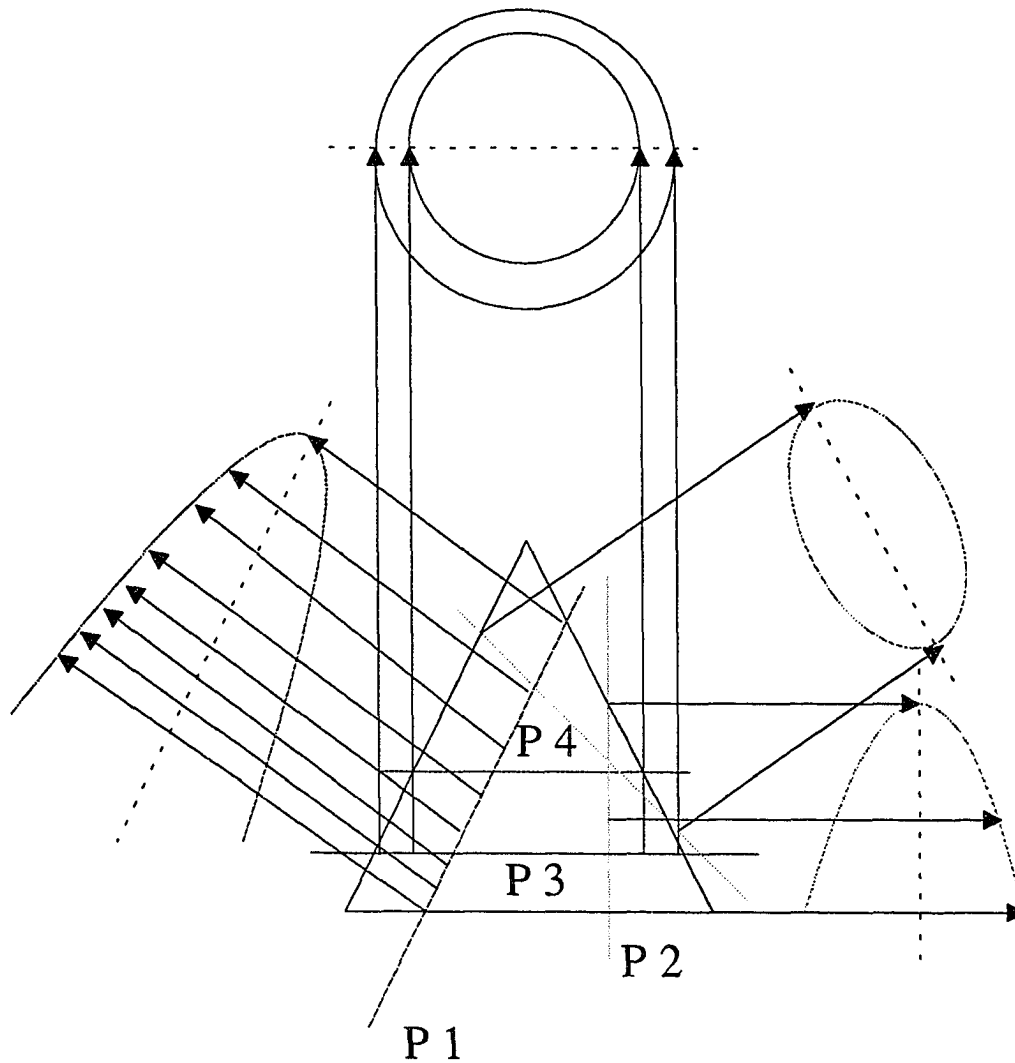


Figure 4-10. P1, P2, P3, and P4 are the four planes which generate all the intersections with the quadric cone. Plane P1 which has the same base angle as that of the cone intercepts a parabola. Plane P2 intercepts a hyperbola. Plane P3 intercepts a circle and finally plane P4 intercepts an ellipse. (The quadric cone under question has a circular base).

PLANE	INTERSECTION
$Z = K$	Circle, Ellipse
$X = K$	Hyperbola
Inclined sub-planes of $Z=K$, $L \geq 0$	Hyperbolas
Inclined sub-planes of $Z=K$, $-C < L < 0$	Ellipses
Inclined sub-planes of $Z=K$, $L = -C + \frac{C}{\sqrt{2}}$	Parabola
Inclined sub-planes of $X=K$, $L = 2A$	Parabola
Inclined sub-planes of $X=K$, $L < 2A$	Hyperbolas
Inclined sub-planes of $X=K$, $L > 2A$	Ellipses

Table 4-4. Intersection of quadric cone with planes.

Equation (4.26) upon completion of squares reduces to

$$F(x,y,z) = \frac{(x + \frac{p}{b})^2}{\frac{1}{b}} + \frac{(y + \frac{q}{b})^2}{\frac{1}{b}} + \frac{-(z + \frac{r}{c})^2}{\frac{-1}{c}} = 1,$$

where $d = \frac{p^2}{b} + \frac{q^2}{b} + \frac{r^2}{c} - 1$.

If $c < 0$, i.e., $b > 0$, intersection of the hyperboloid with plane **1**, i.e., $z = k$, where $-r/c - \sqrt{\frac{-1}{c}} < k < -r/c + \sqrt{\frac{-1}{c}}$, results in

$$\frac{(y + \frac{q}{b})^2}{\frac{1}{b}} + \frac{(x + \frac{p}{b})^2}{\frac{1}{b}} = 1 + \frac{(k + \frac{r}{c})^2}{\frac{-1}{c}}, \quad (4.27)$$

where $-1/c$ is a positive quantity. Equation (4.27) represents a circle. For a hyperboloid with elliptic base, this intersection will be an ellipse.

Intersection of the hyperboloid with plane **2**, i.e., $y = k$, where $-q/b - \sqrt{\frac{-1}{b}} < k < -q/b + \sqrt{\frac{-1}{b}}$, generates

$$\frac{(x + \frac{p}{b})^2}{\frac{1}{b}} - \frac{(z + \frac{r}{c})^2}{\frac{-1}{c}} = 1 - \frac{(k + \frac{q}{b})^2}{\frac{-1}{b}},$$

where $-1/c$ is a positive quantity. This equation is that of a hyperbola. Similar results are obtained when the hyperboloid has elliptic bases.

Step 2:

As in the case of the other quadric surfaces, the elliptic hyperboloid of one sheet shown in Figure 4-11 is assumed to have undergone translation such that its center is aligned with the origin of the coordinate system. The axis of the hyperboloid coincides with the z axis. Under these conditions the quadric representation of the hyperboloid is

$$\frac{X^2}{A^2} + \frac{Y^2}{B^2} - \frac{Z^2}{C^2} = 1. \quad (4.28)$$

The intersection of the hyperboloid with horizontal planes ranging from $Z = 0$ to $Z = |K|$ are ellipses, where $-C < K < C$ and A , B , and C are the semi-axes of the surface. The angular bounds of the various sub-planes with respect to the $Z = 0$ plane which intersects the hyperboloid in ellipses is determined next.

As shown in Figure 4-11, the equation of the plane passing through the points $D(A,0,0)$, $E(0,-B,0)$, and $F(K,0,C)$ where $|K| > 0$ is

$$-ACY + B(A-K)Z - BCX - ABC = 0.$$

Solving for Z and substituting in Equation (4.28) results in

$$X^2[B^2(A-K)^2 - A^2B^2] + Y^2[A^2(A-K)^2 - A^4] - 2A^3BXY + \dots = 0.$$

Proceeding with the discriminant test,

$$\delta = 4A^2B^2[A^2 + K^2 - 2AK][A^2 - K^2 + 2AK].$$

Since A and K are always positive, based upon the term

$$[A^2 - K^2 + 2AK],$$

DETAILED VIEW : HORIZONTAL INTERSECTIONS

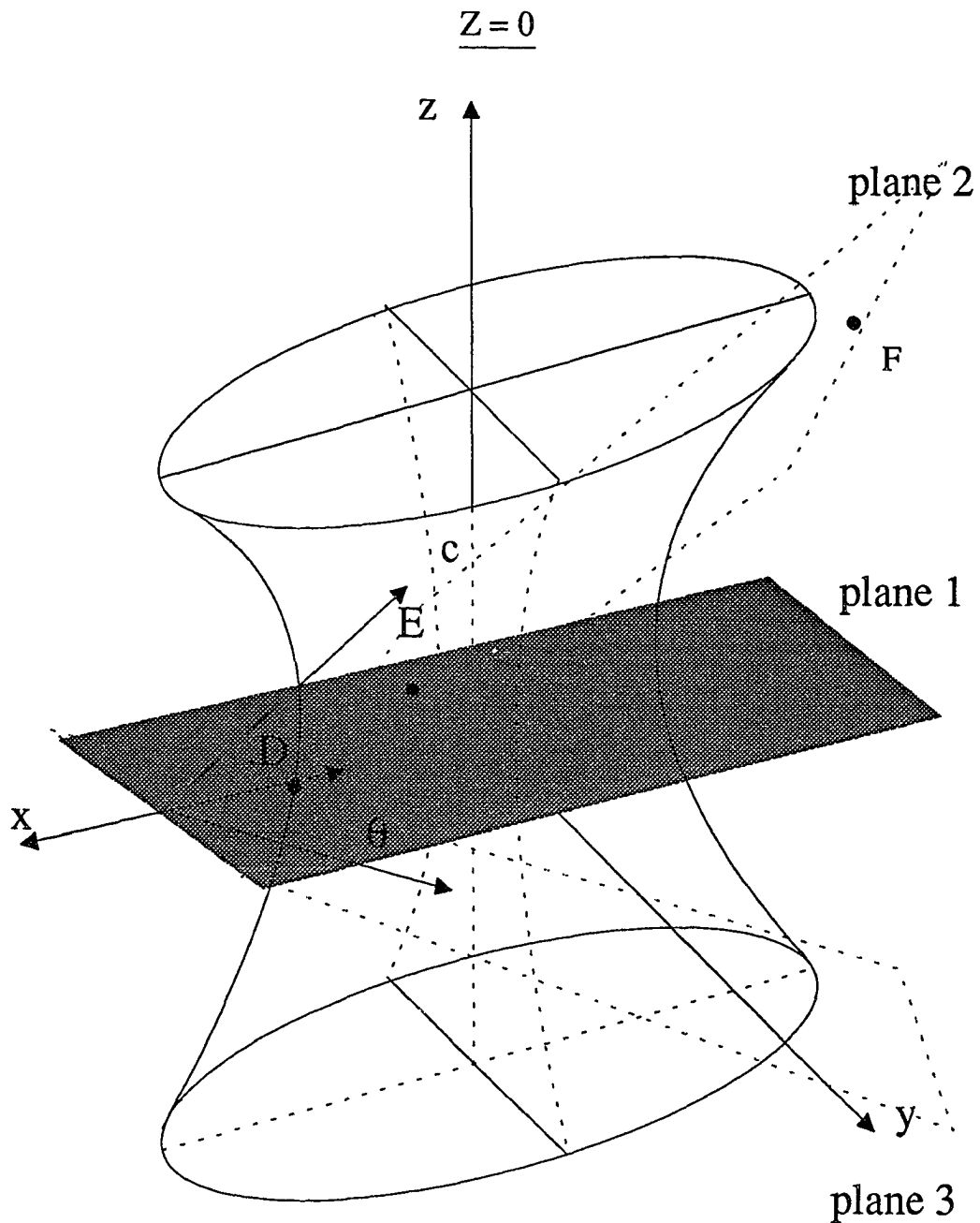


Figure 4-11. Plane 1 ($z = 0$) and all sub-planes parallel to it intersect the hyperboloid in ellipses. Plane 2 and plane 3 denote the maximum bound or inclination, within which the hyperboloid still intercepts ellipses.

a decision can be made whether the intersection is an ellipse, a hyperbola or a parabola. Solving for K , we determine that for

$K = A(-\sqrt{2} + 1)$, the intersection is a parabola,

$K > A(-\sqrt{2} + 1)$, the intersection is an ellipse, and

$K < A(-\sqrt{2} + 1)$, the intersections are hyperbolas. The inclination of the plane at each of these intersections is given as

$$\cos\theta = \frac{B(A - K)}{\sqrt{B^2(A-K)^2 + A^2C^2 + B^2C^2}}.$$

Next, consider intersection of the plane $Z = -C$ with the hyperboloid as shown in Figure 4-12. Substituting $Z = -C$ in Equation (4.28) results in the intersection

$$\frac{X^2}{A^2} + \frac{Y^2}{B^2} = 2,$$

which is an ellipse as expected. To determine the bounds at which the inclined $Z = -C$ plane still generates ellipses, consider the plane passing through the points $G(L,0,-C)$, $H(0,-B,-C)$, and $I(M,0,K)$, where $-C < K < C$, $|L| > |A|$. The equation of the plane results in

$$B(C + K)X - L(C + K)Y - B(L - M)Z - (2BCL + BLK - BCM) = 0.$$

Solving for Z and substituting in Equation (4.28) results in the intersection

$$X^2[C^2B^2(L - M)^2 - A^2B^2(C + K)^2] + Y^2[C^2B^2(L - M)^2 - A^2L^2(C + K)^2] + 2LBA^2(C + K)^2XY + \dots = 0.$$

Evaluating the discriminant leads to the following:

$$\delta = 4A^2B^2[L^2A^2(C + K)^4 - [C^2(L - M)^2 - A^2(C + K)^2][C^2(L - M)^2 - L^2(C + K)^2]]$$

The bounds for the various intercepts are obtained as follows:

$M = L$, the intersection is a parabola,

DETAILED VIEW : HORIZONTAL INTERSECTIONS

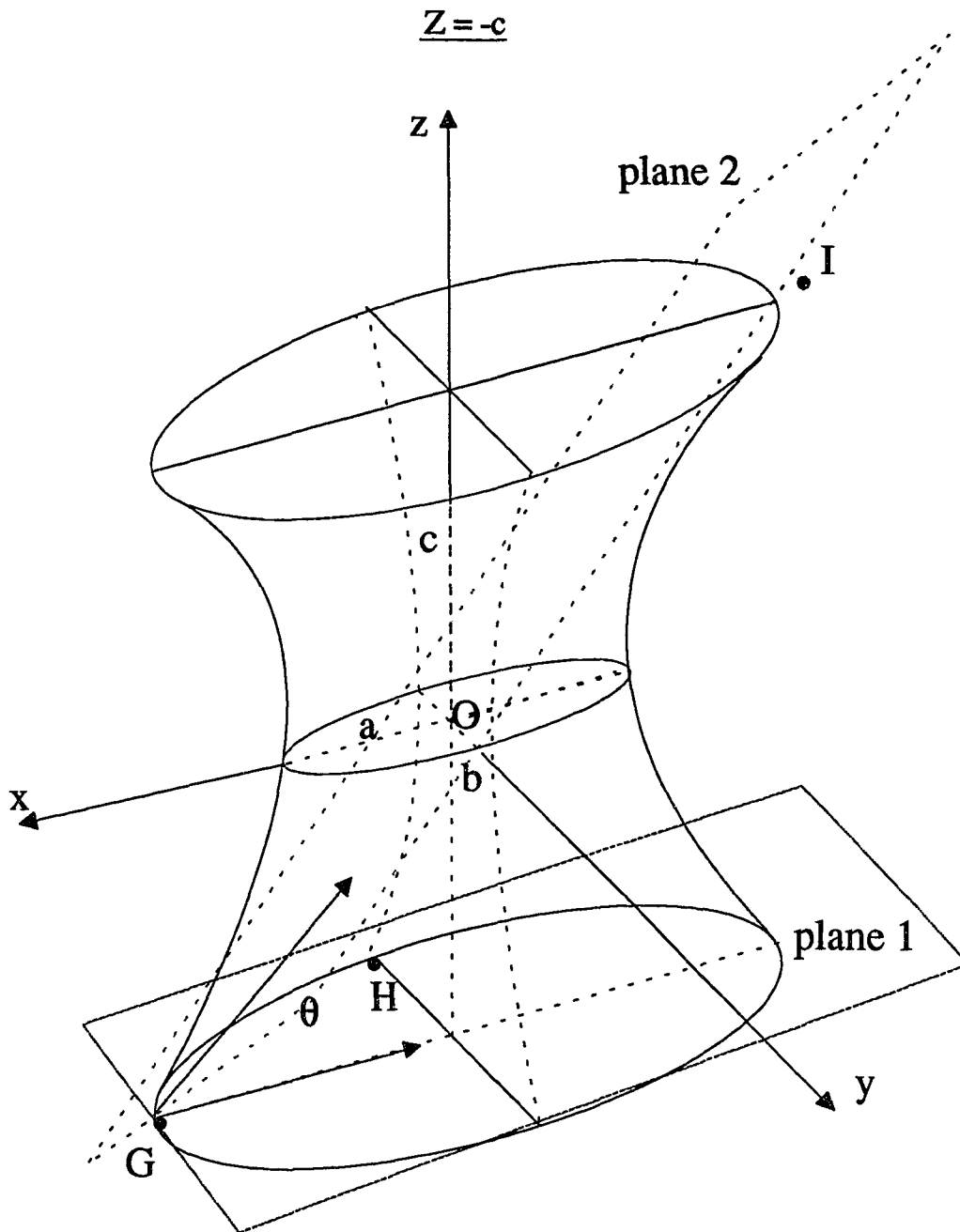


Figure 4-12. Plane 1 ($z = -c$) and all sub-planes parallel to it intersect the hyperboloid in ellipses. Plane 2 denotes the maximum bound or inclination, within which the hyperboloid still intercepts ellipses.

$M > L$, the intersection is a hyperbola, and

$M < L$, the intersection is an ellipse.

In terms of the angle,

$$\cos\theta = \frac{B(L - M)}{\sqrt{B^2(C + K)^2 + L^2(C + K)^2 + B^2(L - M)^2}}.$$

Next, consider the various intersections of the plane $X = 0$ and its inclined sub-planes as shown in Figure 4-13 with the hyperboloid. As seen before, for $-K < X < K$, the intercepts are hyperbolas. The equation of the plane passing through the points $J(0, B, -C)$, $M(0, B, -C)$, and $N(K, 0, C)$ is

$$-KZ + 2CX - KC = 0.$$

Solving for Z and substituting in Equation (4.28) results in the intersection

$$X^2(K^2 - 4A^2) + A^2K^2Y^2 + \frac{4X}{K} + \dots = 0.$$

It is observed that for all $K < |2A|$ the intersections are hyperbolas. However for the case $K = 2A$, the intersection takes the form

$$A^2K^2Y^2 + \frac{4X}{K} + \dots = 0,$$

which is a parabola. Similarly for the case $K > |2A|$ the intersections are ellipses. In terms of the angle, the bounds for the plane $X = 0$ are

$$\cos\theta < \frac{2C}{\sqrt{K^2 + 4C^2}}.$$

Figure 4-14 shows the lateral view of the various curves intercepted in a hyperboloid by various planes. Table 4-5 summarizes the results obtained in this section.

DETAILED VIEW : VERTICAL INTERSECTIONS

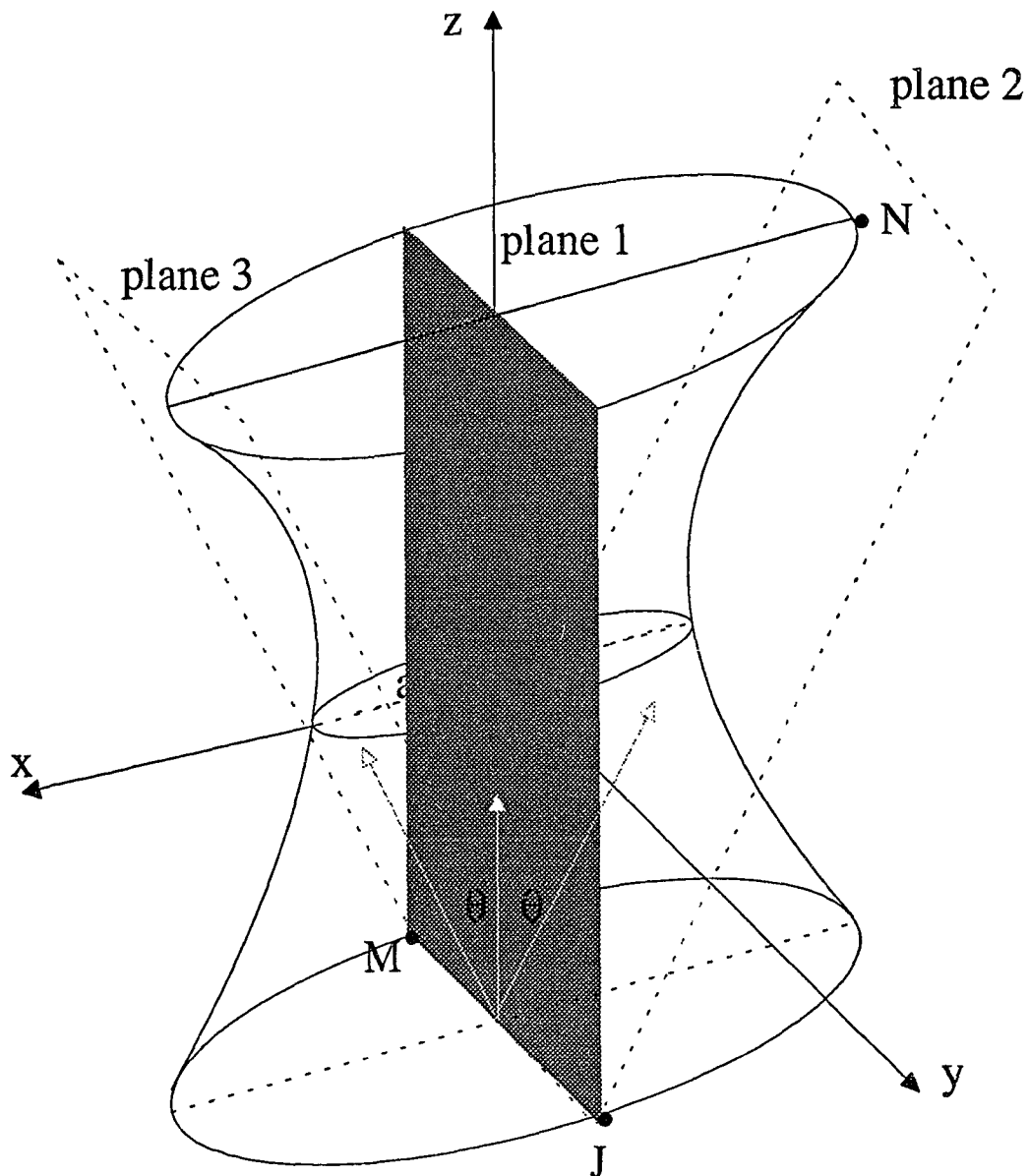


Figure 4-13. Plane 1 and all sub-planes parallel to it intersect the hyperboloid in hyperbolas. The inclined sub-planes of plane 1 which are denoted in the above figure by plane 2 and plane 3 determine the maximum range or bound wherein hyperbolas are still intercepted. Beyond this range the hyperboloid intersects various planes in ellipses except the case when the plane makes an angle of δ , under which case the intercepted curve is a parabola.

LATERAL VIEW

INTERSECTION OF A PLANE AND HYPERBOLOID OF ONE SHEET

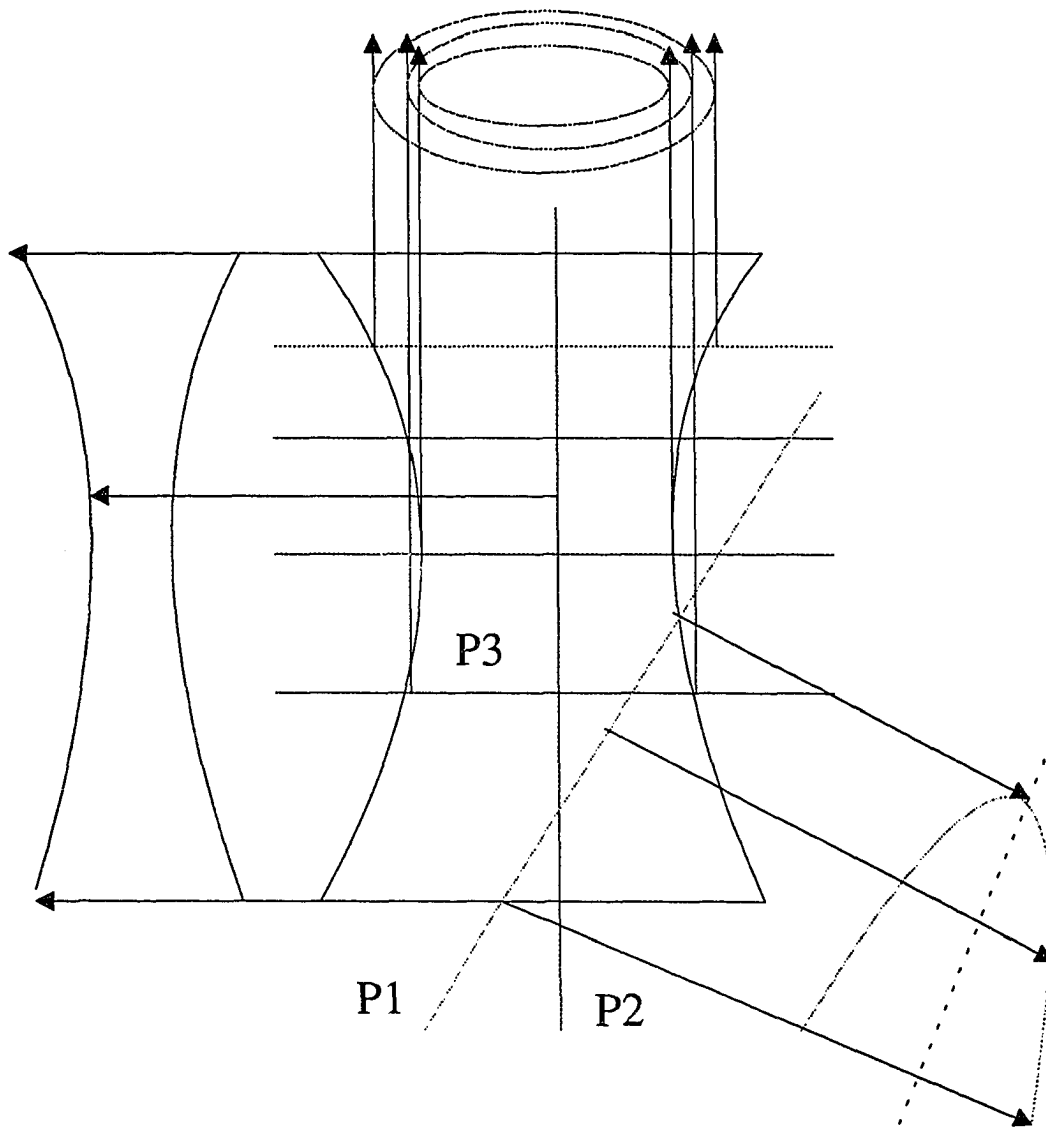


Figure 4-14. Plane P1 intersects the hyperboloid in a parabola, plane P2 and all planes parallel to it intersect the hyperboloid in hyperbolas. Plane P3 and all planes parallel to it in the range $-c$ to $+c$ intersect the hyperboloid in ellipses.

PLANE	INTERSECTION
$Z = K$	Circle, Ellipse
$X = K$	Hyperbola
Inclined sub-planes of $Z=0$, $K=A(-\sqrt{2} + 1)$	Parabola
Inclined sub-planes of $Z=0$, $K>A(-\sqrt{2} + 1)$	Ellipse
Inclined sub-planes of $Z=0$, $K<A(-\sqrt{2} + 1)$	Hyperbola
Inclined sub-planes of $Z=-C$, $ Z < C$	Ellipse
Inclined sub-planes of $Z=-C$, $ Z > C$	Hyperbola
Inclined sub-planes of $X=K$, $K < 2A $	Hyperbola
Inclined sub-planes of $X=K$, $K = 2A$	Parabola
Inclined sub-planes of $X=K$, $K > 2A $	Ellipses

Table 4-5. Intersection of hyperboloid of one sheet with planes.

4.3.6 Hyperboloid of two sheets

Step 1:

Unlike the hyperboloid of one sheet, the hyperboloid of two sheets consists of two separate pieces. The quadric representation of a hyperboloid of two sheets lying on a plane parallel to the xy plane is

$$bx^2 + by^2 + cz^2 + 2px + 2qy + 2rz + d = 0, \quad (4.29)$$

where the base of the hyperboloid is circular, $bc < 0$. Completing squares results in

$$F(x,y,z) = \frac{(x + \frac{p}{b})^2}{\frac{1}{b}} + \frac{(y + \frac{q}{b})^2}{\frac{1}{b}} + \frac{-(z + \frac{r}{c})^2}{\frac{-1}{c}} = -1,$$

where $d = \frac{p^2}{b} + \frac{q^2}{b} + \frac{r^2}{c} + 1$, and $-1/c$ is a positive quantity. Intersection of the object with the plane 1, i.e., $z = k$, where $|k| > \sqrt{-1/c}$, results in

$$\frac{(x + \frac{p}{b})^2}{\frac{1}{b}} + \frac{(y + \frac{q}{b})^2}{\frac{1}{b}} = -1 + \frac{(k + \frac{r}{c})^2}{\frac{-1}{c}},$$

where $-1/c$ is a positive quantity. This equation is of a circle. For a hyperboloid with an elliptic base, this intersection will be an ellipse. However, when $|k| = \sqrt{-1/c}$, the intersection will result in a point.

Consider the case when the object is intersected with the plane 2, i.e., $y = k$, where $-q/b - \sqrt{\frac{1}{b}} < k < -q/b + \sqrt{\frac{1}{b}}$. This intersection results in

$$\frac{-(x + \frac{p}{b})^2}{\frac{1}{b}} + \frac{-(z + \frac{r}{c})^2}{\frac{-1}{c}} = \frac{(k + \frac{q}{b})^2}{\frac{-1}{b}} + 1,$$

which is an equation of a hyperbola. Similar results are obtained for a hyperboloid with an elliptic base.

Step 2:

As in the case of the hyperboloid of one sheet, the elliptic hyperboloid of two sheets is assumed to have undergone translation so that its center is aligned with the origin of the coordinate system as shown in Figure 4-15. The axis of the hyperboloid coincides with the z axis. Under these conditions the quadric representation of the hyperboloid is

$$\frac{X^2}{A^2} + \frac{Y^2}{B^2} - \frac{Z^2}{C^2} = -1. \quad (4.30)$$

The intersection of the hyperboloid with the horizontal plane $Z = K$, $|K| < C$, is an imaginary ellipse. For $|K| > C$, the horizontal plane will intersect ellipses as seen from Equation (4.30).

Consider the case where $Z = -T$, where T refers to the length of segment OG . Substituting in Equation (4.30) leads to the intersection

$$\frac{X^2}{A^2} + \frac{Y^2}{B^2} = \frac{T^2}{C^2} - 1,$$

which is an ellipse. Let us now determine the bounds wherein the inclined sub-planes of the plane $Z = -T$ still intersect the hyperboloid in an ellipse. Equation of the plane passing through the points $D(A,0,-T)$, $E(0,-B,-T)$, and $G(0,0,L)$, where $-T < L < T$ is

$$A(T+L)Y - ABZ - B(T+L)X + ABL = 0.$$

Solving for Z , and substituting in Equation (4.30) yields

$$B^2(C^2 - (T+L)^2)X^2 + A^2(C^2 - (T+L)^2)Y^2 + 2AB(T+L)^2XY + \dots = 0.$$

Discriminant

$$\delta = 4A^2B^2[(T+L)^4 - [(C^2 - (T+L)^2)^2]].$$

The bounds for the various curves are obtained as follows:

For $L = \frac{C}{\sqrt{2}} - T$, the intersection is a parabola,

for $L > \frac{C}{\sqrt{2}} - T$, the intersection is a hyperbola, and

for $L < \frac{C}{\sqrt{2}} - T$, the intersection is an ellipse.

DETAILED VIEW : HORIZONTAL INTERSECTIONS

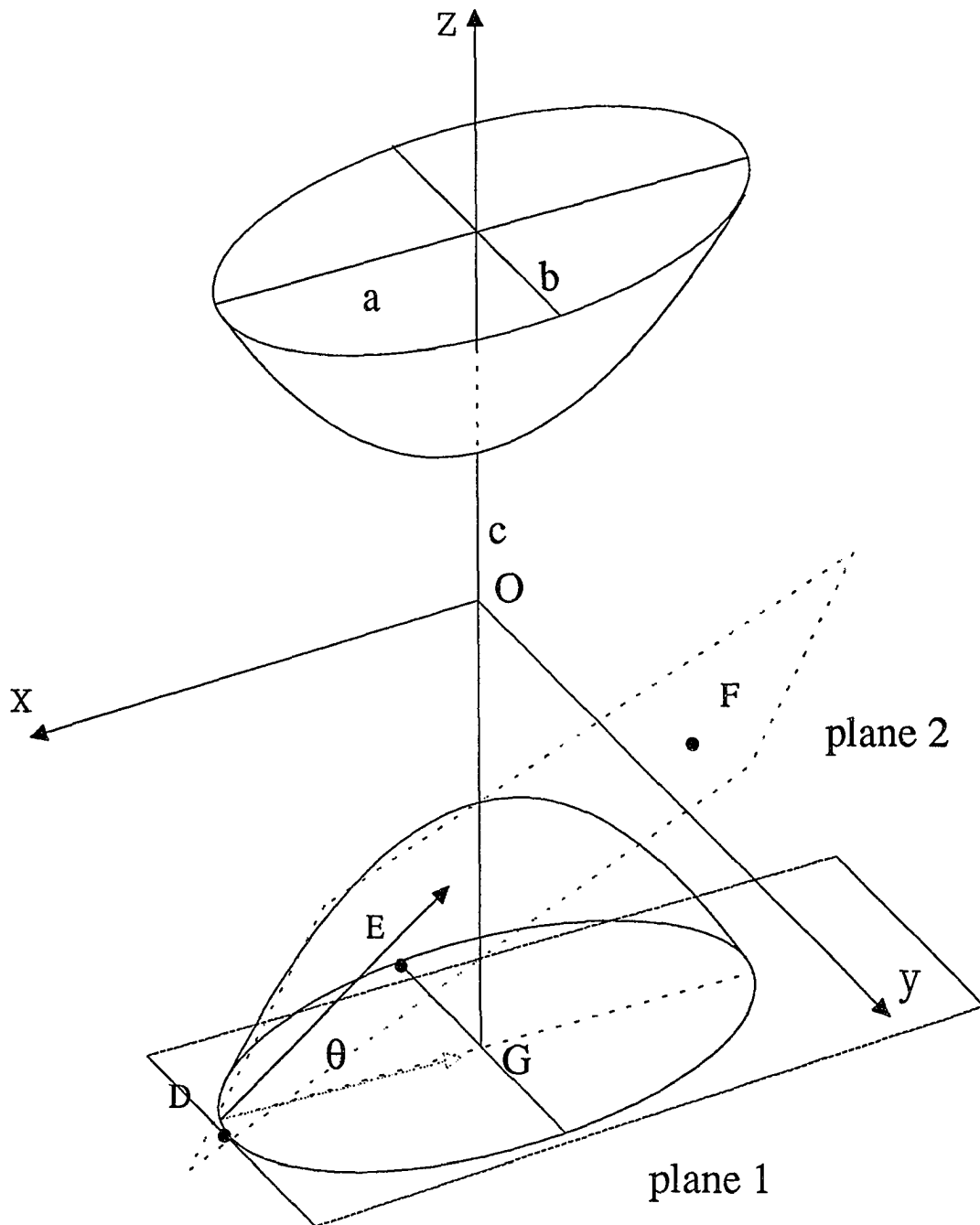


Figure 4-15. Plane 1 ($z=-k, |k| > |c|$) and all its inclined sub-planes which span angle θ intersect the hyperboloid (of two sheets) in ellipses.

Angle θ at each of these values of L is determined as

$$\cos\theta = \frac{AB}{\sqrt{-A^2(-T+C)^2 + A^2B^2 + B^2(-T+C)^2}}.$$

Next, consider the vertical plane $X = 0$ and its inclined sub-planes. Substituting $X = 0$ in Equation (4.30) yields the equation of a hyperbola.

To determine the angular bounds of the various intercepts formed through the intersection of the inclined sub-planes and the hyperboloid, consider the plane shown in Figure 4-16. The equation of the plane passing through the points $H(0,B,-T)$, $I(0,-B,-T)$, and $J(L,0,T)$ is

$$LZ + 2TX + LT = 0.$$

Solving for Z and substituting in Equation (4.30) yields

$$\frac{X^2}{A^2} + \frac{Y^2}{B^2} - \frac{[2TX + LT]^2}{L^2C^2} = -1.$$

Expanding and re-arranging the terms, leads to the equation of the intercept as

$$B^2(L^2C^2 - 4A^2T^2)X^2 + A^2L^2C^2Y^2 + 4T^2A^2B^2LX - A^2B^2L^2(C^2 - T^2) + \dots = 0.$$

Based upon the term $L^2C^2 - 4A^2T^2$ which is the coefficient of X^2 , a decision can be made about the nature of the intercept. Since $C < T$, for all values $L \leq 2A$, the intercept will be a hyperbola. The coefficient of X^2 will disappear when $L = \frac{2AT}{C}$, which case the intersection is a parabola. For all other cases, i.e., $L \geq 2A$, the intersections are ellipses.

In terms of θ , where hyperbolas are intersected, the angle between the two planes is

$$\cos\theta = \frac{2T}{\sqrt{L^2 + 4T^2}}.$$

DETAILED VIEW : VERTICAL INTERSECTIONS

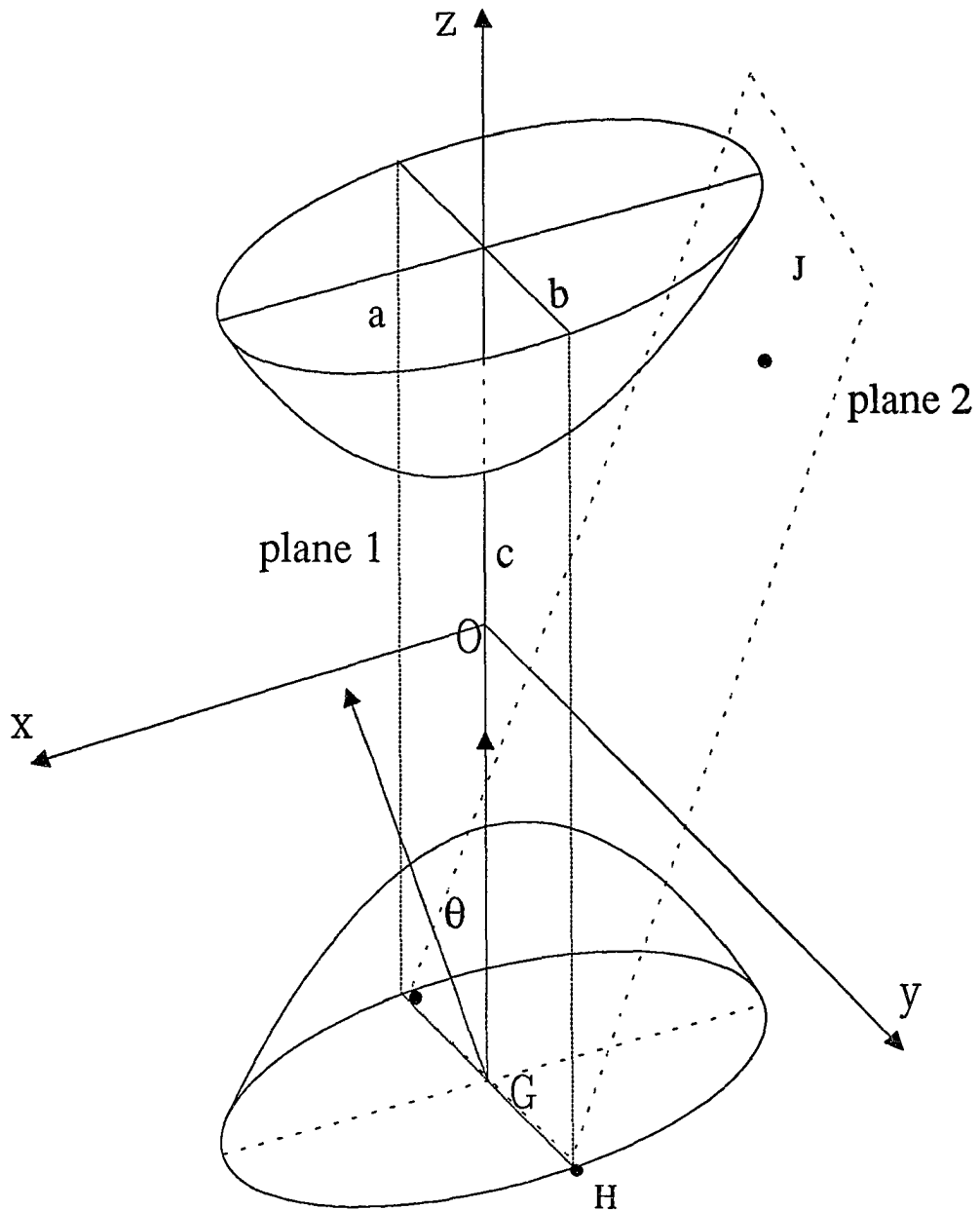


Figure 4-16. Plane 1 ($x=0$) and all its inclined sub-planes, plane 2 being one of them, spans angle θ while intersecting the hyperboloid (of two sheets) in hyperbolas.

Figure 4-17 shows the lateral view of all the curves intercepted in a hyperboloid of two sheets by various planes. Table 4-6 summarizes the results obtained above.

PLANE	INTERSECTION
$Z = K$	Circle, Ellipse
$Z = K, K > c$	Circle, ellipse
$Z = K, K = c$	Point
$Z = K, K < c$	Imaginary ellipse
$Z = -T$	Ellipse
$X = K$	Hyperbola
Inclined sub-planes of $Z=-T, L = -C$	Hyperbola
Inclined sub-planes of $Z=-T, L = \frac{C}{\sqrt{2}} - T$	Parabola
Inclined sub-planes of $Z=-T, L > \frac{C}{\sqrt{2}} - T$	Hyperbola
Inclined sub-planes of $Z=-T, L < \frac{C}{\sqrt{2}} - T$	Ellipse
Inclined sub-planes of $X = K, L \leq 2A$	Hyperbola
Inclined sub-planes of $X = K, L \leq \frac{2AT}{C}$	Parabola
Inclined sub-planes of $X = K, L \geq 2A$	Ellipse

Table 4-6. Intersection of hyperboloid of two sheets with planes.

LATERAL VIEW

INTERSECTION OF THE HYPERBOLOID OF TWO SHEETS

WITH PLANES

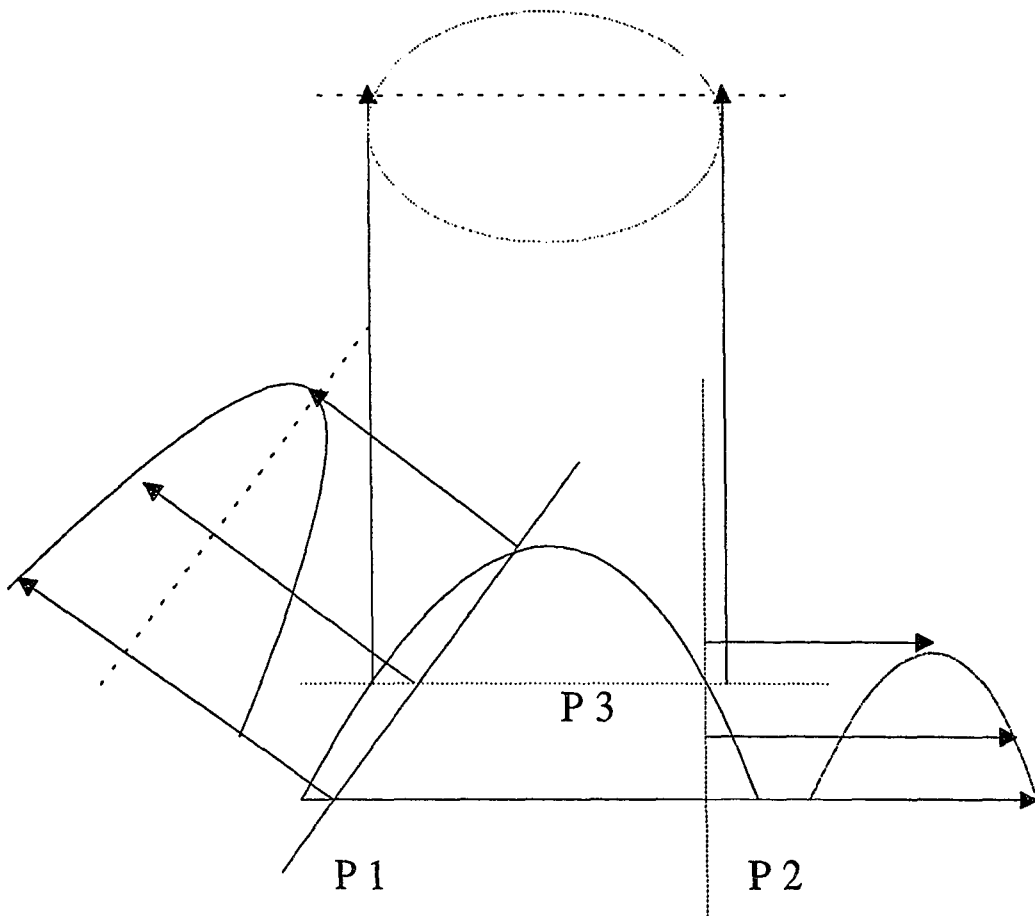


Figure 4-17. Plane P1 intersects the hyperboloid in a parabola, plane P3 and all planes parallel to it intersect the hyperboloid in ellipses, and finally, plane P2 and all planes parallel to it intersect the hyperboloid in hyperbolas.

4.3.7 Elliptic paraboloid

Step 1:

The quadric representation of the elliptic paraboloid resting on a plane parallel to the xy plane is

$$ax^2 + by^2 + 2px + 2qy + 2rz + d = 0. \quad (4.31)$$

Equation (4.31) upon completing squares, reduces to the form

$$\frac{(x + \frac{p}{a})^2}{\frac{1}{a}} + \frac{(y + \frac{q}{b})^2}{\frac{1}{b}} + \frac{z}{\frac{1}{2r}} = 0$$

only if $d = \frac{p^2}{a} + \frac{q^2}{b}$. $\sqrt{\frac{1}{a}}$, $\sqrt{\frac{1}{b}}$ are the semi-major and minor axes of the paraboloid, whereas $1/2r$ is the height of the paraboloid.

Consider the intersection of the elliptic paraboloid with the plane **1**, i.e., $z = k$, where $0 < k < 1/2r$. The equation of the intercept is

$$\frac{(x + \frac{p}{a})^2}{\frac{1}{a}} + \frac{(y + \frac{q}{b})^2}{\frac{1}{b}} = \frac{-k}{\frac{1}{2r}}, \quad (4.32)$$

where $\frac{-k}{1/2r}$ is a positive quantity. Equation (4.32) is that of an ellipse.

Consider the intersection of the surface with the plane **2**, i.e., $y = k$, where $\frac{-q}{b} - \sqrt{\frac{1}{b}} < k < \frac{-q}{b} + \sqrt{\frac{1}{b}}$. The curve intercepted is the parabola

$$\frac{(x + \frac{p}{a})^2}{1/a} = - \left[\frac{z}{1/2r} - \frac{(k + \frac{q}{b})^2}{1/b} \right].$$

Step 2:

Unlike step 1, the elliptic paraboloid in this section has undergone translation. Hence, its center is aligned with the origin of the coordinate system as shown in Figure 4-18. The axis of the paraboloid coincides with the z axis. Thus, the quadric representation of the surface is

$$\frac{X^2}{A^2} + \frac{Y^2}{B^2} + 2Z = 0. \quad (4.33)$$

Intersection of the elliptic paraboloid with planes $X = K$ and $Y = K$ where $-A \leq K \leq A$, and $-B \leq K \leq B$, respectively, will yield parabolas as discussed in step 1. Also, the planes $Z = K$, where $K < 0$, intersect the paraboloid in ellipses. Consider the intersection of the horizontal plane $Z = -L$ (where L is the length of the segment OG) and its inclined sub-planes with the paraboloid. The equation of the plane passing through the points $D(A,0,-L)$ (where L is the length of the segment OG , and "a" is the semi-minor axis), $E(0,-B,-L)$, and $F(0,0,K)$, $|K| \geq 0$, is

$$-A(K+L)Y + ABZ + B(L+K)X - ABK = 0.$$

Solving for Z and substituting in Equation (4.32) yields the equation of the intercept as

$$\frac{X^2}{A^2} + \frac{Y^2}{B^2} + 2\left(\frac{A(K+L)Y - B(K+L)X + ABK}{AB}\right) = 0.$$

Substituting $K = -L$ will intercept the ellipse

$$\frac{X^2}{A^2} + \frac{Y^2}{B^2} = 2L.$$

Consider the case where $K = 0$. Under this condition the resultant intercept is

$$\frac{X^2}{A^2} + \frac{Y^2}{B^2} + \frac{LY}{B} - \frac{LX}{A} = 0,$$

which is an ellipse. Hence in the range $-L \leq Z \leq 0$, the inclined sub-planes of

DETAILED VIEW : HORIZONTAL INTERSECTIONS

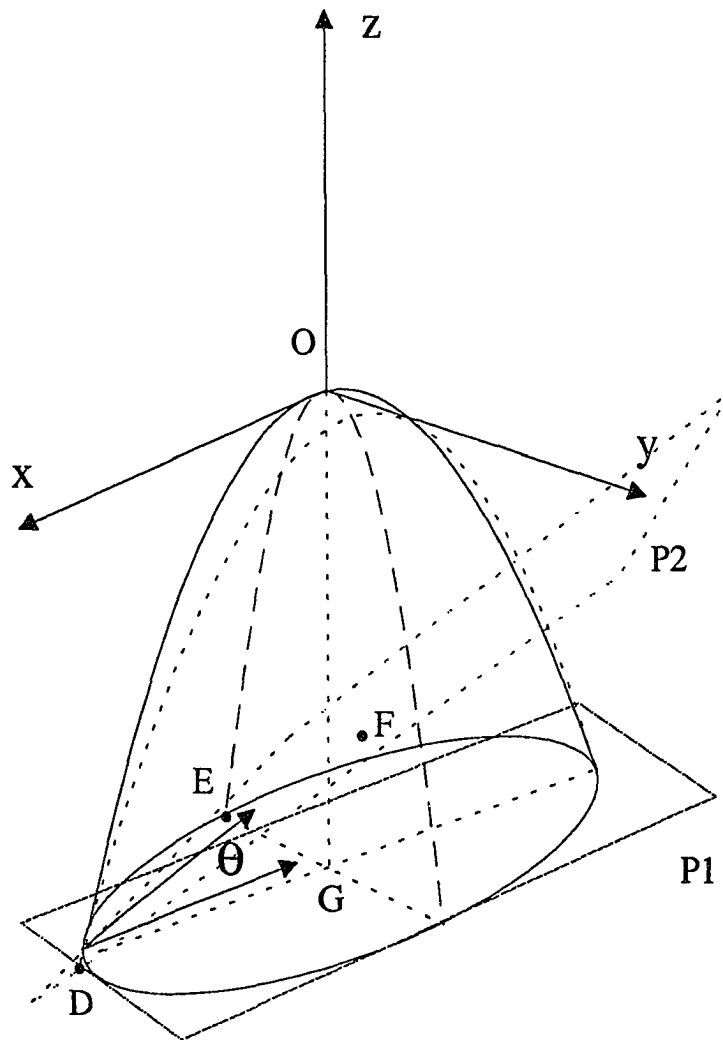


Figure 4-18. Plane P1 and planes parallel to it intersect the paraboloid in ellipses. Plane P2 is one of the inclined sub-planes which determines the maximum inclination or range (of plane P1) within which ellipses are still generated. θ is the angular bound in terms of the angle.

$Z = -L$, intercept ellipses. Analyzing the discriminant δ leads to the following bounds:

$$0 < \cos\theta \leq \frac{AB}{\sqrt{(A^2(K+L)^2 - A^2B^2 - B^2(L+K)^2)}}.$$

Next, consider the various intersections made by the plane $X = 0$ and its inclined sub-planes as illustrated in Figure 4-19. The plane $X = 0$ generates the intercept

$$\frac{Y^2}{B^2} + 2Z = 0,$$

which is a parabola. Consider the plane passing through the points $H(0,-B,-L)$, $I(0,B,-L)$, and $J(N,0,M)$, where $-L < M < 0$, and $0 < N < A$. The equation of the plane is found to be

$$NZ - (L+M)X + LN = 0.$$

Solving for X and substituting in Equation (4.32) yields the intercept

$$\frac{N^2Z^2}{(L+M)^2A^2} + \frac{2LN^2Z}{A^2(L+M)} + 2Z + \frac{Y^2}{B^2} = 0,$$

which represents ellipses, except when $N = 0$.

Hence all inclined sub-planes of the plane $X = K$, where $-A < K < A$, yield intercepts as ellipses. In terms of θ ,

$$\cos\theta < \frac{+(L+M)}{\sqrt{(N^2 - (L+M)^2)}}. \quad (4.34)$$

Equation (4.34) denotes the angular bounds within which the intersections are all ellipses. Table 4-7 summarizes the various conics obtained when various planes intersect the elliptic paraboloid.

DETAILED VIEW : VERTICAL INTERSECTIONS

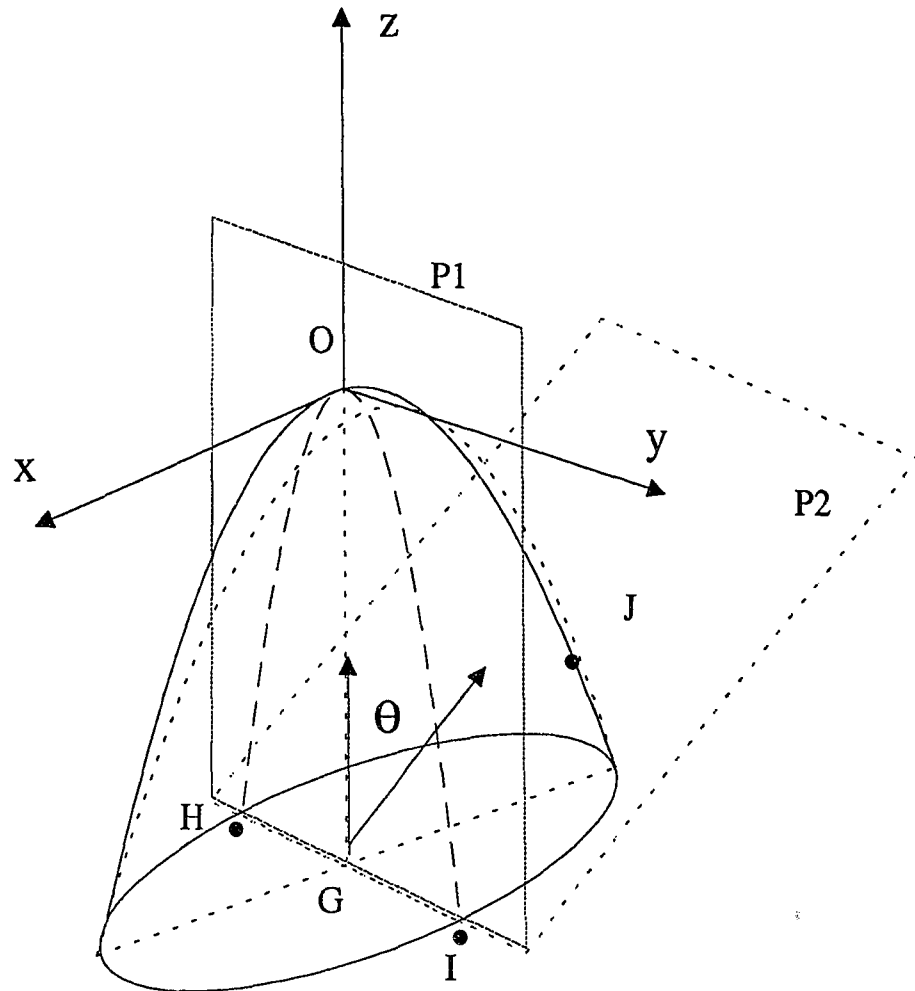


Figure 4-19. Plane P1 ($x=0$) and all planes parallel to it intersect the paraboloid in parabolas. The inclined plane P2 determines the range within which parabolas are still intersected. After an angular span of θ , the plane intersects the paraboloid in ellipses.

PLANE	INTERSECTION
$Z = K$	Ellipse
$X = K$	Parabola
$Y = K$	Parabola
Inclined sub-planes of $Z = -L$	Ellipse
Inclined sub-planes of $X = 0$	Ellipse

Table 4-7. Intersection of elliptic paraboloid with planes.

4.3.8 Hyperbolic paraboloid

Step 1:

Unlike the elliptic paraboloid, the hyperbolic paraboloid is symmetrical with respect to the xz plane, the yz plane and the z axis. Its representation is as follows:

$$ax^2 + by^2 + 2px + 2qy + 2rz + d = 0. \quad (4.35)$$

In this case, however, $ab < 0$. Upon completing squares we have

$$\frac{(x + \frac{p}{a})^2}{\frac{1}{a}} - \frac{(y + \frac{q}{b})^2}{-\frac{1}{b}} + \frac{z}{\frac{1}{2r}} = 0$$

only if $d = \frac{p^2}{a} + \frac{q^2}{b}$ and $\frac{-1}{b}$ is a positive quantity.

Intersecting the surface with plane **1**, i.e, $z = k$, results in

$$\frac{(x + \frac{p}{a})^2}{\frac{1}{a}} - \frac{(y + \frac{q}{b})^2}{-\frac{1}{b}} = \frac{-k}{\frac{1}{2r}},$$

where $-1/b$ is a positive quantity. This equation is that of a hyperbola. In the case when $z = k = 0$, it results in a pair of parallel lines which is a degenerate case of a hyperbola.

Consider the case when the object is intersected with plane 2, i.e., $y = k$, then

$$\frac{(x + \frac{p}{a})^2}{\frac{1}{a}} + \frac{z}{\frac{1}{2r}} = \frac{(k + \frac{q}{a})^2}{-\frac{1}{b}},$$

which is an equation of a parabola. The two planes considered in step 1 by themselves prove sufficient enough to distinguish the hyperbolic paraboloid from all the other quadric surfaces considered for the recognition process. Hence, angular bounds to extract the regions where a unique set of features (curves) is obtained are not necessary in the case of this quadric surface. However, Figures 4-20 and 4-21 illustrate the regions, if necessary, where extra features (curves) can be evaluated. Table 4-8 summarizes the curves intercepted by planes 1 and 2 with the hyperbolic paraboloid.

PLANE	INTERSECTION
Z = K	Hyperbola
X = K	Parabola
Y = K	Parabola

Table 4-8. Intersection of hyperbolic paraboloid with planes.

DETAILED VIEW : HORIZONTAL INTERSECTIONS

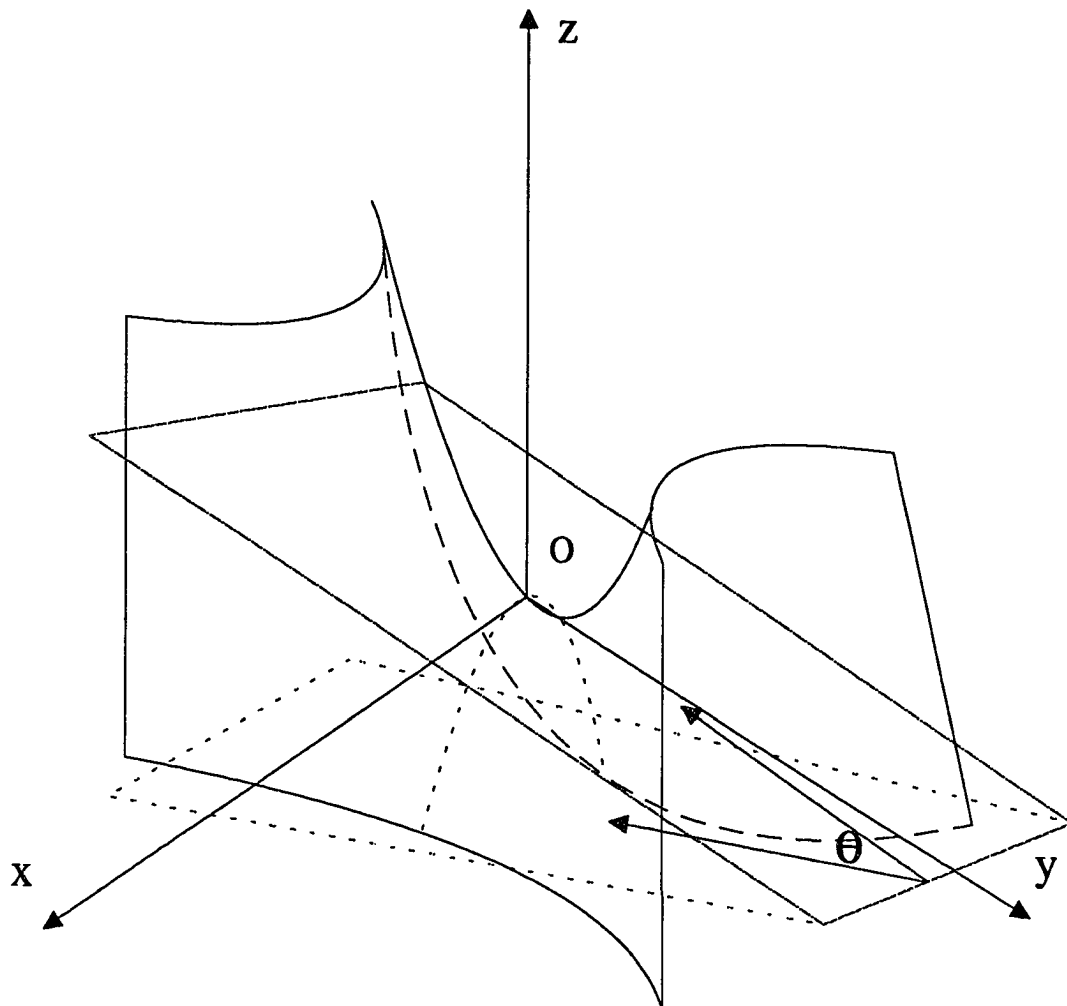


Figure 4-20. Planes parallel to the xy -plane ($z=k$) and all its inclined sub-planes intersect the hyperbolic paraboloid in hyperbolas.

DETAILED VIEW : VERTICAL INTERSECTIONS

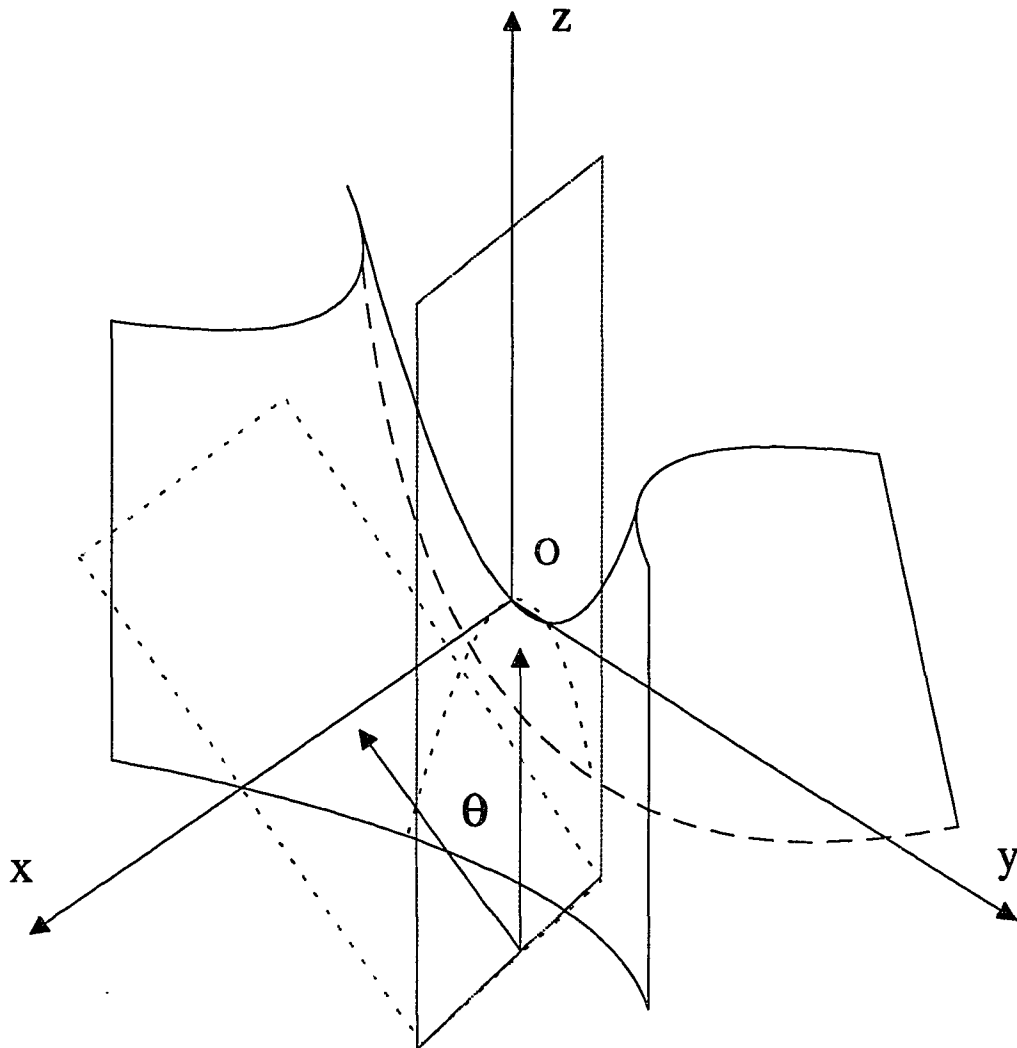


Figure 4-21. Planes parallel to the xz -plane ($y=k$) and all its inclined sub-planes intersect the hyperbolic paraboloid in parabolas.

4.3.9 Hyperbolic cylinder

Step 1:

As in the case of a regular circular or elliptic cylinder, the surface of the hyperbolic cylinder is parallel to the z axis. Subsequently, the variable z is not present in its quadric representation. It's general representation when resting on a plane parallel to the xy plane is

$$ax^2 + by^2 + 2px + 2qy + d = 0, \quad (4.36)$$

where $ab < 0$. Completing squares

$$\frac{(x + \frac{p}{a})^2}{\frac{1}{a}} - \frac{(y + \frac{q}{b})^2}{-\frac{1}{b}} + 1 = 0$$

only if $d = \frac{p^2}{a} + \frac{q^2}{b} + 1$. Also, $-1/b$ is a positive quantity. Intersection of the cylinder with plane **1**, i.e., $z = k$, generates a hyperbola. Since Equation (4.36) is independent of the variable z , the curve intercepted is the one represented by Equation (4.36).

Intersection of the hyperbolic cylinder with plane **2**, i.e., $y = k$ results in the equation

$$\frac{(x + \frac{p}{a})^2}{\frac{1}{a}} = \frac{(k + \frac{q}{b})^2}{-\frac{1}{b}} - 1,$$

which when solved results in a pair of straight lines. As in the case of the hyperbolic paraboloid, angular bounds to extract the regions where a unique set of features (curves) are determined are not necessary, since the two planes considered in step **1** by themselves prove sufficient to distinguish this surface from all the other quadric

surfaces considered in the recognition process. A follow-up on the various inclined sub-planes of the $z = k$ and $y = k$ planes leads to a similar set of intercepts as with the $x = k$ plane. Figures 4-22 and 4-23 illustrate the regions, if required, where extra features (curves) can be determined. Table 4-9 displays the intercepts formed when the hyperbolic cylinder is intersected with the two planes.

PLANE	INTERSECTION
Z = K	Hyperbola
X = K	Lines
Y = K	Lines

Table 4-9. Intersection of the hyperbolic cylinder with planes.

4.3.10 Parabolic cylinder

Step 1:

Unlike the two quadric cylinder considered before, i.e., the circular (elliptic) and the hyperbolic, this surface is parallel to the y axis. Hence the variable y is not present in its quadric representation. It's general representation when resting on a plane parallel to the xy plane is

$$f(x,y,z) = ax^2 + 2px + 2rz + d = 0. \quad (4.37)$$

Upon completing squares it reduces to

$$\frac{(x + \frac{p}{a})^2}{1/a} + \frac{z}{1/2r} = 0 \quad (4.38)$$

DETAILED VIEW : HORIZONTAL INTERSECTIONS

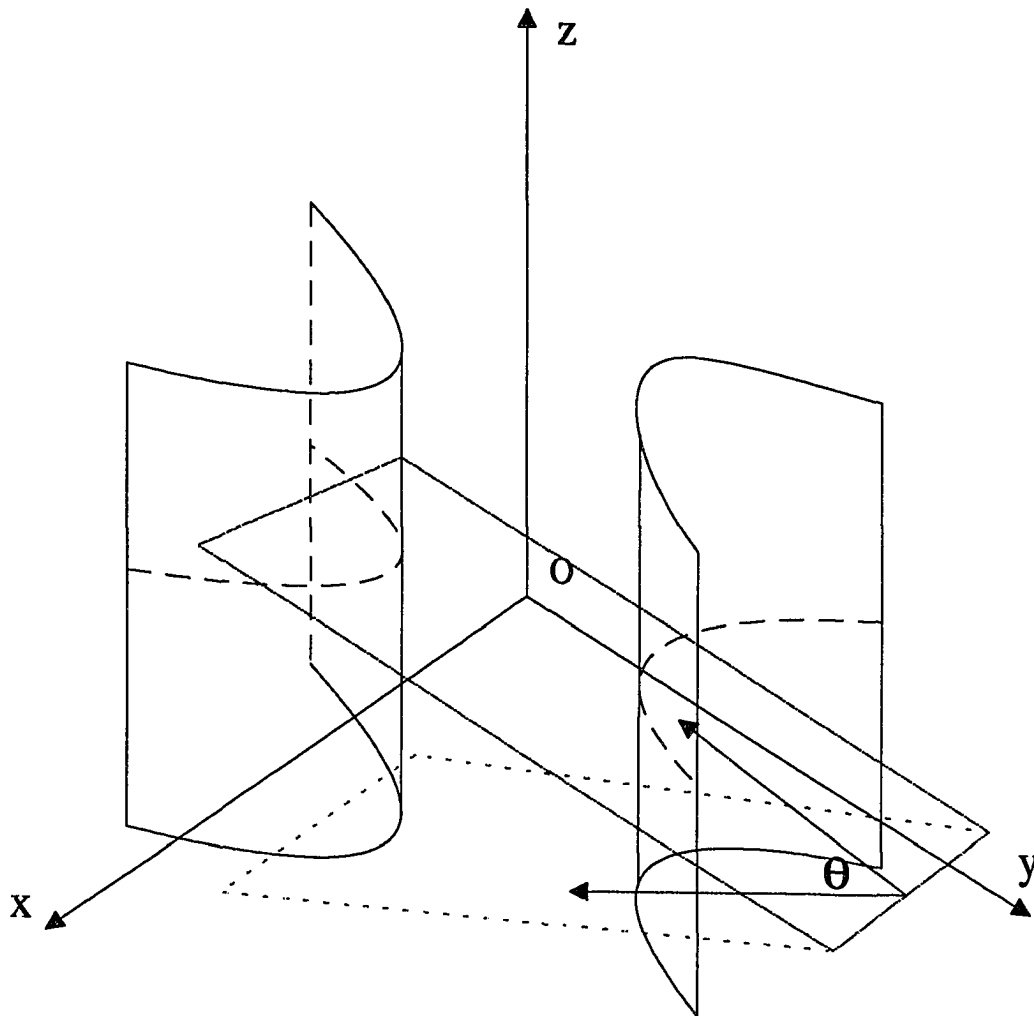


Figure 4-22. Planes parallel to the xy -plane ($z=k$) and all its inclined sub-planes intersect the hyperbolic cylinder in hyperbolas.

DETAILED VIEW : VERTICAL INTERSECTIONS

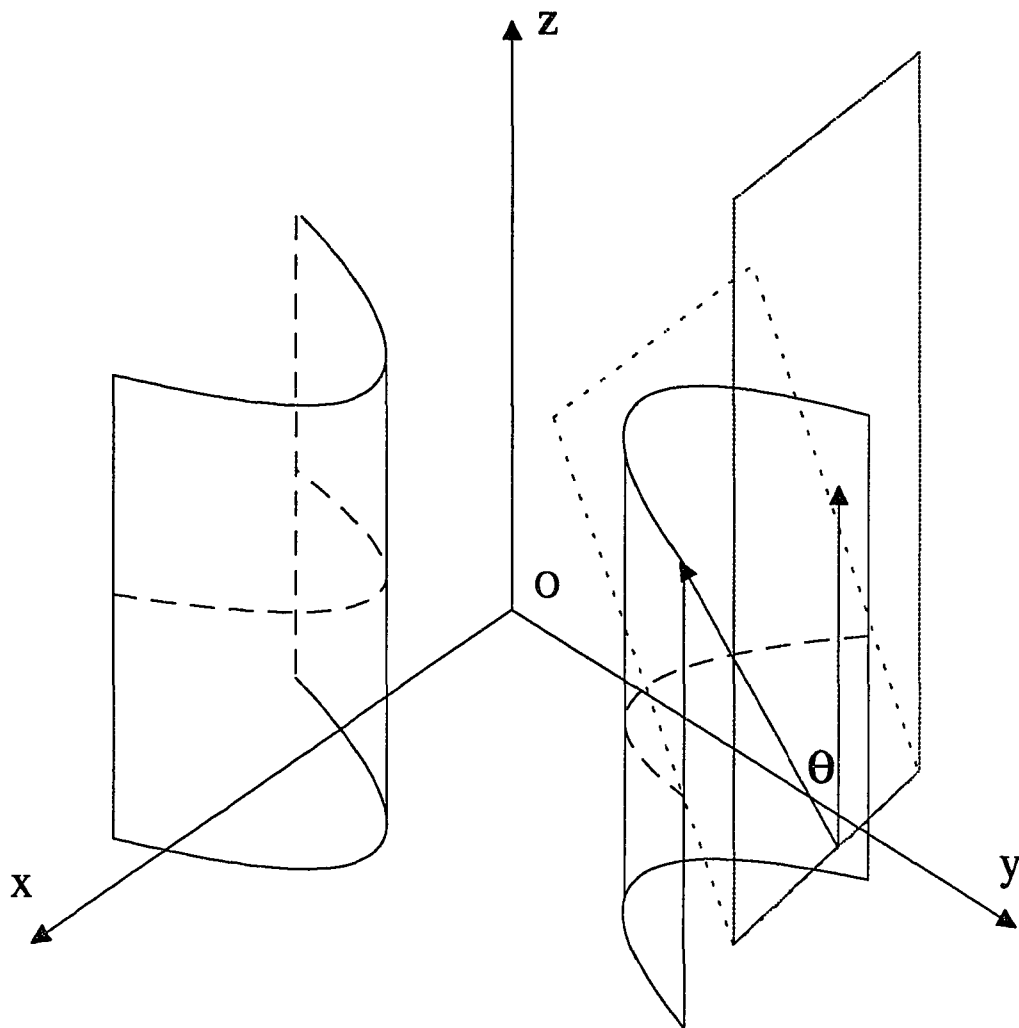


Figure 4-23. Planes parallel to the xz -plane ($y=k$) and all its inclined sub-planes intersect the hyperbolic cylinder in lines.

only if $d = \frac{p^2}{a}$. Intersection of the parabolic cylinder with plane **1**, i.e., $z = k$, $0 < k < 2r/ab$, where b is any finite positive quantity signifying the width of the base of the cylinder, yields

$$\frac{(x + \frac{p}{a})^2}{\frac{1}{a}} = \frac{k}{\frac{1}{2r}},$$

which, when solved, results in a pair of parallel lines.

Consider the intersection of the parabolic cylinder with plane **2**, i.e., $y = k$. Since Equation (4.37) is independent of the variable y , the resultant curve intersected is the same as Equation (4.37), which is a equation of a parabola. As in the case of the hyperbolic paraboloid and the hyperbolic cylinder, angular bounds to extract the regions wherein a unique set of features (curves) are determined are is not necessary. The two planes considered in step **1** by themselves proved sufficient enough to distinguish this surface from all the other quadric surfaces considered from the recognition process. Figures (4-24) and (4-25) illustrate the regions, if required, where extra features (curves) can be determined. Table 4-10 displays the intercepts formed when the parabolic cylinder is intersected with the two planes.

PLANE	INTERSECTION
Z = K	Lines
Y = K	Parabola

Table 4-10. Intersection of the parabolic cylinder with planes.

DETAILED VIEW : HORIZONTAL INTERSECTIONS

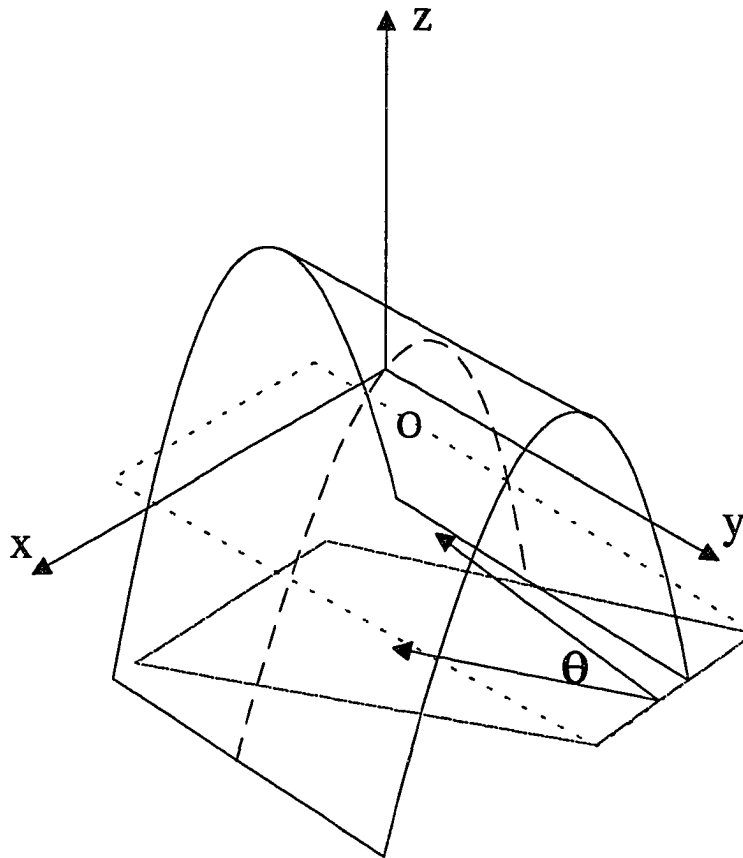


Figure 4-24. Planes parallel to the xy -plane ($z=k$) and all its inclined sub-planes intersect the parabolic cylinder in lines.

DETAILED VIEW : VERTICAL INTERSECTIONS

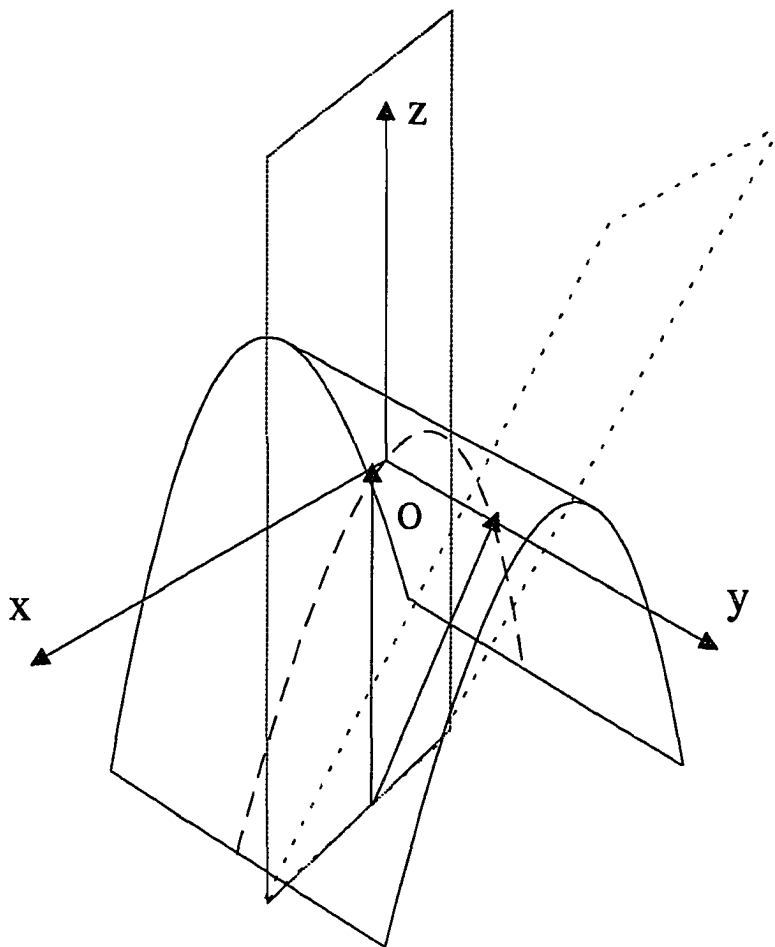


Figure 4-25. Planes parallel to the xz -plane ($y=k$) and all its inclined sub-planes intersect the parabolic cylinder in parabolas.

4.3.11 Parallelepiped

Since planar surfaces cannot be represented with quadratic equations, we consider a plane of the parallelepiped. The general equation of a plane from Equation (4.1) is of the form

$$2px + 2qy + 2rz + d = 0. \quad (4.39)$$

Intersection with plane **1**, i.e., $z = k$, will generate

$$2px + 2qy + d + 2rk = 0,$$

which is the equation of a line. Similarly, intersection of the plane denoted by Equation (4.39) with plane **2** will generate the line

$$2px + 2rz + d + 2qk = 0.$$

Table 4-11 summarizes the short results obtained for the parallelepiped.

PLANE	INTERSECTION
$Z = K$	Line
$X = K$	Line
$Y = K$	Line

Table 4-11. Intersection of the parallelepiped with planes.

Table 4-12 summarizes the various curves (conics) derived from intersecting each of the eleven surfaces with the two planes $z = k$ and $y = k$. These observations follow the results obtained in step 1 of each of the quadric surfaces. As seen from Table 4-12, the quadric cone and the hyperboloid of one and two sheets all generate similar curves. However, after using the results of step 2 (where angular bounds have been determined), we are able to distinguish each of the quadric surfaces from one another. Each of the quadric surfaces can be represented by a binary five-tuple, where the numeral 1 indicates the presence of a particular curve and the numeral 0 refers to the non-existence of that curve. Table 4-13 below presents the feature vector for each of the quadric surfaces.

Quadric surfaces which seem to have identical feature vectors in the table above, get differentiated when the angular bounds theory as defined and derived for each of the surfaces (step 2) is applied. The next section briefly presents one other surface recognition approach which is very similar to the two-dimensional discriminant approach utilized to distinguish two-dimensional curves. It is one of our primary areas for future investigation.

4.4 Mapping of Explicit to Implicit Representations for Quadric Surfaces

Another objective which should be discussed is the formulation of a three-dimensional discriminant similar to the two-dimensional discriminant described earlier as means of recognizing three-dimensional objects. Consider the general quadratic representation of quadrics again, i.e.,

$$F(x,y,z) = ax^2 + by^2 + cz^2 + 2fyz + 2gzx + 2hxy + 2px + 2qy + 2rz + d = 0. \quad (4.40)$$

This equation can be written implicitly, such that

$$z = F(x,y) = Ax^2 + By^2 + Cxy + Dx + Ey + F. \quad (4.41)$$

OBJECT	PLANE 1 : $x = k$	PLANE 2 : $y = k$
Ellipsoid	Ellipse	Circle
Circular cylinder	Circle	Line
Sphere	Circle	Circle
Quadric cone	Circle	Hyperbola, Parabola
Hyperboloid of one sheet	Circle	Hyperbola, Parabola
Hyperboloid of two sheets	Circle, Point	Hyperbola, Parabola
Elliptic paraboloid	Ellipse	Parabola
Hyperbolic cylinder	Hyperbola	Line
Parabolic cylinder	Line	Parabola
Hyperbolic paraboloid	Hyperbola	Line
Parallelepiped	Line	Line

Table 4-12. The various curves intercepted by the quadric surfaces when intersected with the planes $z = k$ and $y = k$.

3-D SURFACE	CIRCLE	ELLIPSE	PARABOLA	HYPERBOLA	LINE
Ellipsoid	1	1	0	0	0
Circular cylinder	1	1	0	0	1
Sphere	1	0	0	0	0
Quadric cone	1	1	1	1	1
Hyperboloid of one sheet	1	1	1	1	0
Hyperboloid of two sheets	1	1	1	1	0
Elliptic paraboloid	1	1	1	0	0
Hyperbolic cylinder	0	0	0	1	1
Parabolic cylinder	0	0	1	0	1
Hyperbolic paraboloid	0	0	1	1	1
Parallelepiped	0	0	0	0	1

Table 4-13. Feature vectors (representing the presence or absence of curves) for each of the quadric surfaces.

Equation (4-40) characterizes the complete surface through its representation, whereas Equation (4-41) characterizes surface patches on three-dimensional surfaces. As discussed in Chapter Two, where surface curvatures are utilized to describe surface patches as being planar or curved (hyperbolic, parabolic, or elliptic), we wish to utilize the ten coefficients of Equation (4.40) in the form of a discriminant to represent patches on three-dimensional surfaces. In case we justify the existence of the implicit form, we would like to derive a mapping from $F(x,y,z)$ to $F(x,y)$; i.e., we would like to investigate the relations between $A, B, C, D, E,$ and F and a, b, c, d, p, q, r and d . If this is possible, then we can attempt to derive a discriminant using $A, B, C, D, E,$ and F , the combination of which can distinguish three-dimensional objects.

We approach this problem in two directions. In the first approach we would numerically solve and derive relations for each coefficient in Equation (4-41) in terms of the coefficients of Equation (4-40). For example, while solving for F we arrive at its representation as

$$F = \frac{-2r \pm \sqrt{4r^2 - 4cd}}{2c}.$$

Similarly, expressions for the coefficient B have been found to be

$$B = \pm \frac{\sqrt{2(f+g+r)^2 - 4c(a+b+2h+2p+2q+d)}}{4c}.$$

Each of the above coefficients were derived while setting the variables x and y as zero. Similarly the remaining coefficients can be derived after solving several linear and non-linear equations. In the second approach, derivatives are utilized to obtain a pattern vector based on the coefficients of Equation (4-40). Rewriting Equation (4-40) in terms of a quadratic of z ,

$$-[cz^2 + 2fyz + 2rz + 2gxz] = f(x,y) = ax^2 + by^2 + 2hxy + 2px + 2qy + d, \quad (4.42)$$

which is similar to Equation (4-41), i.e., to

$$z = F(x,y) = Ax^2 + By^2 + Cxy + Dx + Ey + F.$$

Differentiating Equation (4-42) with respect to each of the variables, x , y , and z , yields the following equations:

$$\frac{\partial F}{\partial y} = 2fy = 2by + 2hx + 2q,$$

$$\frac{\partial F}{\partial x} = 2gx = 2ax + 2hy + 2p,$$

and

$$\frac{\partial F}{\partial z} = 2cz + 2fy + 2x + 2gx = 0.$$

Each of these expressions are utilized individually in Equation (4-40) to yield an expression of the form

$$Ax^2 + C^2 + Bxy + Ex + Fy + D = 0,$$

from which the discriminant $B^2 - 4AC$ again produces results which are either less than zero, equal to zero, or greater than zero. A list of pattern vectors which seem to be invariant has been derived for some of the quadric surfaces. Much more work has to be done on simulated as well as real data before arriving at definite conclusions.

The theory developed in chapters Three and Four were experimented with several sets of real and simulated range data. Results of which are summarized in Chapter Five.

CHAPTER FIVE

EXPERIMENTAL RESULTS

5.1 Introduction

Section 5.2 discusses our study of median filtering on range images. Section 5.3 explains the process whereby filtered range images of spheres, cylinders, and quadric cones undergo the recognition criterion. Subsequently, Section 5.4 discusses the application of the rotation alignment algorithm to the processed as well as simulated range images. Section 5.5 briefly presents the results obtained while using the three-dimensional discriminant approach to simulated and real range data.

Range data obtained using a laser radar three-dimensional vision system is similar to intensity images obtained from a normal camera. However, instead of intensity (brightness) information, range (depth) information is available. Thus it is possible to interpret intensity information as range information when a range image is displayed on a image processing monitor. The nearer the object, the brighter it appears on the screen.

The experimental work was performed in the following order :

- (i) The effect of median filtering on range images was studied.
- (ii) The proposed recognition scheme was applied to filtered range images.
- (iii) The quadric alignment algorithm was applied to simulated and real data.
- (iv) The three-dimensional discriminant approach was tested with simulated data.

5.2 Median Filtering on Range Images

Range images of objects like spheres, cylinders and cones were segmented in order to separate the object from its background. The resulting image, which is referred to as the raw image, was then median filtered with mask sizes 3×3 , 5×5 and 7×7 .

Consider Figure 5-1 which is the actual range image of a sphere with its background. Figure 5-2 is the image after segmentation. The effect of median filtering on Figure 5-2 can be observed in Figure 5-3 (3×3 mask), Figure 5-4 (5×5 mask), and Figure 5-5 (7×7 mask). The curvature sign map, which is discussed in Chapter Three, was then utilized to study the effect of median filtering on the original range image shown in Figure 5-2. Evaluating the first and second derivatives with respect to the x and y axes and comparing each of these maps determines whether or not the median filtering has altered the original range data to any extent. Figures 5-6a, 5-6b, 5-6c, and 5-6d are the first and second derivatives with respect to the x and y axes, respectively, for figure 5-2. Similarly figures 5-7a, 5-7b, 5-7c, 5-7d; figures 5-8a, 5-8b, 5-8c, 5-8d; and figures 5-9a, 5-9b, 5-9c, 5-9d are the first and second derivatives for the images in figures 5-3, 5-4, and 5-5, respectively.

In all of these figures, "+" is assigned to a particular pixel position if the magnitude of the derivative (first or second) of that pixel is greater than the magnitude of the derivative (first or second) of the pixel to its right. Similarly "-" is assigned to a particular pixel position if the magnitude of the derivative (first or second) of that pixel is less than the magnitude of the derivative (first or second) of the pixel to its right. In the case when the magnitudes of the derivatives (first or second) of either pixels is the same, a blank is assigned.

Sign maps are also generated to check the integrity of the image data before and after the filtering process. Based on the magnitude of the depth value of a pixel and

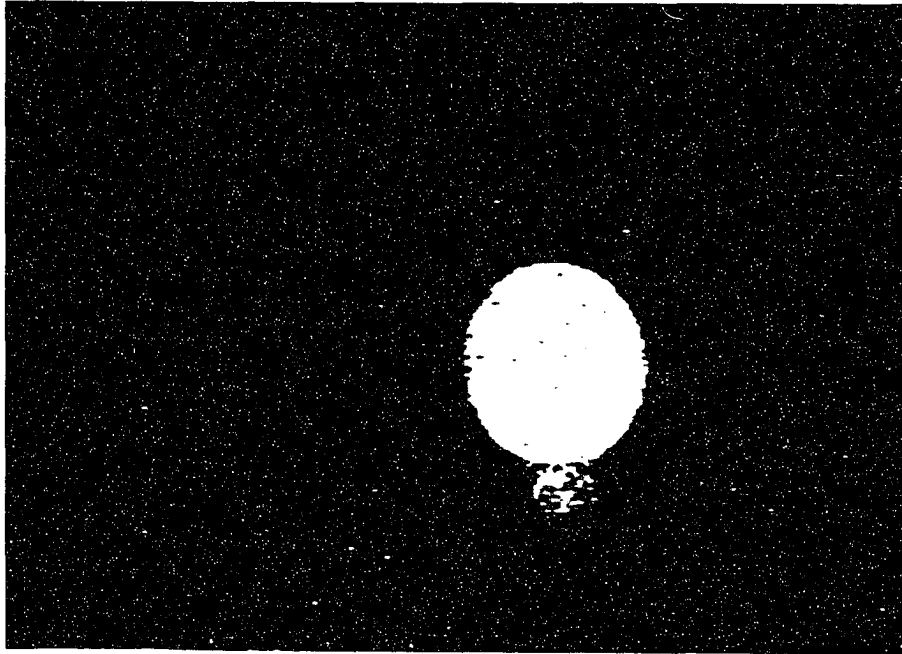


Figure 5-1. Raw range image of the sphere with its background.

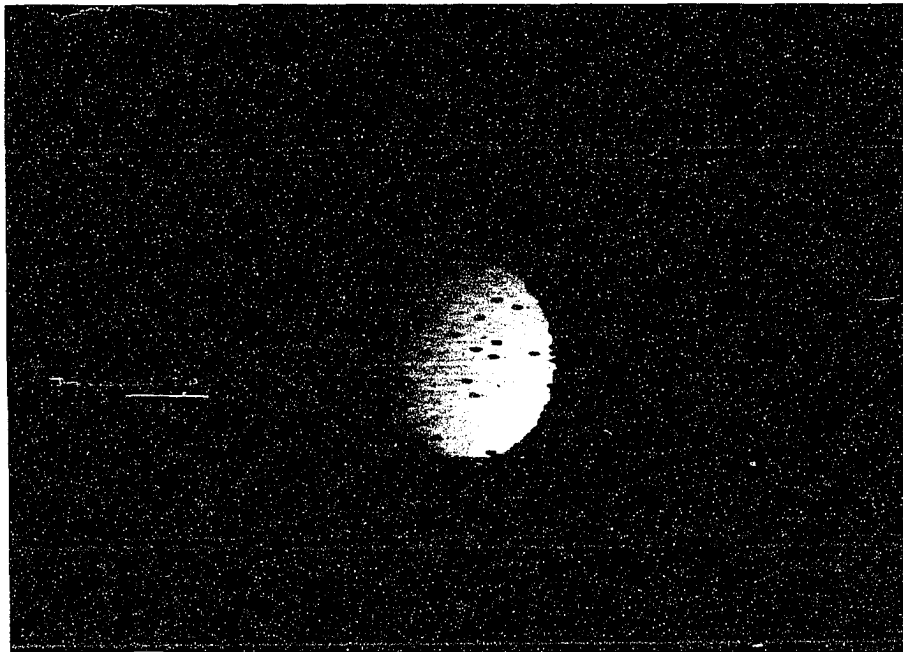


Figure 5-2. Range image of the sphere after segmentation.

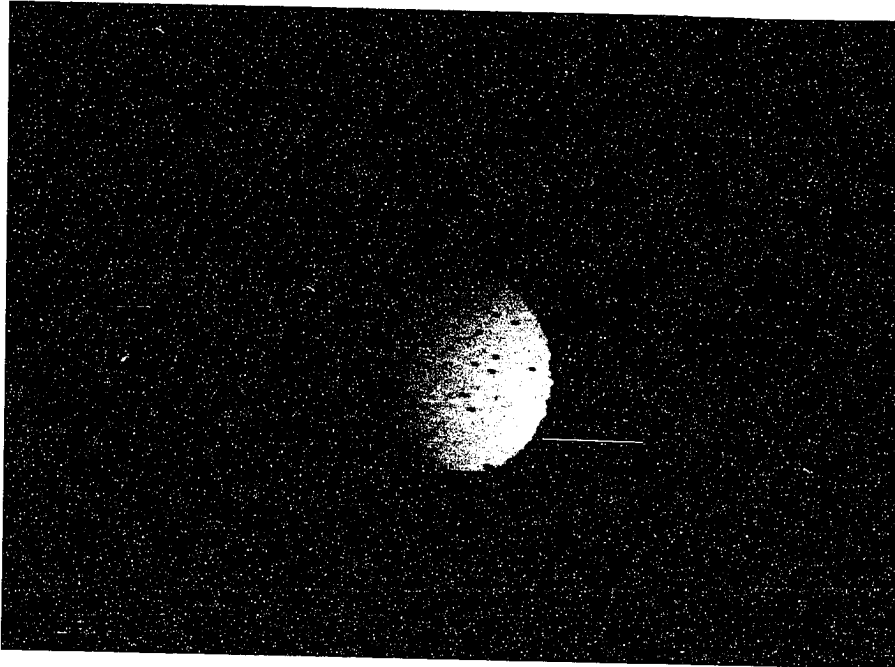


Figure 5-3. 3 x 3 median filtered image of the raw sphere.

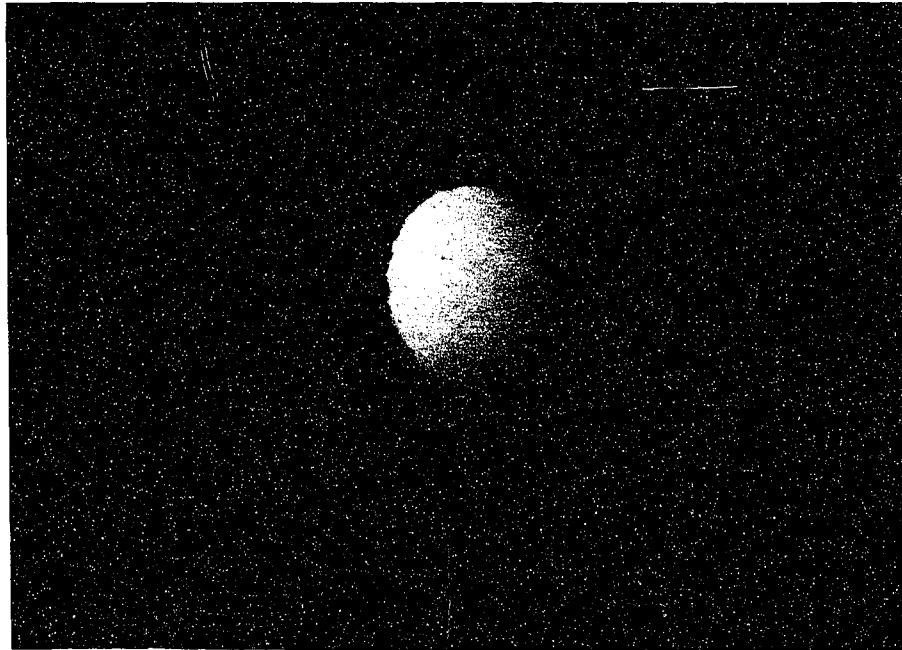


Figure 5-4. 5 x 5 median filtered image of the raw sphere.

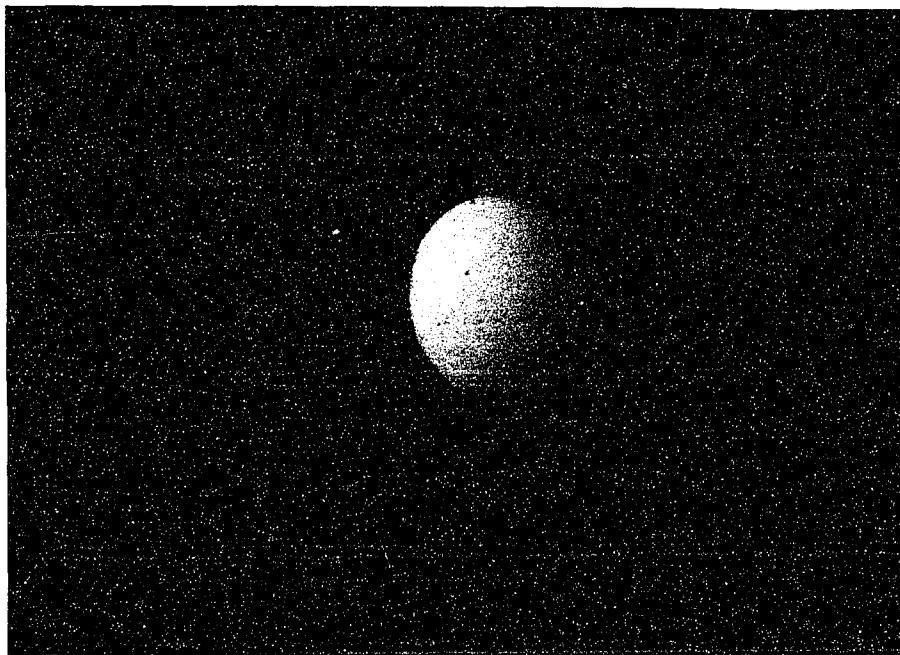


Figure 5-5. 7 x 7 median filtered image of the raw sphere.

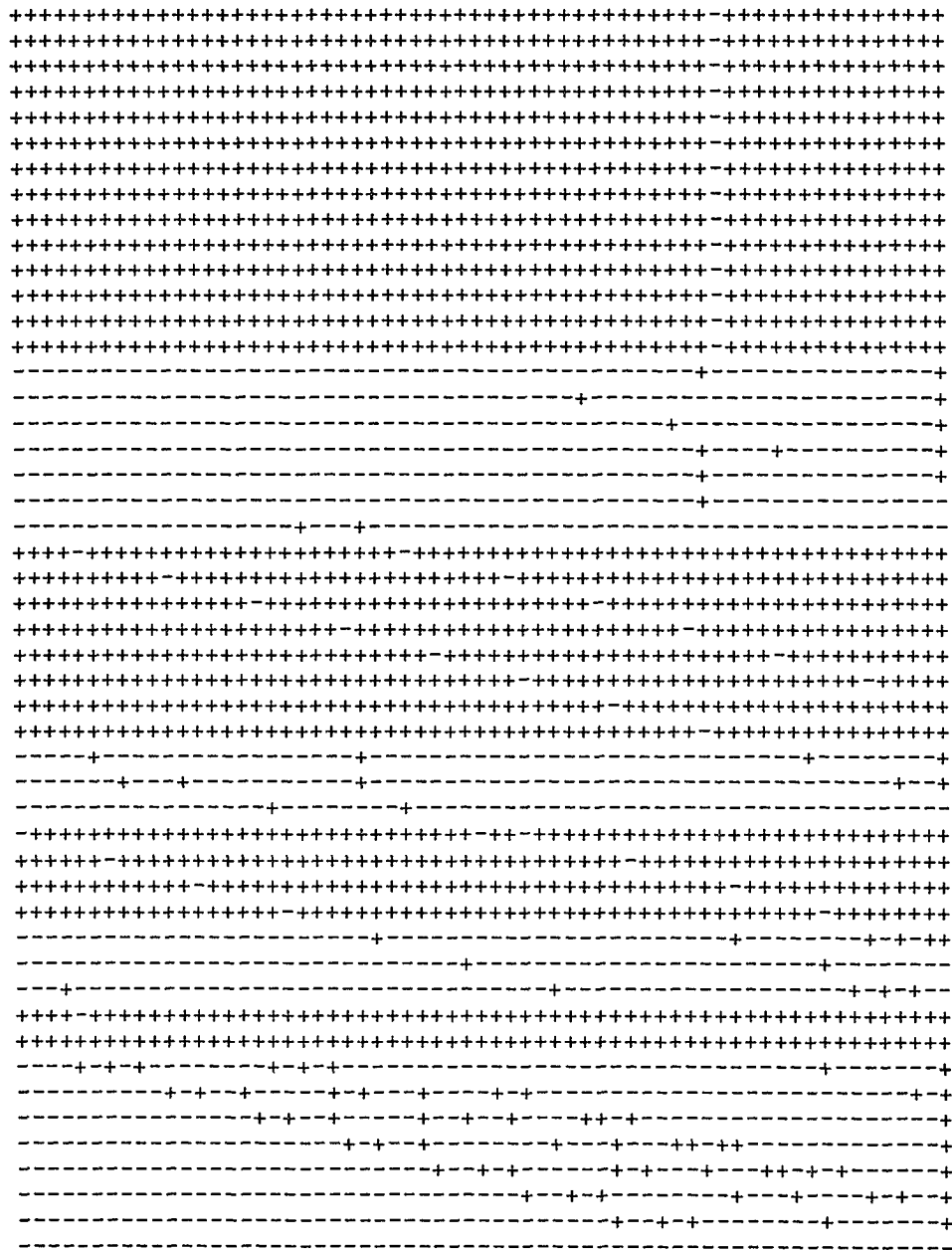


Figure 5-6a. Second derivative w.r.t x-axis of the original sphere.

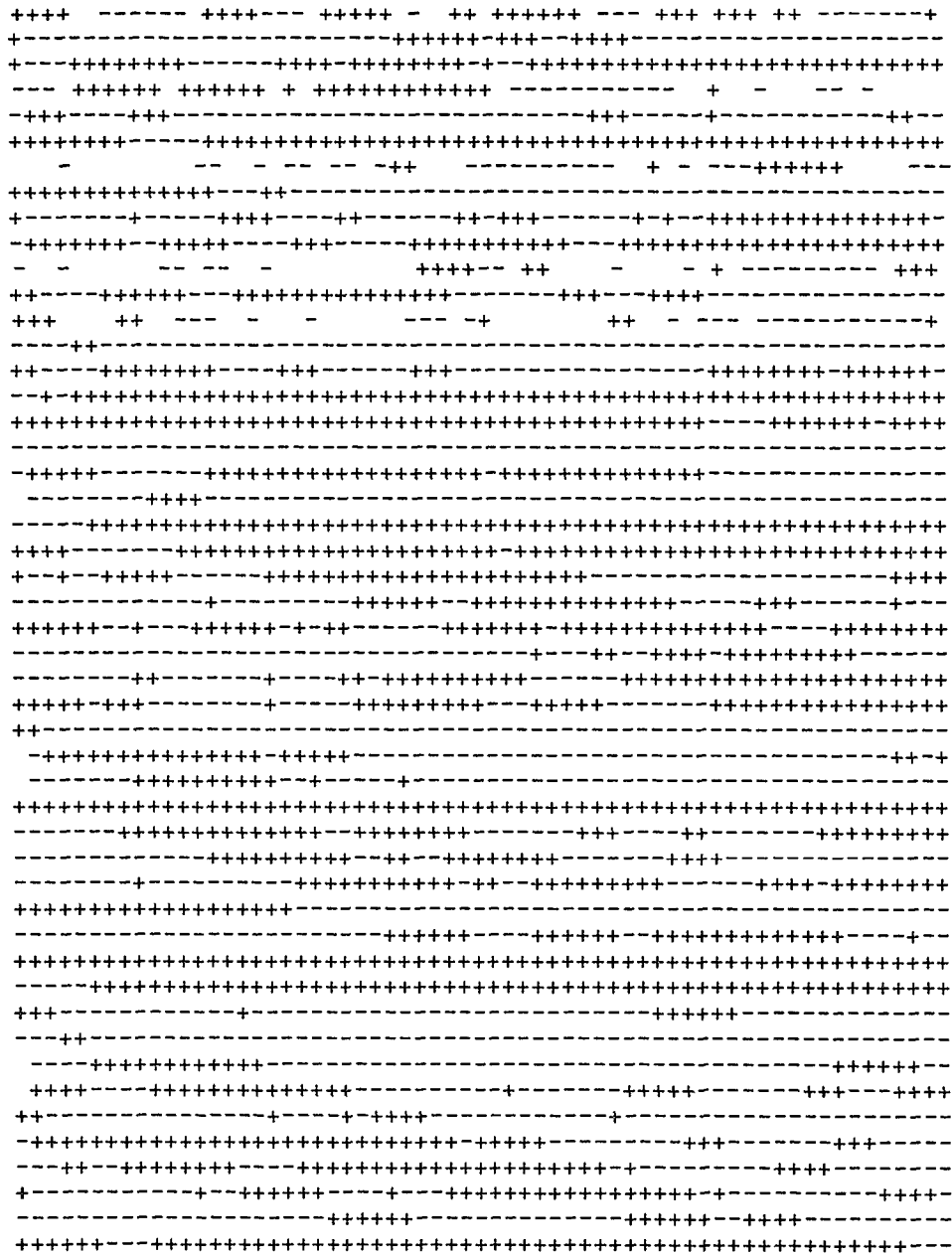


Figure 5-6b. First derivative w.r.t y-axis of the original sphere.

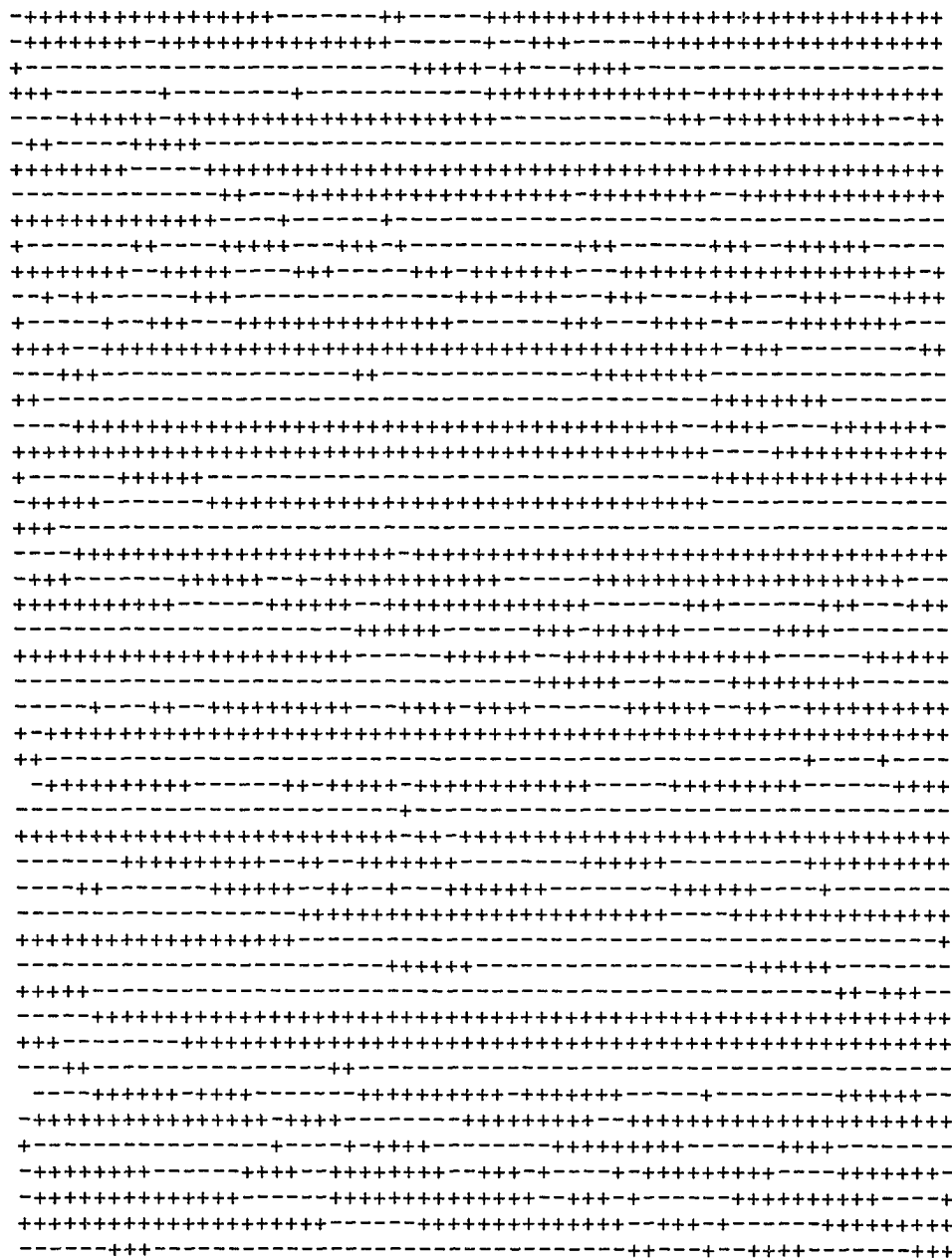


Figure 5-6d. Second derivative w.r.t y-axis of the original sphere.

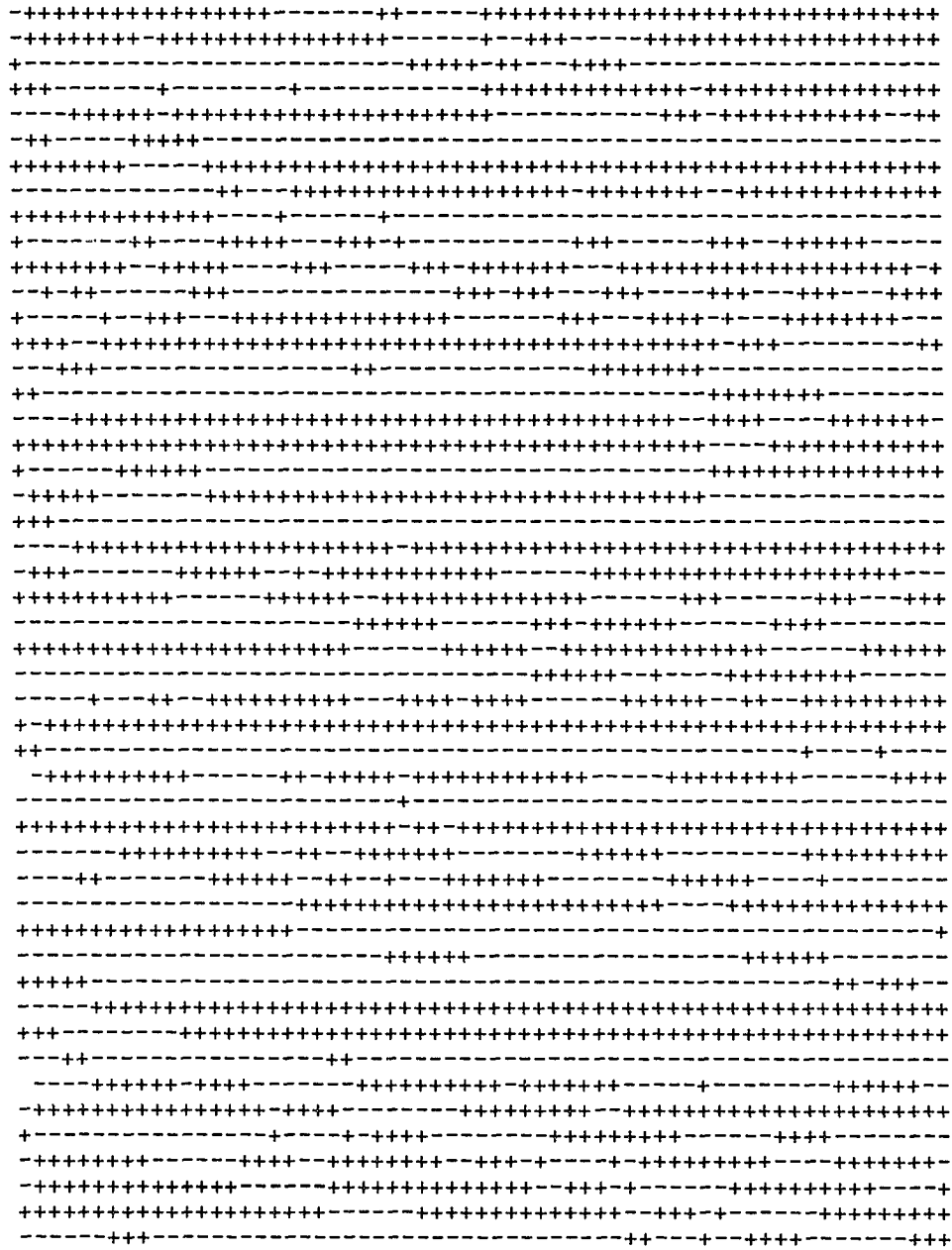


Figure 5-6d. Second derivative w.r.t y-axis of the original sphere.

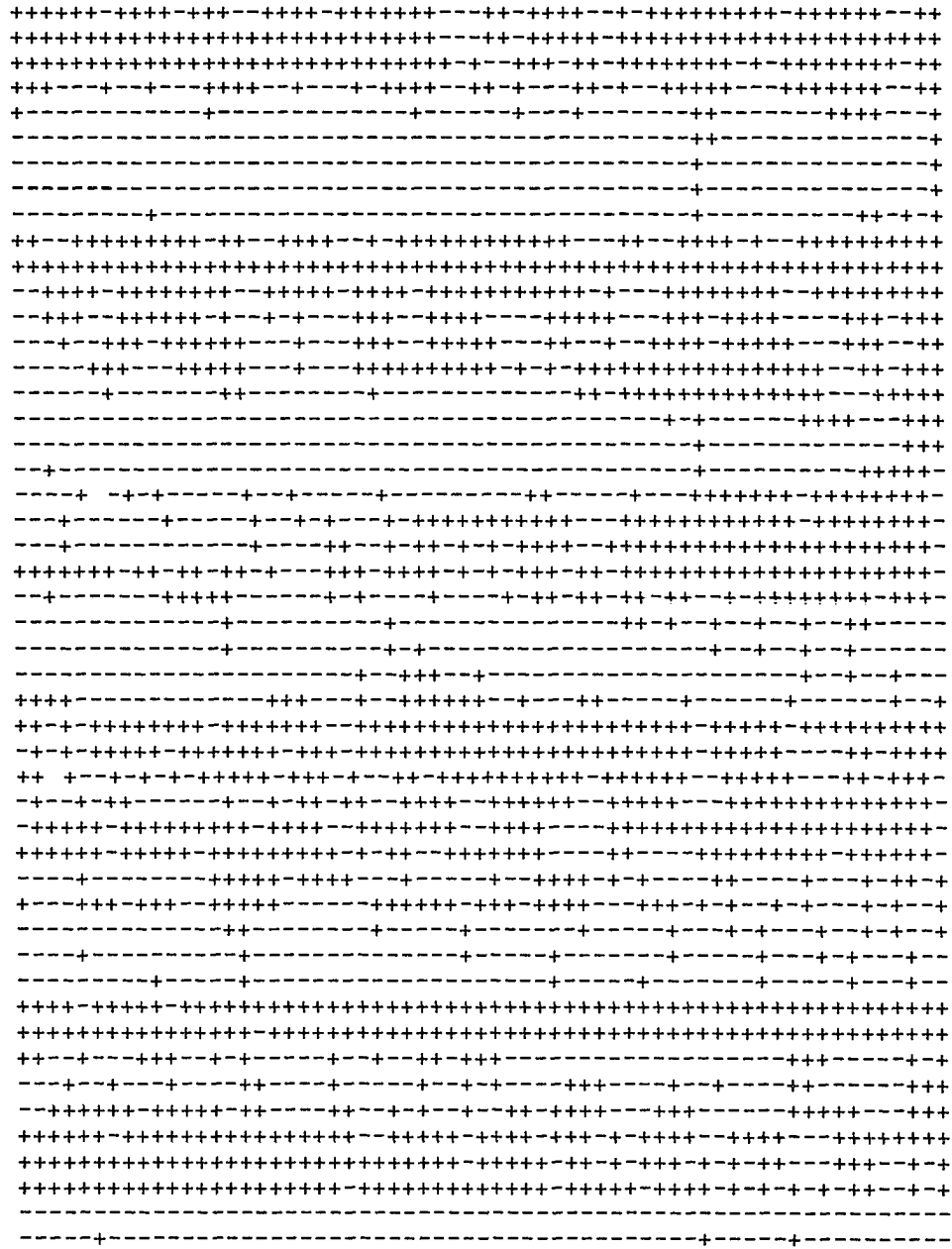


Figure 5-7a. First derivative w.r.t x-axis of the sphere filtered with a mask size of 3 X 3.

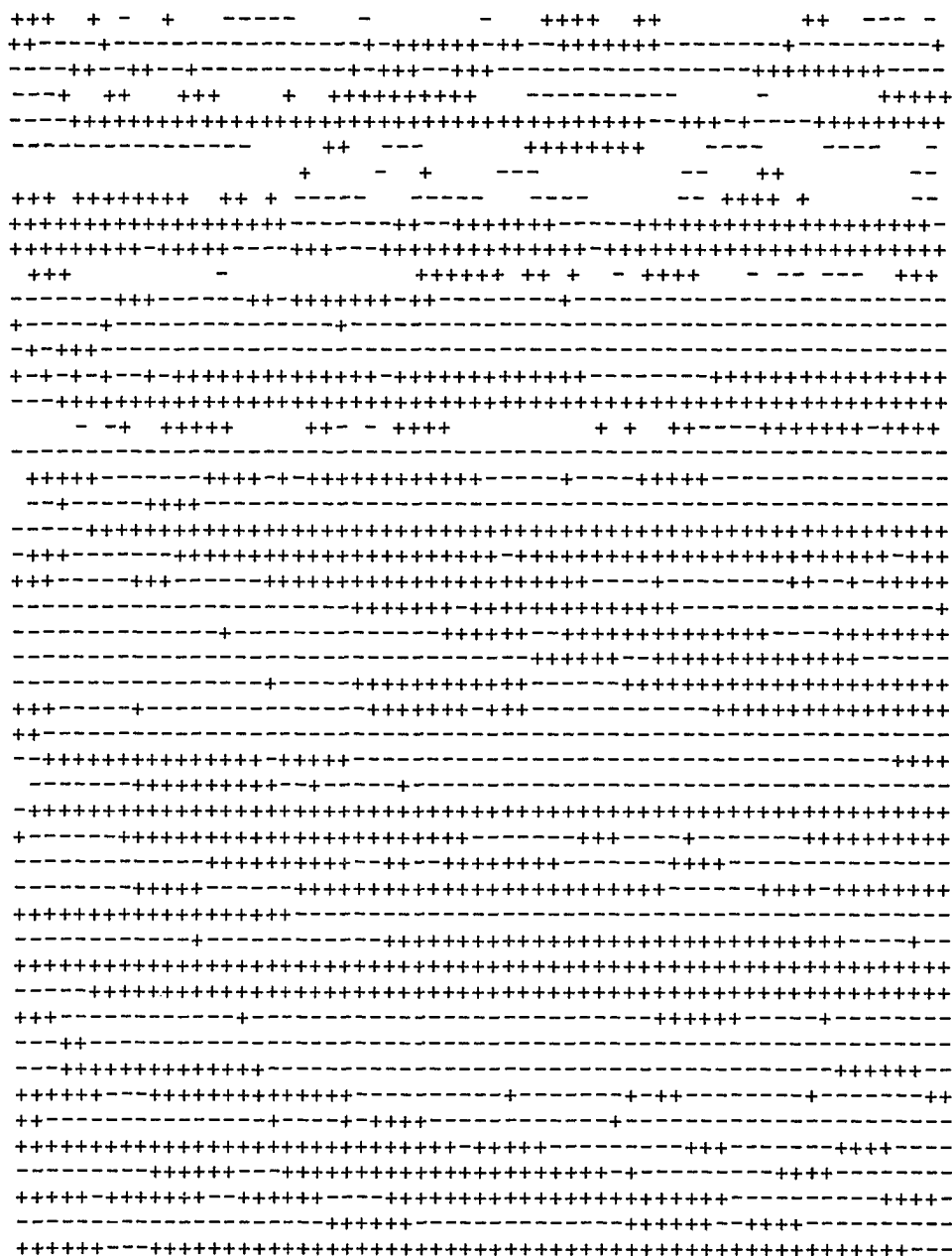


Figure 5-7b. First derivative w.r.t y-axis of the sphere filtered with a mask size of 3 X 3.

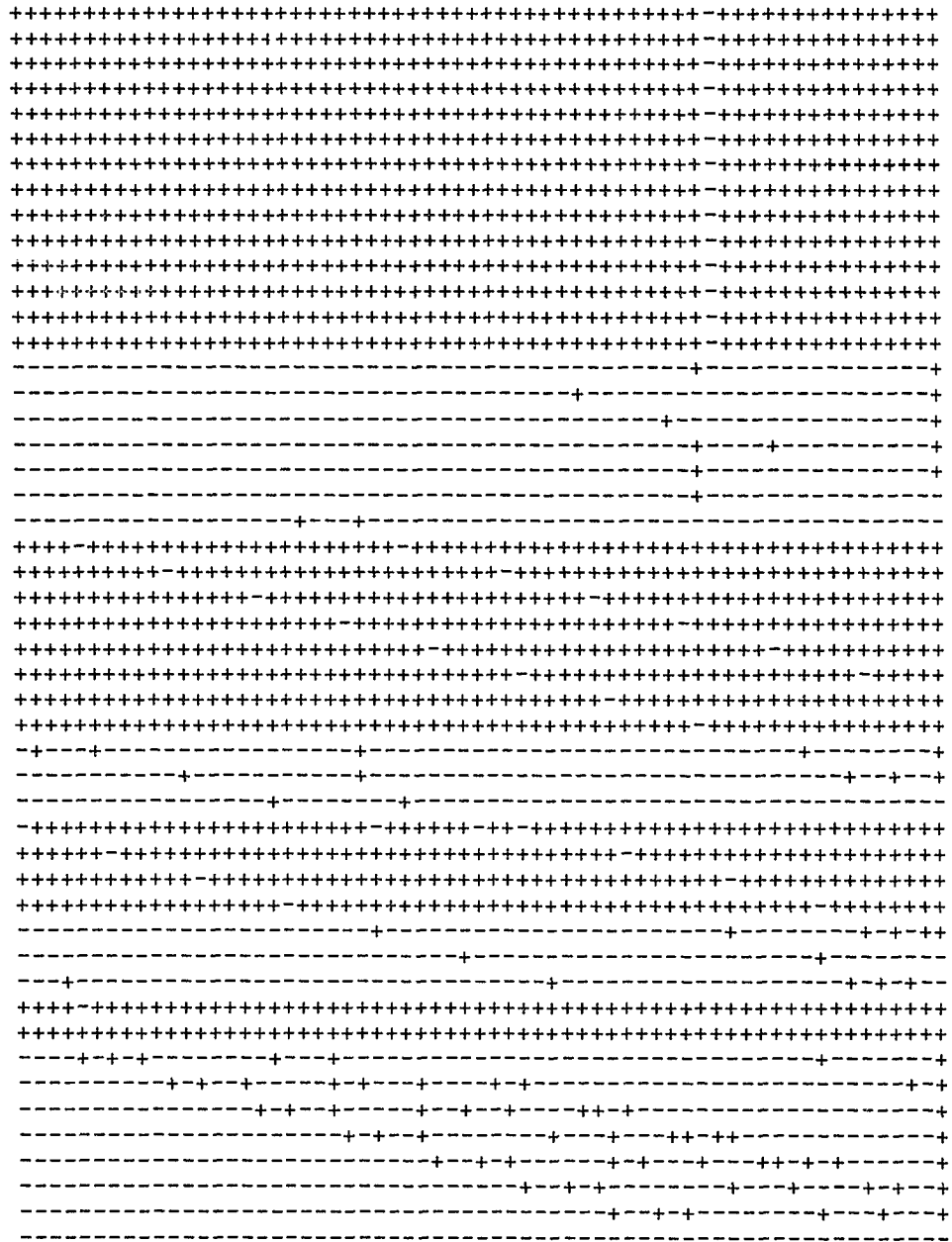


Figure 5-7c. Second derivative w.r.t x-axis of the sphere filtered with a mask size of 3 X 3.

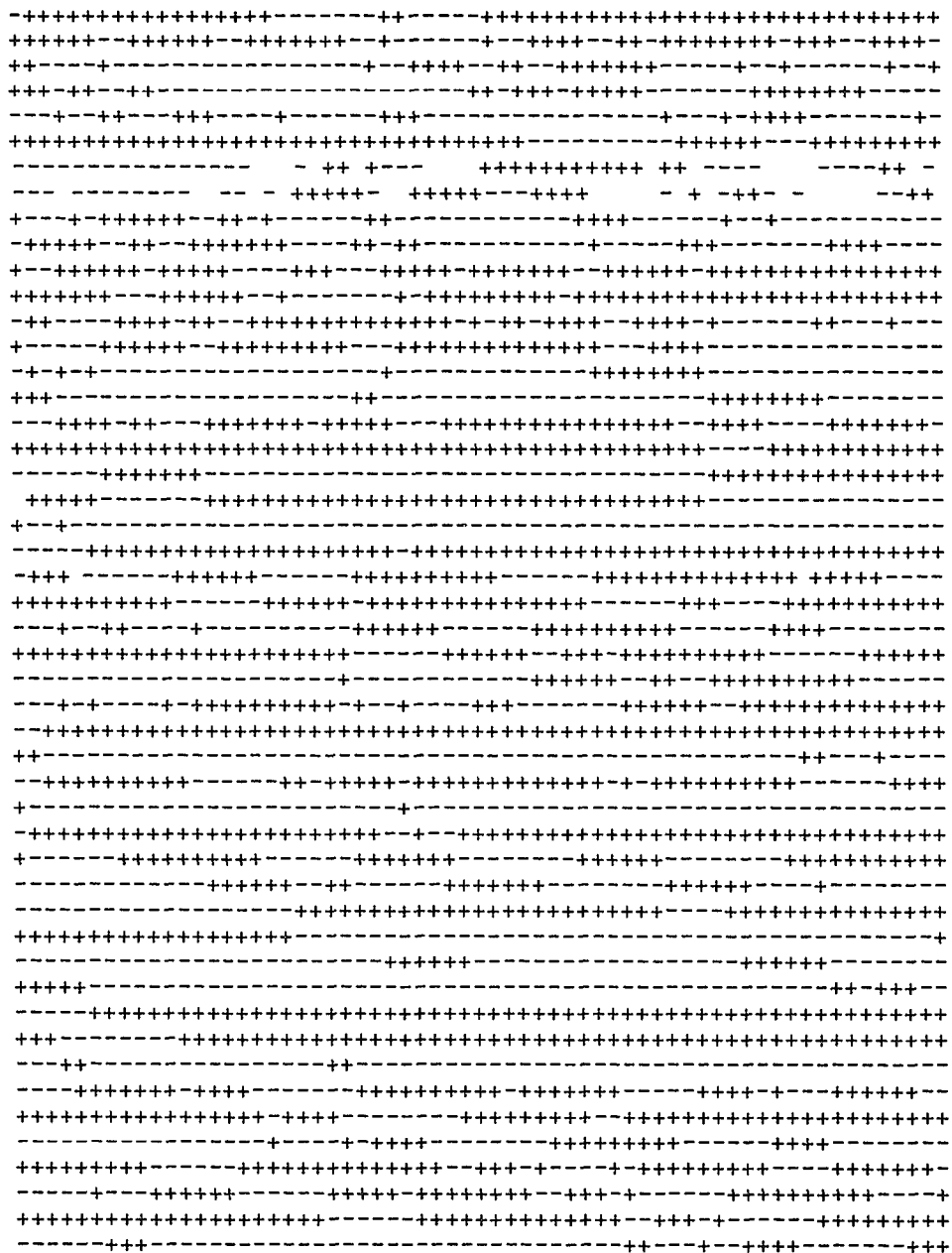


Figure 5-7d. Second derivative w.r.t y-axis of the sphere filtered with a mask size of 3 X 3.

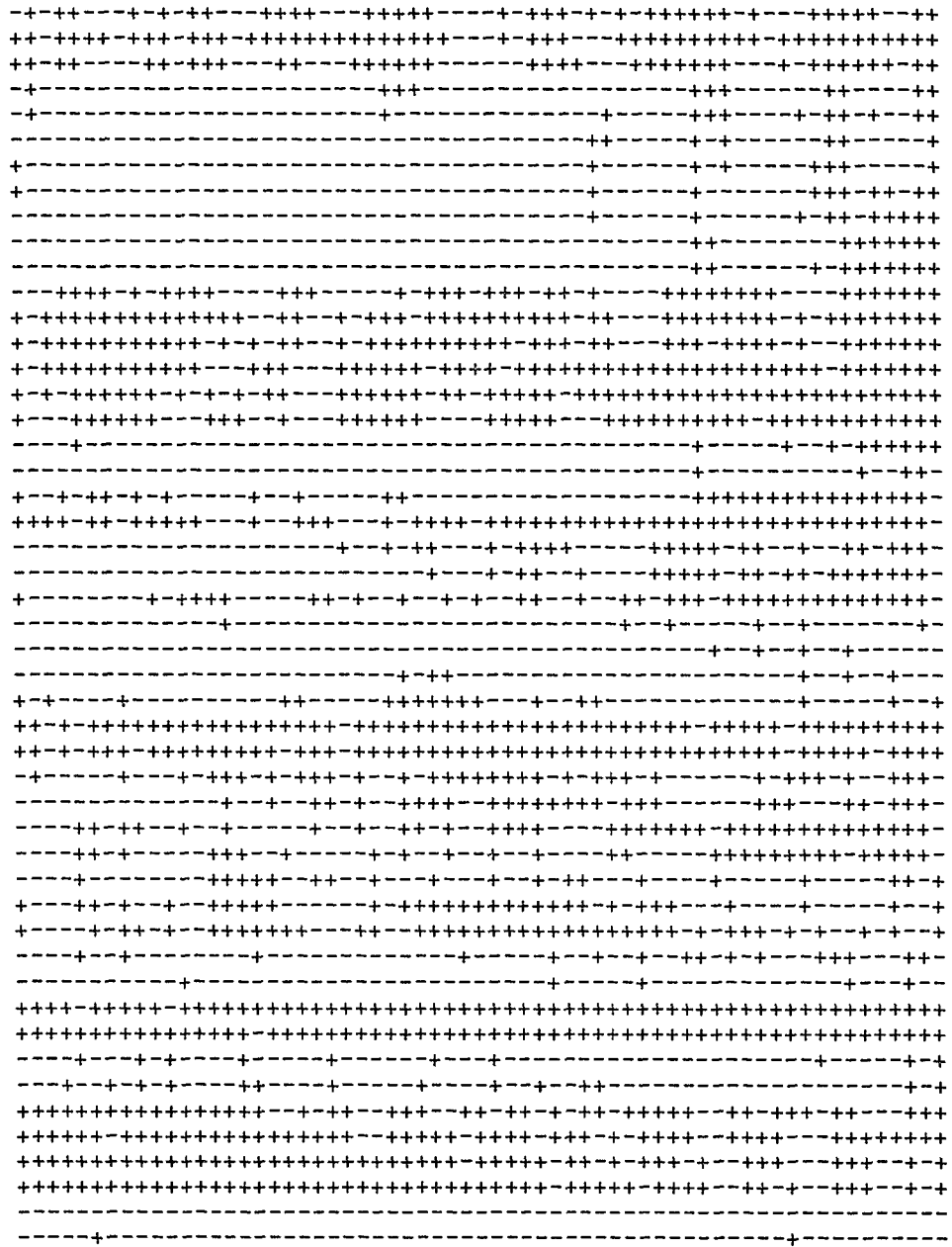


Figure 5-8a. First derivative w.r.t x-axis of the sphere filtered with a mask size of 5 X 5.

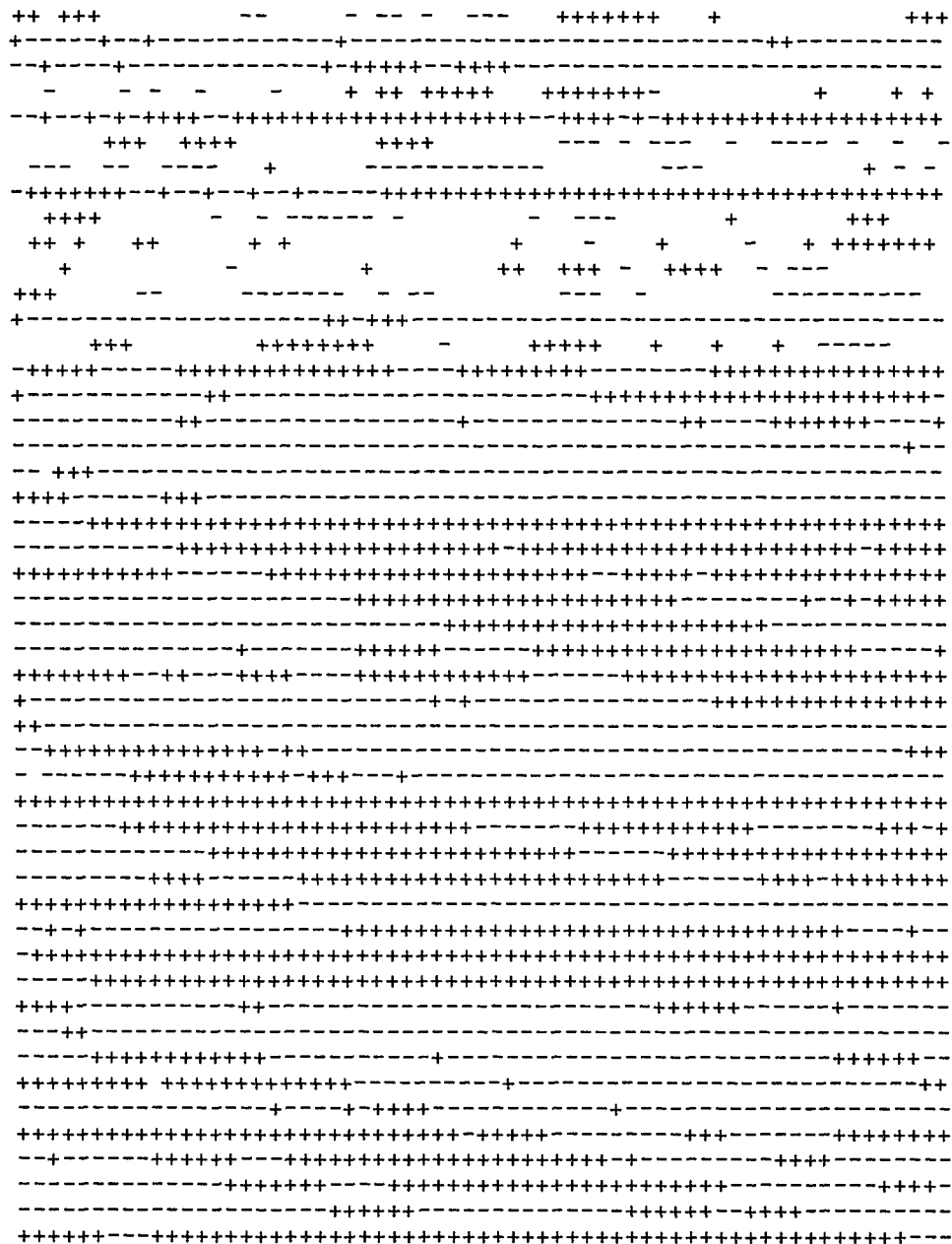


Figure 5-8b. First derivative w.r.t y-axis of the sphere filtered with a mask size of 5 x 5.

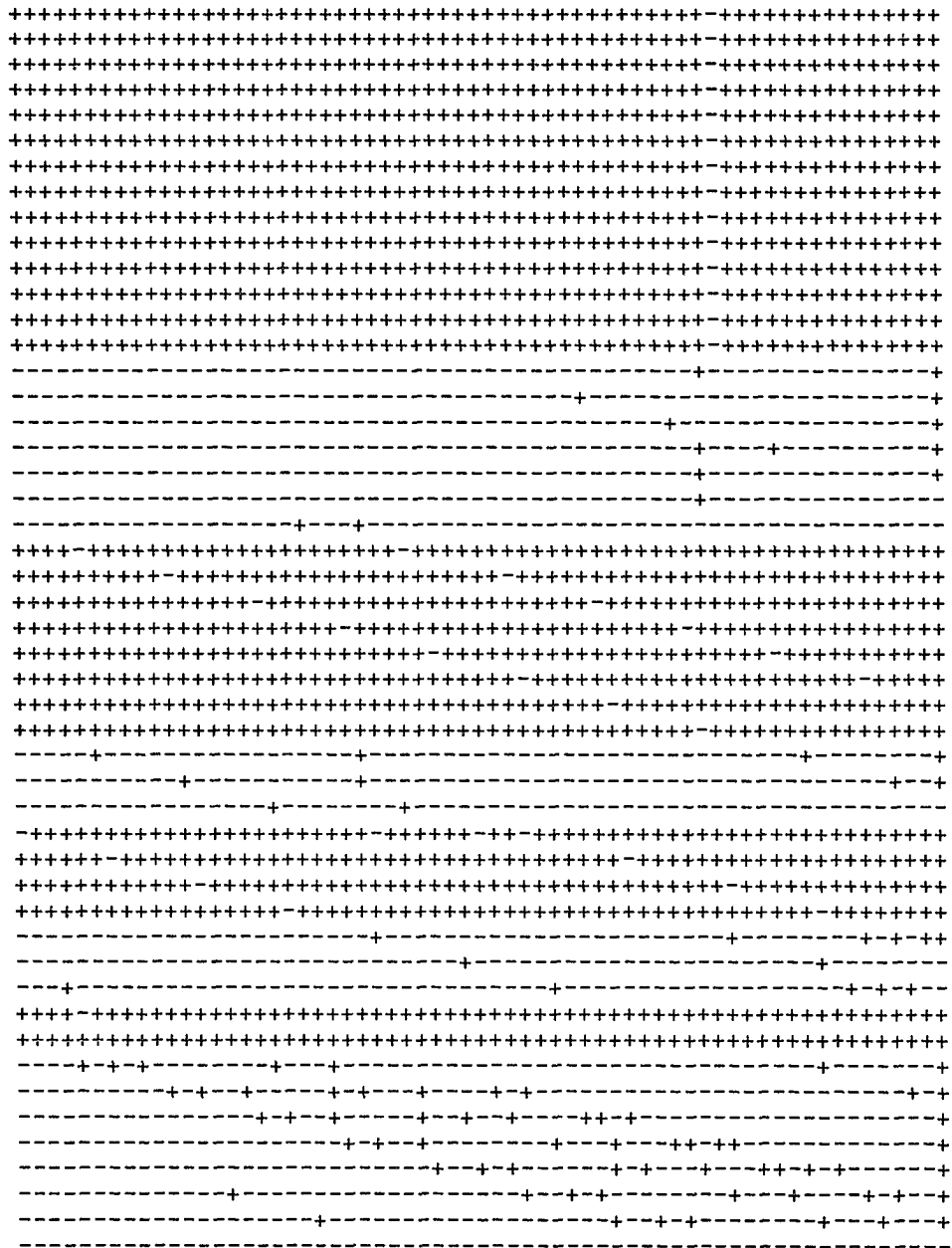


Figure 5-8c. Second derivative w.r.t x-axis of the sphere filtered with a mask size of 5 X 5.

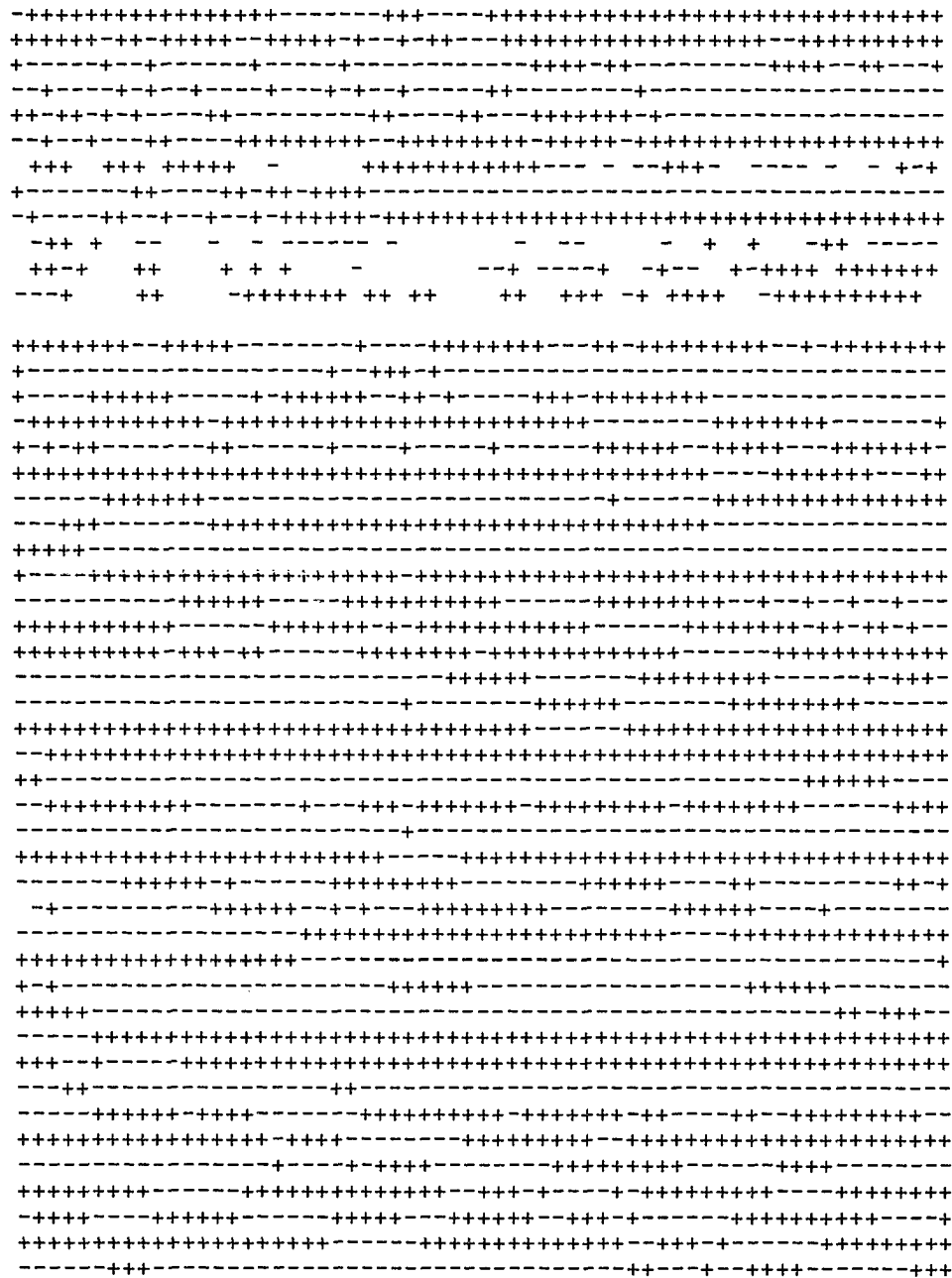


Figure 5-8d. Second derivative w.r.t y-axis of the sphere filtered with a mask size of 5 X 5.

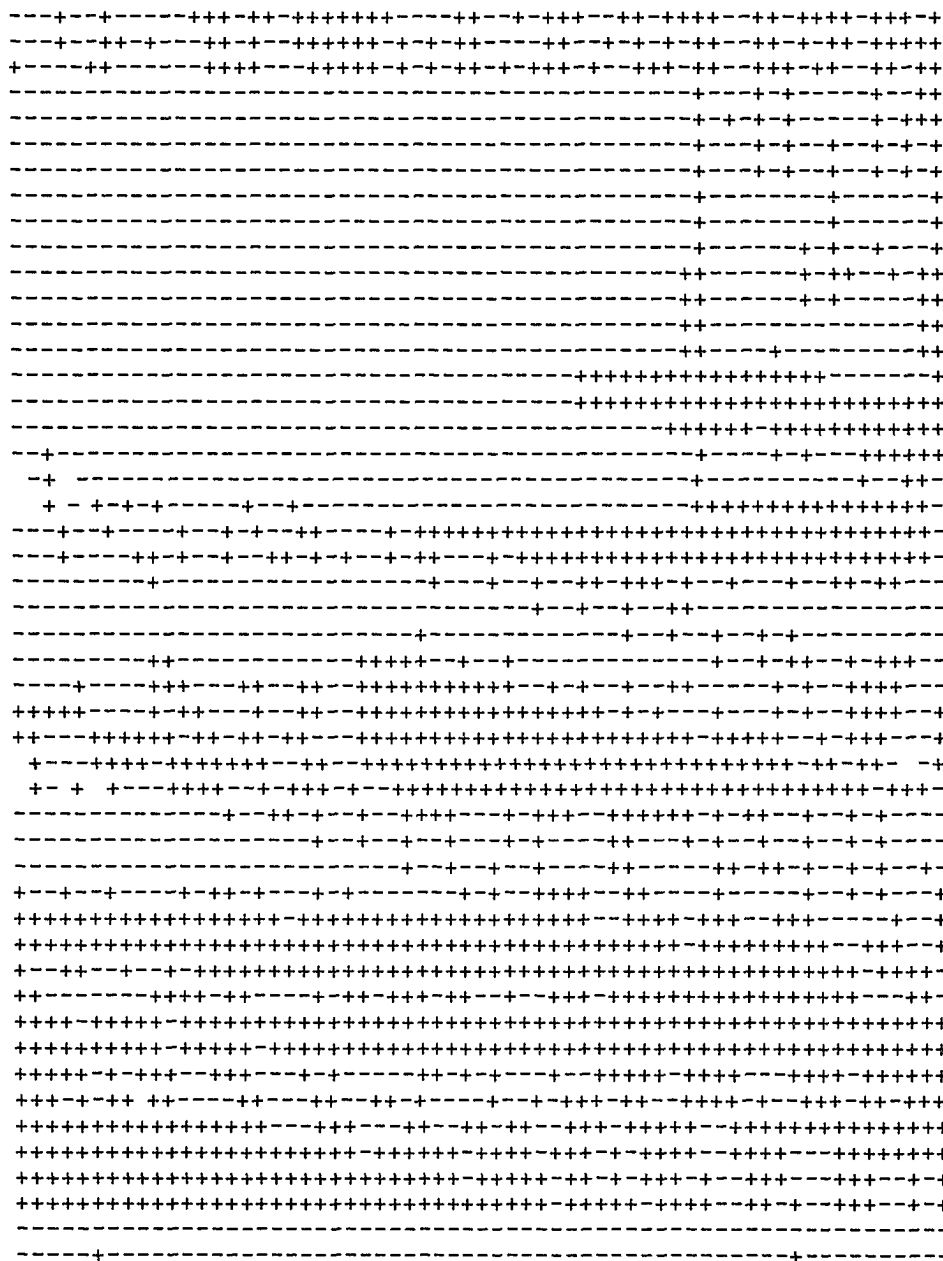


Figure 5-9a. First derivative w.r.t x-axis of a sphere filtered with a mask size of 7 x 7.

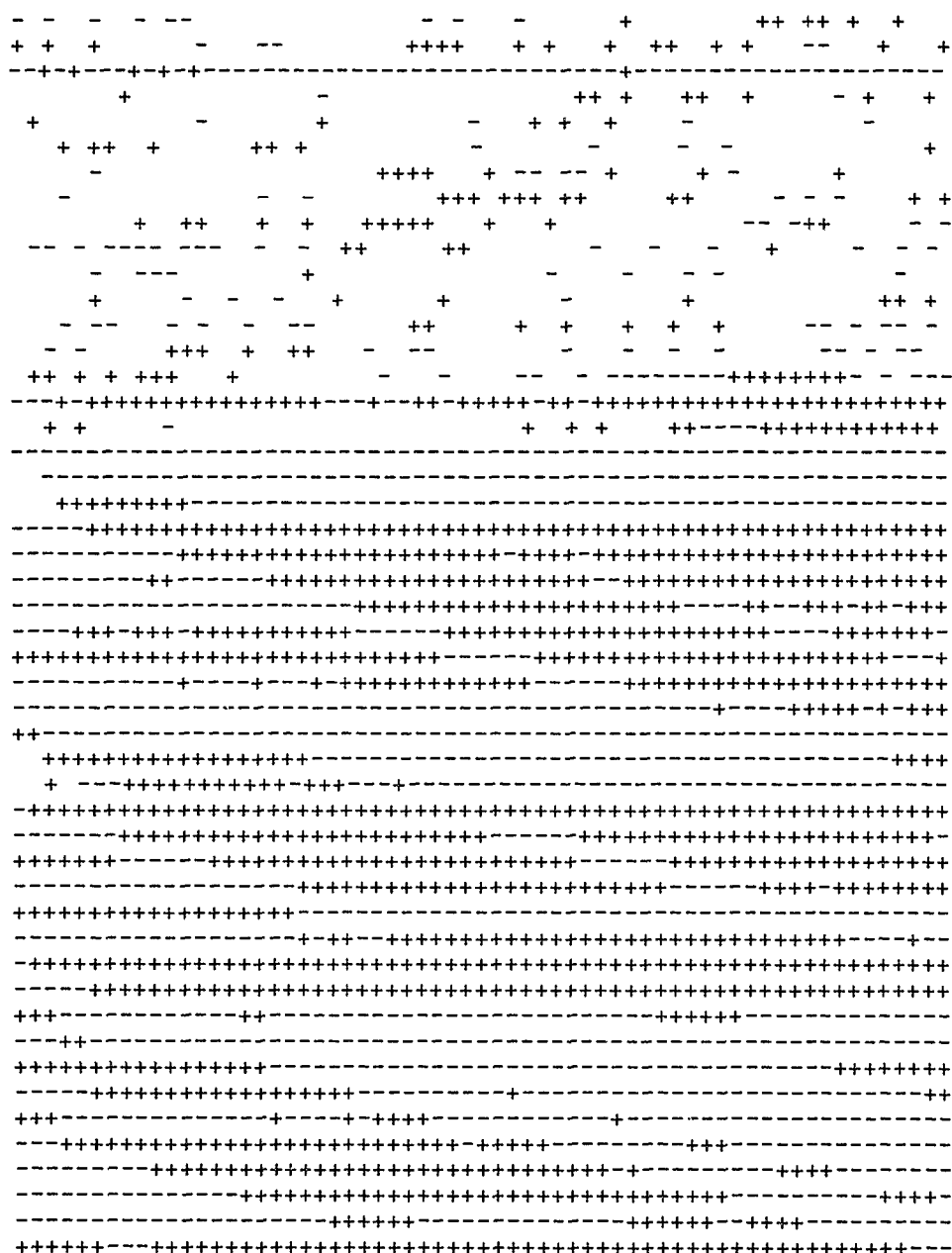


Figure 5-9b. First derivative w.r.t y-axis of a sphere filtered with a mask size of 7 x 7.

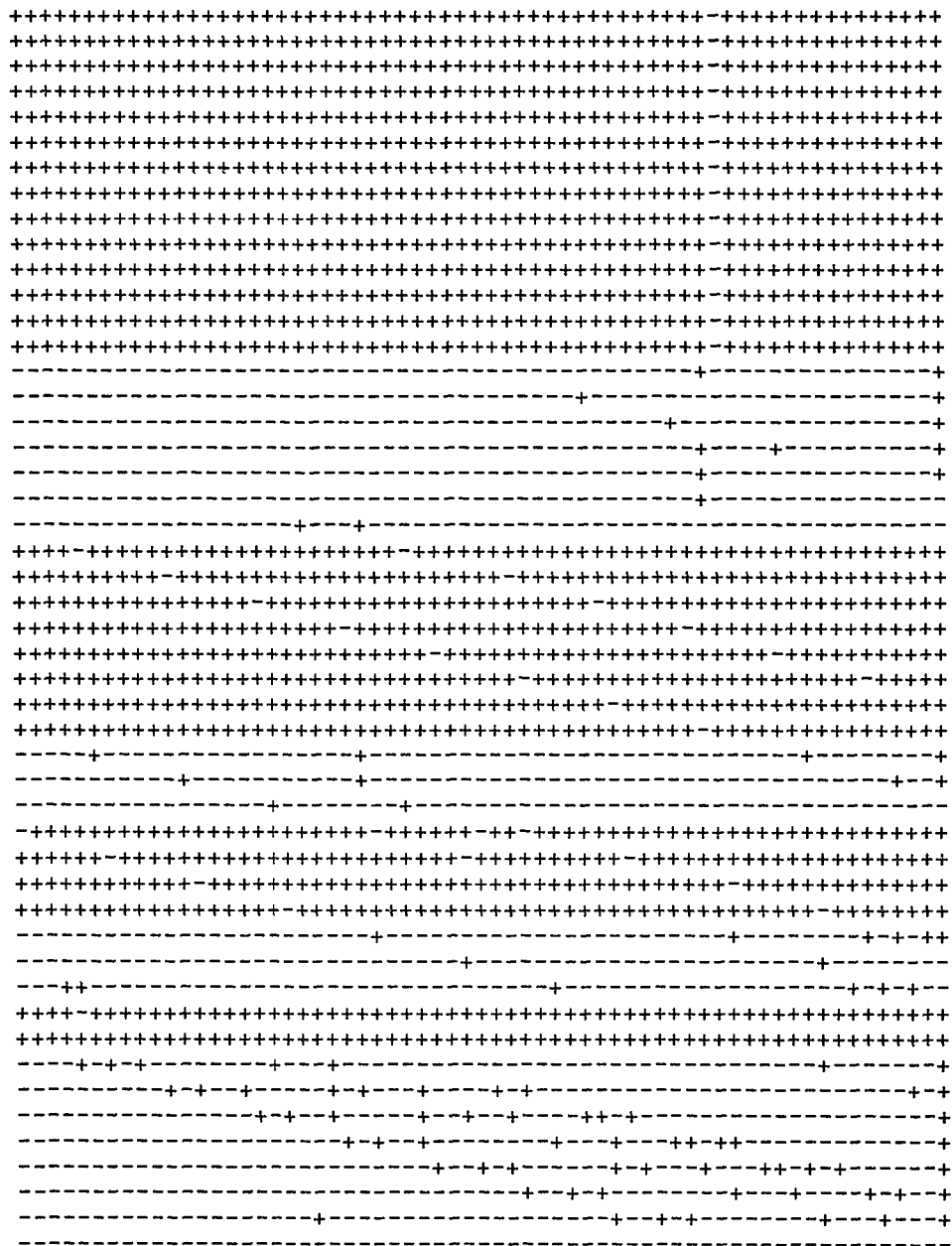


Figure 5-9c. Second derivative w.r.t x-axis of the sphere filtered with a mask size of 7 x 7.

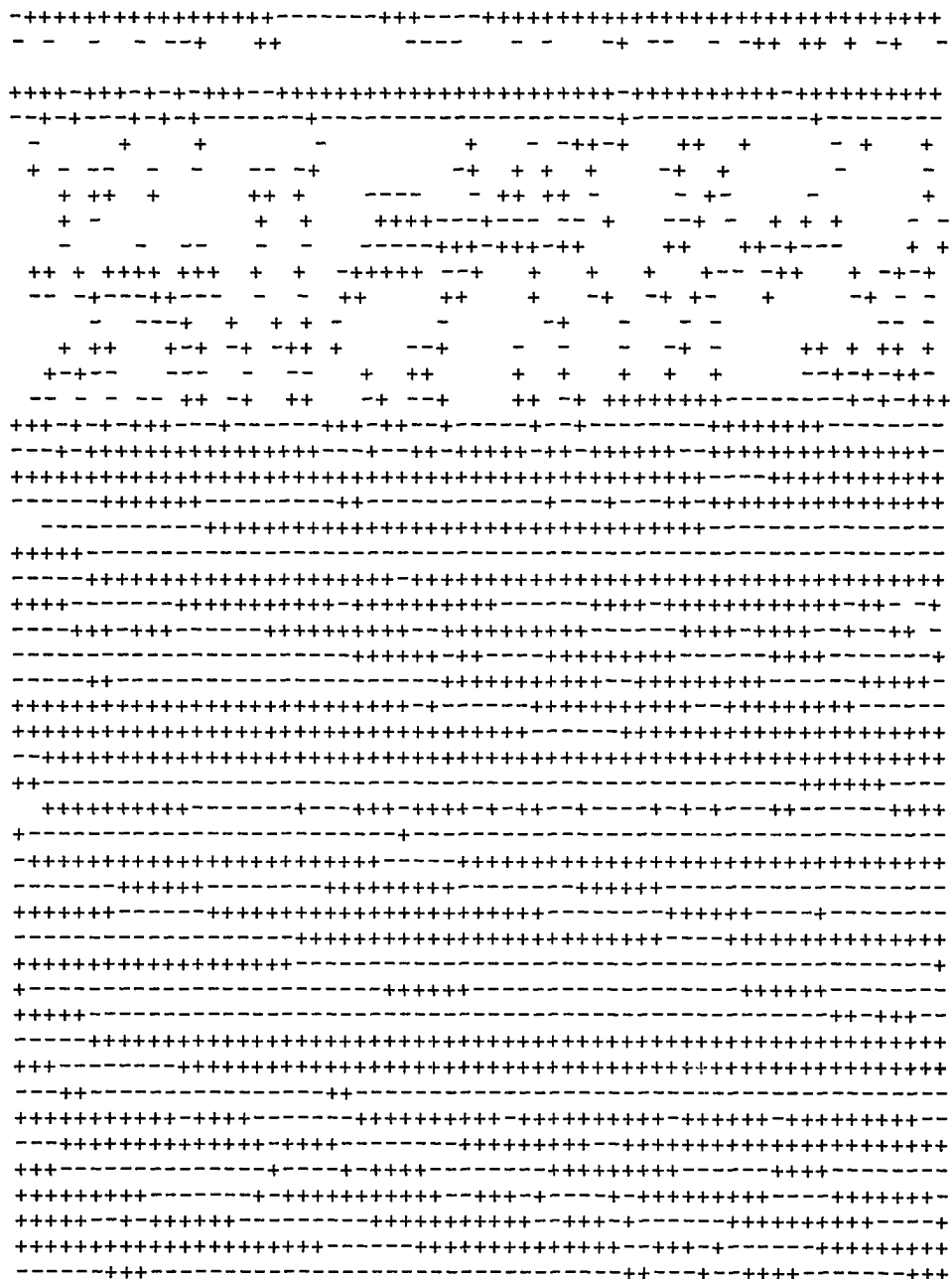


Figure 5-9d. Second derivative w.r.t y-axis of the sphere filtered with a mask size of 7 x 7.

its adjacent neighbor, a "+" or "-" or " " (blank) is assigned to the pixel location in the sign map. Figure 5-10 is the sign map generated for the original raw image data of the sphere. Similarly figures 5-11, 5-12, and 5-13 are the sign maps generated for the 3 x 3, the 5 x 5, and the 7 x 7 filtered images of the sphere. A careful observation of these sign maps suggests that only a small variation has been brought about due to the filtering process.

The prime objective of median filtering is to remove salt and pepper noise in the range images and thus present a noise free range image for the evaluation of the objects coefficients [27]. It can be seen from figures 5-3, 5-4, and 5-5 that these filters met the objective. However, looking at the curvature maps it is observed that as the filter size increases, the apparent curvature is distorted relative to the original curvature. The 3 x 3 filtered image, being the closest to the original raw image, can be utilized for further processing and for describing the surface features. The validity of the curvature map calculations were checked using a "best fit" analysis.

Once the data files were obtained for each of the filtered images, the depth information of each of these files was converted into rectangular coordinates. The operation manual for the laser radar three-dimensional vision system [31] describes the equations used for the transformations of the range information from spherical coordinates to rectangular coordinates:

$$X = (R - L)\sin\theta_f, \quad (5.1)$$

$$Y = (R - \frac{\delta}{\cos\theta_f} - L)\sin\theta_g\cos\theta_f, \quad (5.2)$$

and

$$Z = (R - \frac{\delta}{\cos\theta_f} - L)\cos\theta_g\cos\theta_f, \quad (5.3)$$

where θ_f is the horizontal scanning angle and θ_g is the vertical scanning angle.

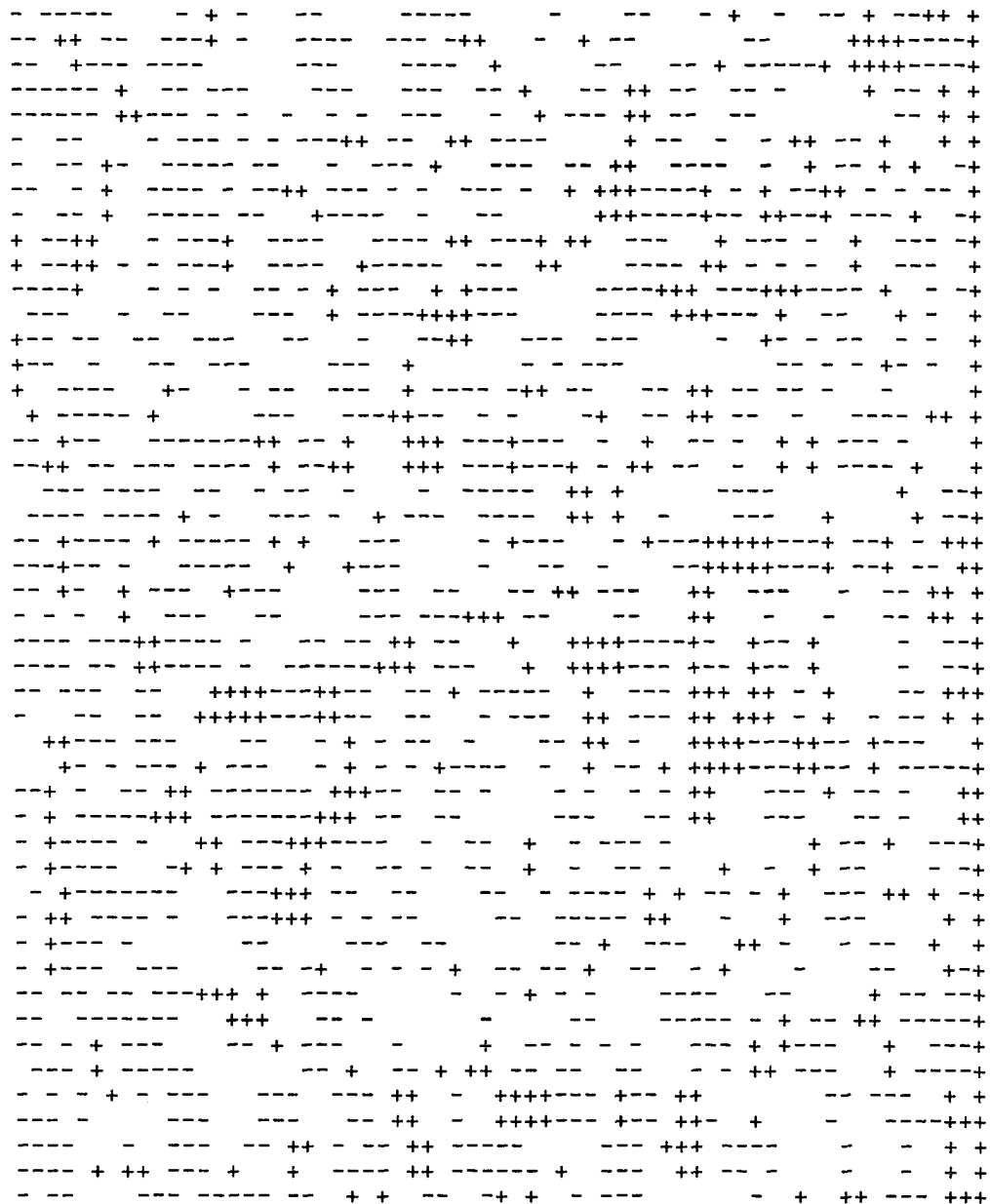


Figure 5-10. Sign map generated for the original raw image of the sphere taking into consideration the magnitude of the depth value at a particular pixel and its neighboring pixel.



Figure 5-11. Sign map generated for the 3 x 3 filtered image of the sphere taking into consideration the magnitude of the depth value at a particular pixel and its neighboring pixel.



Figure 5-12. Sign map generated for the 5 x 5 filtered image of the sphere taking into consideration the magnitude of the depth value at a particular pixel and its neighboring pixel.

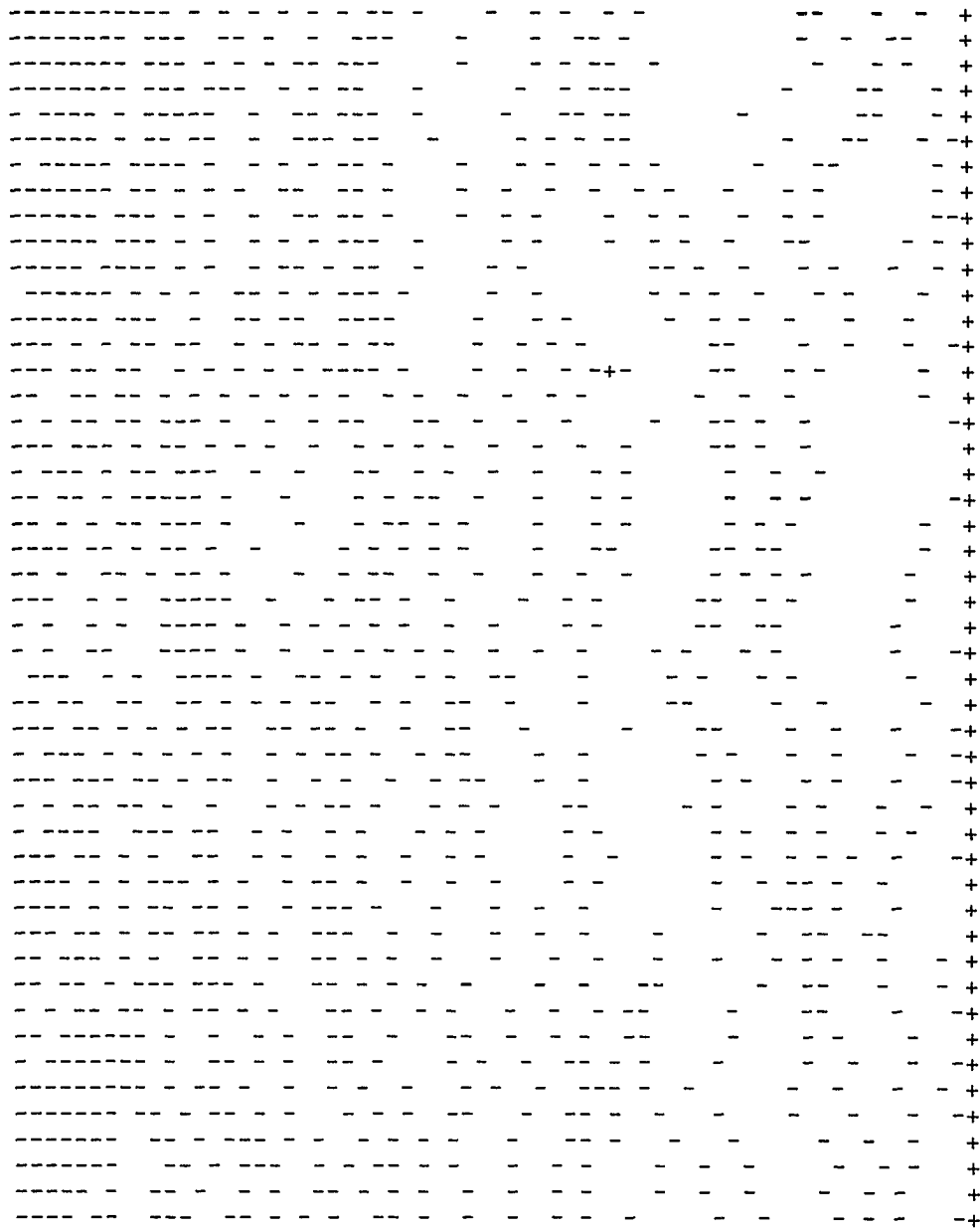


Figure 5-13. Sign map generated for the 7 x 7 filtered image of the sphere taking into consideration the magnitude of the depth value at a particular pixel and its neighboring pixel.

$$\theta_f = 25^\circ - (\text{horizontal pixel \#}) (0.1961 \text{ deg/pixel}). \quad (5.4)$$

$$\theta_g = (\text{vertical pixel \#}) (0.1961 \text{ deg/pixel}) - 25^\circ. \quad (5.5)$$

$$L = 0.362\text{m}. \quad (5.6)$$

$$R \text{ is Range in meters} = (0.00459 \text{ m/pixel})(\text{Range pixel}) + (n - 1/2), \quad (5.7)$$

where n is the electronic range in meters set by the operator. The cartesian coordinate information was then utilized for determining the coefficients which describe each of the three-dimensional surfaces.

Experiments were conducted on range data for spheres and cylinders. Results of median filtering for one such set of range data is presented.

Figure 5-14 is the actual range image of a cylinder. Figure 5-15 is the range image after segmentation. Similarly, figures 5-16 and 5-17 illustrate the 3×3 and the 5×5 median filtered images of the cylinder range data.

Curvature maps for studying the effect of median filtering on the range data are illustrated in figures 5-18(a,b,c,d), figures 5-19(a,b,c,d), and figures 5-20(a,b,c,d), which are the first and second derivatives with respect to the x and y axes for the original cylinder image, the 3×3 filtered cylinder image, and the 5×5 filtered cylinder image, respectively.

Sign maps similar to the ones derived for the sphere are generated for the cylinder and are shown in figures (5-21), (5-22), and (5-23). The figures correspond to the original, the 3×3 filtered image, and the 5×5 filtered images of the cylinder, respectively. Analyzing the curvature maps for the cylinder indicates the filtering process removed the noise and smoothed the image data without effecting significant distortions. The sign maps, much like the curvature maps, seem not much affected by the filtering process other than some information (range data) being lost at the edges. Listed in tables 5-1 and 5-2 are the coefficients obtained for the original range images,

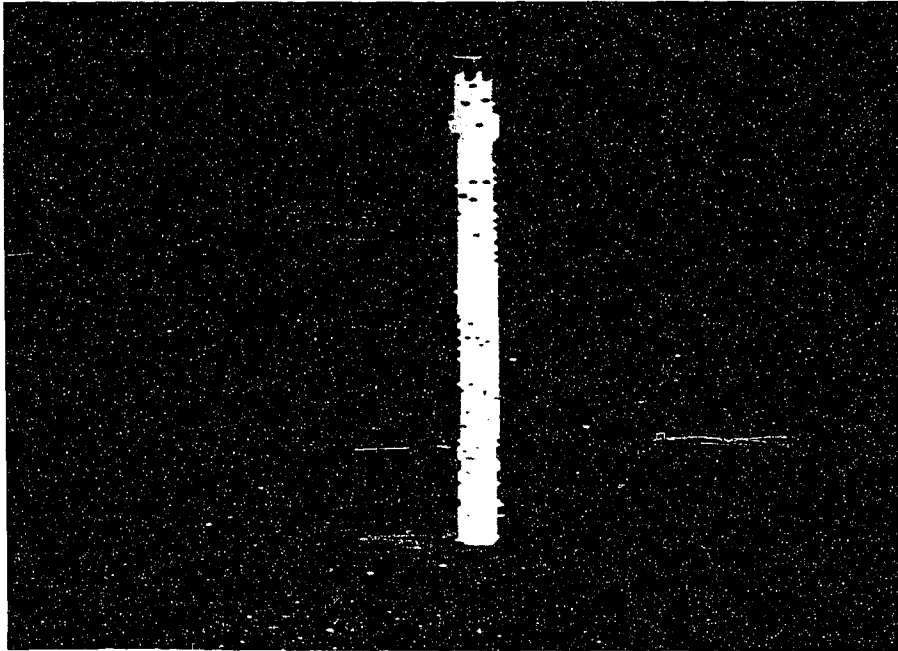


Figure 5-14. Raw range image of the cylinder with its background.

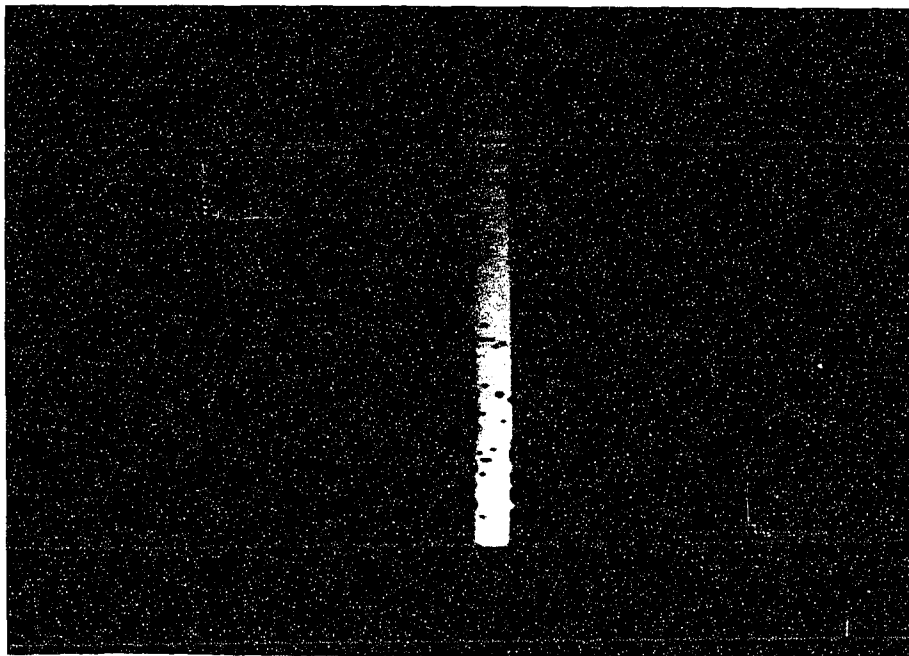


Figure 5-15. Range image of the cylinder after segmentation.

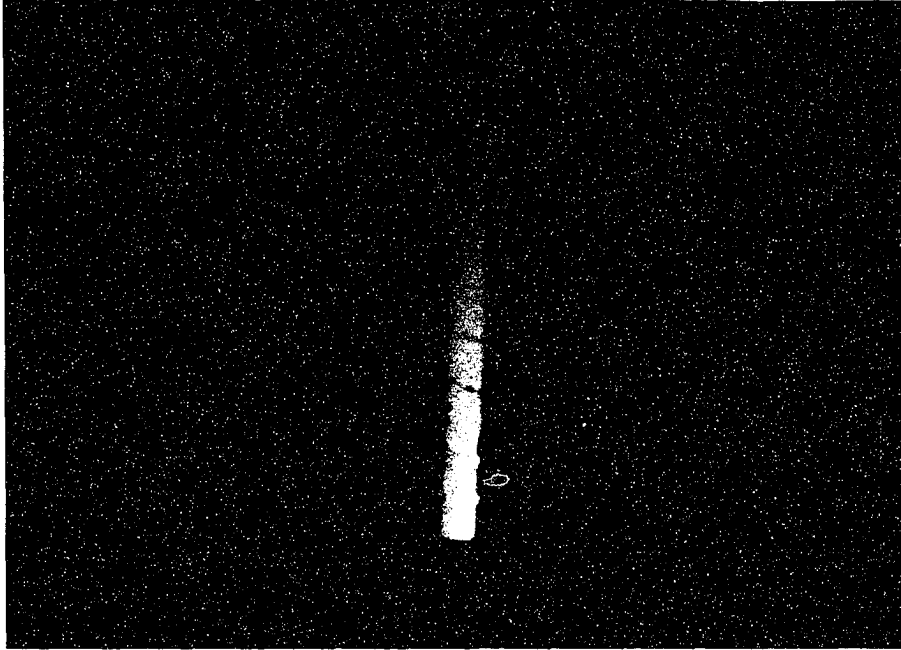


Figure 5-16. 3 x 3 median filtered image of the raw cylinder.



Figure 5-17. 5 x 5 median filtered image of the raw cylinder.

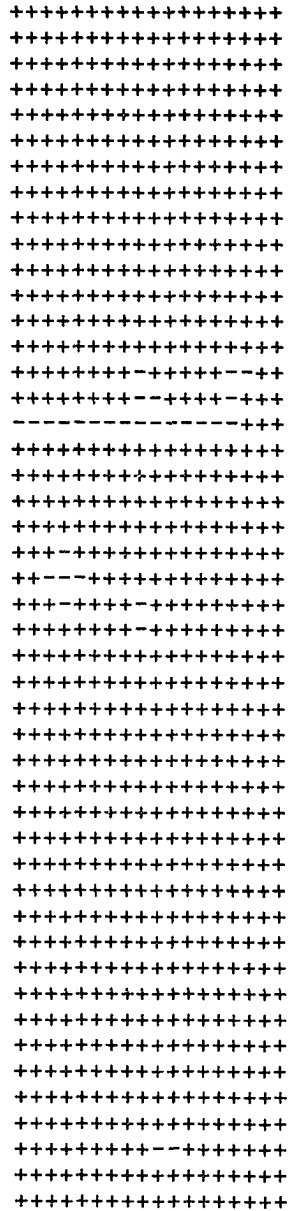


Figure 5-18a. First derivative w.r.t x-axis of the original cylinder.

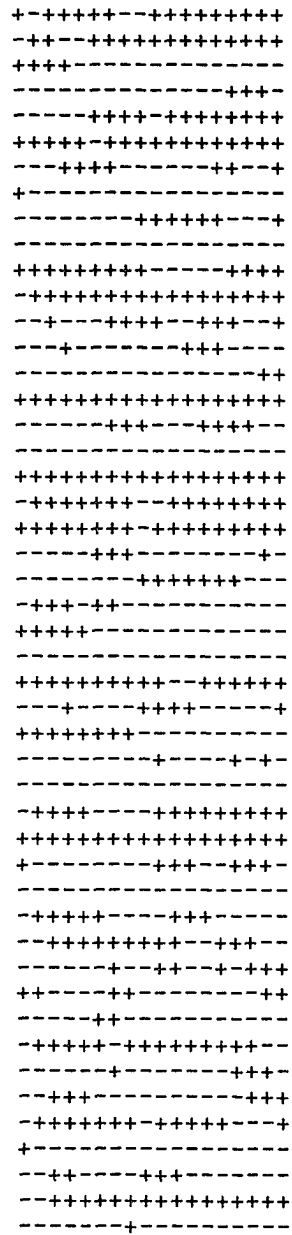


Figure 5-18b. First derivative w.r.t y-axis of the original cylinder.

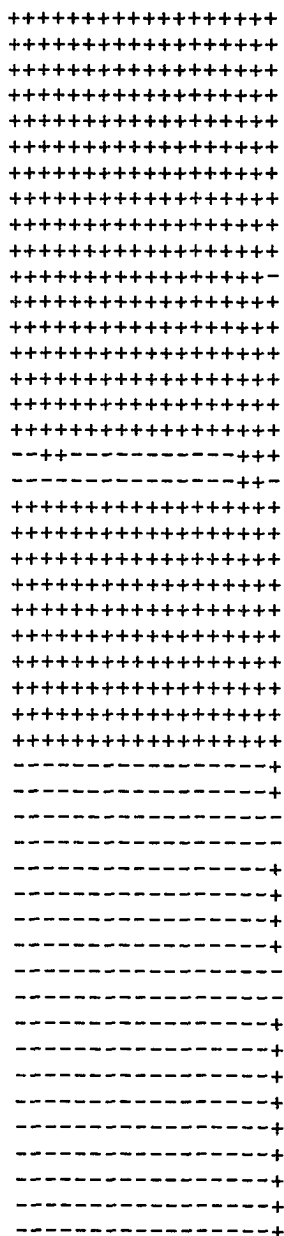


Figure 5-18c. Second derivative w.r.t x-axis of the original cylinder.

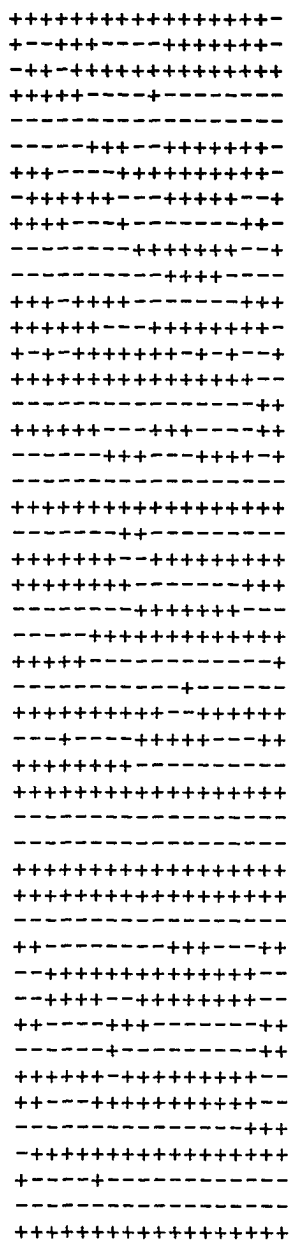


Figure 5-18d. Second derivative w.r.t y-axis of the original cylinder.

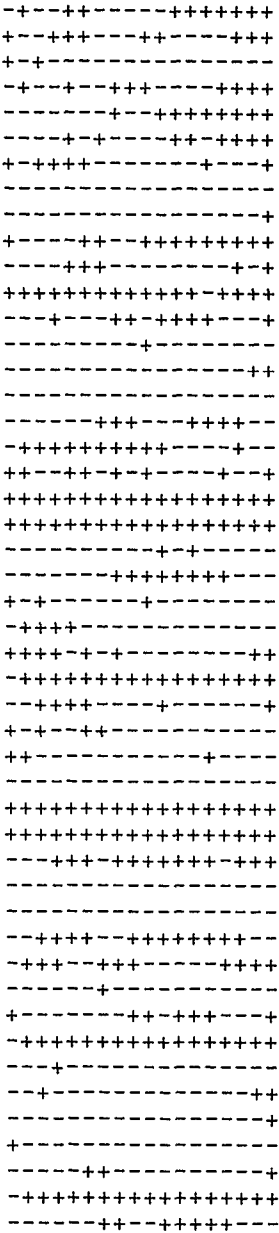


Figure 5-19b. First derivative w.r.t y-axis of the cylinder filtered with a mask size of 3 X 3.

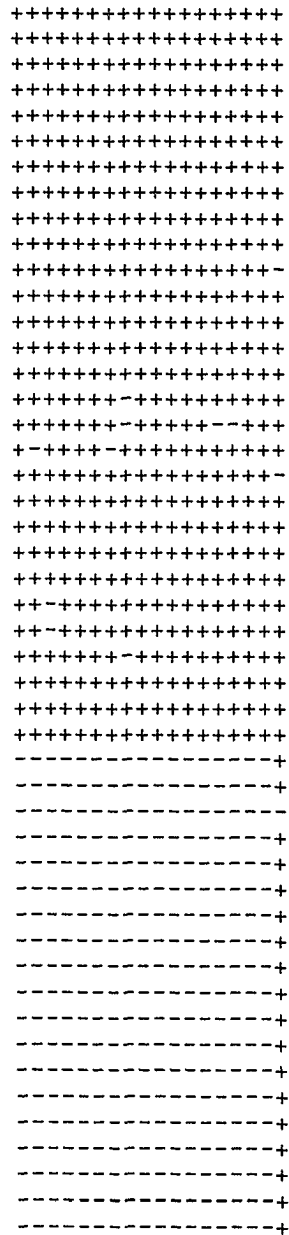


Figure 5-19c. Second derivative w.r.t x-axis of the cylinder filtered with a mask size of 3 X 3.

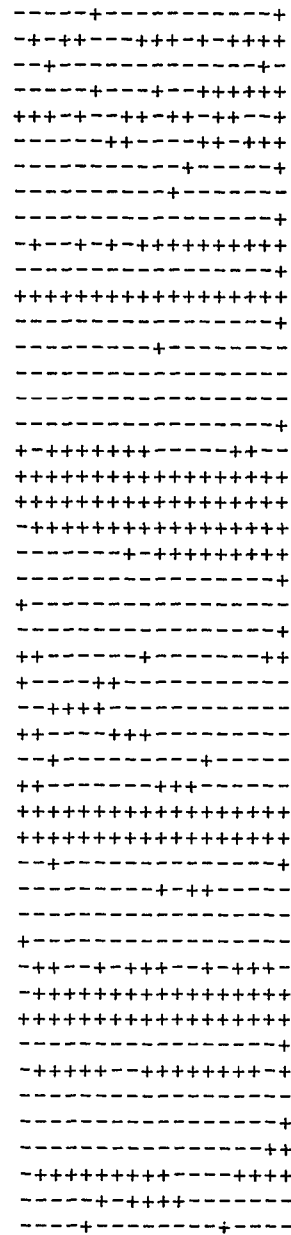


Figure 5-20b. First derivative w.r.t y-axis of the cylinder filtered with a mask size of 5 X 5.

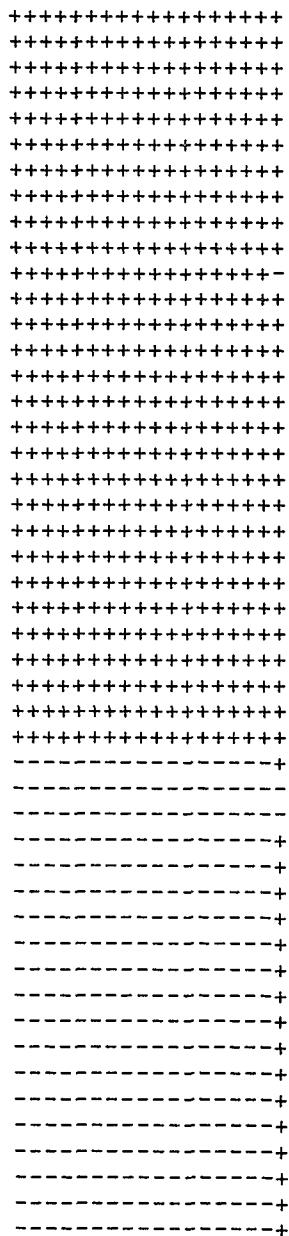


Figure 5-20c. Second derivative w.r.t x-axis of the cylinder filtered with a mask size 5 X 5.

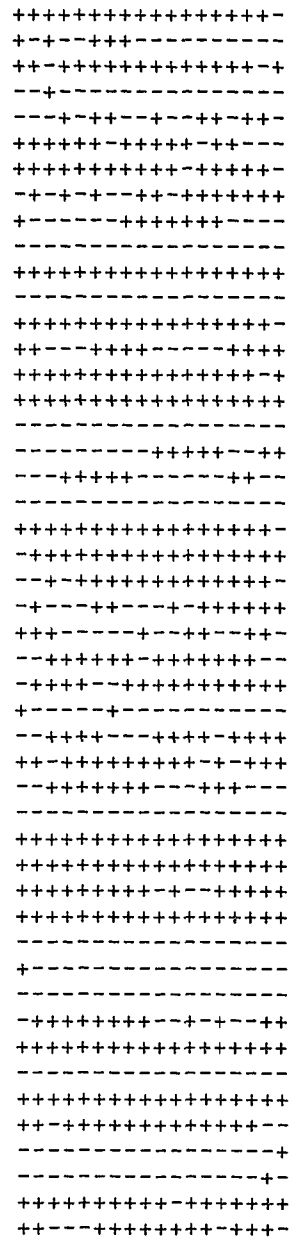


Figure 5-20d. Second derivative w.r.t y-axis of the cylinder filtered with a mask size of 5 X 5.

```

-  --      -  -  ++++++
-  --      -  ++  -  +++++
-  -  --  ---+++  --  +++++
-  --  -  +-  -  ---  +++
-  ---  +-  -  --  +++
-  ---  +++-  ---+++++
-  --      +  ---  +++++
-+  --  ---  +  ++++++
-+  --  ---  +  ++++++
-+  --      +  ---  +++
-+  ---  -  +  ---  +++
-  ---  +++-  ---+++++
-+  ---  +++-  ---  ++++++
-+  +++-  ---  ---  +
-+  --  +  -  +++++
-  --  --  ++  ---+++++
-  --  --  +  ---+++++
-  --  +  ---  -  +++++
-  ---++  --  --  +++++
++++---  ---+  ++++++
++++---+---  ++++++
-+---+++---  +---+++++
-+  +++-  ---+---+++++
-  ---      +  ---  -+++
-  ---  -+  +  --  -+++
-+  ---+++  +  --  +++++
-+  ---+++  ++  ---+++++
-+++---  +  --  +++++
-+  ---  +  --  +++++
---+  --  +  -  +  ++
---+  --      +  +++
-  -  --      -  +  +++
-  --  +  ---  +++  +++
---++---  +  ---+++++
---++  --  +  -  +++++
-+  ---+++  ---  ++
-+  ---++  --  -+++

```

Figure 5-21. Sign plot for the original cylinder. The sign "+" or "-" is assigned depending whether the adjacent pixel has a range value lesser or greater than the pixel to its left.

the 3 x 3 filtered images, the 5 x 5 filtered images and finally the 7 x 7 filtered images of a sphere and a cylinder.

These tables show that none of the coefficient sets describe a real sphere or cylinder with any certainty. The following procedure was utilized to determine which particular set of coefficients best describes the original range data of the object. A small surface patch of the object is chosen. In the quadratic form,

$$F(x,y,z) = ax^2 + by^2 + cz^2 + 2fyz + 2gzx + 2hxy + 2px + 2qy + 2rz + d = 0,$$

the coefficients a, b, c, d, f, g, h, p, q, and r are inserted and for each (x,y,z) of the object patch, the error is evaluated for each set of coefficients. A plot is generated in which every point of the surface patch is replaced with the numerals 1, 3, 5, and 7 signifying that the minimum error was obtained for that particular set of coefficients. Figure 5-24 is one such plot for the raw segmented image of the sphere. Numeral 1 refers to the situation when the original set of coefficients fits best, and similarly numerals 3, 5, and 7 are used depending whether the 3 x 3 or the 5 x 5 or the 7 x 7 set of coefficients, listed in Table 5-1, of the sphere fits best. As seen from Figure 5-24, the presence of excess number of the numeral 3 confirms the results obtained from the curvature maps for the sphere range data. Figure 5-25 is the plot using the coefficients listed in Table 5-2 for the cylinder. Both of these plots validate our findings from the analysis of the curvature maps.

The experiments mentioned above were performed on a large number of real range data sets for spheres, cylinders, and cones, the results of which are shown in appendix A.

5.3 Application of the Recognition Process to the Processed Image Data

The next objective was to apply our recognition schemes to the processed images of a sphere, a cylinder and a quadric cone. Each of the processed images of the sphere, the cylinder, and the cone were intersected with two planes (one parallel to the

11111111311111337
 1111333111131153337
 111111111111153537
 113533511531111137
 115515117571111117
 11111117711177757
 11111117711177777
 11555577717777711
 13555577711777717
 1111111177777137
 113111111337777117
 113111311111111137
 113135111113111737
 113115535751117111
 1131355557711355311
 111111333131133155
 1131131333131133155
 3113311353133315315
 311511115711111117
 1355355157771137317
 1135555137771177117
 113115511177777115
 113113531117777135
 113531131577777135
 113531351357777135
 1131331353177177115
 1131331333137177711
 111133377111117773
 111115577711111175
 135555777771177711
 155555777771177735
 1531113777111777115
 1333133177711777111
 73155335777771113
 75135515777777775
 1351155317771171111
 1155555111777771113
 113535533777777111
 1111151117771177111
 13555557777777773
 15555557777777775

Figure 5-25. Best fit plot obtained for the cylinder belonging to set A. Numerals "1, 3, 5, 7" denote the original image, the 3 x 3 image, the 5 x 5 image, and the 7 x 7 image respectively.

COMPARISON OF COEFFICIENTS EVALUATED FOR THE ORIGINAL AND THE PROCESSED IMAGES OF A SPHERE				
COEFFICIENT	RAW IMAGE	3 X 3 FILT. IMAGE	5 X 5 FILT. IMAGE	7 X 7 FILT. IMAGE
A, COEFF. OF X ²	0.3026	0.2211	-0.3260	0.4242
B, COEFF. OF Y ²	0.2734	0.2802	-0.4860	0.2178
C, COEFF. OF Z ²	0.6545	0.7747	-0.3338	0.5845
F, COEFF. OF YZ	0.5310	-0.5348	0.4834	-0.3417
G, COEFF. OF XZ	0.6357	-0.4860	0.7194	-0.7452
H, COEFF. OF XY	0.3524	0.2339	-0.5801	0.4353
P, COEFF. OF X	0.3036	0.1999	-0.3159	0.3127
Q, COEFF. OF Y	0.4199	0.4401	-0.3524	0.1996
R, COEFF. OF Z	-0.8172	-1.0163	0.3191	-0.5858
D, CONSTANT	0.2847	0.3717	-0.0973	0.1516

Table 5-1. Comparison of the coefficients evaluated for the original and the processed images of a sphere.

COMPARISON OF COEFFICIENTS EVALUATED FOR THE ORIGINAL AND THE PROCESSED IMAGES OF A CYLINDER			
COEFFICIENT	RAW IMAGE	3 X 3 FILTERED IMAGE	5 X 5 FILTERED IMAGE
A, COEFF. OF X ²	0.8338	0.6636	0.0572
B, COEFF. OF Y ²	0.0041	0.0209	0.599
C, COEFF. OF Z ²	0.059	-0.0923	0.4416
F, COEFF. OF YZ	-0.00103	-0.0219	-0.807
G, COEFF. OF XZ	-0.636	-0.7604	0.459
H, COEFF. OF XY	0.4437	0.7727	-0.149
P, COEFF. OF X	-0.0141	0.4242	-0.5915
Q, COEFF. OF Y	-0.189	-0.2155	1.089
R, COEFF. OF Z	0.193	0.374	-1.019
D, CONSTANT	-0.1341	-0.253	0.664

Table 5-2. Comparison of the coefficients evaluated for the original and the processed images of a cylinder.

xy plane, the other parallel to the xz plane). The results obtained for the sphere are tabulated in Table 5-3. A decision on the curve being an ellipse or a circle was made based upon the parity and disparity of the x^2 , y^2 , and z^2 coefficients.

Sphere Images			
plane 1, $y = k$	Ellipse	Ellipse	Ellipse
plane 2, $z = k$	Ellipse	Ellipse	Circle

Table 5-3. Curves intercepted by the two planes, $z = k$, $y = k$, with real raw and processed range data of the sphere.

Experiments conducted with the raw and the processed images of the cylinder led to the results tabulated in Table 5-4.

Cylinder Images			
plane 1, $y = k$	Ellipse	Line	Line
plane 2, $z = k$	Ellipse	Ellipse	Ellipse

Table 5-4. Curves intercepted by the two planes, $z = k$, $y = k$, with real raw and processed range data of the cylinder.

As seen from the tabulated results, the raw images come close in generating the desired curves for each of the objects, but at the same time a 5×5 filter in either case generates the exact two-dimensional curves.

Experiments conducted with the raw and the processed images of the quadric cone led to the results tabulated in Table 5-5.

Quadric cone Images			
plane 1, $z = k$	Ellipse	Ellipse	Ellipse
plane 2, $y = k$	Ellipse	Hyperbola	Hyperbola

Table 5-5. Curves intercepted by the two planes, $z = k$, $y = k$, with real raw and processed range data of the quadric cone.

As seen from the tabulated results, the raw images do not come close in generating the desired curves for each of the objects, but at the same time the 3×3 as well as the 5×5 filter in either case generates the exact two-dimensional curves. Coefficients generated for the raw image data of the cone as well as the 3×3 and 5×5 median filtered image data of the quadric cone are listed in Appendix B.

5.4 Application of the Rotation Alignment Algorithm

The rotation alignment algorithm which determines the orientation of the quadric surfaces in space and then aligns them in accordance to our desired coordinate system was applied to simulated data as well as real data.

Consider tables 5-6, 5-7, and 5-8, which compare the coefficients of the sphere range data before and after rotation alignment.

Each of the image data sets, i.e., the original raw image of the sphere and the 3×3 and the 5×5 median filtered images of the sphere, required three iterations to eliminate the product terms. Since a sphere is symmetric about all coordinate axes, no rotation alignment should be needed. The alignment algorithm was performed just to see how the coefficients relate to each other before and after the rotation. The coefficients were basically invariant as expected.

Similarly, tables 5-9, 5-10, and 5-11, show the coefficients obtained before and after the rotation alignment for the cylinder range data. However, in these cases, each of the image data sets, i.e., the original raw image of the cylinder, the 3×3 and the

COEFFICIENT	BEFORE	AFTER ALIGNMENT
A, COEFF. OF X ²	0.3026	0.3206466
B, COEFF. OF Y ²	0.2734	0.184263
C, COEFF. OF Z ²	0.6545	0.7999953
F, COEFF. OF YZ	0.5310	0.0
G, COEFF. OF XZ	0.6357	0.0
H, COEFF. OF XY	0.3524	0.0
P, COEFF. OF X	0.3036	0.252
Q, COEFF. OF Y	0.4199	0.41686
R, COEFF. OF Z	-0.8172	-0.8623
D, CONSTANT	0.2847	0.2847

Table 5-6. New coefficients of the raw image data of sphere after alignment.

COEFFICIENT	BEFORE	AFTER ALIGNMENT
A, COEFF. OF X ²	0.264	0.249
B, COEFF. OF Y ²	0.129	0.1311
C, COEFF. OF Z ²	0.5738	0.634
F, COEFF. OF YZ	-0.6275	0.0
G, COEFF. OF XZ	-0.783	0.0
H, COEFF. OF XY	0.4014	0.0
P, COEFF. OF X	0.4826	0.4405
Q, COEFF. OF Y	0.3670	0.3746
R, COEFF. OF Z	-0.7218	-0.7401
D, CONSTANT	0.2210	0.2210

Table 5-7. New coefficients of the 3 x 3 median filtered image data of sphere after alignment.

COEFFICIENT	BEFORE	AFTER ALIGNMENT
A, COEFF. OF X^2	0.303	0.3765
B, COEFF. OF Y^2	0.392	0.372
C, COEFF. OF Z^2	0.6526	0.6417
F, COEFF. OF YZ	-0.4487	0.0
G, COEFF. OF XZ	-0.8376	0.0
H, COEFF. OF XY	0.2416	0.0
P, COEFF. OF X	0.4047	0.4259
Q, COEFF. OF Y	0.2214	0.2184
R, COEFF. OF Z	-0.7089	-0.7423
D, CONSTANT	0.1913	0.1913

Table 5-8. New coefficients of the 5 x 5 median filtered image data of sphere after alignment.

COEFFICIENT	BEFORE	AFTER ALIGNMENT
A, COEFF. OF X^2	0.8338	0.9812
B, COEFF. OF Y^2	0.00411	-0.1143
C, COEFF. OF Z^2	0.059	0.03255
F, COEFF. OF YZ	-0.00103	0.0
G, COEFF. OF XZ	-0.636	0.0
H, COEFF. OF XY	0.4437	0.0
P, COEFF. OF X	-0.0141	-0.0876
Q, COEFF. OF Y	-0.189	-0.2478
R, COEFF. OF Z	0.193	-0.01125
D, CONSTANT	-0.1341	-0.1341

Table 5-9. New coefficients of the raw image data of cylinder after alignment.

COEFFICIENT	BEFORE	AFTER ALIGNMENT
A, COEFF. OF X ²	0.6636	0.9235
B, COEFF. OF Y ²	0.0209	-0.2967
C, COEFF. OF Z ²	-0.0923	-0.00207
F, COEFF. OF YZ	-0.0219	0.0
G, COEFF. OF XZ	-0.7604	0.0
H, COEFF. OF XY	0.7727	0.0
P, COEFF. OF X	0.4242	0.1923
Q, COEFF. OF Y	-0.2155	-0.5368
R, COEFF. OF Z	0.374	0.05379
D, CONSTANT	-0.253	-0.2533

Table 5-10. New coefficients of the 3 x 3 median filtered image data of cylinder after alignment.

COEFFICIENT	BEFORE	AFTER ALIGNMENT
A, COEFF. OF X ²	0.0572	-0.07251
B, COEFF. OF Y ²	0.599	0.977
C, COEFF. OF Z ²	0.4416	0.1930
F, COEFF. OF YZ	-0.807	0.0
G, COEFF. OF XZ	0.459	0.0
H, COEFF. OF XY	-0.149	0.0
P, COEFF. OF X	-0.5915	-0.1764
Q, COEFF. OF Y	1.089	1.5696
R, COEFF. OF Z	-1.019	-0.1902
D, CONSTANT	0.664	0.664

Table 5-11. New coefficients of the 5 x 5 median filtered image data of cylinder after alignment.

5 x 5 median filtered images of the cylinder, required four iterations to eliminate the product terms. Except for the coefficients of the raw image data, both the 3 x 3 and 5 x 5 filtered coefficients after alignment yielded the desired curves when intersected with various planes. Making use of the coefficients of the 5 x 5 filtered image, the diameter of this particular cylinder was calculated to be 4.99 centimeters. The actual diameter of the cylinder was 5 centimeters. Appendix C contains more results obtained while carrying out the rotation alignment algorithm for other cylinder range images.

The rotation alignment technique was utilized for a large group of simulated data. Listed in tables 5-12, 5-13, and 5-14 are several upon which the utilization of our recognition scheme correctly identified the surfaces. Upon application of our recognition scheme the quadric surfaces represented in Tables 5-12, 5-13, and 5-14 were correctly recognized as an ellipsoid, a hyperboloid of one sheet, and a hyperbolic cylinder, respectively.

All the simulated data sets of quadric surfaces could be recognized after conducting the rotation alignment technique on the original quadratic representation. The three-dimensional discriminant approach which was described in Chapter Two was applied to several simulated data of quadrics.

5.5 Application of Three-Dimensional Discriminant Technique

Results for the simulated data are illustrated in Table 5-15 and are very effective as predicted by the theory. Object (1) refers to a parabolic cylinder, (2) refers to a hyperbolic paraboloid, (3) refers to a hyperboloid of one sheet, (4) refers to an ellipsoid, (5) refers to a hyperbolic cylinder, (6) refers to a quadric cone, (7) refers to a hyperboloid of two sheets, and (8) refers to an elliptic paraboloid. A listing of a sample data file is included in Appendix D. However, as expected, unsatisfactory results were obtained while experimenting with real data. A listing of all the programs

COEFFICIENT	BEFORE	AFTER ALIGNMENT
A, COEFF. OF X ²	103	49.84
B, COEFF. OF Y ²	125	96.887
C, COEFF. OF Z ²	66	145.3905
F, COEFF. OF YZ	-60	0.0
G, COEFF. OF XZ	-12	0.0
H, COEFF. OF XY	-48	0.0
P, COEFF. OF X	0.0	0.0
Q, COEFF. OF Y	0.0	0.0
R, COEFF. OF Z	0.0	0.0
D, CONSTANT	-294	-294

Table 5-12. New coefficients of an unknown simulated data obtained after alignment.

COEFFICIENT	BEFORE	AFTER ALIGNMENT
A, COEFF. OF X ²	0.0	2.0
B, COEFF. OF Y ²	2.0	-4.0
C, COEFF. OF Z ²	1.0	-1.0
F, COEFF. OF YZ	-4.0	0.0
G, COEFF. OF XZ	-4.0	0.0
H, COEFF. OF XY	0.0	0.0
P, COEFF. OF X	0.0	0.0
Q, COEFF. OF Y	0.0	0.0
R, COEFF. OF Z	0.0	0.0
D, CONSTANT	-4.0	-4.0

Table 5-13. New coefficients of an unknown simulated data obtained after alignment.

COEFFICIENT	BEFORE	AFTER ALIGNMENT
A, COEFF. OF X ²	0.0	3.0
B, COEFF. OF Y ²	0.0	0.0
C, COEFF. OF Z ²	0.0	-3.0
F, COEFF. OF YZ	-1.414	0.0
G, COEFF. OF XZ	0.0	0.0
H, COEFF. OF XY	1.0	0.0
P, COEFF. OF X	0.0	0.0
Q, COEFF. OF Y	0.0	0.0
R, COEFF. OF Z	0.0	0.0
D, CONSTANT	-3.0	-3.0

Table 5-14. New coefficients of an unknown simulated data obtained after alignment.

SURFACE CHARACTERIZATION USING THREE-DIMENSIONAL DISCRIMINANT APPROACH FOR SIMULATED DATA								
COEFFICIENTS OF THE SIMULATED OBJECTS								
A, COEFF. OF X ²	1	0	0	1	0	0	1	3
B, COEFF. OF Y ²	4	1	0	3	0	0	0	0
C, COEFF. OF Z ²	9	20	0	2	6	1	3	2
F, COEFF. OF YZ	-6	-4.5	1.5	-1	1.5	3	1	0
G, COEFF. OF XZ	3	-2.5	1	0	1	-2	-1	-2
H, COEFF. OF XY	-2	0.5	0.5	1	0.5	1	0	0
P, COEFF. OF X	1	0.5	-1	2	-2	2	0	0
Q, COEFF. OF Y	7	0	0	5	3	3	1	1
R, COEFF. OF Z	0	0	3	0	0	0	3	0
D, CONSTANT	10	0	0	8	0	12	9	19
OBJECT IS	(1)	(2)	(3)	(4)	(5)	(6)	(7)	(8)

Table 5-15. Surface characterization using three-dimensional discriminant approach for simulated data.

utilized in this research is included in Appendix E. The program that generates the ten coefficients for quadric surfaces and the program which aligns the quadric surfaces to a desired coordinate system are among those listed.

CHAPTER SIX

CONCLUSIONS

6.1 Overview

We have presented a new approach based on two-dimensional analytic geometry to recognize a series of three-dimensional objects. Among the various three-dimensional objects considered are the hyperboloids of one and two sheets, the ellipsoids, the spheres, the circular and elliptical quadric cones, the circular and elliptical cylinders, the parabolic and hyperbolic cylinders, the elliptic and hyperbolic paraboloids, and the parallelepipeds.

Our proposed method utilizes a two-dimensional discriminant which is a measure for distinguishing curves. Instead of evaluating the ten generated coefficients and attempting to recognize the surface from its quadric representation, we can identify the quadrics using the information resulting from the intersection of the surface with different planes. If the surface is one of those listed above, there are five possible two-dimensional curves that may result from such intersections: (i) a circle, (ii) an ellipse, (iii) a parabola, (iv) a hyperbola, and (v) a line. Thus, a feature or pattern vector with five independent components can be formed for characterizing each of the surfaces.

Although all of the quadric surfaces considered have been symmetric, our recognition system can be extended to other three-dimensional objects. Figures 6-1, 6-2, and 6-3 are examples of these surfaces which exist in the real world. To recognize complex objects a suitable segmentation technique is required for the isolation of each individual surface.

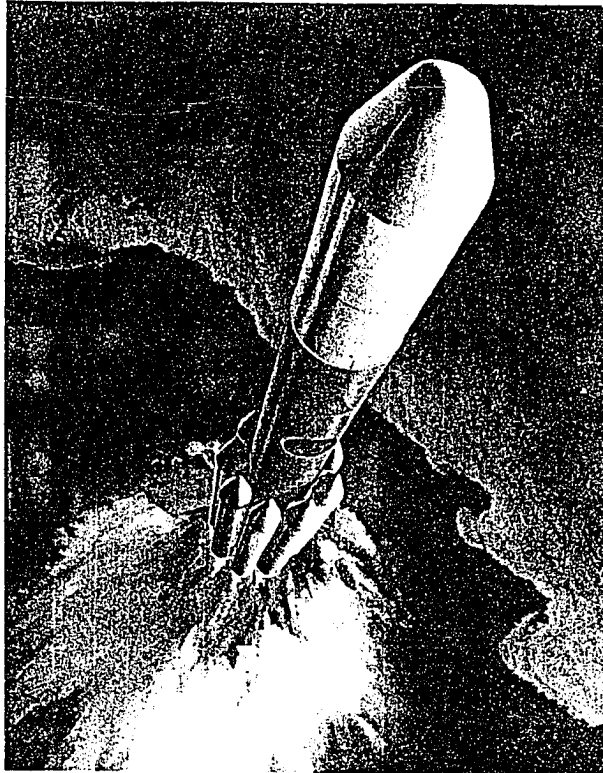


Figure 6-1. This delta rocket is composed of cylindrical and conical shapes (*Courtesy NASA*).

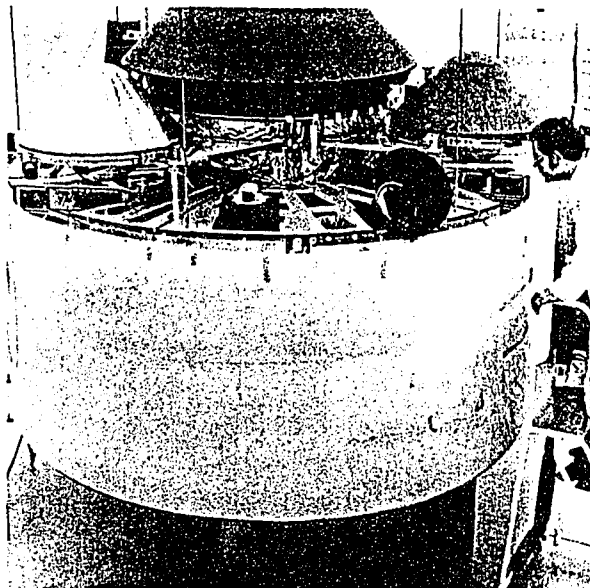


Figure 6-2. Conical domes and cylinderlike body make up this space probe (*Courtesy NASA*).

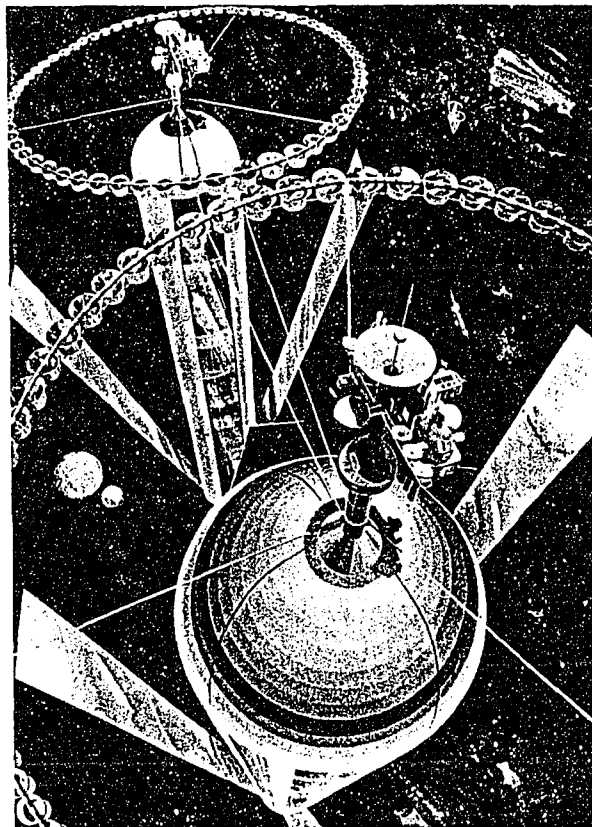


Figure 6-3. Cylindrical space station with a half sphere dome top (*Courtesy NASA*).

6.2 Advantages of the Recognition Scheme

Some of the advantages of our recognition scheme are listed below:

- (1) Recognition systems using the curvature approach (evaluation of the mean and Gaussian curvatures) are very computationally intensive. These approaches never really describe the quadric surface in question. Our proposed recognition system is computationally efficient. All of the quadric surfaces are recognized as well as described in terms of their dimensions.
- (2) The three-dimensional discriminant approach discussed in Chapter Two works only on ideal or simulated data. It is not useful for real range data. Our recognition system is shown to work for both simulated and real range data.
- (3) The best-fit plot technique used for analyzing processed range images is a new and efficient technique to determine the validity and integrity of the processed range images.
- (4) The rotation alignment technique is a new method which systematically and effectively eliminates the product terms and aligns the quadric surfaces in our desired coordinate system through an iterative technique.
- (5) The curvature analysis technique and the best-fit plot can be used to determine performances of various laser range mappers.

The equations of the planes which determine distinct feature vectors for each of the quadric surfaces are very sensitive to the quality of the digitized range data. In case the coefficient determining algorithm does not perform as expected, errors might be encountered while forming the feature sets. Active sensors like laser range mappers have only recently been developed. Much improvement is expected in the quality of range images in the near future. This will make the various recognition schemes much more reliable and flexible.

6.3 Future Goals and Research Directions

As seen from the best-fit plot in Chapter Five, regions within the range images have been marked to indicate which particular filter size (median) fits the image data the best at a particular pixel. While arriving at the coefficients of a second degree polynomial which describe a quadric surface, the range data considered were either the original, the 3×3 , the 5×5 , or the 7×7 median filtered range images. A filter whose mask size varies from region to region could possibly be a more effective filter which would not significantly distort the images.

Though experiments were performed on a large sample of range images belonging to spheres, cylinders, and cones, the effectiveness and accuracy of the developed recognition system can be tested further by using real range images of paraboloids, hyperboloids and cylinders (hyperbolic and parabolic). The recognition algorithm, however, has been very accurate when applied to simulated data.

We propose to extend our recognition algorithm to recognize quadric surfaces from complex scenes (scenes composed of more than two objects). This can be achieved by first utilizing an effective (existing) segmentation process, whereby range data of various surfaces will be separated. We could extend our recognition system to recognize irregular surfaces which are made up piece-by-piece of regular quadric surfaces.

Finally, we would like to investigate fully the mapping of the extrinsic and intrinsic representations of quadric surfaces. This process will lead to a three-dimensional discriminant analogous to the two-dimensional discriminant, which will distinguish all of the quadric surfaces considered for the recognition process in the course of this research. The development of such a discriminant will not only reduce the computational complexity, but will also eliminate the process of eliminating the product terms (rotation parameters) from the representation of the quadric surfaces. This approach will be invariant to pose and orientation.

REFERENCES

- [1] P. J. Besl and R. C. Jain, "Three-Dimensional Object Recognition," *ACM Comput. Surveys*, vol 17, pp. 77-145, March 1985.
- [2] R. A. Jarvis, "A Perspective on Range Finding Techniques for Computer Vision," *IEEE Trans. on Pattern Analysis and Machine Intelligence*, PAMI-5, pp. 122-139, March 1983.
- [3] M. Ishii and T. Nagata, "Feature Extraction of Three-Dimensional Objects and Visual Processing in a Hand-Eye System using Laser Tracker," *Pattern Recognition* vol. 8, pp. 229-237, 1976.
- [4] O. D. Faugeras et.al, "Towards a Flexible Vision System," *Robot Vision*, U.K., 1982.
- [5] M. Oshima and Y. Shirai, "Object Recognition using Three-Dimensional information," *IEEE Trans. on Pattern Analysis and Machine Intelligence*, PAMI-5, No. 4, pp. 353-361, July 1983.
- [6] B. Bhanu, "Representation and Shape Matching of 3-D Objects," *IEEE Trans. on Pattern Analysis and Machine Intelligence* , PAMI-6, No. 3, pp. 340-350, 1984.
- [7] R. Nevatia and T. O. Binford, "Description and Recognition of Curved Objects," *Artificial Intelligence*, 8, pp. 77-98, 1977.
- [8] I. K. Sethi and S. N. Jayaramamurthy, "Surface Classification using Characteristic Contours," Proc. 7th Intl. Conf. on Pattern Recognition, Montreal-Canada, pp. 438-440, 1984.

- [9] P. J. Besl and R. C. Jain, "Invariant Surface Characteristics for 3D Object Recognition in Range Images," *IEEE Trans. on Computer Vision, Graphics and Image Processing*, 33, 1, pp. 33-80, January 1986.
- [10] N. Alvertos and I. D'Cunha, "Three-Dimensional Description of Symmetric Objects from Range Images," SPIE vol 1382, Intelligent Robots and Computer Vision IX: Neural, Biological, and 3-D Methods, pp. 388-396, 1990.
- [11] N. Yokoya and M. D. Levine, "Range Image Segmentation based on Differential Geometry: A Hybrid Approach," McRCIM-TR-CIM 87-16, 1987.
- [12] W. E. L. Grimson and T. Lozano-Perez, "Model Based Recognition and Localization from Sparse Range data," *Techniques for 3-D Machine perception*, Elsevier Science Publishers (North Holland), pp. 113-148, 1986.
- [13] O. D. Faugeras and M. Hebert, "The Representation, Recognition, and Positioning of 3-D Shapes from Range Data," *Techniques for 3-D Machine Perception*, Elsevier Science Publishers (North Holland), 1986.
- [14] G. Hu and G. Stockman, "3-D Surface Solution using Structured Light and Constraint Propagation," *IEEE Trans. on Pattern Analysis and Machine Intelligence*, vol. 11, No. 4, April 1989.
- [15] M. Nagao, S. Hashimoto, and T. Saka, *Automatic Model Generation and Recognition of Simple Three-Dimensional Bodies*, " New York: Academic Press, Inc., 1973.
- [16] S. Ullman and R. Basri, "Recognition by Linear Combination of Models," *IEEE Trans. on Pattern Analysis and Machine Intelligence*, vol. 13, No. 10, pp. 992-1006, October 1991.
- [17] T. J. Fan, G. Medioni, and R. Nevatia, "Recognizing 3-D Objects using Surface Descriptors," *IEEE Trans. on Pattern Analysis and Machine Intelligence*, vol. 11, No. 11, pp. 1140-1157, November 1989.

- [18] D. Forsyth, J. L. Mundy, A. Zisserman, C. Coelho, A. Heller, and C. Rothwell, "Invariant Descriptors for 3-D Object Recognition and Pose," *IEEE Trans. on Pattern Analysis and Machine Intelligence*, vol. 13, No. 10, pp. 971-991, October 1991.
- [19] S. Lee and H. Hahn, "An Optimal Sensing Strategy for Recognition and Localization of 3-D Natural Quadric Objects," *IEEE Trans. on Pattern Analysis and Machine Intelligence*, vol. 13, No. 10, pp. 1018-1037, October 1992.
- [20] N. C. Grisworld and C. P. Yeh, "A New Stereo Vision Model Based upon the Binocular Fusion Concept," *IEEE Trans. on Computer Vision, Graphics, and Image Processing*, 41, pp. 153-171, 1988.
- [21] D. Marr and T. Poggio, "A Computational Theory of Human Stereo Vision," *Proc. R. Soc. London*, B 204, pp. 301-308, 1979.
- [22] W. E. L. Grimson, "Computational Experiments with Feature Based Stereo Algorithms," *IEEE Trans. on Pattern Analysis and Machine Intelligence*, PAMI-7, pp. 17-34, 1985.
- [23] R. P. Wilder, "Qualitative Three-Dimensional Shape from Stereo," *Proc. SPIE, Intelligent Robots and Computer Vision IX: Neural, Biological, and 3-D Methods*, vol 13382, pp. 453-463, 1990.
- [24] J. M. H. Olmstead, *Solid Analytical Geometry*. New York: Appleton-Century-Crofts. Inc., 1947.
- [25] B. Spain, *Analytical Quadrics*. London: Pergamon press Ltd., 1960.
- [26] B. Groshong and G. Bilbro, "Fitting a Quadric Surface to Three-Dimensional Data," technical Report, January 1986.
- [27] N. Alvertos and I. D'Cunha, "Curvature Effect of Median Filtering on Range Images," *IEEE proc. of Southeastcon 1991*, vol. 2, pp. 910- 914, 1991. %br

- [28] A. E. Taylor and W. R. Mann, *Advanced Calculus*, New York: J. Wiley, 1972.
- [29] O. D. Faugeras, "Segmentation of Range Data into Planar and Quadric Patches," *Proc. of the IEEE Conf. on Computer Vision and Pattern Recognition*, pp. 8-13, 1983.
- [30] G. B. Thomas Jr., *Calculus and Analytic Geometry*, Massachusetts: Addison-Wesley Publishing Company Inc., 1972.
- [31] Digital Signal Corporation, *Laser Radar 3-D Vision System Operation Manual*, contract no. NAS-18522, October 1988.

APPENDIX A

Appendix A consists of the ten coefficients generated for the original and processed range images of a sphere and a cylinder whose data is mapped using a different type of laser range mapper. Files with extension *.cod refer to the range data converted into cartesian coordinates, and files with extension *.coe consist of the coefficients generated for each of the images.

The input file was "spavgmed1.cod "
The output file is "spavgmed1.coe "
The coeff of x-squared is 0.2963710
The coeff of y-squared is -7.1920902E-03
The coeff of z-squared is 0.6404306
The coeff of yz is -0.2438449
The coeff of zx is -0.9575970
The coeff of xy is 0.1657399
The coeff of x is 0.5431624
The coeff of y is 0.1216914
The coeff of z is -0.6774822
The constant d is 0.1

Coefficients for an averaged sphere image.

The input file was "SPAMED31.COD "
The output file is "SPAMED31.COE "
The coeff of x-squared is 0.1939911
The coeff of y-squared is -6.4082608E-02
The coeff of z-squared is 0.7181194
The coeff of yz is -0.1474224
The coeff of zx is -0.9272834
The coeff of xy is 5.9526406E-02
The coeff of x is 0.6028971
The coeff of y is 6.9603384E-02
The coeff of z is -0.8269780
The constant d is 0.2249310

Coefficients for a 3 x 3 median filtered averaged sphere image.

The input file was "SPAMED51.COD "
The output file is "SPAMED51.COE "
The coeff of x-squared is 0.2154791
The coeff of y-squared is 0.1832946
The coeff of z-squared is 0.6808279
The coeff of yz is 0.8267535
The coeff of zx is -0.2360811
The coeff of xy is -0.4166962
The coeff of x is -0.2436151
The coeff of y is -0.4302364
The coeff of z is -0.4764909
The constant d is 9.0547577E-02

Coefficients for a 5 x 5 median filtered averaged sphere image.

The input file was "stavgmed1.cod "
The output file is "stavgmed1.coe "
The coeff of x-squared is -0.1682273
The coeff of y-squared is 4.3279368E-02
The coeff of z-squared is 0.7034476
The coeff of yz is 4.8151415E-02
The coeff of zx is 0.9669251
The coeff of xy is 0.1127514
The coeff of x is -0.7436121
The coeff of y is -8.4567606E-02
The coeff of z is -1.537530
The constant d is 0.7877931

Coefficients for an averaged cylinder image.

The input file was "STAMED31.COD "
The output file is "STAMED31.COE "
The coeff of x-squared is 0.2759137
The coeff of y-squared is 2.7527343E-02
The coeff of z-squared is 0.7029013
The coeff of yz is 0.1449835
The coeff of zx is -0.9098228
The coeff of xy is -9.6383080E-02
The coeff of x is 0.5634921
The coeff of y is -8.9731783E-02
The coeff of z is -0.8506840
The constant d is 0.2536311

Coefficients for a 3 x 3 median filtered averaged cylinder image.

The input file was "STAMED51.COD "
The output file is "STAMED51.COE "
The coeff of x-squared is 0.1115851
The coeff of y-squared is 3.1368352E-02
The coeff of z-squared is 0.8936580
The coeff of yz is 0.1347357
The coeff of zx is -0.5961419
The coeff of xy is -4.8396215E-02
The coeff of x is 0.4117958
The coeff of y is -9.9320240E-02
The coeff of z is -1.295335
The constant d is 0.4731036

Coefficients for a 5 x 5 median filtered averaged cylinder image.

APPENDIX B

This appendix consists of the ten coefficients generated for the original and processed range images of a quadric cone. Files with extension *.cod refer to the range data converted into cartesian coordinates, and files with extension *.coe consists of the coefficients generated for each of the images.

The input file was "coner.cod "
The output file is "coner.coe "
The coeff of x-squared is 0.9966836
The coeff of y-squared is -4.400091E-03
The coeff of z-squared is -1.723930E-03
The coeff of yz is 2.299275E-02
The coeff of zx is -0.1116501
The coeff of xy is -1.4285150E-02
The coeff of x is 9.4580045E-04
The coeff of y is -4.7494676E-03
The coeff of z is 1.7082826E-03
The constant d is -2.6372296E-04

Coefficients for a raw quadric cone image.

The input file was "conep.cod "
The output file is "conep.coe "
The coeff of x-squared is 0.9950956
The coeff of y-squared is -3.4555167E-02
The coeff of z-squared is -8.4933117E-03
The coeff of yz is 5.0487362E-02
The coeff of zx is -0.1104977
The coeff of xy is -4.7736488E-02
The coeff of x is 9.5897805E-04
The coeff of y is -1.6880523E-02
The coeff of z is 6.8076607E-03
The constant d is -1.0696481E-03

Coefficients for a median filtered quadric cone image.

APPENDIX C

This appendix consists of a sample executed file generated using the surface alignment algorithm. The coefficients considered are that of a 3 x 3 filtered image of a raw cylinder.

OUTPUT DATA FILE OF THE SURFACE ALIGNMENT PROGRAM

THE COEFFICIENTS CONSIDERED ARE OF THE 3 X 3 FILTERED IMAGE OF THE RAW CYLINDER.

THE NUMBER OF ITERATIONS COMPLETED IS : 3

COEFF. OF X SQUARE TERM IS : -0.5819000
COEFF. OF Y SQUARE TERM IS : -2.5060000E-02
COEFF. OF Z SQUARE TERM IS : -0.4078000
COEFF. OF YZ SQUARE TERM IS : -9.1289997E-02
COEFF. OF XZ SQUARE TERM IS : 0.9860000
COEFF. OF XY SQUARE TERM IS : 8.9539997E-02
COEFF. OF X TERM IS : -0.3951000
COEFF. OF Y TERM IS : 4.5000002E-02
COEFF. OF Z TERM IS : 0.3026000
CONSTANT OF PROP. IS : -4.4810001E-02

-0.5854765 -2.1506138E-02 -0.4078000 -1.2481645E-02 0.9838626
0.0000000E+00 -0.3974287 1.3208531E-02 0.3026000
-0.5854765 -2.1405339E-02 -0.4079008 0.0000000E+00 0.9837343
-1.5888708E-02 -0.3974287 8.3200261E-03 0.3027738
-0.9965052 -2.1405339E-02 3.1279027E-03 -1.0188361E-02 0.0000000E+00
-1.2192142E-02 -0.4991140 8.3200261E-03 -2.2511929E-02
-0.9965433 -2.1367228E-02 3.1279027E-03 -1.0188161E-02 -6.3691252E-05
0.0000000E+00 -0.4990523 1.1440012E-02 -2.2511929E-02
-0.9965433 -2.2384373E-02 4.1450467E-03 0.0000000E+00 -6.2458355E-05
-1.2471168E-05 -0.4990523 6.8105781E-03 -2.4316186E-02
-0.9965433 -2.2384373E-02 4.1450476E-03 3.8919640E-10 0.0000000E+00
-1.2471168E-05 -0.4990530 6.8105781E-03 -2.4300613E-02
-0.9965433 -2.2384373E-02 4.1450476E-03 3.8919640E-10 2.4912431E-15
0.0000000E+00 -0.4990530 6.8137725E-03 -2.4300613E-02
-0.9965433 -2.2384373E-02 4.1450476E-03 0.0000000E+00 2.4912431E-15
-1.8273728E-23 -0.4990530 6.8137725E-03 -2.4300613E-02
0.0000000E+00 0.0000000E+00 0.0000000E+00 0.0000000E+00 0.0000000E+00
0.0000000E+00 0.0000000E+00 0.0000000E+00 0.0000000E+00

THE NEW COEFF. OF X SQUARE TERM IS : -0.9965433
THE NEW COEFF. OF Y SQUARE TERM IS : -2.2384373E-02
THE NEW COEFF. OF Z SQUARE TERM IS : 4.1450476E-03
THE NEW COEFF. OF X TERM IS : -0.4990530
THE NEW COEFF. OF Y TERM IS : 6.8137725E-03
THE NEW COEFF. OF Z TERM IS : -2.4300613E-02
THE NEW CONSTANT OF PROP. IS : -4.4810001E-02

```

*****
A      B      C      F      G      H      P      Q      R
-----
-0.58548 -0.02151 -0.40780 -0.01248 0.98386 0.00000 -0.39743 0.01321 0.30260
-0.58548 -0.02141 -0.40790 0.00000 0.98373 -0.01589 -0.39743 0.00832 0.30277
-0.99651 -0.02141 0.00313 -0.01019 0.00000 -0.01219 -0.49911 0.00832 -0.02251
-0.99654 -0.02137 0.00313 -0.01019 -0.00006 0.00000 -0.49905 0.01144 -0.02251
-0.99654 -0.02238 0.00415 0.00000 -0.00006 -0.00001 -0.49905 0.00681 -0.02432
-0.99654 -0.02238 0.00415 0.00000 0.00000 -0.00001 -0.49905 0.00681 -0.02430
-0.99654 -0.02238 0.00415 0.00000 0.00000 0.00000 -0.49905 0.00681 -0.02430
-0.99654 -0.02238 0.00415 0.00000 0.00000 0.00000 -0.49905 0.00681 -0.02430
0.00000 0.00000 0.00000 0.00000 0.00000 0.00000 0.00000 0.00000 0.00000
*****
*****
*****
*****
*****
Alpha      Beta      Gamma
-----
4.567488      0.9253277      39.88381
-0.3581797      -11.29185      -1.7880693E-03
-3.6674985E-04      4.2027511E-07      0.0000000E+00
*****
*****
ALPTOT      BETTOT      GAMTOT
4.208942      -10.36652      39.88202
*****
*****
*****
*****
THE ROTATION MATRIX IS :
0.7640848      -7.1428910E-02      -0.6411492
7.9622917E-02      0.9966942      -1.6149314E-02
0.6401832      -3.8710725E-02      0.7672463

```

APPENDIX D

This appendix consists of a sample data file which is generated while executing the 3-D discriminant algorithm. The unknown quadric surface is later classified as a parabolic cylinder.

C***** SAMPLE DATA OF 3-D DISCRIMINANT PROGRAM

Coeff. of x^2 (A):

A =

1

Coeff. of y^2 (B):

B =

4

Coeff. of z^2 (C):

C =

9

Coeff. of yz (F):

F =

-6

Coeff. of xz (G):

G =

3

Coeff. of xy (H):

H =

-2

Coeff. of x (P):

P =

1

Coeff. of y (Q):

$$Q =$$

$$7$$

Coeff. of z (R):

$$R =$$

$$0$$

Constant of prop. (D):

$$D =$$

$$10$$

$$e =$$

$$\begin{array}{ccc} 1 & -2 & 3 \\ -2 & 4 & -6 \\ 3 & -6 & 9 \end{array}$$

$$EE =$$

$$\begin{array}{cccc} 1 & -2 & 3 & 1 \\ -2 & 4 & -6 & 7 \\ 3 & -6 & 9 & 0 \\ 1 & 7 & 0 & 10 \end{array}$$

$$dt_e =$$

$$0$$

$$dt_{EE} =$$

$$0$$

K_K =

-0.0000
0.0000
14.0000

rho_3 =

1

rho_4 =

3

s_d_EE =

0

s1 =

-1

s2 =

1

s3 =

1

flag =

0

The sign of the ch. roots are not the same

The rank of EE is : 1.0000

The rank of e is : 3.0000

The sign of the determinant of EE is : 0.0000

The characteristics roots have the same sign? : 0.0000

The object is a PARABOLIC CYLINDER

APPENDIX E

This appendix consists of the listings of the following programs:

1. Program "Median Filtering", which performs the 3 x 3 and 5 x 5 median filtering on range images.
2. Program "Derivatives" that evaluates the first and second derivative with respect to x and y axes of the data files and then transforms it into a sign map.
3. Program "Rangediff" that generates the sign map for each of the range images based upon the magnitude of the range value of neighboring pixels.
4. Program "Surface" that generates the ten coefficients which describe each of the range images.
5. Program "Surface Alignment" which eliminates the product terms from the representation of quadric surfaces thereby aligning them according to a desired coordinate system.
6. Program "3-D discriminant" which implements the classification of the quadrics based upon the discriminant procedure.


```

C      PROGRAM MEDIAN FILTERING
      PARAMETER (N=512)
      INTEGER*2  A(N,N),MED(N,N)
      CHARACTER*12  INFILE,OUTFILE

C
C      MAIN PROGRAM
C
      WRITE(*,123)
123    FORMAT(5X,'INPUT FILE NAME : INFILE')
      READ(*,*)INFILE
      WRITE(*,223)
223    FORMAT(5X,'OUTPUT FILENAME : OUTFILE')
      READ(*,*)OUTFILE

      OPEN (UNIT=1,FILE=INFILE,RECL=2048,STATUS='OLD')
      READ (1,9)((A(I,J),J=1,N),I=1,N)
9      FORMAT(512I4)
      M=3
c      CLOSE(1,DISPOSE='SAVE')
      CALL MEDFLT(A,MED,N,M)
      OPEN (UNIT=2,FILE=OUTFILE,RECL=2048,STATUS='NEW')

      WRITE (2,11)((MED(I,J),J=1,N),I=1,N)
11     FORMAT(512I4)
c      CLOSE(2,DISPOSE='SAVE')
      STOP
      END

CC
CC      SUBROUTINE MEDIAN FILTER
CC
      SUBROUTINE MEDFLT(A,MED,N,M)
      INTEGER*2  A(N,N),MED(N,N),SORT(50)
      LOGICAL    NEXCHAN

C
C
C
      MM=M ** 2
      X=(M+1)/2
      Y=X-1
      M1=(MM+1)/2
      DO 7 I=X,(N-Y)
      DO 9 J=X,(N-Y)

```

```

        K1=0
    DO 11 K=(I-Y),(I+Y)
    DO 13 L=(J-Y),(J+Y)
        K1=K1+1
        SORT(K1)=A(K,L)
13  CONTINUE
11  CONTINUE
    DO 15 I1=1,(MM-1)
    DO 17 K1=1,(MM-I1)
        IF (SORT(K1).GT.SORT(K1+1)) THEN
            TEMP=SORT(K1)
            SORT(K1)=SORT(K1+1)
            SORT(K1+1)=TEMP
        END IF
17  CONTINUE
15  CONTINUE
    MED(I,J)=SORT(M1)
9   CONTINUE
7   CONTINUE
    DO 19 I=1,Y
    DO 21 J=1,N
        MED(I,J)=A(I,J)
        MED(N+1-I,J)=A(N+1-I,J)
        MED(J,N+1-I)=A(J,N+1-I)
        MED(J,I)=A(J,I)
21  CONTINUE
19  CONTINUE
    RETURN
    END

```

C***** PROGRAM DERIVATIVES

C***** This program determines the derivative along the x and the

C***** y axes. A group of files can be compared to see whether a

C***** a particular location has the same curvature or not.

```

      INTEGER*2  I1,J1,T1,P1,K,L,I,J
      REAL      DX1,DX2,DX3,DY1,DY2,DY3
      REAL      DX11,DX22,DX33,DY11,DY22,DY33
      REAL      D(70,350),E(70,350),A(1000,3),AA(60,50)
      REAL      D1(70,350),E1(70,350)
      INTEGER*2  STREC,ENDREC
      CHARACTER*12  INFILE1,INFILE2,INFILE3,POINT
      CHARACTER*2  GRAPH1(70,100),GRAPH2(70,100),GRAPH3(70,100)
      CHARACTER*2  GRAPH4(70,100)
      WRITE(*,20)
20    FORMAT(5X,'INPUT FILE NAME : INFILE1')
      READ(*,*)INFILE1
      OPEN(UNIT=1, FILE=INFILE1, STATUS='UNKNOWN')
      DO 100 I=1,969
      READ(1,*)(A(I,J),J=1,3)
100   CONTINUE
      DO 811 K=1,51
      DO 815 L=1,19
      AA(K,L)=A(L+(19*(K-1)),3)
815   CONTINUE
811   CONTINUE

300   FORMAT(512I4)

C**   TO FIND THE DERIVATIVE ALONG X-AXIS

C1111 WRITE(*,908)
C908  FORMAT('INPUT THE STARTING RECORD NUMBER: STREC')
C     READ(*,*)STREC
C9008 FORMAT('INPUT THE ENDING RECORD NUMBER: ENDREC')

      OPEN(UNIT=2,FILE='FILE1.X',STATUS='UNKNOWN')
      OPEN(UNIT=3,FILE='FILE1.Y',STATUS='UNKNOWN')

```

```

OPEN(UNIT=4,FILE='FILE1.XX',STATUS='UNKNOWN')
OPEN(UNIT=8,FILE='FILE1.YY',STATUS='UNKNOWN')
11178 DO 1104 I1=1,51
      DO 1204 J1=1,19
      D(I1,J1)=0.5*((AA(I1,J1+1)-AA(I1,J1))+AA(I1+1,J1+1)-AA(I1+1,J1)))

      D1(I1,J1)=(AA(I1,J1-1)-2*(AA(I1,J1))+AA(I1,J1+1))

      E1(I1,J1)=(AA(I1+1,J1)-2*(AA(I1,J1))+AA(I1-1,J1))
      E(I1,J1)=0.5*((AA(I1,J1+1)-AA(I1,J1))+AA(I1,J1)-AA(I1+1,J1)))
1204 CONTINUE
1104 CONTINUE
1965      DO 11104 I1=1,51
      WRITE(2,*)(D(I1,J1),J1=1,19)
      WRITE(3,*)(E(I1,J1),J1=1,19)
      WRITE(4,*)(D1(I1,J1),J1=1,19)
      WRITE(8,*)(E1(I1,J1),J1=1,19)
11104 CONTINUE
      CLOSE(2)
      CLOSE(3)
      CLOSE(4)
      CLOSE(8)

OPEN(UNIT=2,FILE='FILE1.X',STATUS='UNKNOWN')
OPEN(UNIT=3,FILE='FILE1.Y',STATUS='UNKNOWN')
OPEN(UNIT=4,FILE='FILE1.XX',STATUS='UNKNOWN')
OPEN(UNIT=5,FILE='FILE1.YY',STATUS='UNKNOWN')
DO 324 I1=1,51,1
READ(2,*)(D(I1,J1),J1=1,19)
324 CONTINUE
DO 325 I1=1,51,1
DO 326 J1=1,19
IF (D(I1,J1).GT.D(I1,J1+1))THEN
GRAPH1(I1,J1)= '-'
ENDIF
IF (D(I1,J1).LT.D(I1,J1+1))THEN
GRAPH1(I1,J1)= '+'

ENDIF
IF (D(I1,J1).EQ.D(I1,J1+1))THEN
GRAPH1(I1,J1)= ' '
ENDIF
326 CONTINUE
325 CONTINUE

```

```

DO 328 I1=1,51,1
READ(3,*)(D1(I1,J1),J1=1,19)

328 CONTINUE
DO 329 I1=1,51,1
DO 330 J1=1,19
    IF (D1(I1,J1).GT.D1(I1,J1+1))THEN
GRAPH2(I1,J1)= '-'
ENDIF
    IF (D1(I1,J1).LT.D1(I1,J1+1))THEN
GRAPH2(I1,J1)= '+'
ENDIF
    IF (D1(I1,J1).EQ.D1(I1,J1+1))THEN
GRAPH2(I1,J1)= ' '
ENDIF
330 CONTINUE
329 CONTINUE
DO 332 I1=1,51,1
READ(4,*)(E(I1,J1),J1=1,19)
332 CONTINUE
DO 333 I1=1,51,1
DO 334 J1=1,19
    IF (E(I1,J1).GT.E(I1,J1+1))THEN
GRAPH3(I1,J1)= '-'
ENDIF
    IF (E(I1,J1).LT.E(I1,J1+1))THEN
GRAPH3(I1,J1)= '+'
ENDIF
    IF (E(I1,J1).EQ.E(I1,J1+1))THEN
GRAPH3(I1,J1)= ' '
ENDIF
334 CONTINUE
333 CONTINUE

DO 336 I1=1,51,1
READ(5,*)(E1(I1,J1),J1=1,19)
336 CONTINUE
DO 337 I1=1,51,1
DO 338 J1=1,19
    IF (E1(I1,J1).GT.E1(I1,J1+1))THEN
GRAPH4(I1,J1)= '-'
ENDIF
    IF (E1(I1,J1).LT.E1(I1,J1+1))THEN
GRAPH4(I1,J1)= '+'
ENDIF

```

```
IF (E1(I1,J1).EQ.E1(I1,J1+1))THEN
GRAPH4(I1,J1)= ' '
ENDIF

338 CONTINUE
337 CONTINUE
1324 CONTINUE
OPEN(UNIT=13,FILE='GRAPH.X',STATUS='UNKNOWN')
OPEN(UNIT=14,FILE='GRAPH.Y',STATUS='UNKNOWN')
OPEN(UNIT=15,FILE='GRAPH.XX',STATUS='UNKNOWN')
OPEN(UNIT=16,FILE='GRAPH.YY',STATUS='UNKNOWN')
DO 21104 I1=1,51,1
WRITE(13,1234)(GRAPH1(I1,J1),J1=1,19)
WRITE(14,1234)(GRAPH2(I1,J1),J1=1,19)
WRITE(15,1234)(GRAPH3(I1,J1),J1=1,19)
WRITE(16,1234)(GRAPH4(I1,J1),J1=1,19)

21104 CONTINUE
1234 FORMAT(30X,20A1)
C WRITE(*,21)
C GOTO 64
END
```

C***** PROGRAM RANGE SIGN MAP (RANGEDIFF)
 C***** THIS PROGRAM GENERATES A SIGN MAP FOR DATA FILES
 C***** BY TAKING INTO CONSIDERATION THE ABSOLUTE
 C***** DIFFERENCE IN RANGE VALUE OF NEIGHBORING PIXELS.

```

      INTEGER*2 A(0:511,0:512),D(100,100)
      INTEGER*2 I1,J1,T1,P1,ZZ,XX
      CHARACTER*12 INFILE1,INFILE2,INFILE3,POINT
      CHARACTER*2  GRAPH1(100,100)
      WRITE(*,20)
20    FORMAT(5X,'INPUT FILE NAME : INFILE1')
      READ(*,*)INFILE1
      OPEN(UNIT=1, FILE=INFILE1, STATUS='UNKNOWN', RECL=2048)
      DO 100 I=1,511
      READ(1,300)(A(I,J),J=1,512)
100   CONTINUE
300   FORMAT(512I4)
      ZZ=1
      C   XX=1
      DO 43 I=165,215
      XX=1
      DO 53 J=260,278
      D(ZZ,XX)=A(I,J)
      C   ZZ=ZZ+1
      XX=XX+1
53    CONTINUE
      C   XX=1
      ZZ=ZZ+1
      C   XX=1
43    CONTINUE
      WRITE(*,*)XX,ZZ
      OPEN(UNIT=2,FILE='rangeval.dat',STATUS='UNKNOWN')
      OPEN(UNIT=3,FILE='rangediff.dat',STATUS='UNKNOWN')
      c   OPEN(UNIT=4,FILE='FILE1.XX',STATUS='UNKNOWN')

      DO 325 I=1,ZZ-1
      DO 326 J=1,XX-1
      IF (D(I,J).GT.D(I,J+1))THEN
      GRAPH1(I,J)= '+'

```

```
ENDIF
  IF (D(I,J).LT.D(I,J+1))THEN
    GRAPH1(I,J)= '-'
  ENDIF
  IF (D(I,J).EQ.D(I,J+1))THEN
    GRAPH1(I,J)= ' '
  ENDIF
326 CONTINUE
325 CONTINUE
  DO 21104 I=1,ZZ-1
    WRITE(3,1234)(GRAPH1(I,J),J=1,XX-1)
    WRITE(2,3000)(D(I,J),J=1,XX-1)
21104 CONTINUE
1234 FORMAT(35X,20A1)
3000 FORMAT(I4)
  STOP
  END
```


C Program Surface

```
C *****
C This program approximates the coefficients of a surface
C generated by given data points. The input file consists of
C the rectangular coordinates of points on some surface.
C *****
```

```
integer i,j,k,ip
real x(9000),y(9000),z(9000),x_2(9000)
real y_2(9000),z_2(9000),p(9000,10)
real yz(9000),zx(9000),xy(9000),p_ptr(9000,10,10),sc(10,10)
real a(4,4),b(6,4),b_tr(4,6),c(6,6),h(6,6),h_inv(6,6)
real ris(4,8),a_inv(4,4),ba_inv(6,4),ba_invbt(6,6),m(6,6)
real h_invm(6,6),m_pr(6,6),ai(6,6),bi(6,6),ci(6,6)
real eigval(6,6),eigvec(6,6),ei_vec(6),a_invbt(4,6)
real alpha(4),beta(6),a_vect(10)
character*18 infile,outfile
Type*, ' Enter coordinates file : '
Accept*,infile
Type*, ' Enter output coefficients file : '
Accept*,outfile
open(unit=1,file=infile,status='old')
open(unit=2,file=outfile,status='new')
c***** The constraint matrix h and h_inv is created *****

write(*,3)
3 format(5x,'Input total points not exceeding 7750: ip=')
read(*,*) ip
root=1/(sqrt(2.))
do 24 i=1,6
do 26 j=1,6
h(i,j)=0
26 continue
24 continue
h(1,1)=1
h(2,2)=1
h(3,3)=1
h(4,4)=root
h(5,5)=root
h(6,6)=root
```

```

root1=sqrt(2.)
  do 20 i=1,6
    do 22 j=1,6
      h_inv(i,j)=0
22    continue
20    continue
h_inv(1,1)=1
h_inv(2,2)=1
h_inv(3,3)=1
h_inv(4,4)=root1
h_inv(5,5)=root1
h_inv(6,6)=root1

c***** Data is read here *****

  do 30 i=1,ip
    read(1,*) (x(i),y(i),z(i))
30    continue

c ***** the vector P for scatter matrix is formed here *****

  do 32 i=1,ip
    x_2(i)=x(i)**2
    y_2(i)=y(i)**2
    z_2(i)=z(i)**2
    yz(i)=y(i)*z(i)
    zx(i)=z(i)*x(i)
    xy(i)=x(i)*y(i)
32    continue
  do 34 i=1,ip
    p(i,1)=x_2(i)
    p(i,2)=y_2(i)
    p(i,3)=z_2(i)
    p(i,4)=yz(i)
    p(i,5)=zx(i)
    p(i,6)=xy(i)
    p(i,7)=x(i)
    p(i,8)=y(i)
    p(i,9)=z(i)
    p(i,10)=1
34    continue
  do 36 i=1,ip
    do 38 j=1,10
      do 40 k=1,10
        p_ptr(i,j,k)=p(i,j)*p(i,k)

```

```

40     continue
38     continue
36     continue
      do 42 j=1,10
          do 44 k=1,10
              sc(j,k)=0
44         continue
42     continue

c**** The Scatter Matrix is formed here *****

      do 46 j=1,10
          do 48 k=1,10
              do 50 i=1,ip
                  sc(j,k)=sc(j,k)+p_ptr(i,j,k)
50         continue
48     continue
46     continue

c***** The Scatter matrix sc is decomposed into a,b,b_tr,c **

      do 52 i=1,6
          do 54 j=1,6
              c(i,j)=sc(i,j)
54         continue
52     continue
      do 56 i=1,6
          do 58 j=1,4
              b(i,j)=sc(i,j+6)
58         continue
56     continue
      do 60 i=1,4
          do 62 j=1,6
              b_tr(i,j)=sc(i+6,j)
62         continue
60     continue
      do 64 i=1,4
          do 66 j=1,4
              a(i,j)=sc(i+6,j+6)
66         continue
64     continue
      do 68 i=1,4
          do 70 j=1,4
              ris(i,j)=a(i,j)

```

```

70     continue
68     continue
    call invers(ris,4,4,8)
        do 72 i=1,4
            do 74 j=1,4
                a_inv(i,j)=ris(i,j)
74         continue
72     continue
c ***** Now to compute M *****
        do 76 i=1,6
            do 78 j=1,4
                ba_inv(i,j)=0
78         continue
76     continue
        do 80 i=1,6
            do 82 j=1,4
                do 84 k=1,4
                    ba_inv(i,j)=ba_inv(i,j)+b(i,k)*a_inv(k,j)

84         continue
82         continue
80         continue
        do 86 i=1,6
            do 88 j=1,6
                ba_invbt(i,j)=0
88         continue
86         continue
        do 90 i=1,6
            do 92 j=1,6
                do 94 k=1,4
                    ba_invbt(i,j)=ba_invbt(i,j)+ba_inv(i,k)*b_tr(k,j)
94         continue
92         continue
90         continue
        do 96 i=1,6
            do 98 j=1,6
                m(i,j)=c(i,j)-ba_invbt(i,j)
98         continue
96         continue
c
c ***** Now to compute M' *****
c
        do 100 i=1,6
            do 102 j=1,6

```

```

        h_invm(i,j)=0
102    continue
100    continue
        do 104 i=1,6
            do 106 j=1,6
                do 108 k=1,6
                    h_invm(i,j)=h_invm(i,j)+h_inv(i,k)*m(k,j)
108    continue
106    continue
104    continue
        do 110 i=1,6
            do 112 j=1,6

                m_pr(i,j)=0
112    continue
110    continue
                do 114 i=1,6
                    do 116 j=1,6
                        do 118 k=1,6
                            m_pr(i,j)=m_pr(i,j)+h_invm(i,k)*h_inv(k,j)
118    continue
116    continue
114    continue
c
c ***** Now to find the eigen values of M' *****
c
        nd=6
        call eig(nd,m_pr,eigval,eigvec)
c
c ***** To find the smallest eigen value and its corresponding **
c ***** eigen vector *****
c
        s_eig=eigval(1,1)
        kount=1
        do 120 i=2,6
            if (s_eig.gt.eigval(i,i)) then
                s_eig=eigval(i,i)
                kount=i
            endif
120    continue
        do 122 i=1,6
            ei_vec(i)=eigvec(i,kount)
122    continue
        do 124 i=1,6

```

```

        beta(i)=0
        do 126 j=1,6
            beta(i)=beta(i)+h_inv(i,j)*ei_vec(j)
126     continue
124     continue
        do 128 i=1,4
            do 130 j=1,6
                a_invbt(i,j)=0
                do 132 k=1,4
                    a_invbt(i,j)=a_invbt(i,j)+a_inv(i,k)*b_tr(k,j)
132     continue
130     continue
128     continue
        do 134 i=1,4
            alpha(i)=0
            do 136 j=1,6
                alpha(i)=alpha(i)+a_invbt(i,j)*beta(j)
136     continue
            alpha(i)=-alpha(i)
134     continue
        do 138 i=1,6
            a_vect(i)=beta(i)
138     continue
        do 140 i=1,4
            a_vect(i+6)=alpha(i)
140     continue
c     do 142 i=1,10
        write(2,*) (' The input file was "',infile,'"')
        write(2,*) (' The output file is "',outfile,'"')
        write(2,*) (' The coeff of x-squared is ',a_vect(1))
        write(2,*) (' The coeff of y-squared is ',a_vect(2))
        write(2,*) (' The coeff of z-squared is ',a_vect(3))
        write(2,*) (' The coeff of yz is ',a_vect(4))
        write(2,*) (' The coeff of zx is ',a_vect(5))
        write(2,*) (' The coeff of xy is ',a_vect(6))
        write(2,*) (' The coeff of x is ',a_vect(7))
        write(2,*) (' The coeff of y is ',a_vect(8))
        write(2,*) (' The coeff of z is ',a_vect(9))
        write(2,*) (' The constant d is ',a_vect(10))
c142     continue
        close(unit=2,dispose='save')
        close(unit=1,dispose='save')
        end

```

c *****

```

Subroutine Invers(ris,N,Nx,Mx)
Dimension ris(Nx,Mx)
N1=N-1
N2=2*N
  Do 2 i=1,N
    Do 1 j=1,N
      j1=j+N
1    ris(i,j1)=0.
      j1=i+N
2    ris(i,j1)=1.
      Do 10 k=1,N1
        C=ris(k,k)
        If (Abs(C)-0.000001) 3,3,5
5        k1=k+1
          Do 6 j=k1,N2
6          ris(k,j)=ris(k,j)/C
          Do 10 i=k1,N
            C=ris(i,k)
            Do 10 j=k1,N2
              ris(i,j)=ris(i,j)-C*ris(k,j)
10         Continue
          Np1=N+1
          If (Abs(ris(N,N))-0.000001) 3,3,19
19        Do 20 j=Np1,N2
20        ris(N,j)=ris(N,j)/ris(N,N)
          Do 200 l=1,N1
            k=N-l
            k1=k+1
            Do 200 i=Np1,N2
              Do 200 j=k1,N
200         ris(k,i)=ris(k,i)-ris(k,j)*ris(j,i)
            Do 250 i=1,N
              Do 250 j=1,N
                j1=j+N
250         ris(i,j)=ris(i,j1)
          Return
3    Type*, 'Singularity in row found'
      Return
      End

Subroutine eig(nd,ai,bi,ci)
dimension ai(nd,nd),bi(nd,nd),ci(nd,nd)

```

```

integer n1,m1,n2,m2
n1=nd
M1=nd
n2=nd
m2=nd
ANorm=0.0
Sn=Float(N2)
  Do 100 i=1,N2
    Do 101 j=1,N2
      If (i-j) 72,71,72
71      Bi(i,j)=1.0
        Goto 101
72      Bi(i,j)=0.0
        ANorm=ANorm+Ai(i,j)*Ai(i,j)
101      Continue
100      Continue
ANorm=Sqrt(ANorm)
FNorm=ANorm*(1.0E-09/Sn)
Thr=ANorm
23  Thr=Thr/Sn
3   Ind=0
    Do 102 i=2,N2
      i1=i-1
      Do 103 j=1,i1
        If (Abs(Ai(j,i))-Thr) 103,4,4
4         Ind=1
          Al=-Ai(j,i)
          Am=(Ai(j,j)-Ai(i,i))/2.0
          Ao=Al/Sqrt((Al*Al)+(Am*Am))
          If (Am) 5,6,6
5           Ao=-Ao
6           Sinx=Ao/Sqrt(2.0*(1.0+Sqrt(1.0-Ao*Ao)))
            Sinx2=Sinx*Sinx
            Cosx=Sqrt(1.0-Sinx2)
            Cosx2=Cosx*Cosx
          Do 104 k=1,N2
            If (k-j) 7,10,7
7             If (k-i) 8,10,8
8             At=Ai(k,j)
              Ai(k,j)=At*Cosx-Ai(k,i)*Sinx
              Ai(k,i)=At*Sinx+Ai(k,i)*Cosx
10            Bt=Bi(k,j)
              Bi(k,j)=Bt*Cosx-Bi(k,i)*Sinx
              Bi(k,i)=Bt*Sinx+Bi(k,i)*Cosx

```



```

104      Continue
      Xt=2.0*Ai(j,i)*Sinx*Cosx
      At=Ai(j,j)
      Bt=Ai(i,i)
      Ai(j,j)=At*Cosx2+Bt*Sinx2-Xt
      Ai(i,i)=At*Sinx2+Bt*Cosx2+Xt
      Ai(j,i)=(At-Bt)*Sinx*Cosx+Ai(j,i)*(Cosx2-Sinx2)
      Ai(i,j)=Ai(j,i)
      Do 105 k=1,N2
        Ai(j,k)=Ai(k,j)
        Ai(i,k)=Ai(k,i)
105      Continue
103      Continue
102      Continue
      If (Ind) 20,20,3
20      If (Thr-FNorm) 25,25,23
25      Do 110 i=2,N2
        j=i
29      If ((Abs(Ai(j-1,j-1)))-(Abs(Ai(j,j)))) 30,110,110
30      At=Ai(j-1,j-1)
        Ai(j-1,j-1)=Ai(j,j)
        Ai(j,j)=At
        Do 111 k=1,N2
          At=Bi(k,j-1)
          Bi(k,j-1)=Bi(k,j)
          Bi(k,j)=At
111      Continue
        j=j-1
        If (j-1) 110,110,29
110      Continue
      do 112 i=1,N2
        do 114 j=1,N2
          ci(i,j)=bi(i,j)
          bi(i,j)=ai(i,j)
114      continue
112      continue
      return
      end

```

C**** PROGRAM SURFACE ALIGNMENT

C**** This program is used to eliminate the product terms
 C**** from the quadratic representation of any 3D surface.
 C**** The new coefficients generated consists of the square terms,
 C**** the x, y, z, and the constant term.

```

REAL AA,BB,CC,DD,FF,GG,HH,PP,QQ,RR,D,Test_f,Test_g,test_h
REAL A(50,50),B(50,50),C(50,50),F(50,50)
REAL G(50,50),H(50,50),ALPHA(100),BETA(100)
REAL RESULT(200,200),P(50,50),Q(50,50),R(50,50)
REAL AAA,BBB,CCC,DDD,EEE,FFF,GGG,HHH,III,ROT(3,3)
REAL DEL1,DEL2,DEL3,A_A,B_B,C_C,F_F,G_G,H_H,GAMMA(100)
REAL VV,VVV,VVVV,VVVVV,THRESHLD,INITMIN,ABSA,ABSB,ABSC
REAL A_AA,B_BB,C_CC,D_DD,P_PP,Q_QQ,R_RR
REAL ABSF,ABSG,ABSH,ABSP,ABSQ,ABSR,RRR(50),alptot,bettot
REAL gamtot
INTEGER N,M,I,J
C F(X,Y,Z)=Ax**2+By**2+Cz**2+2Fyz+2Gxz+2Hxy+2Px+2Qy+2Rz+D
C =0
C PARAMETER (THRESHLD= 0.00000000000000001)

OPEN(UNIT=1,FILE='CONVERGENCE.DAT',STATUS='NEW')
TYPE*, 'ENTER VALUE FOR THRESHLD:'
ACCEPT*, THRESHLD

Type*, 'Enter coef. of x ** 2 :'
Accept*, AA
Type*, 'Enter coef. of y ** 2 :'
Accept*, BB
Type*, 'Enter coef. of z ** 2 :'
Accept*, CC
Type*, 'Enter coef. of yz :'
Accept*, FF
Type*, 'Enter coef. of xz :'
Accept*, GG
Type*, 'Enter coef. of xy :'
Accept*, HH
Type*, 'Enter coef. of x :'
Accept*, PP
Type*, 'Enter coef. of y :'
Accept*, QQ
Type*, 'Enter coef. of z :'
```

```

Accept*,RR
Type*,'Enter constant of prop. :'
Accept*,D

```

```

A(1,1)=AA
B(1,1)=BB
C(1,1)=CC
F(1,1)=FF
G(1,1)=GG
H(1,1)=HH
P(1,1)=PP
Q(1,1)=QQ
R(1,1)=RR
ABSA=ABS(AA)
ABSB=ABS(BB)
ABSC=ABS(CC)
ABSF=ABS(FF)
ABSG=ABS(GG)
ABSH=ABS(HH)
ABSP=ABS(PP)
ABSQ=ABS(QQ)
ABSR=ABS(RR)
RRR(1)=ABSA
RRR(2)=ABSB
RRR(3)=ABSC
RRR(4)=ABSF
RRR(5)=ABSG
RRR(6)=ABSH
RRR(7)=ABSP
RRR(8)=ABSQ
RRR(9)=ABSR
DO 3980 I=1,9
IF (RRR(I).EQ.0)THEN
RRR(I)=10000
ENDIF
3980 CONTINUE
INITMIN=AMIN1(RRR(1),RRR(2),RRR(3),RRR(4),RRR(5),RRR(6),RRR(7)
+ ,RRR(8),RRR(9))
WRITE(*,*)INITMIN
IF (ABS(INITMIN).LT.1.0)THEN
A(1,1)=A(1,1)/INITMIN
B(1,1)=B(1,1)/INITMIN

```

```

C(1,1)=C(1,1)/INITMIN
F(1,1)=F(1,1)/INITMIN
G(1,1)=G(1,1)/INITMIN
H(1,1)=H(1,1)/INITMIN
P(1,1)=P(1,1)/INITMIN
Q(1,1)=Q(1,1)/INITMIN
Q(1,1)=Q(1,1)/INITMIN
DD_D=D/INITMIN
ELSE
GOTO 3405
ENDIF
3405 A(1,1)=AA
      B(1,1)=BB
      C(1,1)=CC
      F(1,1)=FF
      G(1,1)=GG
      H(1,1)=HH
      P(1,1)=PP
      Q(1,1)=QQ
      R(1,1)=RR

345  if (b(1,1).eq.a(1,1)) then

      goto 1167
      else
c     goto 57
c     endif
c     else
      goto 57
      endif
57   alpha(1)=(0.5*ATAND((H(1,1)/(B(1,1)-A(1,1))))
      A(1,1)=A(1,1)*COSD(ALPHA(1))*COSD(ALPHA(1))+B(1,1)*
+ SIND(ALPHA(1))*SIND(ALPHA(1))- H(1,1)*SIND(ALPHA(1))*
+ COSD(ALPHA(1))
      B(1,1)=B(1,1)*COSD(ALPHA(1))*COSD(ALPHA(1))+A(1,1)*
+ SIND(ALPHA(1))*SIND(ALPHA(1))+H(1,1)*SIND(ALPHA(1))*
+ COSD(ALPHA(1))
      C(1,1)=C(1,1)
      F(1,1)=G(1,1)*SIND(ALPHA(1))+F(1,1)*COSD(ALPHA(1))
      G(1,1)=G(1,1)*COSD(ALPHA(1))-F(1,1)*SIND(ALPHA(1))
      H(1,1)=0

```

```

P(1,1)=P(1,1)*COSD(ALPHA(1))-Q(1,1)*SIND(ALPHA(1))
Q(1,1)=Q(1,1)*COSD(ALPHA(1))+P(1,1)*SIND(ALPHA(1))

R(1,1)=R(1,1)

IF (ABS(F(1,1)).LT.THRESHLD)THEN
GOTO 1005
ELSE
GOTO 1167
ENDIF
1005 IF (ABS(G(1,1)).LT.THRESHLD)THEN
GOTO 1812
ELSE
GOTO 1167
ENDIF
1167 IF (C(1,1).EQ.B(1,1))THEN
GOTO 1169
ELSE
GOTO 1200
ENDIF
1200 BETA(1)=(0.5*ATAND((F(1,1)/(C(1,1)-B(1,1))))
A(1,2)=A(1,1)
B(1,2)=B(1,1)*COSD(BETA(1))*COSD(BETA(1))+C(1,1)*
+ SIND(BETA(1))*SIND(BETA(1))-F(1,1)*SIND(BETA(1))*COSD(BETA(1))

C(1,2)=C(1,1)*COSD(BETA(1))*COSD(BETA(1))+B(1,1)*
+ SIND(BETA(1))*SIND(BETA(1))+F(1,1)*SIND(BETA(1))*COSD(BETA(1))
F(1,2)=0
G(1,2)=G(1,1)*COSD(BETA(1))
H(1,2)=-G(1,1)*SIND(BETA(1))
P(1,2)=P(1,1)
Q(1,2)=Q(1,1)*COSD(BETA(1))-R(1,1)*SIND(BETA(1))

R(1,2)=R(1,1)*COSD(BETA(1))+Q(1,1)*SIND(BETA(1))
IF (ABS(H(1,2)).LT.THRESHLD)THEN
GOTO 1007
ELSE
GOTO 1169
ENDIF
1007 IF (ABS(G(1,2)).LT.THRESHLD)THEN

```

```

GOTO 1812
ELSE
GOTO 1169
ENDIF

1169 IF (C(1,2).EQ.A(1,2))THEN
GOTO 67
ELSE
GOTO 1235
ENDIF

1235 GAMMA(1)=(0.5*ATAND((G(1,2)/(C(1,2)-A(1,2))))
A(1,3)=A(1,2)*COSD(GAMMA(1))*COSD(GAMMA(1))+C(1,2)*
+ SIND(GAMMA(1))*SIND(GAMMA(1))-G(1,2)*SIND(GAMMA(1))
+ *COSD(GAMMA(1))
B(1,3)=B(1,2)
C(1,3)=C(1,2)*COSD(GAMMA(1))*COSD(GAMMA(1))+A(1,2)*
+ SIND(GAMMA(1))*SIND(GAMMA(1))+G(1,2)*SIND(GAMMA(1))
+ *COSD(GAMMA(1))
F(1,3)=H(1,2)*SIND(GAMMA(1))
G(1,3)=0
H(1,3)=H(1,2)*COSD(GAMMA(1))

P(1,3)=P(1,2)*COSD(GAMMA(1))-R(1,2)*SIND(GAMMA(1))
Q(1,3)=Q(1,2)
R(1,3)=R(1,2)*COSD(GAMMA(1))+P(1,2)*SIND(GAMMA(1))

IF (ABS(F(1,3)).LT.THRESHLD)THEN
GOTO 1009
ELSE
GOTO 67
ENDIF
1009 IF (ABS(H(1,3)).LT.THRESHLD)THEN
GOTO 1812
ELSE
GOTO 67
ENDIF

```

```

67   DO 10 I=2,100
C    DO 20 J=1

71   if((b(i-1,3).eq.a(i-1,3)))then
      goto 167
C    else
c    if(h(i,3).eq.0)then

c    goto 67
c    else
c    goto 67
c    endif
c    else
      goto 177
      endif

177  alpha(I)=(0.5*ATAND((H(I-1,3)/(B(I-1,3)-A(I-1,3))))
      A(I,1)=A(I-1,3)*COSD(ALPHA(I))*COSD(ALPHA(I))+(B(I-1,3))*
+ SIND(ALPHA(I))*SIND(ALPHA(I))- H(I-1,3)*SIND(ALPHA(I))*
+ COSD(ALPHA(I))
      B(I,1)=B(I-1,3)*COSD(ALPHA(I))*COSD(ALPHA(I))+A(I-1,3)*
+ SIND(ALPHA(I))*SIND(ALPHA(I))+H(I-1,3)*SIND(ALPHA(I))*
+ COSD(ALPHA(I))
      C(I,1)=C(I-1,3)
      F(I,1)=F(I-1,3)*COSD(ALPHA(I))
      G(I,1)=-F(I-1,3)*SIND(ALPHA(I))
      H(I,1)=0
      P(I,1)=P(I-1,3)*COSD(ALPHA(I))-Q(I-1,3)*SIND(ALPHA(I))
      Q(I,1)=Q(I-1,3)*COSD(ALPHA(I))+P(I-1,3)*SIND(ALPHA(I))
      R(I,1)=R(I-1,3)

      IF (ABS(F(I,1)).LT.THRESHLD)THEN
        GOTO 1011
      ELSE
        GOTO 167
      ENDIF
1011 IF (ABS(G(I,1)).LT.THRESHLD)THEN
      N=I
      GOTO 666
      ELSE
        GOTO 167
      ENDIF
167  if((c(i,1).eq.b(i,1)))then

```

```

        goto 69
    else
c      goto 59
c      endif
c      else
        goto 59
    endif
59    BETA(I)=(0.5*ATAND((F(I,1)/(C(I,1)-B(I,1))))))
        A(I,2)=A(I,1)
        B(I,2)=B(I,1)*COSD(BETA(I))*COSD(BETA(I))+C(I,1)*
+     SIND(BETA(I))*SIND(BETA(I))-F(I,1)*SIND(BETA(I))*COSD(BETA(I))

        C(I,2)=C(I,1)*COSD(BETA(I))*COSD(BETA(I))+B(I,1)*
+     SIND(BETA(I))*SIND(BETA(I))+F(I,1)*SIND(BETA(I))*COSD(BETA(I))
        F(I,2)=0
        G(I,2)=G(I,1)*COSD(BETA(I))
        H(I,2)=-G(I,1)*SIND(BETA(I))
        P(I,2)=P(I,1)
        Q(I,2)=Q(I,1)*COSD(BETA(I))-R(I,1)*SIND(BETA(I))

        R(I,2)=R(I,1)*COSD(BETA(I))+Q(I,1)*SIND(BETA(I))

        IF (ABS(G(I,2)).LT.THRESHLD)THEN
            GOTO 1013
        ELSE
            GOTO 69
        ENDIF
1013 IF (ABS(H(I,2)).LT.THRESHLD)THEN
            N=I
            GOTO 666
        ELSE
            GOTO 69
        ENDIF

c69  if(g(i,2).eq.0)then
69    if((c(i,2).eq.a(i,2)))then
        goto 10
    else
c      goto 63
c      endif

```



```

c      else
      goto 63
      endif
63     GAMMA(I)=(0.5*ATAND((G(I,2)/(C(I,2)-A(I,2))))
      A(I,3)=A(I,2)*COSD(GAMMA(I))*COSD(GAMMA(I))+C(I,2)*
+     SIND(GAMMA(I))*SIND(GAMMA(I))-G(I,2)*SIND(GAMMA(I))
+     *COSD(GAMMA(I))
      B(I,3)=B(I,2)
      C(I,3)=C(I,2)*COSD(GAMMA(I))*COSD(GAMMA(I))+A(I,2)*
+     SIND(GAMMA(I))*SIND(GAMMA(I))+G(I,2)*SIND(GAMMA(I))
+     *COSD(GAMMA(I))
      F(I,3)=H(I,2)*SIND(GAMMA(I))
      G(I,3)=0
      H(I,3)=H(I,2)*COSD(GAMMA(I))

      P(I,3)=P(I,2)*COSD(GAMMA(I))-R(I,2)*SIND(GAMMA(I))
      Q(I,3)=Q(I,2)
      R(I,3)=R(I,2)*COSD(GAMMA(I))+P(I,2)*SIND(GAMMA(I))

      IF (ABS(F(I,3)).LT.THRESHLD)THEN
      GOTO 1015
      ELSE
      GOTO 10
      ENDIF
1015  IF (ABS(H(I,3)).LT.THRESHLD)THEN
      N=I
      GOTO 666
      ELSE
      GOTO 10
      ENDIF

20    CONTINUE
10    CONTINUE
1812  N=1
666   WRITE(*,*)N
      WRITE(*,123)
123   FORMAT(5X,'*****')
+     *****')
      WRITE(*,*)('THE NUMBER OF ITERATIONS COMPLETED IS:',N)

```

```

M=N*3
DO 1000 I=1,N
DO 1001 J=1,3
RESULT(3*(I-1)+J,1)=A(I,J)
RESULT(3*(I-1)+J,2)=B(I,J)
RESULT(3*(I-1)+J,3)=C(I,J)
RESULT(3*(I-1)+J,4)=F(I,J)
RESULT(3*(I-1)+J,5)=G(I,J)
RESULT(3*(I-1)+J,6)=H(I,J)
RESULT(3*(I-1)+J,7)=P(I,J)
RESULT(3*(I-1)+J,8)=Q(I,J)
RESULT(3*(I-1)+J,9)=R(I,J)

1001 CONTINUE
1000 CONTINUE
WRITE(1,*)('THE NUMBER OF ITERATIONS COMPLETED IS :',N)
WRITE(1,123)

WRITE(1,*)('COEFF. OF X SQUARE TERM IS : ', AA)
198 WRITE(1,*)('COEFF. OF Y SQUARE TERM IS : ', BB)
298 WRITE(1,*)('COEFF. OF Z SQUARE TERM IS : ', CC)
398 WRITE(1,*)('COEFF. OF YZ SQUARE TERM IS : ', FF)
498 WRITE(1,*)('COEFF. OF XZ SQUARE TERM IS : ', GG)
598 WRITE(1,*)('COEFF. OF XY SQUARE TERM IS : ', HH)
WRITE(1,*)('COEFF. OF X TERM IS : ', PP)
WRITE(1,*)('COEFF. OF Y TERM IS : ', QQ)
WRITE(1,*)('COEFF. OF Z TERM IS : ', RR)
WRITE(1,*)('CONSTANT OF PROP. IS : ', D)

write(1,123)
write(1,123)
write(1,123)
DO 2000 I=1,M
WRITE(1,*)(RESULT(I,J),J=1,9)
2000 CONTINUE

A_AA=RESULT(M-2,1)
B_BB=RESULT(M-2,2)
C_CC=RESULT(M-2,3)
P_PP=RESULT(M-2,7)

```

```

Q_QQ=RESULT(M-2,8)
R_RR=RESULT(M-2,9)
D_DD=D

do 30001 i=1,3
write(1,123)
30001 continue
WRITE(1,*)('THE NEW COEFF. OF X SQUARE TERM IS : ', A_AA)
WRITE(1,*)('THE NEW COEFF. OF Y SQUARE TERM IS : ', B_BB)
WRITE(1,*)('THE NEW COEFF. OF Z SQUARE TERM IS : ', C_CC)
WRITE(1,*)('THE NEW COEFF. OF X TERM IS : ', P_PP)
WRITE(1,*)('THE NEW COEFF. OF Y TERM IS : ', Q_QQ)
WRITE(1,*)('THE NEW COEFF. OF Z TERM IS : ', R_RR)
WRITE(1,*)('THE NEW CONSTANT OF PROP. IS : ',D_DD)

do 3001 i=1,3
write(1,123)
3001 continue

write(1,1278)
1278 format(6x,'A',9x,'B',9x,'C',9x,'F',9x,'G',9x,'H',9x,'P',
+ 9x,'Q',9x,'R')
write(1,1897)
1897 format(5x,'-----'
+ -----')

DO 2001 I=1,M
WRITE(1,1234)(RESULT(I,J),J=1,9)
2001 CONTINUE
1234 format(9F10.5)
DO 3000 I=1,5
WRITE(1,123)
3000 CONTINUE
write(1,1908)
1908 format(6x,'Alpha',9x,'Beta',9x,'Gamma')
write(1,1897)
DO 4000 I=1,N
WRITE(1,*)ALPHA(I),BETA(I),GAMMA(I)
4000 CONTINUE

```

```

alptot=alpha(1)+alpha(2)+alpha(3)
bettot=beta(1)+beta(2)+beta(3)
gamtot=gamma(1)+gamma(2)+gamma(3)
write(1,123)
write(1,123)
write(1,1998)
1998 format(6x,'ALPTOT',9x,'BETTOT',9x,'GAMTOT')
write(1,*)alptot,bettot,gamtot
write(1,123)
c*****      To evaluate coeff. of yz, xz, and xy once alpha, beta
c*****      and gamma are evaluated.
write(*,*)alpha(1),beta(1),gamma(1)
AAA=BB*cosd(alpha(1))*cosd(alpha(1))+(AA*sind(alpha(1))
+ *sind(alpha(1)))+(HH/2)*sind(2*alpha(1))-CC
BBB=gg*sind(alpha(1))+(ff*cosd(alpha(1)))
CCC=((aa-bb)*sind(2*alpha(1))+(hh*cosd(2*alpha(1)))
DDD=gg*cosd(alpha(1))-(ff*sind(alpha(1)))
EEE=aa*(cosd(alpha(1))*cosd(alpha(1))-(sind(alpha(1))
+ *sind(alpha(1))*sind(beta(1))*sind(beta(1))))
FFF=bb*(sind(alpha(1))*sind(alpha(1))-(cosd(alpha(1))
+ *cosd(alpha(1))*sind(beta(1))*sind(beta(1))))
GGG=cc*cosd(beta(1))*cosd(beta(1))
HHH=(gg/2)*sind(alpha(1))*sind(2*beta(1))+(ff/2)*cosd(alpha(1))*
+ sind(2*beta(1))
III=(hh/2)*sind(2*alpha(1))*(1+sind(beta(1))*
+ sind(beta(1)))

Test_F=(AAA*sind(2*beta(1))+BBB*cosd(2*beta(1)))*
+ cosd(gamma(1))+(CCC*cos(beta(1))-DDD*sind(beta(1)))
+ *sind(gamma(1))

Test_G=(EEE+FFF-GGG-HHH-III)*SIND(2*GAMMA(1)) +
+ (CCC*SIND(BETA(1))+COSD(BETA(1))*DDD)*COSD(2*GAMMA(1))

TEST_H=(CCC*COSD(BETA(1))-DDD*SIND(BETA(1)))*COSD(GAMMA(1)) -
+ (AAA*SIND(2*BETA(1))+BBB*COSD(2*BETA(1)))*SIND(GAMMA(1))

c      write(1,123)
      write(1,123)

```

```

c      write(1,124)
c
c      write(1,*)test_f,test_g,test_h
      write(1,123)
      write(1,123)
      write(1,124)
124   format(5x,'THE ROTATION MATRIX IS : ')
c**** To evaluate the rotation matrix

      rot(1,1)=cosd(alpha(1))*cosd(gamma(1))-(sind(alpha(1))*
+   sind(beta(1))*sind(gamma(1)))
      rot(1,2)=-sind(alpha(1))*cosd(gamma(1))-(cosd(alpha(1))*
+   sind(beta(1))*sind(gamma(1)))
      rot(1,3)=-sind(gamma(1))*cosd(beta(1))

      rot(2,1)=sind(alpha(1))*cosd(beta(1))
      rot(2,2)=cosd(beta(1))*cosd(alpha(1))
      rot(2,3)=-sind(beta(1))

      rot(3,1)=cosd(alpha(1))*sind(gamma(1))+(sind(alpha(1))*
+   sind(beta(1))*cosd(gamma(1)))
      rot(3,2)=cosd(alpha(1))*cosd(gamma(1))*sind(beta(1))
+   -(sind(alpha(1))*sind(gamma(1)))
      rot(3,3)=cosd(gamma(1))*cosd(beta(1))

      DO 989 I=1,3
      WRITE(1,*)(ROT(I,J),J=1,3)
989   CONTINUE
      stop
end

```

```

C***** PROGRAM 3-D DISCRIMINANT
C***** Implementation of the 3-D discriminant approach
C***** Implemented on MATLAB
diary on
input('Coeff. of x^2 (A): ');
A=ans
input('Coeff. of y^2 (B): ');
B=ans
input('Coeff. of z^2 (C): ');
C=ans
input('Coeff. of yz (F): ');
F=ans
input('Coeff. of xz (G): ');
G=ans
input('Coeff. of xy (H): ');
H=ans
input('Coeff. of x (P): ');
P=ans
input('Coeff. of y (Q): ');
Q=ans
input('Coeff. of z (R): ');
R=ans
input('Constant of prop. (D): ');
D=ans
F=F/2;
G=G/2;
H=H/2;
P=P/2;
Q=Q/2;
R=R/2;

e=[A H G
  H B F
  G F C ]

EE=[ A H G P
  H B F Q
  G F C R
  P Q R D ]

dt_e=det(e)
dt_EE=det(EE)

K_K=eig(e)
rho_3=rank(e)
rho_4=rank(EE)
s_d_EE=sign(dt_EE)

```

```

s1=sign(K_K(1))
s2=sign(K_K(2))
s3=sign(K_K(3))
flag=0
if s1 == s2;
flag=flag+1
end;
if s1 == s3;
flag=flag+1
end;
if flag == 2;
an_w=1;
fprintf('\n\n The sign of the ch. roots are the same \n')
else;
an_w=0;
end;
fprintf('\n\n The sign of the ch. roots are not the same \n')
fprintf('\n\n The rank of EE is : %9.4f \n ', rho_3 )
fprintf('\n\n The rank of e is : %9.4f \n ', rho_4 )
fprintf('\n\n The sign of the determinant of EE is : %9.4f \n',s_d_EE )
fprintf('\n\n The characteristics roots have the same sign? : %9.4f \n', an_w)

if rho_3==3
if rho_4==4
if s_d_EE==-1
if an_w==1
fprintf('\n\n The object is an ELLIPSOID \n\n')
end
end
end
end
if rho_3==3
if rho_4==4
if s_d_EE==1
if an_w==0
fprintf('\n\n The object is a HYPERBOLOID OF ONE SHEET \n\n')
end
end
end
end
if rho_3==3
if rho_4==4
if s_d_EE==-1

if an_w==0
fprintf('\n\n The object is a HYPERBOLOID OF TWO SHEETS \n')
end
end
end
end

```

```

end
if rho_3==3
if rho_4==3
if an_w==0
fprintf('\n\n The object is a REAL QUADRIC CONE \n')
end
end
end
if rho_3==2
if rho_4==4
if s_d_EE==-1
if an_w==0
fprintf('\n\n The object is an ELLIPTIC PARABOLOID \n')
end
end
end
end
if rho_3==2
if rho_4==4
if s_d_EE==1
if an_w==0
fprintf('\n\n The object is a HYPERBOLIC PARABOLOID \n')
end
end
end
end
if rho_3==2
if rho_4==3
if an_w==1
fprintf('\n\n The object is an ELLIPTIC CYLINDER \n')
end
end
end
if rho_3==2
if rho_4==3
if an_w==0
fprintf('\n\n The object is a HYPERBOLIC CYLINDER \n')
end
end
end

if rho_3==1
if rho_4==3
fprintf('\n\n The object is a PARABOLIC CYLINDER \n')
end
end
diary off

```


AUTOBIOGRAPHICAL STATEMENT

The author was born in Jullundur, India on February 18, 1965. He received the Bachelor of Engineering degree from Osmania University, Hyderabad in 1987 and the Master of Engineering degree from Old Dominion University in 1989. His research interests are in the fields of Character Recognition, Pattern Recognition, Three-Dimensional Object Recognition and Computer Vision.